

Picosecond Hydration Dynamics at the Protein Core and the Effect of Perturbed Environment

A Thesis

*Submitted in Partial Fulfillment of the Requirements
for the Degree of*

DOCTOR OF PHILOSOPHY

by

VAISAKH MOHAN K.



to the

**Department of Chemistry
Indian Institute of Technology Kanpur
Kanpur, India**

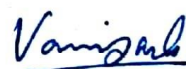
December, 2018

STATEMENT

I hereby declare that the work presented in the thesis entitled “**Picosecond Hydration Dynamics at the Protein Core and the Effect of Perturbed Environment**” is the result of original work carried out by me in the Department of Chemistry, Indian Institute of Technology Kanpur under the supervision of **Prof. Pratik Sen**.

In keeping with the general practice of reporting scientific observations, due acknowledgements have been made wherever the described work is based on the findings of other investigators.

December, 2018
IIT Kanpur


(Vaisakh Mohan K.)
Roll no. 12107084

CERTIFICATE



It is certified that the work reported in the thesis entitled **“Picosecond Hydration Dynamics at the Protein Core and the Effect of Perturbed Environment”** has been carried out by **Mr. Vaisakh Mohan K.** under my supervision and has not been submitted elsewhere for a degree.

December, 2018
IIT Kanpur

Dr. Pratik Sen
(Thesis Supervisor)
Professor, Department of Chemistry
Indian Institute of Technology Kanpur
Kanpur-208016, U.P., India

**Department of Chemistry
Indian Institute of Technology Kanpur**

Certificate of course work

This is to certify that **Mr. Vaisakh Mohan K.** has satisfactorily completed all the courses required for the Ph.D. degree. The courses include:

CHM 629 Principles of Physical Chemistry
CHM 646 Bio-Inorganic Chemistry
CHM 664 Modern Physical Methods in Chemistry
CHM 679 Molecular Reaction Dynamics
AE 698 Introduction to Virtual Instrumentation
CHM 695 Molecular Modelling in Chemistry
CHM 799 Research
CHM 800 General Seminar
CHM 801 Graduate Seminar

Mr. Vaisakh Mohan K. was admitted to the candidacy of the Ph.D. degree in September, 2013 after he successfully completed the written and oral qualifying examinations.

 31/12/18

Head
Department of Chemistry
Indian Institute of Technology Kanpur
Kanpur – 208016, U.P., India

Amalendu Chandra
Professor & Head
Department Of Chemistry
I.I.T. Kanpur



Convenor, DPGC
Department of Chemistry
Indian Institute of Technology Kanpur
Kanpur – 208016, U.P., India

Dedicated to my Father and Mother

Acknowledgements

First and foremost, I express my sincere gratitude to my Ph.D. thesis advisor, Prof. Pratik Sen who taught, guided and supported me throughout my Ph.D. life. He is the kind of person who leads by example. I could learn valuable lessons about being a good researcher from his disciplined and methodological ways. He is an excellent teacher who can explain the toughest of concepts in simple terms. From the very first days of my Ph.D., he has mentored me while doing experiments, while carrying out data analysis and while writing manuscripts. He has patiently corrected my mistakes. His meticulous instructions have helped me to hone my skills as an experimentalist and to write manuscripts in the best possible ways. He has always given space for my ideas. I am sure that the experience I gained with him will be helpful for my future as a researcher.

I am thankful to Prof. S. Manogaran, Prof. K. Srihari, Prof. A. Chandra, Prof. S. P. Rath and Prof. K. Poddar for the highly informative courses they taught me during my course work. I have learnt much from the various seminars conducted in Department of Chemistry. The discussions during physical chemistry group meetings were particularly helpful. My sincere thanks to Dr. S. Matheshwaran of department of Biological Sciences and Bioengineering for letting me use his lab facilities.

I extend my gratitude towards Department of Chemistry for making me a part of it. Thanks are due to our former heads of department, Prof. P. K. Bharadwaj and Prof. S. Verma and current head of department, Prof. A. Chandra. The staff members of Chemistry Department deserve special mention for being very cooperative and helpful whenever I needed them. I thank Mr. Santhosh Kumar for helping me with circular dichroism measurements.

My sincere gratitude is due to School of Chemical Sciences, National Institute of Science Engineering and Research, Bhubaneswar from where I pursued my Master's program. Special thanks to Dr. Moloy Sarkar, Prof. A. C. Dash and Prof.

C. S. Panda for being excellent teachers and mentors. I extend my gratitude to Dr. Ayan Datta with whom I carried out my first research project at Indian Institute of Science Education and Research Thiruvananthapuram.

I thank Rajeev, Shahnawaz and Shradhey who were my seniors at the time I joined my lab. They have helped to make my learning process easier. Bhaswati and Puspall were two of my close friends in the lab and we had many enjoyable moments together. I also want to thank my juniors Vipin, Navin, Nilimesh, Aritra and Shovon. I had a good time working with Barun who joined our lab for carrying out his Master's project. I want to thank Faizi, Vijaykant and Gulab Singh who had done their post-doctoral research at our lab at different times.

I was blessed to have many loving friends at IIT with whom I have shared numerous happy moments. Sharon, Kurian, Sreejith, Rahul, Ravi, Aswathy, Greeshmaja, Sreenath, Dileep, Shamini, Vinithra and Nithin are a few among them. My heartfelt thanks to all my friends who had made IIT a home away from home.

I thank IIT Kanpur for my fellowship and for providing the infrastructure for carrying out my research work.

My parents have been my motivation all through my life. My father has always cared for me more than he cared for himself, chosen the best things for me and taught many practical things in life. My mother was the one who always believed in me more than I ever did. I would never be able to thank them enough. Many hugs to my little sister, Sisira who has been my inspiration. I thank Anupama for being a part of this journey called life. Last but not the least, I thank God Almighty for all the blessings.

Vaisakh Mohan K.

SYNOPSIS

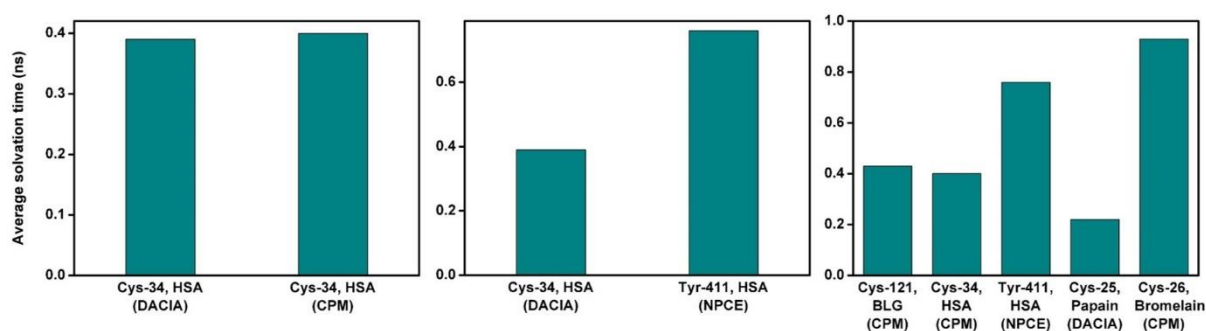
Name of student:	Vaisakh Mohan K.
Roll number:	12107084
Degree for which thesis is submitted:	Ph.D.
Department:	Chemistry
Supervisor:	Prof. Pratik Sen
Thesis title:	Picosecond Hydration Dynamics at the Protein Core and the Effect of Perturbed Environment
Month and year of submission:	December, 2018

In this thesis work, hydration dynamics inside four different proteins, β -lactoglobulin, human serum albumin, papain and bromelain, has been studied at picosecond timescale. Covalent fluorescent probes have been used for site-specific studies by binding them to specific amino acids of the proteins. The effect of the probe molecule and the local environment on solvation dynamics has been monitored. Two of these proteins, human serum albumin (HSA) and papain have been subjected to change in environmental conditions and the effect of such changes have been studied by steady-state and time-resolved techniques. The perturbations in the environment of proteins were created by the introducing external agents, by increasing the temperature and by imposing the confinement. HSA has also been subjected to the simultaneous action of two denaturing agents, GnHCl and temperature, and their effect on overall structure and specific domains of HSA have been studied. The stabilizing effect of sucrose on HSA has been studied as well under the denaturing conditions imposed by urea. Papain, was encapsulated inside cationic and anionic reverse micelles of different sizes and the effect of encapsulation on the solvation dynamics have been studied. The aggregate formation of papain in ethanol-water binary mixtures was also studied using different spectroscopic techniques.

Summary of the work done

(a) A Comparative Study of Hydration Dynamics inside Different Proteins: The Effect of Probe and the Protein Site

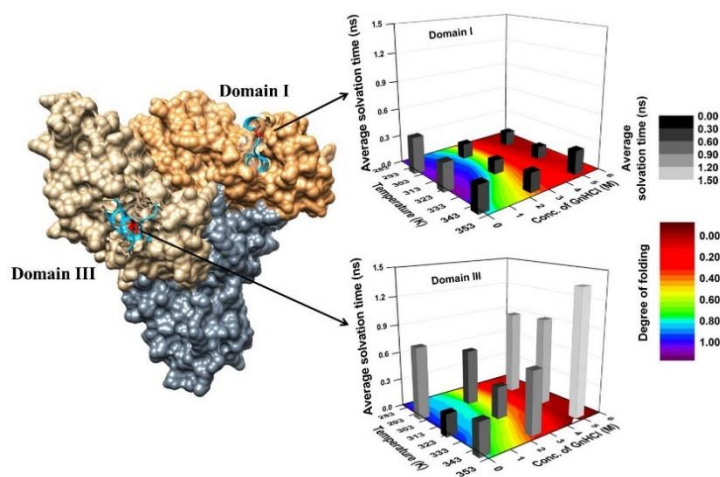
Hydration dynamics inside four different proteins was studied and compared using three different fluorescent tags as probes. The probe molecules were covalently bonded to a particular amino acid residues of the proteins. The average solvation time when monitored using probe molecules N-(7-dimethylamino-4-methylcoumarin-3-yl) iodoacetamide (DACIA) and 7-dimethylamino-3-(4-maleimidophenyl)-4-methylcoumarin (CPM) at Cys-34 position of human serum albumin (HSA), was found to vary only by 2.5%, indicating that the dynamics of solvation at a particular site does not depend on the probe molecule, as expected. However, when monitored at two different sites of HSA, Cys-34 and Tyr-411, the average solvation time was found to differ by 90%. This clarifies the different local environments even within the same protein. Further, solvation dynamics at different proteins were found to exhibit different rates of solvation depending on the environment in which the probe molecule is located. Among the proteins that we have studied, the solvation time was found to be slowest inside bromelain (at Cys-26) and was the fastest inside papain (at Cys-25).



(b) Region-Specific Double Denaturation of Human Serum Albumin: Combined Effect of Temperature and GnHCl on Structural and Dynamic Responses

The effects of two denaturing agents, guanidine hydrochloride (GnHCl) and temperature on the overall structure, domain-I and domain-III of human serum

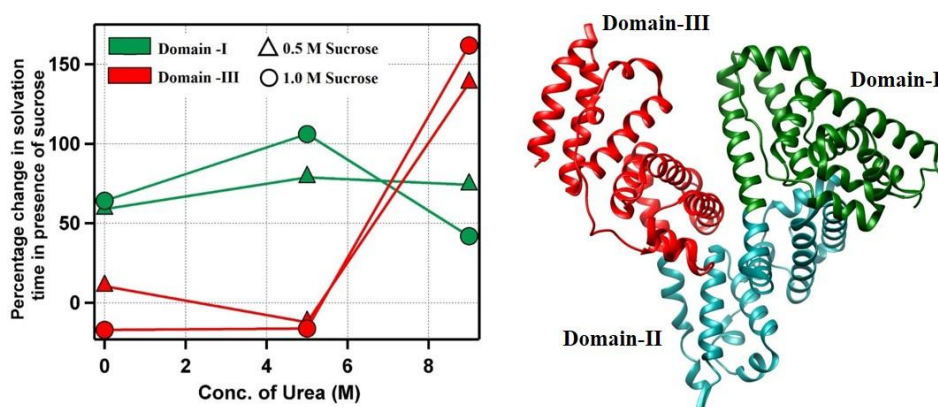
albumin have been investigated. CD spectroscopy studies reveal that the overall denaturation of the protein follows the expected direction in which protein is denatured with an increase in concentration of GnHCl or temperature. α -helicity of the native state of HSA was found to be 64.2% and the minimum value of α -helicity was found to be 14.8% in presence of 6 M of GnHCl at room temperature. Steady state emission studies were carried out on domain-I and domain-III of HSA using site specific fluorescent tags. The degree of folding of the two domains at different combinations of temperature and GnHCl concentration was calculated and was found to follow somewhat different courses of denaturation. Variation of solvation time was also found to be quite different for these two domains. Solvation time inside domain-I tends to decrease with the action of either temperature or GnHCl. On the other hand, inside domain-III of HSA, solvation time does not show any regular change at higher temperatures or in presence of GnHCl. This difference could be attributed to the different microenvironments inside the protein cores of the two domains.



(c) Domain-Specific Stabilization of Structural and Dynamic Responses of Human Serum Albumin by Sucrose

In this work, we have investigated the denaturing and renaturing effects of urea and sucrose respectively, on the overall structure and on two different domains (domain-I and domain-III) of human serum albumin (HSA). From circular dichroism measurements it could be seen that, the α -helicity of the overall structure, which is

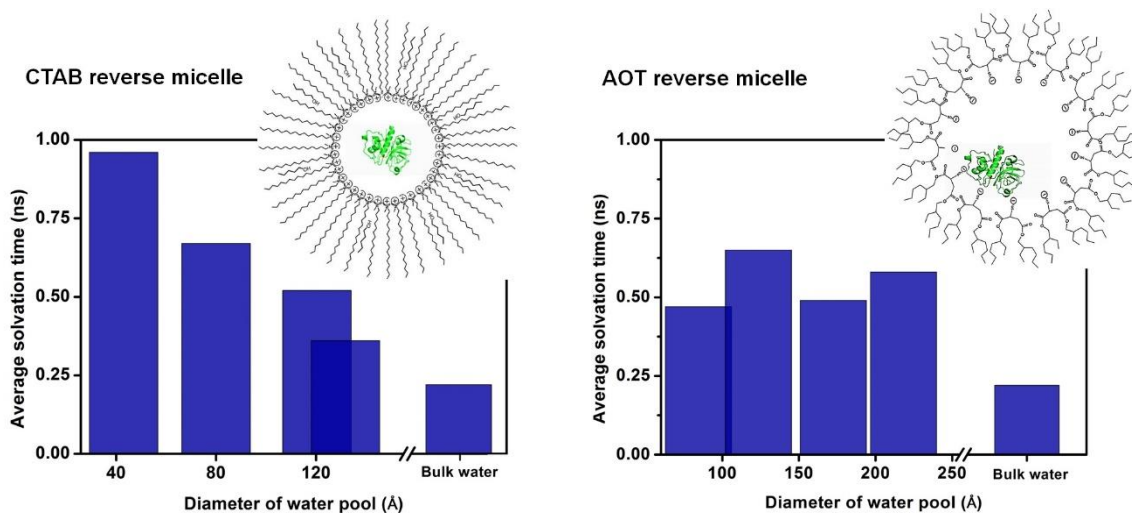
65% in its native state, decreases to 11% in presence of 9 M urea and further increases to 25% with the addition of 1 M sucrose. In order to study the domain-specific responses towards these external agents, HSA covalently tagged with fluorescent probes N-(7-dimethylamino-4-methylcoumarin-3-yl) iodoacetamide (DACIA) and p-nitrophenyl coumarin ester (NPCE) at Cys-34 of domain-I and Tyr-411 of domain-III, respectively were used. The domain-wise unfolding/folding studies of HSA by steady state fluorescence spectroscopy reveal that the renaturing effect of sucrose is more pronounced on domain-I. The calculation of free energy change during denaturation due to urea divulges the presence of an intermediate state, which gets stabilized in the presence of sucrose. The renaturing or stabilizing effect of sucrose is attributed to the stabilization of this intermediate. From solvation dynamics studies it can be seen that the solvation dynamics near binding site of DACIA inside domain-I becomes faster in presence of urea and it becomes slower in presence of sucrose. However, in the case of NPCE-tagged domain-III, the effect of sucrose on solvation time is evident only at high concentrations of urea and the denaturing effect of urea is evident only at very low or zero concentration of sucrose.



(d) Elucidation of Active Site Dynamics of Papain and the Effect of Encapsulation within Cationic and Anionic Reverse Micelles

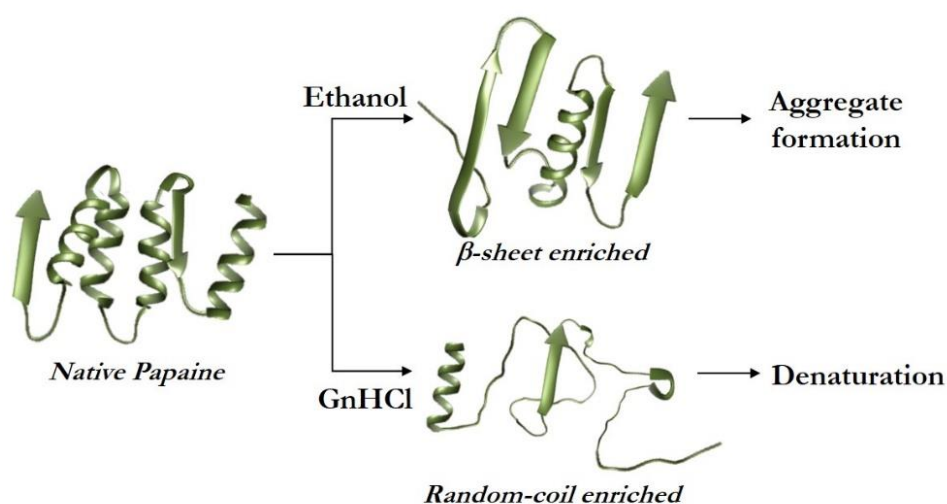
In this study, steady state, solvation dynamics and rotational dynamics experiments have been carried out on a system of DACIA-tagged papain in bulk water and inside the water pool of cationic (cetyltrimethylammonium bromide, CTAB) and anionic (sodium bis(2-ethylhexyl)sulfosuccinate, AOT) reverse

micelles with varying water contents ($W_0 = 20$ to 50). While the absorption and emission maxima and the excited state lifetime did not show any noticeable change with the variation of the size of the reverse micelle, the change in solvation time, Stokes shift, rotational correlation time and residual anisotropy with the change in reverse micellar size were quite revealing. The average solvation time and Stokes shift of papain in bulk water are 0.22 ns and 125 cm^{-1} respectively, which increase to 0.96 ns and 718 cm^{-1} while inside CTAB reverse micelle of $W_0 = 20$. The solvation time and Stokes shift values decrease with the increase in the size of reverse micelle, approaching the corresponding values in bulk water when $W_0 = 50$. The solvation time and Stokes shift of the DACIA-tagged papain was found to be high while inside AOT reverse micelle also (0.47 ns and 438 cm^{-1} respectively when $W_0 = 20$), but there was no monotonous variation with the change in size of micellar size as in the case with CTAB reverse micelle. From the anisotropy studies, it was seen that inside CTAB and AOT reverse micelles, there is a significant amount of residual anisotropy, which is absent in the case of DACIA-tagged papain in bulk water. The rotational correlation times were also found to be higher inside the reverse micelles than those in bulk water. Both residual anisotropy and rotational correlation time were found to be more in the case with AOT reverse micelle than with CTAB reverse micelle. These behaviours could be explained based on the electrostatic forces acting between the papain having a positive surface charge and the reverse micelles of cationic CTAB and anionic AOT.



(e) A spectroscopic Insight on Ethanol Induced Aggregation of Papain

In this contribution, the structural and dynamical changes occurring to papain molecules in ethanol-water binary solvent mixture have been investigated and compared with its denatured state induced by guanidine hydrochloride. Steady-state fluorescence, solvation dynamics, time-resolved rotational anisotropy, circular dichroism and single molecular level fluorescence correlation spectroscopic studies were carried out for this purpose. In ethanol-water mixture with $\chi_{\text{EtOH}} = 0.6$, DACIA-tagged papain was found to undergo a blue shift of 12 nm, while in presence of 5 M GnHCl, a red shift of 5 nm was observed. Solvation dynamics of the system was also found to be different in presence of these external agents. In ethanol-water mixture, the average solvation time was found to increase almost 2 fold as compared to that in water, while in presence of GnHCl only a marginal increase could be observed. These changes of DACIA-tagged papain in ethanol-water mixture is attributed to the aggregation of the protein in presence of ethanol. Rotational anisotropy study further confirmed the formation of aggregates as the residual anisotropy was found to increase 14 fold and the rotational time component corresponding to the rotation of the probe molecule was found to increase by 4 fold in the ethanol-water mixture.



From fluorescence correlation spectroscopic (FCS) study, the hydrodynamic radius of the protein aggregates in ethanol-water mixture was calculated to be ~ 155 Å as compared to the corresponding value of 18.4 Å in the case of native papain

molecule. Also, it is confirmed that aggregate formation takes place even in nanomolar concentration of papain. Analysis of circular dichroism spectra of papain showed that an increase in the β -sheet content of papain at the expense of α -helix and the random coil with an increase of ethanol mole fraction may be responsible for this aggregation process.

Table of Contents

Acknowledgements	xi
Synopsis	xiii
Chapter 1. Introduction	1-24
1.1. Solvation Dynamics	3
1.2. Proteins: A Brief Overview	8
1.2.1. Structure of proteins	8
1.2.2. Protein denaturation	9
1.2.3. Protein aggregation	10
1.3. Solvation Dynamics in Proteins	10
References	17
Chapter 2. Experimental Methods	25-60
2.1. Experimental Techniques	27
2.1.1. Steady-state absorption spectroscopy	27
2.1.2. Steady-state emission spectroscopy	29
2.1.3. Time-correlated single photon counting (TCSPC)	33
2.1.3.1. Basic principle of TCSPC	33
2.1.3.2. Instrumentation for TCSPC	36
2.1.3.3. Analysis of the data obtained from TCSPC	41
2.1.3.4. Construction of TRES from TCSPC data	44
2.1.4. Fluorescence anisotropy measurements	47
2.1.5. Fluorescence correlation spectroscopy	50
2.1.6. Circular dichroism spectroscopy	52
2.2. Materials Used	54
2.3. Tagging of Proteins	55
2.3.1. Tagging of proteins with CPM	55
2.3.2. Tagging of proteins with DACIA	56
2.3.3. Tagging of HSA with NPCE	56
2.3.3.1. Synthesis of NPCE	56
2.3.3.2. Tagging of HSA	57
References	58
Chapter 3. A Comparative Study of Hydration Dynamics inside Different Proteins: The Effect of Probe and the Protein Site	61-84
3.1. Introduction	63
3.2. Results	65
3.2.1. Solvation dynamics inside β -lactoglobulin monitored using CPM	65

3.2.2. Solvation dynamics inside domain-I of HSA monitored using DACIA	67
3.2.3. Solvation dynamics inside domain-I of HSA monitored using CPM	70
3.2.4. Solvation dynamics inside domain-III of HSA monitored using NPCE	72
3.2.5. Solvation dynamics inside papain monitored using DACIA	74
3.2.6. Solvation dynamics inside bromelain monitored using CPM	76
3.3. Discussion	78
3.4. Conclusion	82
References	83

Chapter 4. Region-Specific Double Denaturation of Human Serum Albumin: Combined Effects of Temperature and GnHCl on Structural and Dynamical Responses

85-112

4.1. Introduction	87
4.2. Results	89
4.2.1. Effect of double denaturation on the overall structure of HSA	89
4.2.2. Effect of double denaturation on domain-I of HSA	91
4.2.2.1. Steady state measurements	91
4.2.2.2. Lifetime measurements	93
4.2.2.3. Solvation dynamics measurements	94
4.2.3. Effect of double denaturation on domain-III of HSA	98
4.2.3.1. Steady state measurements	98
4.2.3.2. Lifetime measurements	99
4.2.3.3. Solvation dynamics measurements	100
4.3. Discussion	101
4.4. Conclusion	108
References	109

Chapter 5. Domain-Specific Stabilization of Structural and Dynamical Responses of Human Serum Albumin by Sucrose

113-141

5.1. Introduction	115
5.2. Results	117
5.2.1. Effect of urea and sucrose on the overall structure of HSA	117
5.2.2. Effect of urea and sucrose on domain-I of HSA	118
5.2.2.1. Steady state measurements	118

5.2.2.2. Lifetime measurements	120
5.2.2.3. Solvation dynamics measurements	121
5.2.3. Effect of urea and sucrose on domain-III of HSA	125
5.2.3.1. Steady state measurements	125
5.2.3.2. Lifetime measurements	126
5.2.3.3. Solvation dynamics measurements	127
5.3. Discussion	128
5.4. Conclusion	136
References	137
Chapter 6. Elucidation of Active Site Dynamics of Papain and the Effect of Encapsulation within Cationic and Anionic Reverse Micelles	143-170
6.1. Introduction	145
6.2. Results	148
6.2.1. Steady state experiments	148
6.2.2. Lifetime measurements	150
6.2.3. Solvation dynamics study	151
6.2.4. Fluorescence anisotropy study	156
6.3. Discussion	159
6.4. Conclusion	164
References	166
Chapter 7. A Spectroscopic Insight on Ethanol Induced Aggregation of Papain	171-195
7.1. Introduction	173
7.2. Results	174
7.2.1. Steady state fluorescence spectroscopy study	174
7.2.2. Solvation dynamics study	175
7.2.3. Fluorescence anisotropy study	179
7.2.4. Fluorescence correlation spectroscopy study	180
7.2.5. Circular dichroism spectroscopy study	182
7.3. Discussion	183
7.4. Conclusion	189
References	191
List of Publications	197

Chapter 1

Introduction

In this chapter, I have presented a brief introduction on solvation dynamics. Some basic details of protein molecules have also been discussed. I have also tried to present a very brief history of solvation dynamics studies in different confined environments with emphasis on proteins.

1.1 Solvation Dynamics

Solvation is the process by which solute molecules get stabilized in a solution by virtue of the interaction with the surrounding solvent molecules, and solvation dynamics refers to the dynamics of this process.^{1,2} When a solute molecule having a non-zero dipole moment is present in a solution, it polarizes the solvent molecules around it, both electronically and orientationally. Electronic polarization refers to the rearrangement of electrons within the solvent molecules while orientational polarizability is due to the reorientation of the solvent molecules around the solute dipole. These changes in the solvent creates an electric field around the solute. The interaction of the solute with this electric field eventually decreases the energy of the system and thus stabilizes it. The magnitude of the electric field and the extent of stabilization depends on the dipole moment of the solute and the polarizability of the solvent.

The stabilization due to solute-solvent interaction can occur both in the ground state and the excited states of a solute. If the solute molecule is having a higher dipole moment in the excited state as compared to the ground state, the excited state will be more stabilized. For such cases, the energy gap between the ground and excited states will decrease as we increase the polarity of the solvent. This decrease in energy gap will be reflected by a red shift in the absorption spectrum of the solute molecule. Such a change in absorption spectrum (or colour) of the solute molecule while dissolved in solvents of different polarity is known as solvatochromism.

Lippert-Mataga equation (equation (1.1)) is a good first approximation to describe these solvent dependent spectral shifts.^{3,4}

$$\bar{\nu}_A - \bar{\nu}_F = \frac{2}{hc} \left(\frac{\varepsilon - 1}{2\varepsilon + 1} - \frac{n^2 - 1}{2n^2 + 1} \right) \frac{(\mu_E - \mu_G)}{a^3} + \text{constant} \quad (1.1)$$

In equation (1.1), h is the Planck's constant, c is the speed of light in vacuum, n and ε are the refractive index and dielectric constant of the solvent, respectively. μ_G and μ_E are the dipole moments of the solute in the ground and excited states,

respectively and a is the radius of the cavity in which the solute molecule resides. $\bar{\nu}_A$ and $\bar{\nu}_F$ are the wavenumbers of absorption and emission maxima, respectively. The quantity, $\bar{\nu}_A - \bar{\nu}_F$ is known as the Stokes shift of the molecule. The constant mentioned in the equation accounts for the inherent Stokes shift of the molecule due to vibrational relaxation. In this model, the solute or fluorophore is considered to be a dipole in a continuous medium of uniform dielectric constant. It does not take into account any other chemical interactions. Using Lippert-Mataga equation, by recording the absorption and emission spectra of a fluorophore in different solvents, with known refractive index and dielectric constant, one can estimate either μ_G or μ_E .

In the ground state, the fluorophore and solvent molecules will be in their equilibrium solvated state. However, when the fluorophore is excited using an electromagnetic radiation, the final solvated state will not be achieved instantaneously around the newly created excited state of the molecule. Although the electronic polarization will take place at a very fast rate (at a time scale of 10^{-15} s), the orientational polarization is a much slower process as it involves the motion of solvent molecules around the newly created excited state. If the fluorophore emits during this reorientation/relaxation process, by monitoring the emission at different times following an instantaneous excitation, we would be able to get information about the time required for this relaxation and the energy difference between the relaxed and unrelaxed states, which is schematically represented in figure 1.1. The relaxation time depends on the mobility of the solvent molecules around the fluorophore. If the solvent is a viscous liquid, the relaxation time will be longer. Similarly, if the fluorophore is located in a confined environment (for example, inside the water pool of a reverse micelle or inside a biomolecule where the movement of solvent is restricted), the relaxation time will be longer. So, by studying this relaxation process, we can have an understanding about the immediate environment of the fluorophore.

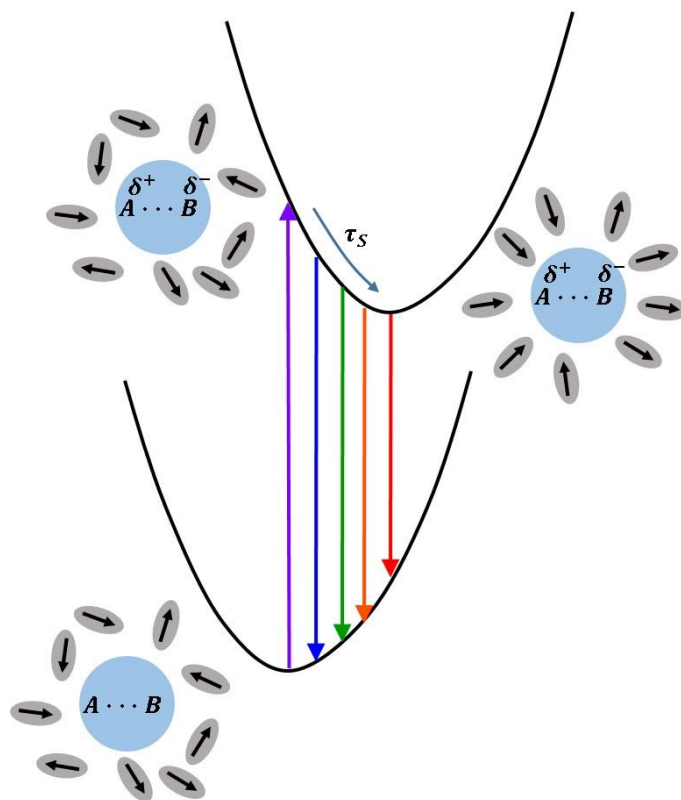


Figure 1.1. Schematic representation of solvation dynamics.

The higher energy excited state of the molecule created by the irradiation of light is known as the Frank-Condon state and the lower energy state after the complete solvation is known as the solvated or relaxed state. The time required for the molecule to reach the solvated state from the Frank-Condon state is known as the solvation time. If we can find out the emission spectra at different times following the excitation of the fluorophore until the system is solvated, we can calculate the solvation time and the energy difference between the Frank-Condon and solvated states. This method of studying solvation dynamics using emission spectra at different times is known as the time dependent fluorescence Stokes shift (TDFSS) method.⁵⁻⁷ The shift in the emission spectrum during the solvation process is known as the dynamic Stokes shift.

Over the years many other techniques including photon echo spectroscopy and incoherent quasi elastic neutron scattering have been used to study solvation dynamics.⁸⁻¹⁰ More recently terahertz spectroscopy¹¹⁻¹⁷ and optical Kerr effect spectroscopy¹⁸⁻²⁰ have been successfully employed for this purpose. However, TDFSS still remains the most commonly used method in the research community.

For studying solvation dynamics in a particular solvent or at a particular environment, we normally select a fluorophore, which has a very small dipole moment in the ground state and a very large dipole moment in the excited state. This fluorophore acts as the probe to study solvation dynamics. Some of the common probe molecules used for solvation dynamics studies are 4-aminophthalimide (4-AP), coumarin-480, coumarin-153, coumarin-343, 4-(dicyanomethylene)-2-methyl-6(p-dimethylaminostyryl)-4H-pyran (DCM) and 2-(p-toluidino) naphthalene-6-sulfonate (TNS). To carry out TDFSS experiment, the system containing the probe molecule is excited using a pulsed light source. Following this, the time resolved emission spectra (TRES) are constructed from the fluorescence transients at various wavelengths. The details about the construction of TRES are described in section 2.1.3.4 of Chapter 2. While recording the fluorescent decays at different wavelengths, it could be found that, the decay recorded at a higher wavelength will be much slower than that recorded at a lower wavelength. This is because, the emission recorded at shorter wavelengths, (which corresponds to a higher energy) will occur from the Frank-Condon state. As the emission from that state occurs immediately after irradiation of the sample with a light pulse, the emission will be finished within a short time scale, thus resulting in a faster decay profile. On the other hand, the emission recorded at a longer wavelength occurs from the solvated state of the system. As the formation of the solvated state occurs after some period of time (depending on the solvation time), the fluorescence decay from this state will be observed at a delayed time with an initial rise in the intensity. Such a wavelength dependence of fluorescence transients is represented in figure 1.2.

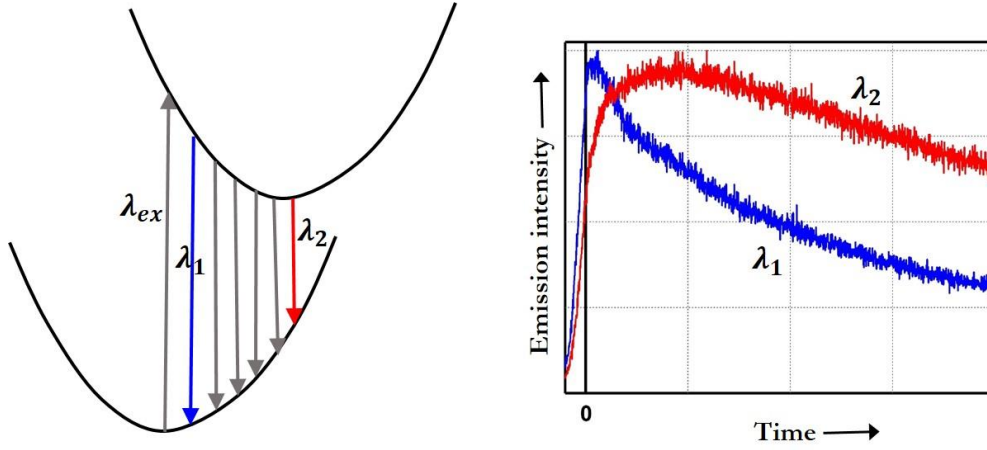


Figure 1.2. Schematic representation of wavelength dependence of fluorescence decay.

Once the time-resolved emission spectra (TRES) are constructed from the fluorescence transients, the normalised time dependent spectral shift (or solvent response function) can be calculated by,^{1,21,22}

$$C(t) = \frac{\nu(t) - \nu(\infty)}{\nu(0) - \nu(\infty)} \quad (1.2)$$

where, $\nu(t)$, $\nu(\infty)$ and $\nu(0)$ are the peak frequencies of emission spectra at time t , ∞ and 0, respectively. The time dependence of $C(t)$ gives us information about the time-dependent change occurring in the solvent due to the sudden change in charge distribution in the probe. The time dependence can be represented as an exponential function.^{1,21,22}

$$C(t) = e^{-t/\tau_s} \quad (1.3)$$

where, τ_s is the solvation time. The single exponential decay of $C(t)$ stems from the simple continuum dielectric model of solvation. However, in a heterogeneous environment, the processes involved in solvation can be quite different. For this reason, when solvation is monitored in a heterogeneous environment inside biomolecules, the decay of solvation is almost always non-exponential.

$$C(t) = \sum_i a_i e^{-t/\tau_{s_i}} \quad (1.4)$$

where, τ_{s_i} are components of solvation times and a_i are their corresponding amplitudes. The average solvation time is given by,

$$\langle \tau_S \rangle = \sum_i a_i \tau_{S_i} \quad (1.5)$$

Solvation dynamics influences many excited state processes like proton transfer and electron transfer. Solvation dynamics studies have been particularly found useful inside biological moieties like proteins and DNA as such studies can deliver information about the local environment inside these moieties.^{8,23–26}

1.2 Proteins: A Brief Overview

Proteins are large macromolecules which carry out numerous functions throughout the biological world. Some of them transport nutrients all through the body, some catalyse metabolic reactions and some others form the structures that make up living things.^{27,28} All proteins are made up of basic building blocks, amino acids, which are in turn made of an alpha carbon, a carboxyl group, an amino group and a side chain. Studies about the structure and structural changes of proteins under different conditions are of prime importance, due to the important roles they play in living systems.

1.2.1 Structure of proteins

Most proteins fold into a three dimensional structure as a result of different interactions between atoms.^{29,30} The shape of the protein in which it folds into naturally is known as the native or folded structure of the protein which is essential for its regular functions. The structure of a folded protein is usually referred to as having four distinct levels. The primary structure refers to the sequence of amino acids in a protein. Each amino acid is connected to the next one by peptide linkages. Secondary structure is the next level of protein structure in which the hydrogen bond interactions within the polypeptide chains make them to fold into some specific structures. The most common types of secondary structures in a protein are α -helix and β -sheet. Both these structures are held in shape by hydrogen bonds between carbonyl oxygen of one amino acid and hydrogen of the amino group of another amino acid. β -turn and Ω -loops are two less common secondary structural motifs in proteins.

The tertiary structure refers to the three dimensional structure of a protein. The α -helixes and β -sheets fold into globular forms mainly due to different non-covalent interactions. Hydrophobic interactions play an important role at this level as non-polar side chains can cluster together in the interior of a protein. Disulphide bonds are also important for keeping the tertiary structure intact. Disulphide bonds are covalent linkages between sulphur containing cysteine amino acids of different polypeptide chains. These bonds, being stronger than non-covalent interactions, help to keep parts of polypeptide chains attached to each other. Some proteins contain multiple peptide chains, which give rise to multiple 'subunits' of the proteins. When such subunits come together to form a single large protein, it is referred to as the quaternary structure of the protein. Human serum albumin is an example of a protein which consists of such domains and subdomains.

1.2.2 Protein denaturation

Under certain conditions, the covalent and non-covalent interactions, which hold the protein together, can break down, leading to a loss of the three dimensional structure of the protein, and consequently the loss in functionality of the protein. This process by which a protein loses its native structure and functional capacity is known as denaturation of the protein.^{31–33} Some proteins denature by a simpler two-step process, while some follow more complex pathways involving intermediates. Protein denaturation is mostly induced by the action of external agents including temperature, chemical agents and pH. It has been reported that, denatured states by the action of temperature and chemicals are different for most of the proteins.^{34,35} The mechanism by which each denaturant affects proteins can also be different.^{36,37} Lim *et al.* have reported that urea forms hydrogen bonding with NH and CO of the peptide bonds, thus disrupting the bonding within the proteins.³⁸ Meuzelaar *et al.* have reported that GnHCl acts by breaking down the salt bridges (salt bridges are the non-covalent interaction between two ionized sites) within the proteins thus causing the denaturation.³⁹

1.2.3 Protein aggregation

Protein aggregation is the process by which misfolded proteins form aggregates among themselves.^{40,41} The aggregation can be either reversible or irreversible.^{42,43} Usually, in the early stages, the aggregation is reversible in nature and in later stages, it is irreversible. The formation of aggregates can depend on factors such as temperature, pH or solvents.^{44–47} Aggregate formation in proteins is related to many human disorders including Alzheimer's disease and Parkinson's disease.^{48–50} Due to its effects on human health, protein aggregation has been widely studied.

1.3 Solvation Dynamics in Proteins

The dynamics of solvation of bulk water had been well studied by 1994. In a paper published in *Nature* in 1994, Fleming and co-workers had reported the solvation dynamics of coumarin 343 dissolved in water, monitored by upconversion technique and classical molecular dynamics simulations.⁵¹ They had demonstrated that aqueous solvation dynamics is dominated by a solvent response of timescale faster than 50 fs and had suggested that water seemed to be the 'fastest' solvent studied thus far. In 1995, Fleming and co-workers reported the slow solvation of water when confined inside the cavity of γ -cyclodextrin (γ CD).⁵² They had carried out experiments with limited number of water molecules in an inclusion complex of coumarin dyes with γ CD. When coumarin 480 was used as the probe inside γ CD, they observed very slow solvation time components of 13, 109 and 1200 ps in addition to solvation at femtosecond time scale. This was in sharp contrast to the solvation dynamics in bulk water, where solvation takes place in femtosecond timescale. This was one of the first reports on the slow solvation of water when restricted inside a cavity.

In the years that followed, hydration dynamics was studied inside many systems, which provide a confined environment to water molecules. Bhattacharyya and co-workers have studied such processes inside micelles and reverse micelles extensively.^{53–60} When solvation inside AOT-heptane reverse micelles was

monitored with the help of coumarin 480, it was found that slow solvation occurs in the range of nanoseconds inside the reverse micelle.⁵³ Also, it was noted that the solvation became faster with an increase in the size of reverse micelle. Solvation inside anionic, neutral and cationic micelles was also studied using the same probe molecule, coumarin 480.⁵⁴ In this case, the relaxation of water molecules in the Stern layer of micelles was found to occur in the time range 180-550 ps, which is considerably slower than that in bulk water.

Other research groups had also carried out similar studies inside micelles and reverse micelles.⁶¹⁻⁷³ Levinger and co-workers had reported that, inside water/AOT/isooctane reverse micelles, the water molecules were essentially frozen when W_0 of reverse micelle was 1.1.⁶¹ With an increase in size of reverse micelle, mobility of water increased. The solvation inside lecithin reverse micelles were found to be even more restricted than inside AOT reverse micelle.⁶² They had also monitored the solvation dynamics inside AOT reverse micelles when formamide is present inside reverse micelle instead of water.⁶⁶ They found that even though the vibrational spectra of formamide inside reverse micelle is almost unchanged from the bulk liquid spectrum, the solvation dynamics inside formamide was extremely slow, rendering the solvent almost immobilised inside reverse micelle.

In addition to monitoring solvation times inside different micelles and reverse micelles, the effect of slow solvation in confined environments on processes like excited state proton transfer and intramolecular charge transfer were also studied. The excited state deprotonation of 1-naphthol was studied in neutral (triton X 100, reduced), cationic (CTAB) and anionic (SDS) micelles.⁵⁵ The deprotonation which occurs in 35 ps in aqueous solution, was found to be significantly retarded inside all the three micelles. However, when intramolecular charge transfer (ICT) of Nile red was monitored inside AOT, the ICT is slower only by a factor of 8 inside reverse micelles as compared to bulk water.⁵⁶ This decrease is much less when compared to the thousands of fold decrease of solvation dynamics inside reverse micelle compared to bulk water. It was proposed that while solvation dynamics is

governed by dielectric relaxation time, dynamics of ICT is governed by static polarity of the medium.

Hydration dynamics inside proteins was studied by Marzola and Gratton using frequency domain fluorescence spectroscopy as early as in 1991.⁷⁴ They had studied three proteins, lysozyme, human serum albumin and liver alcohol dehydrogenase in reverse micelle. In their report, they have noted that the effect of presence of water on fluorescence lifetimes was less clear and have speculated that structural modifications in proteins hosted in reverse micelles might be causing the changes in fluorescence lifetime. After the detection of the very slow solvation time in γ CD, reverse micelles and in other confined media, the interest in studying hydration dynamics inside protein and other biomolecules was reignited among researchers due to their obvious biological importance. In 1995, Bright and co-workers had reported the presence of a relaxation term in nanoseconds when they studied acrylodan-labelled human serum albumin inside a reverse micelle. Many subsequent works by Zewail, Bhattacharyya and Bagchi confirmed the presence of slow solvation dynamics of water inside proteins.^{75–78} The water molecules in the hydration shell in the immediate vicinity of a biomolecule is referred to as ‘biological water’. Dynamics of biological water differs considerably from the bulk water as they form hydrogen bonds with protein, which is stronger than water-water hydrogen bonds. The first theoretical model of the dielectric relaxation of biological water was provided by Nandi and Bagchi in 1997.⁷⁹ According to this model, biological water has two main components, the free water – where water molecules are hydrogen bonded to other water molecules only, and the bound water – where water molecules are attached to the biomolecule by a strong hydrogen bond. Only the free water molecules can undergo orientational motion and contribute to the solvation process. The bound and free water are always in equilibrium.



The equilibrium constant for this dynamic equilibrium can be written as,

$$K = \frac{k_{bf}}{k_{fb}} = e^{\frac{-\Delta G^o}{RT}} \quad (1.7)$$

where, ΔG^o is the difference in hydrogen bond free energy per mole for biomolecule-water and water-water bonds. k_{fb} and k_{bf} are the rate constants of exchange between free and bound states. The rate constant of bound to free conversion can thus be calculated, from which the time component for the slow solvation has been estimated.⁷⁹

Over the last two decades, solvation dynamics inside different proteins has been studied and documented using various experimental techniques and computer simulations. Solvation inside protein is normally studied either by utilizing the intrinsic fluorescence of proteins or by using covalent or non-covalent probes. Tryptophan is one of the major sources of intrinsic fluorescence of proteins.^{75,80–87} The advantage of using tryptophan fluorescence is that we do not have to worry about any structural changes of protein that might occur due to an external probe. Shen and co-workers have reported the solvation time constant of tryptophan in water to be ~ 1.2 ps⁸⁰ while Zewail and co-workers measured it to be biexponential with time components 180 fs (20%) and 1.1 ps (80%).⁷⁵ When they studied the solvation of tryptophan in the proteins, subtilisin *Carlsberg* and monellin, they detected the slow solvation time constants of 38 ps and 16 ps, respectively.⁷⁵ Solvation monitored inside *Pyrococcus furiosus* rubredoxin protein demonstrated that solvation occurs for 10 ps or longer.⁸¹ In the case of denatured protein, solvation was faster as compared to the protein in its native state. More recently, Biesso *et al.* have utilised tryptophan fluorescence in a small protein GB1, to study the dynamics at the protein-water interface.⁸³ They found that the interfacial water retains sub-picosecond relaxation speed. Although tryptophan fluorescence is widely used to study solvation in proteins, in the case of proteins with more than one tryptophan residues, site-specific information would be lost if it is used as probe. For this reason, many covalent and non-covalent probe molecules have been used as solvation probes for the measurement of solvation dynamics inside proteins.

Several groups have studied protein solvation using non-covalent probe molecules attached to the protein.^{8,77,88,89} Fleming and co-workers have monitored solvation dynamics in lysozyme using a fluorescent dye eosin which binds in a hydrophobic pocket present in lysozyme.⁸ They could find out a solvation time component of ~535 ps, which corresponds to the slow solvation in lysozyme. DCM (4-(dicyanomethylene)-2-methyl-6-(p-dimethylaminostyryl) 4H-pyran),⁷⁷ ANS (1-anilinonaphthalene-8-sulfonate)⁸⁸ and TNS (2,6-p-toluidinonaphthalene sulfonate)⁸⁹ are some of the non-covalent probes used to study the solvation dynamics inside proteins. However, covalent probes are preferred over non-covalent probes due to their stronger attachment with amino acid residues in protein. Some of the covalent probe molecules that has been used to bind with specific amino acid moieties inside proteins are dansyl chromophore, acrylodan, 7-diethylamino-3-(4-maleimidophenyl)-4-methylcoumarin (CPM), N-(7-dimethylamino-4-ethylcoumarin-3-yl) iodoacetamide (DACIA), *p*-nitrophenylcoumarin ester (NPCE) and tetramethylrhodamine-5-maleimide (TMR).^{76,90-94} In most of these cases, cysteine was used as the tagging site. Cysteine is a sulphur containing amino acid which forms disulphide bonds within the protein and plays significant role in maintaining the three dimensional structure of proteins. However, sometimes, single cysteine moieties can also be seen in proteins that do not take part in disulphide bonds. Some proteins including human serum albumin and papain have a single ‘free’ cysteine moiety, which can be targeted during tagging of probe molecule to give site-specific information. Sengupta *et al.* have used *p*-nitrophenylcoumarin ester (NPCE) to selectively tag only one among the 19 tyrosine amino acid residues of human serum albumin by controlling pH and the protein to probe ratio during the tagging process.⁹⁴

Apart from measuring the solvation dynamics in the native state of proteins, efforts have been made to understand its change during the denaturation process. Bright and co-workers carried out time-resolved studies during chemical and thermal denaturation of HSA.⁹⁰ They observed a decrease in excited state lifetime, when HSA was denatured, either chemically or thermally. Abou-Zied *et al.* have observed similar effects when they observed subdomain II-A of HSA in its native, unfolded and refolded

states using time-resolved measurements.⁹⁵ They observed a decrease in lifetime when HSA is unfolded by guanidine hydrochloride and an increase in lifetime as refolding progresses by dilution. Recently, Yadav *et al.* have monitored the change in solvation time during thermal and chemical unfolding and sucrose induced refolding of domain-I of HSA.⁹⁶ It was reported that while denaturation results in faster solvation, the stabilizing of the protein due to sucrose results in slower solvation dynamics.

In recent years, solvation dynamics has been monitored in systems that are biomedically more relevant. Bhattacharyya and co-workers have monitored solvation dynamics in live Chinese hamster ovary (CHO) cell with coumarin 153 as the probe.⁹⁷ They have found that average solvation times are 3600 ps, 1100 ps and 750 ps inside lipid droplets, cytoplasm and nucleus, respectively. In another work, they have mentioned average solvation times inside cytoplasm (monitored by CPM) and nucleus (monitored by DAPI) of CHO to be 1250 ps and 775 ps, respectively.⁹⁸ When solvation was monitored in thiol containing membrane proteins of CHO using CPM, the average solvation time was found to be 475 ps.⁹⁹ In all the cases, the solvation was much slower than that in bulk water as expected.

Molecular dynamics simulation, when combined with experimental results helps to get a clearer picture about the solvation dynamics associated with biomolecules.^{14,100–107} Zhong and co-workers have reported the direct mapping of global hydration dynamics around a protein, apoMb.¹⁰⁰ They have observed two distinct water dynamics in hydration layer, first one corresponding to initial local relaxation (1-8 ps) and the other one representing collective network reconstruction (20-200 ps). Mitchell-Koch and co-workers have modelled an enzyme, *Candida antarctica* lipase B using molecular dynamics simulations. They found that regional flexibilities of the enzyme were found to correlate with the regional dynamics of the hydration layer, which means flexible regions of the proteins have fast-moving water molecules near them and less mobile regions are surrounded with slower hydration layer water molecules.¹⁰¹

From the above discussions, it is clear that studies of solvation have provided us with important information regarding the environments inside many

biomolecules. It is important to carry on such studies to clearly understand the processes occurring inside them.

References

- (1) Lakowicz, J. R. *Principles of Fluorescence Spectroscopy*, 3rd ed.; Springer: Boston, MA, 2006.
- (2) Valeur, B.; Berberan-Santos, M. N. *Molecular Fluorescence: Principles and Applications*; Wiley-VCH Verlag GmbH: Weinheim, 2001.
- (3) Lippert, E. von. Spektroskopische Bestimmung Des Dipolmomentes Aromatischer Verbindungen Im Ersten Angeregten Singulettzustand. *Zeitschrift für Elektrochemie, Berichte der Bunsengesellschaft für Phys. Chemie* **1957**, *61*, 962–975.
- (4) Mataga, N.; Kaifu, Y.; Koizumi, M. Solvent Effects upon Fluorescence Spectra and the Dipolemoments of Excited Molecules. *Bull. Chem. Soc. Jpn.* **1956**, *29*, 465–470.
- (5) Bagchi, B.; Oxtoby, D. W.; Fleming, G. R. Theory of the Time Development of the Stokes Shift in Polar Media. *Chem. Phys.* **1984**, *86*, 257–267.
- (6) Maroncelli, M.; Fleming, G. R. Comparison of Time-resolved Fluorescence Stokes Shift Measurements to a Molecular Theory of Solvation Dynamics. *J. Chem. Phys.* **1988**, *89*, 875–881.
- (7) Hsu, C.-P.; Song, X.; Marcus, R. A. Time-Dependent Stokes Shift and Its Calculation from Solvent Dielectric Dispersion Data. *J. Phys. Chem. B* **1997**, *101*, 2546–2551.
- (8) Jordanides, X. J.; Lang, M. J.; Song, X.; Fleming, G. R. Solvation Dynamics in Protein Environments Studied by Photon Echo Spectroscopy. *J. Phys. Chem. B* **1999**, *103*, 7995–8005.
- (9) Lang, M. J.; Jordanides, X. J.; Song, X.; Fleming, G. R. Aqueous Solvation Dynamics Studied by Photon Echo Spectroscopy. *J. Chem. Phys.* **1999**, *110*, 5884–5892.
- (10) Perrin, J.-C.; Lyonnard, S.; Volino, F. Quasielastic Neutron Scattering Study of Water Dynamics in Hydrated Nafion Membranes. *J. Phys. Chem. C* **2007**, *111*, 3393–3404.
- (11) Heugen, U.; Schwaab, G.; Bründermann, E.; Heyden, M.; Yu, X.; Leitner, D. M.; Havenith, M. Solute-Induced Retardation of Water Dynamics Probed Directly by Terahertz Spectroscopy. *Proc. Natl. Acad. Sci.* **2006**, *103*, 12301–12306.
- (12) Leitner, D. M.; Gruebele, M.; Havenith, M. Solvation Dynamics of Biomolecules: Modeling and Terahertz Experiments. *HFSP J.* **2008**, *2*, 314–323.
- (13) Charkhesht, A.; Regmi, C.; Mitchell-Koch, K. R.; Cheng, S.; Vinh, N. Q. High-Precision Megahertz-to-Terahertz Dielectric Spectroscopy of Protein Collective Motions and Hydration Dynamics. *J. Phys. Chem. B* **2018**, *122*, 6341–6350.
- (14) Ebbinghaus, S.; Kim, S. J.; Heyden, M.; Yu, X.; Heugen, U.; Gruebele, M.; Leitner, D. M.; Havenith, M. An Extended Dynamical Hydration Shell around

- Proteins. *Proc. Natl. Acad. Sci.* **2007**, *104*, 20749–20752.
- (15) Ebbinghaus, S.; Kim, S. J.; Heyden, M.; Yu, X.; Gruebele, M.; Leitner, D. M.; Havenith, M. Protein Sequence-and PH-Dependent Hydration Probed by Terahertz Spectroscopy. *J. Am. Chem. Soc.* **2008**, *130*, 2374–2375.
- (16) Kim, S. J.; Born, B.; Havenith, M.; Gruebele, M. Real-time Detection of Protein–water Dynamics upon Protein Folding by Terahertz Absorption Spectroscopy. *Angew. Chemie Int. Ed.* **2008**, *47*, 6486–6489.
- (17) Yang, X.; Zhao, X.; Yang, K.; Liu, Y.; Liu, Y.; Fu, W.; Luo, Y. Biomedical Applications of Terahertz Spectroscopy and Imaging. *Trends Biotechnol.* **2016**, *34*, 810–824.
- (18) Smith, N. A.; Lin, S.; Meech, S. R.; Yoshihara, K. Ultrafast Optical Kerr Effect and Solvation Dynamics of Liquid Aniline. *J. Phys. Chem. A* **1997**, *101*, 3641–3645.
- (19) Jaye, A. A.; Hunt, N. T.; Meech, S. R. Temperature-and Solvation-Dependent Dynamics of Liquid Sulfur Dioxide Studied through the Ultrafast Optical Kerr Effect. *J. Chem. Phys.* **2006**, *124*, 24506.
- (20) Zolotov, B.; Gan, A.; Fainberg, B. D.; Huppert, D. Resonance Heterodyne Optical Kerr Spectroscopy of Solvation Dynamics in Water and D₂O. *Chem. Phys. Lett.* **1997**, *265*, 418–426.
- (21) Maroncelli, M.; Fleming, G. R. Picosecond Solvation Dynamics of Coumarin 153: The Importance of Molecular Aspects of Solvation. *J. Chem. Phys.* **1987**, *86*, 6221–6239.
- (22) Fee, R. S.; Maroncelli, M. Estimating the Time-Zero Spectrum in Time-Resolved Emission Measurements of Solvation Dynamics. *Chem. Phys.* **1994**, *183*, 235.
- (23) Pal, S. K.; Peon, J.; Bagchi, B.; Zewail, A. H. Biological Water: Femtosecond Dynamics of Macromolecular Hydration. *J. Phys. Chem. B* **2002**, *106*, 12376–12395.
- (24) Mukherjee, S.; Mondal, S.; Acharya, S.; Bagchi, B. DNA Solvation Dynamics. *J. Phys. Chem. B* **2018**, *122*, 11743–11761.
- (25) Mukherjee, S.; Mondal, S.; Acharya, S.; Bagchi, B. In Search of the Origin of Long-Time Power-Law Decay in DNA Solvation Dynamics. In *Cornell University*; 2018.
- (26) Furse, K. E.; Corcelli, S. A. Molecular Dynamics Simulations of DNA Solvation Dynamics. *J. Phys. Chem. Lett.* **2010**, *1*, 1813–1820.
- (27) Nelson, D. L.; Cox, M. M. *Lehninger Principles of Biochemistry*, 5th ed.; W. H. Freeman Co.: New York, 2008.
- (28) Berg, J. M.; Tymoczko, J. L.; Stryer, L. *Biochemistry*, 5th ed.; W. H. Freeman and company: New York, 2002.
- (29) Orengo, C. A.; Michie, A. D.; Jones, S.; Jones, D. T.; Swindells, M. B.; Thornton, J. M. CATH—a Hierarchic Classification of Protein Domain Structures. *Structure* **1997**, *5*, 1093–1109.

- (30) Berezovsky, I. N.; Guarnera, E.; Zheng, Z. Basic Units of Protein Structure, Folding, and Function. *Prog. Biophys. Mol. Biol.* **2017**, *128*, 85–99.
- (31) Loughlin, W. J. The Denaturation of Proteins: The Effect of the Addition of Electrolytes on the Viscosity of Solutions of Crystalline Egg-Albumin. *Biochem. J.* **1932**, *26*, 1557–1565.
- (32) Neurath, H.; Greenstein, J. P.; Putnam, F. W.; Erickson, J. A. The Chemistry of Protein Denaturation. *Chem. Rev.* **1944**, *34*, 157–265.
- (33) Daggett, V.; Levitt, M. Protein Unfolding Pathways Explored Through Molecular Dynamics Simulations. *J. Mol. Biol.* **1993**, *232*, 600–619.
- (34) Ramprakash, J.; Doseeva, V.; Galkin, A.; Krajewski, W.; Muthukumar, L.; Pullalarevu, S.; Demirkan, E.; Herzberg, O.; Moulton, J.; Schwarz, F. P. Comparison of the Chemical and Thermal Denaturation of Proteins by a Two-State Transition Model. *Anal. Biochem.* **2008**, *374*, 221–230.
- (35) Anand, U.; Mukherjee, S. Binding, Unfolding and Refolding Dynamics of Serum Albumins. *Biochim. Biophys. Acta (BBA)-General Subj.* **2013**, *1830*, 5394–5404.
- (36) Kishore, D.; Kundu, S.; Kayastha, A. M. Thermal, Chemical and PH Induced Denaturation of a Multimeric β -Galactosidase Reveals Multiple Unfolding Pathways. *PLoS One* **2012**, *7*, e50380.
- (37) Singh, K.; Shandilya, M.; Kundu, S.; Kayastha, A. M. Heat, Acid and Chemically Induced Unfolding Pathways, Conformational Stability and Structure-Function Relationship in Wheat α -Amylase. *PLoS One* **2015**, *10*, e0129203.
- (38) Lim, W. K.; Rösgen, J.; Englander, S. W. Urea, but Not Guanidinium, Destabilizes Proteins by Forming Hydrogen Bonds to the Peptide Group. *Proc. Natl. Acad. Sci. U. S. A.* **2009**, *106*, 2595–2600.
- (39) Meuzelaar, H.; Panman, M. R.; Woutersen, S. Guanidinium-Induced Denaturation by Breaking of Salt Bridges. *Angew. Chemie Int. Ed.* **2015**, *54*, 15255–15259.
- (40) Wang, W.; Nema, S.; Teagarden, D. Protein Aggregation—Pathways and Influencing Factors. *Int. J. Pharm.* **2010**, *390*, 89–99.
- (41) Mahler, H.; Friess, W.; Grauschopf, U.; Kiese, S. Protein Aggregation: Pathways, Induction Factors and Analysis. *J. Pharm. Sci.* **2009**, *98*, 2909–2934.
- (42) Cairolì, S.; Iametti, S.; Bonomi, F. Reversible and Irreversible Modifications Of β -Lactoglobulin upon Exposure to Heat. *J. Protein Chem.* **1994**, *13*, 347–354.
- (43) Bosia, A.; Spangenberg, P.; Lösche, W.; Arese, P.; Till, U. The Role of the GSH-Disulfide Status in the Reversible and Irreversible Aggregation of Human Platelets. *Thromb. Res.* **1983**, *30*, 137–142.
- (44) Dong, A.; Prestrelski, S. J.; Allison, S. D.; Carpenter, J. F. Infrared Spectroscopic Studies of Lyophilization-and Temperature-induced Protein Aggregation. *J. Pharm. Sci.* **1995**, *84*, 415–424.

-
- (45) Goyal, K.; Walton, L. J.; Tunnacliffe, A. LEA Proteins Prevent Protein Aggregation Due to Water Stress. *Biochem. J.* **2005**, *388*, 151–157.
- (46) Tanaka, S.; Oda, Y.; Ataka, M.; Onuma, K.; Fujiwara, S.; Yonezawa, Y. Denaturation and Aggregation of Hen Egg Lysozyme in Aqueous Ethanol Solution Studied by Dynamic Light Scattering. *Biopolym. Orig. Res. Biomol.* **2001**, *59*, 370–379.
- (47) Nemzer, L. R.; Flanders, B. N.; Schmit, J. D.; Chakrabarti, A.; Sorensen, C. M. Ethanol Shock and Lysozyme Aggregation. *Soft Matter* **2013**, *9*, 2187–2196.
- (48) Ross, C. A.; Poirier, M. A. Protein Aggregation and Neurodegenerative Disease. *Nat. Med.* **2004**, *10*, S10–S17.
- (49) Koo, E. H.; Lansbury, P. T.; Kelly, J. W. Amyloid Diseases: Abnormal Protein Aggregation in Neurodegeneration. *Proc. Natl. Acad. Sci.* **1999**, *96*, 9989–9990.
- (50) Hashimoto, M.; Rockenstein, E.; Crews, L.; Masliah, E. Role of Protein Aggregation in Mitochondrial Dysfunction and Neurodegeneration in Alzheimer's and Parkinson's Diseases. *Neuromolecular Med.* **2003**, *4*, 21–35.
- (51) Jimenez, R.; Fleming, G. R.; Kumar, P. V.; Maroncelli, M. Femtosecond Solvation Dynamics of Water. *Nature* **1994**, *369*, 471–473.
- (52) Vajda, Š.; Jimenez, R.; Rosenthal, S. J.; Fidler, V.; Fleming, G. R.; Castner, E. W. Femtosecond to Nanosecond Solvation Dynamics in Pure Water and inside the γ -Cyclodextrin Cavity. *J. Chem. Soc. Faraday Trans.* **1995**, *91*, 867–873.
- (53) Sarkar, N.; Das, K.; Datta, A.; Das, S.; Bhattacharyya, K. Solvation Dynamics of Coumarin 480 in Reverse Micelles. Slow Relaxation of Water Molecules. *J. Phys. Chem.* **1996**, *100*, 10523–10527.
- (54) Sarkar, N.; Datta, A.; Das, S.; Bhattacharyya, K. Solvation Dynamics of Coumarin 480 in Micelles. *J. Phys. Chem.* **1996**, *100*, 15483–15486.
- (55) Mandal, D.; Pal, S. K.; Bhattacharyya, K. Excited-State Proton Transfer of 1-Naphthol in Micelles. *J. Phys. Chem. A* **1998**, *102*, 9710–9714.
- (56) Datta, A.; Mandal, D.; Pal, S. K.; Bhattacharyya, K. Intramolecular Charge Transfer Processes in Confined Systems. Nile Red in Reverse Micelles. *J. Phys. Chem. B* **1997**, *101*, 10221–10225.
- (57) Bhattacharyya, K. Solvation Dynamics and Proton Transfer in Supramolecular Assemblies. *Acc. Chem. Res.* **2003**, *36*, 95–101.
- (58) Sen, P.; Mukherjee, S.; Halder, A.; Bhattacharyya, K. Temperature Dependence of Solvation Dynamics in a Micelle. 4-Aminophthalimide in Triton X-100. *Chem. Phys. Lett.* **2004**, *385*, 357–361.
- (59) Mandal, D.; Sen, S.; Bhattacharyya, K.; Tahara, T. Femtosecond Study of Solvation Dynamics of DCM in Micelles. *Chem. Phys. Lett.* **2002**, *359*, 77–82.
- (60) Bhattacharyya, K.; Bagchi, B. Slow Dynamics of Constrained Water in Complex Geometries. *J. Phys. Chem. A* **2000**, *104*, 10603–10613.
- (61) Riter, R. E.; Willard, D. M.; Levinger, N. E. Water Immobilization at Surfactant Interfaces in Reverse Micelles. *J. Phys. Chem. B* **1998**, *102*, 2705–

- 2714.
- (62) Willard, D. M.; Riter, R. E.; Levinger, N. E. Dynamics of Polar Solvation in Lecithin/Water/Cyclohexane Reverse Micelles. *J. Am. Chem. Soc.* **1998**, *120*, 4151–4160.
- (63) Faeder, J.; Ladanyi, B. M. Solvation Dynamics in Aqueous Reverse Micelles: A Computer Simulation Study. *J. Phys. Chem. B* **2001**, *105*, 11148–11158.
- (64) Hazra, P.; Chakrabarty, D.; Sarkar, N. Intramolecular Charge Transfer and Solvation Dynamics of Coumarin 152 in Aerosol-OT, Water-Solubilizing Reverse Micelles, and Polar Organic Solvent Solubilizing Reverse Micelles. *Langmuir* **2002**, *18*, 7872–7879.
- (65) Hazra, P.; Sarkar, N. Intramolecular Charge Transfer Processes and Solvation Dynamics of Coumarin 490 in Reverse Micelles. *Chem. Phys. Lett.* **2001**, *342*, 303–311.
- (66) Riter, R. E.; Undiks, E. P.; Kimmel, J. R.; Levinger, N. E. Formamide in Reverse Micelles: Restricted Environment Effects on Molecular Motion. *J. Phys. Chem. B* **1998**, *102*, 7931–7938.
- (67) Levinger, N. E. Water in Confinement. *Science* (80-.). **2002**, *298*, 1722–1723.
- (68) Levinger, N. E. Ultrafast Dynamics in Reverse Micelles, Microemulsions, and Vesicles. *Curr. Opin. Colloid Interface Sci.* **2000**, *5*, 118–124.
- (69) Riter, R. E.; Kimmel, J. R.; Undiks, E. P.; Levinger, N. E. Novel Reverse Micelles Partitioning Nonaqueous Polar Solvents in a Hydrocarbon Continuous Phase. *J. Phys. Chem. B* **1997**, *101*, 8292–8297.
- (70) Riter, R. E.; Undiks, E. P.; Levinger, N. E. Impact of Counterion on Water Motion in Aerosol OT Reverse Micelles. *J. Am. Chem. Soc.* **1998**, *120*, 6062–6067.
- (71) Tan, H.-S.; Piletic, I. R.; Riter, R. E.; Levinger, N. E.; Fayer, M. D. Dynamics of Water Confined on a Nanometer Length Scale in Reverse Micelles: Ultrafast Infrared Vibrational Echo Spectroscopy. *Phys. Rev. Lett.* **2005**, *94*, 57405.
- (72) Shirota, H.; Horie, K. Solvation Dynamics in Nonaqueous Reverse Micelles. *J. Phys. Chem. B* **1999**, *103*, 1437–1443.
- (73) Hazra, P.; Chakrabarty, D.; Sarkar, N. Solvation Dynamics of Coumarin 153 in Aqueous and Non-Aqueous Reverse Micelles. *Chem. Phys. Lett.* **2003**, *371*, 553–562.
- (74) Marzola, P.; Gratton, E. Hydration and Protein Dynamics: Frequency Domain Fluorescence Spectroscopy of Proteins in Reverse Micelles. *J. Phys. Chem.* **1991**, *95*, 9488–9495.
- (75) Pal, S. K.; Zewail, A. H. Dynamics of Water in Biological Recognition. *Chem. Rev.* **2004**, *104*, 2099–2124.
- (76) Pal, S. K.; Peon, J.; Zewail, A. H. Biological Water at the Protein Surface: Dynamical Solvation Probed Directly with Femtosecond Resolution. *Proc. Natl. Acad. Sci.* **2002**, *99*, 1763–1768.
- (77) Pal, S. K.; Mandal, D.; Sukul, D.; Sen, S.; Bhattacharyya, K. Solvation

- Dynamics of DCM in Human Serum Albumin. *J. Phys. Chem. B* **2001**, *105*, 1438–1441.
- (78) Mondal, S.; Mukherjee, S.; Bagchi, B. Protein Hydration Dynamics: Much Ado about Nothing? *J. Phys. Chem. Lett.* **2017**, *8*, 4878–4882.
- (79) Nandi, N.; Bagchi, B. Dielectric Relaxation of Biological Water. *J. Phys. Chem. B* **1997**, *101*, 10954–10961.
- (80) Shen, X.; Knutson, J. R. Subpicosecond Fluorescence Spectra of Tryptophan in Water. *J. Phys. Chem. B* **2001**, *105*, 6260–6265.
- (81) Zhong, D.; Pal, S. K.; Zhang, D.; Chan, S. I.; Zewail, A. H. Femtosecond Dynamics of Rubredoxin: Tryptophan Solvation and Resonance Energy Transfer in the Protein. *Proc. Natl. Acad. Sci.* **2002**, *99*, 13–18.
- (82) Vivian, J. T.; Callis, P. R. Mechanisms of Tryptophan Fluorescence Shifts in Proteins. *Biophys. J.* **2001**, *80*, 2093–2109.
- (83) Biesso, A.; Xu, J.; Muñio, P. L.; Callis, P. R.; Knutson, J. R. Charge Invariant Protein–water Relaxation in GB1 via Ultrafast Tryptophan Fluorescence. *J. Am. Chem. Soc.* **2014**, *136*, 2739–2747.
- (84) Santra, M. K.; Banerjee, A.; Krishnakumar, S. S.; Rahaman, O.; Panda, D. Multiple-probe Analysis of Folding and Unfolding Pathways of Human Serum Albumin: Evidence for a Framework Mechanism of Folding. *Eur. J. Biochem.* **2004**, *271*, 1789–1797.
- (85) Lu, W.; Kim, J.; Qiu, W.; Zhong, D. Femtosecond Studies of Tryptophan Solvation: Correlation Function and Water Dynamics at Lipid Surfaces. *Chem. Phys. Lett.* **2004**, *388*, 120–126.
- (86) Santra, M. K.; Banerjee, A.; Rahaman, O.; Panda, D. Unfolding Pathways of Human Serum Albumin: Evidence for Sequential Unfolding and Folding of Its Three Domains. *Int. J. Biol. Macromol.* **2005**, *37*, 200–204.
- (87) Yadav, R.; Sen, P. Mechanistic Investigation of Domain Specific Unfolding of Human Serum Albumin and the Effect of Sucrose. *Protein Sci.* **2013**, *22*, 1571–1581.
- (88) Pal, S. K.; Peon, J.; Zewail, A. H. Ultrafast Surface Hydration Dynamics and Expression of Protein Functionality: α -Chymotrypsin. *Proc. Natl. Acad. Sci.* **2002**, *99*, 15297 LP-15302.
- (89) Mukherjee, S.; Sen, P.; Halder, A.; Sen, S.; Dutta, P.; Bhattacharyya, K. Solvation Dynamics in a Protein–surfactant Aggregate. TNS in HSA–SDS. *Chem. Phys. Lett.* **2003**, *379*, 471–478.
- (90) Flora, K.; Brennan, J. D.; Baker, G. A.; Doody, M. A.; Bright, F. V. Unfolding of Acrylodan-Labeled Human Serum Albumin Probed by Steady-State and Time-Resolved Fluorescence Methods. *Biophys. J.* **1998**, *75*, 1084–1096.
- (91) Sasmal, D. K.; Mondal, T.; Sen Mojumdar, S.; Choudhury, A.; Banerjee, R.; Bhattacharyya, K. An FCS Study of Unfolding and Refolding of CPM-Labeled Human Serum Albumin: Role of Ionic Liquid. *J. Phys. Chem. B* **2011**, *115*, 13075–13083.

- (92) Yadav, R.; Sengupta, B.; Sen, P. Detail Modes of Binding Assessed by Bulk and Single Molecular Level Fluorescence, MD Simulation, and Its Temperature Dependence: Coumarin 152 with Human Serum Albumin Revisited. In *Selected Topics in Photonics*; Springer, 2018; pp 1–12.
- (93) Sengupta, B.; Chaudhury, A.; Das, N.; Sen, P. Single Molecular Level Probing of Structure and Dynamics of Papain Under Denaturation. *Protein Pept. Lett.* **2017**, *24*, 1073–1081.
- (94) Sengupta, B.; Acharyya, A.; Sen, P. Elucidation of the Local Dynamics of Domain-III of Human Serum Albumin over the Ps-Ms Time Regime Using a New Fluorescent Label. *Phys. Chem. Chem. Phys.* **2016**, *18*, 28548–28555.
- (95) Abou-Zied, O. K.; Al-Shihi, O. I. K. Characterization of Subdomain IIA Binding Site of Human Serum Albumin in Its Native, Unfolded, and Refolded States Using Small Molecular Probes. *J. Am. Chem. Soc.* **2008**, *130*, 10793–10801.
- (96) Yadav, R.; Sengupta, B.; Sen, P. Effect of Sucrose on Chemically and Thermally Induced Unfolding of Domain-I of Human Serum Albumin: Solvation Dynamics and Fluorescence Anisotropy Study. *Biophys. Chem.* **2016**, *211*, 59–69.
- (97) Ghosh, S.; Chattoraj, S.; Mondal, T.; Bhattacharyya, K. Dynamics in Cytoplasm, Nucleus, and Lipid Droplet of a Live CHO Cell: Time-Resolved Confocal Microscopy. *Langmuir* **2013**, *29*, 7975–7982.
- (98) Sasmal, D. K.; Ghosh, S.; Das, A. K.; Bhattacharyya, K. Solvation Dynamics of Biological Water in a Single Live Cell under a Confocal Microscope. *Langmuir* **2013**, *29*, 2289–2298.
- (99) Ghosh, S.; Chattoraj, S.; Bhattacharyya, K. Solvation Dynamics and Intermittent Oscillation of Cell Membrane: Live Chinese Hamster Ovary Cell. *J. Phys. Chem. B* **2014**, *118*, 2949–2956.
- (100) Zhang, L.; Wang, L.; Kao, Y.-T.; Qiu, W.; Yang, Y.; Okobiah, O.; Zhong, D. Mapping Hydration Dynamics around a Protein Surface. *Proc. Natl. Acad. Sci.* **2007**, *104*, 18461–18466.
- (101) Dahanayake, J. N.; Mitchell-Koch, K. R. How Does Solvation Layer Mobility Affect Protein Structural Dynamics? *Front. Mol. Biosci.* **2018**, *5*.
- (102) Bose, S.; Adhikary, R.; Barnes, C. A.; Fulton, D. B.; Hargrove, M. S.; Song, X.; Petrich, J. W. Comparison of the Dielectric Response Obtained from Fluorescence Upconversion Measurements and Molecular Dynamics Simulations for Coumarin 153– Apomyoglobin Complexes and Structural Analysis of the Complexes by NMR and Fluorescence Methods. *J. Phys. Chem. A* **2010**, *115*, 3630–3641.
- (103) Li, T.; Hassanali, A. A.; Kao, Y.-T.; Zhong, D.; Singer, S. J. Hydration Dynamics and Time Scales of Coupled Water– Protein Fluctuations. *J. Am. Chem. Soc.* **2007**, *129*, 3376–3382.
- (104) Chang, C.-W.; Guo, L.; Kao, Y.-T.; Li, J.; Tan, C.; Li, T.; Saxena, C.; Liu, Z.;

- Wang, L.; Sancar, A. Ultrafast Solvation Dynamics at Binding and Active Sites of Photolyases. *Proc. Natl. Acad. Sci.* **2010**, *107*, 2914–2919.
- (105) Tsui, V.; Case, D. A. Molecular Dynamics Simulations of Nucleic Acids with a Generalized Born Solvation Model. *J. Am. Chem. Soc.* **2000**, *122*, 2489–2498.
- (106) Shivakumar, D.; Williams, J.; Wu, Y.; Damm, W.; Shelley, J.; Sherman, W. Prediction of Absolute Solvation Free Energies Using Molecular Dynamics Free Energy Perturbation and the OPLS Force Field. *J. Chem. Theory Comput.* **2010**, *6*, 1509–1519.
- (107) Patel, S.; Mackerell Jr, A. D.; Brooks III, C. L. CHARMM Fluctuating Charge Force Field for Proteins: II Protein/Solvent Properties from Molecular Dynamics Simulations Using a Nonadditive Electrostatic Model. *J. Comput. Chem.* **2004**, *25*, 1504–1514.

Chapter 2

Experimental Methods

This chapter enlists the experimental methods I have used to carry out the research works presented in this thesis. I have described the basic principle and the instrumentation of steady-state absorption and emission spectroscopy, time-correlated single photon counting technique for the measurement of fluorescence lifetime, fluorescence anisotropy measurements, fluorescence correlation spectroscopy and circular dichroism spectroscopy. I have also described the procedures for tagging of the proteins used for my studies with different probe molecules.

2.1 Experimental Techniques

2.1.1 Steady-state absorption spectroscopy

Absorption of electromagnetic radiation is the process by which the energy of a photon is taken up by matter and is converted into internal energy of absorbing molecules, like thermal energy or other forms of molecular energy. The relationship between the attenuation of the light while passing through a sample to the properties of the material through which it passes through can be represented by Beer-Lambert law, which can be summed up using the following equation.^{1,2}

$$A_{\lambda} = \varepsilon_{\lambda} \cdot c \cdot l \quad (2.1)$$

In the above equation, ε_{λ} is the molar extinction coefficient, which is a measurement of how efficiently a chemical species absorbs light. The molar extinction coefficient is a wavelength-dependent term and will be different for different molecules. c and l are concentration of the sample under study and the length of the sample through which light passes, respectively. A_{λ} is the wavelength dependent absorbance, which is a measure of the amount of light that has been absorbed by a sample. Absorbance can be written as^{3,4}

$$A_{\lambda} = \log \frac{I_0(\lambda)}{I(\lambda)} \quad (2.2)$$

Here, $I_0(\lambda)$ and $I(\lambda)$ are the intensity of the incident light on the sample and that of the light transmitted through the sample, respectively. By measuring $I_0(\lambda)$ and $I(\lambda)$ we can calculate the absorbance of a sample. We can obtain the absorption spectrum by plotting the absorbance at each wavelength (A_{λ}) against the corresponding wavelength (λ). For my experiments, I have used a commercial double beam spectrophotometer (Shimadzu 2450, Japan) for recording absorption spectra. A schematic diagram of the basic instrumentation of a double beam spectrophotometer is given in figure 2.1.

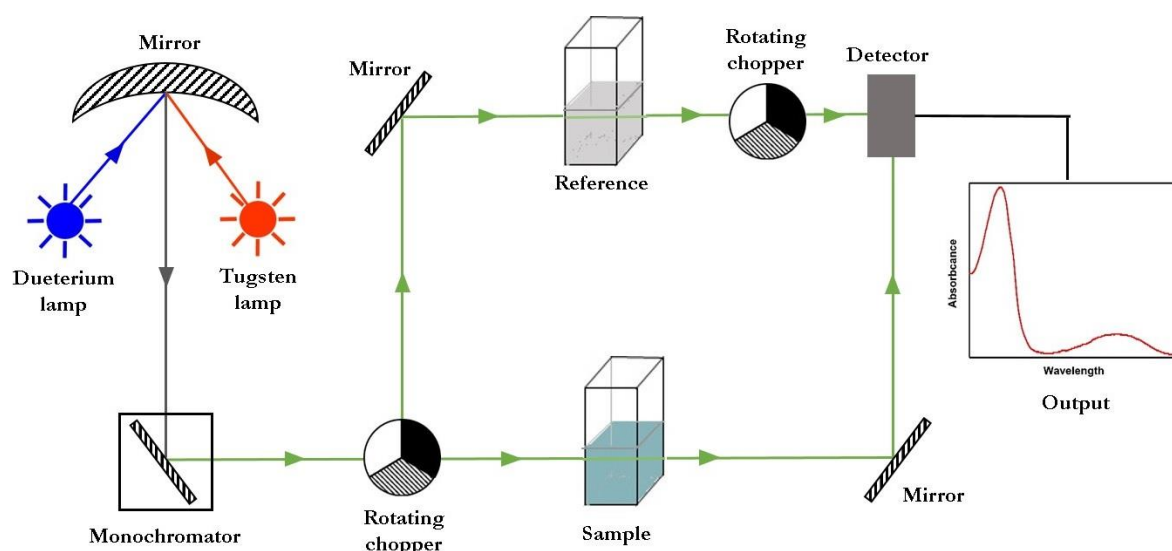


Figure 2.1. Schematic representation of the essential components of a double beam spectrophotometer.

In such a spectrophotometer the two light sources that we usually use are a tungsten filament lamp, which can generate light in visible-wavelength region, and a deuterium lamp, which can generate light in ultra violet region. The generated light passes through a monochromator. A monochromator can transmit a selectable narrow wavelength range with the help of a diffraction grating from a wider range of wavelength generated by the light source. The beam of light that emerges from the monochromator is then split into two beams using a rotating chopper, one of which passes through the sample (for measuring $I(\lambda)$) and the other one passes through a reference (for measuring $I_0(\lambda)$). For my experiments, I have used quartz cuvettes of 10 mm path length for the sample and reference solutions. The two beams of light reach the detector after passing through the respective solutions in the cuvettes. The reference beam passes through one more rotating chopper before reaching the detector. In our case, a photomultiplier tube is used as the detector.

The two rotating choppers we use are divided into an open part, an opaque part and a mirrored part. When the beam coming from the monochromator falls on the open part of the first chopper, the light beam will pass through it and then through the sample which will then reach the detector. When the beam falls on the mirrored part of the chopper, it will be redirected to the reference cuvette which will pass through the second rotating chopper before reaching the detector. The rotation of the

two choppers are synchronised in such a way that when the beam is redirected using the mirrored part of the first chopper, it will pass through the open part of the second chopper. When the beam faces the opaque part of the first chopper, light will not pass through and consequently no signal will be detected on the detector. This arrangement will help minimize the effect of lamp fluctuation as the fluctuation of the lamp will now affect both sample and reference beams equally.

2.1.2 Steady-state emission spectroscopy

The absorption of electromagnetic radiation by a molecule will take the molecule from its ground state to a higher excited state. While in the excited state, the molecule can undergo processes including intersystem crossing, internal conversion, vibrational relaxation, other non-radiative processes and fluorescence.^{5–}

⁷ Among these, fluorescence is the radiative process by which the molecule relaxes back to its ground state from the lowest vibrational level of an excited state. The fluorescence spectrum of a sample, which shows the emission intensity at different wavelengths can be recorded using a fluorimeter.

The schematic diagram of a fluorimeter is given in figure 2.2. The basic components of a fluorimeter include a light source, an excitation monochromator, a sample holder, an emission monochromator, a detector, a beam splitter and a reference detector. The light source which could be a normal tungsten lamp or a xenon lamp produces radiations of a wide range. The excitation monochromator helps us to choose the wavelength at which we want to excite the sample. The radiation of the selected wavelength then excites the sample placed in the sample holder which consequently emits radiations depending upon its fluorescing properties. The emitted light is detected using a photomultiplier tube placed at a perpendicular direction to that of the light source in order to minimize the scattering effects. The emission monochromator placed in front of the detector helps us to monitor the emission at any particular wavelength. Scanning the emission monochromator over a desired range of wavelengths can give us the emission spectrum which is a plot of emission intensity against the wavelength at which

emission is monitored, when the sample is excited using light at a particular wavelength.

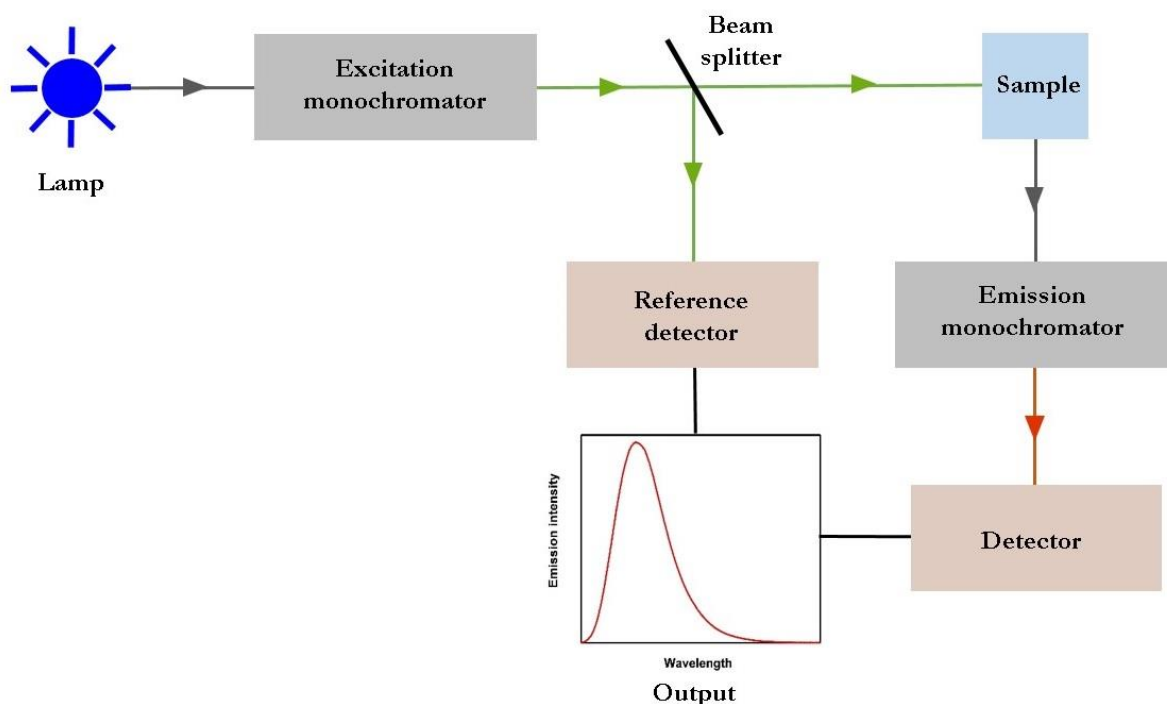


Figure 2.2. Schematic diagram of the essential components of a fluorimeter.

In the case of liquid samples, the solution is normally taken in a quartz cuvette, which is placed in the sample holder. Two major scenarios could result in errors during measurements if proper care has not been given during sample preparations. The first one occurs due to the reabsorption of emitted light by sample molecules. If the absorption spectrum and emission spectrum of a sample have an overlapping region, it means that some of the emitted light is within the absorbing range of the sample. If the concentration of such a sample is very high, some of the emitted light can be again absorbed by the sample molecules in the cuvette which were not initially excited by the excitation light. This will cause errors in the measured emission intensity. The second scenario which will result in an error is also a result of high concentrations. If the concentration of a sample is high, the intensity of exciting light will decrease as it passes through the sample solution. The intensity could also reduce to zero if the sample concentration is very high. In such a case, all the molecules in the path along which light should have been passing through are not excited. This is called the front surface absorption and will modulate

the emission intensity measurement. Both these errors could be rectified by choosing a low sample concentration. If, during dilution of the sample, we could see that the fluorescence intensity is varying proportional to the concentration of the sample, we could be sure that the reabsorption and front surface absorption are not resulting in any errors in our measurements.

Even after taking the above mentioned precautions, the recorded emission spectrum might contain errors arising due to some of the inherent properties of the main components of a fluorimeter, namely the light source, monochromator and detector. The photon to voltage conversion efficiency of the photomultiplier tube (PMT) is not equal for all wavelengths. This means that radiation of different wavelengths but having the same intensity falling on a PMT may give rise to different voltages for different wavelengths, and consequently different emission intensities in the spectrum. Similar are the cases with monochromator and the lamp where the light-throughput of monochromator and the excitation light intensity of the lamp are also far from ideal and vary considerably with wavelength. These fluctuations of fluorimeter components should be nullified in order to obtain the correct emission spectrum of a sample. Moreover, the intensity of excitation light from the lamp at any particular wavelength can also vary from time to time, which also should be taken care of while recording a spectrum.

In order to find out the wavelength-dependent variation of excitation light intensity an arrangement called quantum counter is used in the fluorimeter. The schematic representation of a quantum counter is given in figure 2.3. To measure the lamp profile, we take a highly concentrated sample of a molecule (quinine sulphate, fluorescein, rhodamine B etc. can be used for this purpose) in the quantum counter. As the solution is highly concentrated, all of the excitation light falling on the sample will be absorbed by the solution. The light reaching the detector (without using an emission monochromator) will be the total fluorescence intensity produced by the sample due to the excitation light of a particular wavelength. This fluorescence intensity will be proportional to the excitation light intensity. If we scan the

excitation light over a wide range of wavelength using the excitation monochromator, we can obtain the fluorescence intensity over that particular range which will be proportional to the intensity of lamp over the same range. This particular spectrum collected is called the lamp profile ($L(\lambda)$). The range upon which we can scan the excitation light and collect the lamp profile depends on the absorption range of the molecule we had taken in the quantum counter. The combined range of quinine sulphate, fluorescein and rhodamine B can give us an absorption range of approximately 250 to 600 nm.

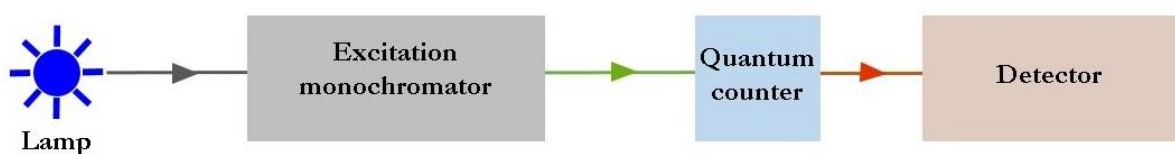


Figure 2.3. Schematic representation of a quantum counter of a fluorimeter.

In order to find out the correction factor which will take care of the wavelength dependent change in efficiency of detector and monochromators, we take a scatterer, Magnesium Oxide (MgO). A solution of MgO will not give out any fluorescence, but will give out scattered light as a result of Rayleigh scattering and this scattering efficiency will be equal at all wavelengths. Further, we scan both the excitation and emission monochromators through the entire range for which we would like to find out the correction factor. The spectrum thus obtained will incorporate the wavelength dependent efficiencies of monochromators, the detector and the lamp. Let the spectrum be represented as $L(\lambda)c(\lambda)$, where $L(\lambda)$ represents the lamp profile and $c(\lambda)$ represents the efficiency of the monochromators and the detector. We can find out $c(\lambda)$ as we already know $L(\lambda)c(\lambda)$ and $L(\lambda)$. This $c(\lambda)$ is constant for a fluorimeter and once measured, can be stored in the system as a correction file. If the emission spectrum recorded using the instrument is represented as $S_1(\lambda)$, $S_1(\lambda).c(\lambda)$ will be the spectrum where the wavelength dependent efficiencies of detector and monochromators are taken care of.

It should be noted that the correction file, $c(\lambda)$ does not incorporate the wavelength dependent efficiency of the lamp or the time-to-time change in the

intensity of excitation light. For taking these factors into account, during a spectrum measurement, we divert a small amount of light coming from the excitation monochromator into a second detector known as reference detector using a beam splitter (figure 2.2). Whenever we record the emission spectrum of a sample, a second reference spectrum will also be recorded using the reference detector. The spectrum thus generated, $(R(\lambda_{ex}))$ will account of the corrections for the lamp – the variation in lamp intensity with wavelength and the change in intensity of lamp at different times. Thus, $S_1(\lambda).c(\lambda)/R(\lambda_{ex})$ will give us the correct steady-state emission spectrum of a sample which has taken into account the various non-ideal behaviours of the components of fluorimeter. For carrying out the works described in this thesis, I have used Fluoromax-4 fluorimeter from Jobin Yvon, USA.

2.1.3 Time-correlated single photon counting (TCSPC)

In the previous two sections I have discussed about the methods to record the steady-state absorption and emission spectra of a chemical species. The steady-state experiments, albeit being very helpful in studying the energy levels of molecules and the changes occurring to them under different circumstances, provide us with spectra which are time integrated and do not contain any time-dependent information. However, time-resolved information is necessary to understand the molecular level changes occurring at small time scales. While there are many techniques that can be used for the measurement of fluorescent lifetime including fluorescence up-conversion and streak camera, for the works carried out in this thesis, I have used time-correlated single photon counting method for carrying out time-resolved studies including solvation dynamics and time-dependent anisotropy measurements.

2.1.3.1 Basic principle of TCSPC

Once a molecule absorbs a photon and gets excited to a higher energy state, it spends some period of time in the excited state before coming back to the ground state. Fluorescence lifetime is the average time spent by molecules in the excited state before decaying back to the ground state. After a system containing a large

number of molecules is excited to higher energy levels using a pulse of light, the excited state population decreases exponentially with time. As the intensity of emitted light is proportional to the number of molecules in the excited state, we can write⁶

$$I(t) = I_0 \cdot e^{\left(-\frac{t}{\tau}\right)} \quad (2.3)$$

Here, I_0 and $I(t)$ are the emission intensities of the system due to the excitation of the sample using a delta pulse, immediately after excitation and after time t respectively. The term τ denotes the excited state lifetime of the species, which can be derived from equation (2.3), as the time taken for the emission intensity to decrease to $\frac{1}{e}$ th of the initial value (ie. τ is the value of t when $I(t) = \frac{1}{e} \cdot I_0$). In more complex systems, the emission can be multi-exponential instead of the single-exponential decay mentioned in equation (2.3). In such a case, the components of lifetime are represented by τ_i where $i = 1, 2, 3, \dots$.

We measure the excited state lifetime of molecules using time-correlated single photon counting (TCSPC) method.⁸⁻¹⁰ TCSPC measurement works on the principle that the probability distribution for the emission of a single photon after an excitation event yields the actual intensity versus time distribution of all photons emitted as the result of a single excitation event using a light pulse. We construct the probability distribution by monitoring the single photon emission following a large number of excitation pulses. In this experiment, a sample containing a large number of molecules placed in a sample holder will be excited using a pulse of light. The excited molecules will emit photons in all directions around the sample holder. Among these photons, only the photons coming in one particular direction – the direction of the detector – will be detected by the instrument. Also, only one photon, the first photon coming in the direction of the detector will be detected during one cycle of excitation, emission and photon detection. The emission of emitted photon towards a particular direction is a random event and the detection of photon can happen at any given time following the excitation. It is also possible that during a

particular cycle, no emitted photon comes in the direction of the detector and no photon is detected during that cycle.

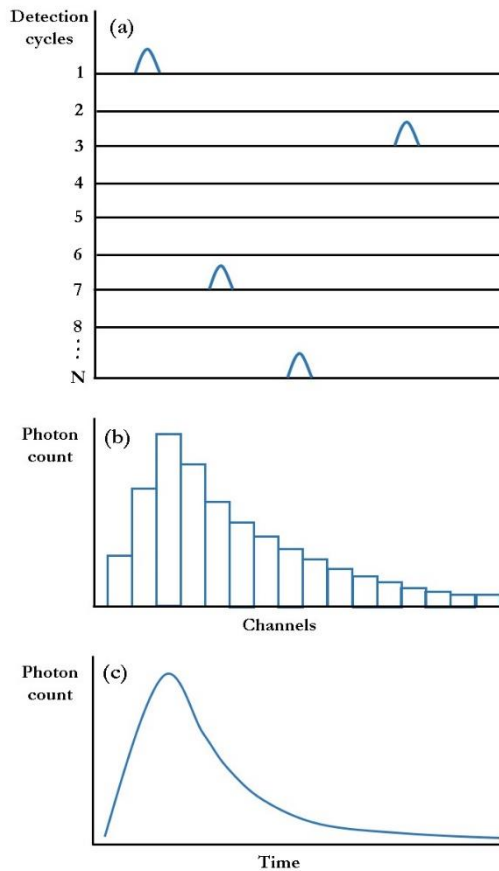


Figure 2.4. Principle of TCSPC: (a) the photon detection during a large number of cycles, (b) the construction of counts vs channels histograms and (c) the counts vs time graph.

We repeat the above experiment a very large number of times. The time period after excitation up to a particular amount of time (say 10 ns) is divided into many small time intervals (say 1 ps). A channel will be designated for each of these time intervals. When a photon is detected after some particular time after the excitation event which falls within one of the time intervals mentioned above, a count of one will be added to the channel corresponding to that time interval. When this experiment is repeated enough number of times (perhaps millions of times), we will end up with a histogram with channels in the x-axis and the number of counts against each channel in the y-axis. As the channels corresponds to some particular time intervals, the x-axis can be converted into time-axis. This graph of counts of photons in the y-axis and time in the x-axis would emulate the actual intensity versus

time plot for fluorescence emission following an excitation event. A schematic representation of the photon detection during many cycles, the construction of histogram in which the number of photons detected are plotted against each channel and the time versus intensity graph are shown in figure 2.4.

2.1.3.2 Instrumentation for TCSPC

The essential components of a TCSPC instrument include a laser, sample holder, polarizers, monochromator, a photomultiplier tube (PMT) detector, a constant fraction discriminator (CFD), a time to amplitude converter (TAC), a multichannel analyser (MCA) and a computer to analyse the data. A schematic diagram showing the basic instrumentation of a TCSPC instrument is shown in figure 2.5.

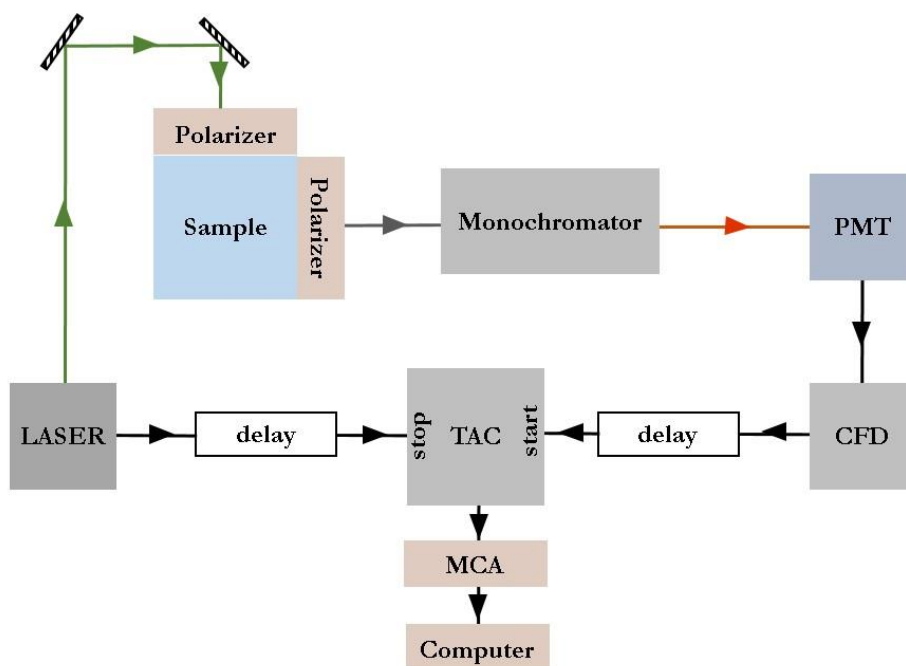


Figure 2.5. Schematic diagram showing the basic instrumentation required for TCSPC measurements.

In my experiments, a picosecond diode laser has been used as the light source. For a light source used in a TCSPC instrument, two parameters are of particular importance. One of them is the pulse width of laser. Ideally for such an experiment, a δ -pulse should be used where pulse width is zero and the molecules in the sample are excited at the exact same time using a very sharp pulse. However, it is not possible to generate such pulses and any light pulse generated will have an

inherent pulse width. It is advisable to use light pulses with much smaller pulse width as compared to the lifetime of the sample we are measuring. If the pulse width of the excitation pulse is comparable to the lifetime of the sample, that might distort the decay profile we obtain. The lasers used for my experiments have a pulse width (full width at half maximum) of approximately 100 ps. The second parameter of laser which is important is the ability to vary the pulse repetition rate or the time delay between successive pulses. For a sample with comparatively longer fluorescence decay, the time delay must be more than the fluorescence decay time, otherwise the second photon may excite the molecules and record a photon detection before the emission due to the first photon is detected. If the fluorescence lifetime is smaller, it is advisable that pulse delay is also proportionally smaller as this will make the experiment faster.

The light pulse from laser reaches the sample placed in the sample holder where it excites the molecule and the emitted photon is detected by the photomultiplier tube. All the samples used in my experiments were liquid solutions which were placed in a quartz cuvette of path length 10 mm. The radiation emitted by laser is linearly polarized. However, we have used an emission polarizer to ensure the vertical polarization of the light reaching the sample. The emitted light is collected through another polarizer oriented at 54.7° to the vertical axis to avoid the effects of rotational diffusion on intensity decay. It could be noted that unlike the steady-state measurements, a monochromator is not used before the light reaches the sample as the radiation emerging from the laser is already monochromatic. However, a monochromator is placed between the sample and the detector as the emission occurs in a broad range of wavelengths. The monochromator helps us to choose the wavelength of the emitted photon we want to monitor.

The emitted photon will be detected by a detector which is a photomultiplier tube (PMT). A PMT consists of a photocathode, a series of dynodes and an anode. When a photon falls on the photocathode of PMT, it causes the ejection of an electron from the photocathode's surface. The ejected electron is accelerated towards

the first dynode due to a potential difference and the collision of the electron on the dynodes causes the ejection of many additional electrons which will then move towards the next dynode. The process is repeated many times and finally the electrons exit from the anode of PMT as an electric pulse. However, there are some inherent errors associated with PMT. The electrons spend some time inside PMT between the photon falling on photocathode and the ejection of electric pulse from the anode. This time is called transit time and had this time been a constant quantity, we could have been able to take care of it while calculating the time between the excitation of a molecule and the emission of photon. Unfortunately, transit time varies from cycle to cycle due to the difference in location on photocathode where the photon falls and the difference in the path followed by the photoelectrons. This is called the transit time spread (TTS) and it causes an error while calculating the lifetime. TTS cannot be avoided in any of the PMTs available today. In our set-up a microchannel plate photomultiplier tube (MCP-PMT) has been used. A MCP-PMT has numerous small holes (microchannels) lined by dynode material. The small size of MCP-PMT decreases the TTS considerably, but still the TTS value would be about 10 ps – 25 ps.

Due to the difference in the path followed by photoelectrons inside PMT, the number of electrons emerging from the anode of PMT will also vary from cycle to cycle. This causes a difference in the amplitude of the electric pulses from the PMT even though each of them are generated as a result of a single photon. As these pulses are having different amplitudes, they will also be having a variation in pulse width, as the pulses with more amplitude will have more pulse width and vice versa. This differential pulse width will cause a problem while calculating the arrival time of the electric pulse. The arrival of electric pulses is detected only if the amplitudes of the pulses are above a certain threshold value in order to remove the thermal noise. In such a case, even if two electric pulses having amplitudes more than that of the threshold value are arriving at the same exact time, if one of the pulses is broader than the other, the broader pulse will appear to reach earlier than the other one

(leading edge discrimination). This time difference caused by different amplitudes of electric pulses is called the time jitter and it causes an error in the measurement of the arrival time and consequently the lifetime of a sample. This problem can be solved to a large extent by using the constant fraction discriminator (CFD). In CFD, whenever the amplitude of the pulse is more than that of the threshold, the pulse is divided into two smaller pulses, one of which is inverted and delayed by about half a pulse width. When the two pulses are recombined, the zero crossing point will be largely independent of the amplitude of the pulse. We use this zero crossing point to determine the arrival time of the pulse which reduces the time jitter significantly.

A time-to-amplitude converter (TAC) measures the time difference between the emission of a photon pulse from the laser and the detection of an electric pulse and is at the heart of a TCSPC instrument. TAC can work by the method mentioned below. When the laser emits a photon pulse, it simultaneously directs a trigger pulse to the TAC, which initiates the charging of a capacitor within the TAC. The photon pulse emitted then excites the sample and the first detected photon is converted into an electric pulse by the PMT which then passes through CFD. The electric pulse then reaches the TAC which acts as the stop pulse for stopping the charging of the capacitor. The capacitor then produces an electric pulse whose voltage will be proportional to the time between the emission of photon from laser and the detection of the electric pulse from PMT. The TAC should be calibrated previously, which allows us to get the excited state lifetime of a molecule from the voltage generated from TAC. The multichannel analyser (MCA) carries out the function of measuring the voltage from TAC and adding a count to the corresponding channel which represents a particular time interval. At this point, it is important to mention that there will be a significant time delay as the electric pulse travels through different components of the instrument, which is corrected by the use of delay lines in the instrument.

However, the above mentioned method has some drawbacks. As mentioned earlier, a photon might not be detected by PMT every time the sample is excited by

a laser pulse. On the contrary, only about 1 to 2% of excitations will result in an emitted photon falling in the photocathode of PMT and thus result in a detection event. In the method mentioned above, the TAC capacitor will start charging every time laser emits a photon and the TAC will be reset to zero if no stop pulse is received. Due to the high repetition rate of laser, TAC will be overloaded because of continuous start pulses. To solve this problem, we operate TAC in the ‘reverse mode’.

In the reverse mode, the electric pulse due to the detection of photon acts as the start pulse after which the capacitor will charge for some time known as the delay time and the charging will be stopped by the emission of next excitation pulse which serves as the stop pulse. The length of the delay time during which the charging of capacitor takes place will not be constant and will vary with variation of the arrival time of electric pulse from PMT (start pulse). On the other hand, the excitation pulse/stop pulse is programmed to occur at a particular time for each cycle and will not vary for different cycles. In the case of a sample with zero lifetime (a scatterer), the delay time will be the longest as the scattering event takes place without any excited state lifetime. For a sample with an excited state lifetime, the arrival of the electric pulse will be delayed due to the time the molecule spends in the excited state before emission. Consequently, the length of decay time will be shorter and the voltage output from TAC will be smaller. In short, the samples with comparatively longer excited state lifetime will give rise to smaller voltages from TAC and those with shorter lifetimes will give rise to larger voltages. As TAC is calibrated to give lifetime values proportional to the voltage generated, the measured lifetimes and thus the decay curves will be mirror images of the actual lifetimes and decay curves. This can be corrected later using a software. The reverse mode has the advantage that the capacitor will be charged and discharged only when a photon is detected by PMT and so TCSPC instruments work in this mode.

An important aspect that should be given care during the measurement of lifetime using TCSPC is ‘pulse pile-up’. As fluorescence emission is an exponential

process, during an emission following an excitation, the number of photons being emitted decreases exponentially with time. The number of molecules emitting at a longer time would be much smaller than those emitting at a shorter time following the excitation. In TCSPC method, only the first photon detected by PMT during each cycle has relevance. If the concentration of the sample is high, it is highly possible that every time (or most of the time), the first photon detected by PMT is the one having a very short lifetime. This would distort the shape of the decay profile with the shorter time having more counts than that is expected. This is known as pulse pile-up. To avoid this problem, we usually decrease the concentration of sample, which decreases the detection rate so that photons with different decay times are detected according to the actual decay profile of the molecule. In my experiments, I have made sure that the detection rate of photon is only about 0.01 times or lesser than that of the excitation pulses.

For all the lifetime measurements mentioned in this thesis, I have used Lifespec II TCSPC setup from Edinburg instruments, UK. Two laser sources were used, EPL-375 and EPL-445, Edinburg instruments, UK which can excite samples at 375.8 nm and 442.0 nm respectively. The detector used is Hamamastu R3809-50 MCP PMT with intrinsic TTS <25 ps. The maximum number of channels in our instrument is 4096. While measuring lifetime with a time scale of 5 ns, this can give a resolution of 1.22 ps per channel.

2.1.3.3 Analysis of the data obtained from TCSPC

The decay profile obtained from TCSPC can be fitted using equation (2.3) to obtain the excited state life of the sample. However, this equation is applicable only when a δ -function is used and the molecules are excited simultaneously. As we had seen, the light pulses from our laser are not δ -pulses and have a certain width. When such a pulse is used for excitation, the molecules will not be excited at a particular point of time, but along a period of time defined by the width of the pulse. We can measure the form of the excitation pulse by recording the instrument response function (IRF). IRF is measured by recording the response of TCSPC to a

zero lifetime sample. Scatterers like ludox solution or a milk solution can be used for this purpose. The emission should be collected at the excitation wavelength itself. An IRF thus obtained, represents the collective response of laser and other components of TCSPC to a zero lifetime sample. I have used dilute ludox solution for recording IRF and the pulse widths were found to be approximately 75 ps and 100 ps for lasers of 442.0 nm and 375.8 nm respectively.

For the purpose of analysing the decay transients, we assume the excitation pulse as a summation of infinite number of δ -pulses of different amplitudes. Each of these δ -pulses will excite the sample and produce its own decay profile. The decay profile obtained will be an integrated sum of all these decay profiles. Mathematically, this can be written as,^{6,8-10}

$$N(t) = \int_0^t L(t') I(t - t') dt' \quad (2.4)$$

where, $N(t)$ is the total intensity at any time t and $I(t - t')$ is the fluorescence intensity at time t due to a δ -pulse at time t' whose amplitude is $L(t')$. This equation is called the convolution integral. In this equation, both $N(t)$ and $L(t')$ are known quantities as we have measured the fluorescence decay of the sample and the lamp profile. $I(t - t')$ can be expressed as an exponential function similar to equation (2.3).

$$I(t - t') = I_0 \cdot e^{-\frac{t-t'}{\tau}} \quad (2.5)$$

Next, we take a guess value for τ and calculate $I(t - t')$. Knowing the value of $I(t - t')$ and $L(t')$, which is a measured quantity, we can calculate $N(t)$ using equation (2.4). We then compare the calculated $N(t)$ with the experimentally obtained $N(t)$ which is the same as the recorded decay profile. If the two are not matching closely, we perturb the value of τ slightly and do the process all over again. This will be repeated until the calculated and experimentally obtained $N(t)$ are satisfactorily close. This process in which we repeatedly convolute the lamp profile,

$L(t')$ with the calculated value of $I(t - t')$ and then calculate $N(t)$ until we get close matching with the experimentally obtained $N(t)$ is known as the iterative reconvolution. The τ value which was used for the calculation of $N(t)$ during the final cycle will be taken as the excited state lifetime of the sample. Equation (2.5) is applicable for single-exponential equations only. If no satisfactory matching could be obtained using a single-exponential fit, multi-exponential functions will need to be considered where more guess values corresponding to τ_i ($i = 1, 2, 3, \dots$) and their fractional components will be needed.

In order to decide the closeness of the calculated and recorded value of $N(t)$ (the goodness of fit), we have used the nonlinear least square (NLLS) method.^{8,11} In this method, the goodness of fit parameter, χ^2 is given by,^{6,8-10}

$$\chi^2 = \sum_{k=1}^n \frac{1}{\sigma_k^2} |N(t_k) - N_c(t_k)|^2 \quad (2.6)$$

In this equation, $N(t_k)$ and $N_c(t_k)$ are the measured and calculated data respectively, σ_k is the standard deviation at each point and the summation is carried over the number of channels or data points (n) used for the particular analysis. As the detection of photon by the detector is a random event and as the detection time of any photon does not depend on that of any other photon, the distribution of photons with time is assumed to follow a Poisson distribution. From Poisson statistics, the standard deviation is known to be the square root of the number of photons. ie. $\sigma_k = \sqrt{N(t_k)}$. So equation (2.6) becomes,

$$\chi^2 = \sum_{k=1}^n \frac{|N(t_k) - N_c(t_k)|^2}{N(t_k)} \quad (2.7)$$

In order to get the best fit for the experimental data for the model we use, we have to minimize the value of χ^2 . However, for a large number of channels, it may not be convenient to use the value of χ^2 as it depends on the value of data points (channels). For this reason, we use the reduced χ^2 as given by,⁶

$$\chi_R^2 = \frac{\chi^2}{n - p} \quad (2.8)$$

Here, n is the number of data points, p is the number of parameters and $(n - p)$ represents the number of degrees of freedom. As the number of data points are much more than the number of parameters in a typical TCSPC experiment, $(n - p)$ will be approximately equal to n . For a Poisson distributed data, χ_R^2 should be close to 1.^{8,12} Even though from equations (2.7) and (2.8), it might seem that χ_R^2 values closer to zero can account for a very good data, values much smaller than 1 (< 0.75) is an indication that the number of data points in the measurement is very small. Also, from a strict Poisson statistics point of view, a value of $\chi_R^2 = 1.02$ would probably invalidate the fit.¹² However, TCSPC experiments can contain some non-Poisson contribution,¹³ and due to this χ_R^2 values between 0.8 and 1.2 are considered to correspond to a good fit. It should also be mentioned that even if the values of χ_R^2 are a good means to decide the acceptability of the fit, a visual comparison should also be made between the recorded data and the fitting curve. For my analysis, the residuals, which are the difference between the data and the fitted function at each data point have also been examined. For all these data analysis, I have used FAST (fluorescence analysis decay technology) software developed by Edinburgh instruments, UK.

2.1.3.4 Construction of time-resolved emission spectra from TCSPC data

As was mentioned earlier, a steady-state emission spectrum is an average spectrum over a very long period of time. Time-resolved emission spectra (TRES) are the spectra that would be observed at any time following the excitation of the molecule. TRES can give us more information about the processes that happen following the excitation of a molecule that is unavailable from the steady-state emission spectrum. Even though TRES can be obtained by direct methods, the TRES recorded, will contain distortions due to instrument response function.^{14–16} So, construction of TRES from TCSPC data is a more preferred method.

For the construction of TRES of a sample, the lifetime decay of the sample at different wavelengths along the steady-state emission spectrum of the molecule should be recorded. The decay at each wavelength should be fitted using a multi-exponential (or single exponential, if it renders a satisfactory fitting) model as given below.

$$I(t) = \sum_{i=1}^n \alpha_i e^{-\frac{t}{\tau_i}} \quad (2.9)$$

Here, $I(t)$ is the intensity decay at time t , τ_i is the i^{th} lifetime components and α_i is the corresponding normalized fractional component of each τ_i . For the construction of TRES, all we need to know is the function $I(\lambda, t)$ which is the intensity of emission at different wavelengths and at different times. If we have this information, we can construct the emission spectrum at any particular time. For the purpose of calculation, $I(\lambda, t)$ can be considered as the product of two functions, one which varies with time and the other which varies with wavelength.^{6,8–10}

$$I(\lambda, t) = A(\lambda)B(t) \quad (2.10)$$

The time-dependent function can be written as the sum of exponentials used to express the time dependent fluorescence decay.

$$B(t) = \sum_{i=1}^n \alpha_i e^{-\frac{t}{\tau_i}} \quad (2.11)$$

To calculate $A(\lambda)$, we use the fact that the steady-state emission spectrum is the time average of TRES. This can be mathematically written as

$$I_{ss}(\lambda) = \int_0^{\infty} I(\lambda, t) dt = \int_0^{\infty} A(\lambda)B(t)dt = A(\lambda) \int_0^{\infty} B(t)dt \quad (2.12)$$

$I_{ss}(\lambda)$ is the steady-state emission spectrum. From equations (2.11) and (2.12) we can get,

$$A(\lambda) = \frac{I_{ss}(\lambda)}{\sum_{i=1}^n \alpha_i \tau_i} \quad (2.13)$$

Knowing the values of $A(\lambda)$ and $B(\lambda)$, we can now write equation (2.10) as

$$I(\lambda, t) = \frac{I_{ss}(\lambda)}{\sum_{i=1}^n a_i \tau_i} \sum_{i=1}^n \alpha_i e^{\frac{-t}{\tau_i}} \quad (2.14)$$

Using this equation, we can calculate the emission intensity at different wavelengths and at different times which will give us the time-resolved emission spectra. The spectra thus obtained are normally fitted using a log-normal function described by Maroncelli and Fleming.^{15,17}

$$I(\nu) = I_0 e^{-\ln(2) \left[\frac{\ln(1+2b(\nu-\nu_p)/\Delta)}{b} \right]^2} \quad (2.15)$$

Here, $I(\nu)$ is the intensity at any frequency ν . I_0 , b , ν_p and Δ are the peak intensity, asymmetry parameter, peak frequency and the width parameter, respectively. The width parameter (Δ) is related to the full width at half maximum (Γ) as

$$\Gamma = \Delta \left(\frac{\sinh(b)}{b} \right) \quad (2.16)$$

The time-dependent Stokes shift is calculated usually from the fitted curves. The dynamic Stokes shift is calculated as $(\nu(0) - \nu(\infty))$, where $\nu(0)$ is the peak intensity at zero time and $\nu(\infty)$ is the peak frequency at infinite time. Normally, $\nu(\infty)$ is taken as the peak frequency of the spectrum at a longer time when the peaks do not shift with time. In solvation dynamics studies, the solvent correlation function (solvent response function) is calculated as,¹⁶

$$C(t) = \frac{\nu(t) - \nu(\infty)}{\nu(0) - \nu(\infty)} \quad (2.17)$$

The solvent correlation function plotted against time can be fitted using either a single exponential or a multi-exponential equation to find out the solvation time.

$$C(t) = \sum a_i e^{\frac{-t}{\tau_{s_i}}} \quad (2.18)$$

Here, τ_{s_i} 's are the components of solvation times with fractional components, a_i 's. In the case of a multi-exponential decay of solvent correlation function, the average solvation time can be calculated as,

$$\tau_S = \sum a_i \tau_{S_i} \quad (2.19)$$

The above-mentioned fittings were carried out using Igor pro software.

2.1.4 Fluorescence anisotropy measurements

In a solution containing fluorescent molecules, the transition moments of absorption and emission of the molecules will be randomly oriented. When excited using a plane-polarized light, those molecules whose absorption transition moments are oriented along the electric vector of the incident radiation will be preferentially excited. This preferential orientation will be lost shortly as the molecules tend to rotate at all times and the random orientation will be restored. However, if the rotational time of the molecule is shorter than or comparable to that of the excited state lifetime of the molecule, we will be able to monitor the emission during the rotational relaxation of the molecules. From this information we would be able to calculate the rotational time of the molecule. Rotational time is an important parameter as it depends on both the size of molecule and the viscosity of the surrounding medium and we can calculate one of these quantities, knowing the other. This is the basic principle of anisotropy measurements.^{6,16}

Fluorescence anisotropy of a molecule is defined by the following equation.⁶

$$r = \frac{I_{\parallel} - I_{\perp}}{I_{\parallel} + 2I_{\perp}} \quad (2.20)$$

Here, r is the anisotropy and I_{\parallel} and I_{\perp} are the intensity of emitted light whose plane polarization is parallel and perpendicular, respectively to the polarized excitation of the molecules. To measure the anisotropy, vertically polarized light is used to excite the sample and the emission is collected at a vertically polarized condition (I_{VV}) and at a horizontally polarized condition (I_{VH}) using the excitation polarizer. I_{VV} and I_{VH} will not be exactly equal to I_{\parallel} and I_{\perp} , as the intensity of detected light will depend on the transmission efficiencies of the monochromator for each polarized component. The relationship between I_{VV} and I_{VH} with I_{\parallel} and I_{\perp} respectively can be given as,⁶

$$I_{VV} = kS_V I_{\parallel} \quad (2.21)$$

$$I_{VH} = kS_H I_{\perp} \quad (2.22)$$

where, k is the proportionality factor to account for the quantum yield of the fluorophore and S_V and S_H are the sensitivities of the emission channel for the vertical and horizontal polarized components. Using equations (2.20), (2.21) and (2.22), we can get,

$$r = \frac{I_{VV} - G \cdot I_{VH}}{I_{VV} + 2 \cdot G \cdot I_{VH}} \quad (2.23)$$

Here, G (known as G-factor) which accounts for the sensitivities of emission channels of different polarized lights is given by,

$$G = \frac{S_V}{S_H} \quad (2.24)$$

To experimentally record the G-factor, the sample is excited using a horizontally polarized light and the emission is collected at vertically (I_{HV}) and horizontally (I_{HH}) polarized conditions. However, in this case both the detected polarized lights will be perpendicular to the polarized excitation light (the detection using horizontal polarization will be perpendicular to the excitation light because the detector is placed perpendicular to the direction of excitation). The directions of the plane-polarised lights during the measurement of anisotropy and during the calculation of G-factor are schematically represented in figure 2.6 (a) and (b) respectively.

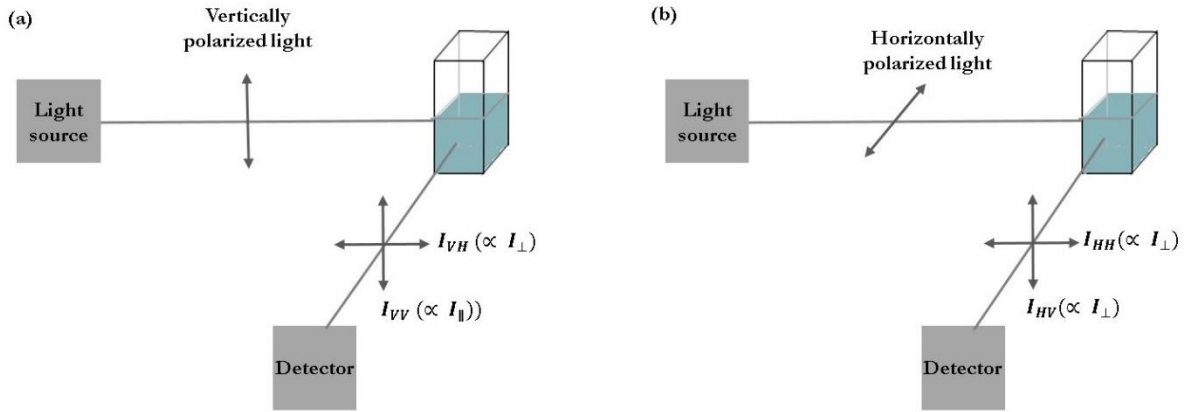


Figure 2.6. Schematic diagram for showing the directions of plane-polarized lights for the calculation of (a) anisotropy and (b) G-factor.

In this case, we have,

$$I_{HV} = kS_V I_{\perp} \quad (2.25)$$

$$I_{HH} = kS_H I_{\perp} \quad (2.26)$$

From equations (2.25) and (2.26) we can get,

$$G = \frac{S_V}{S_H} = \frac{I_{HV}}{I_{HH}} \quad (2.27)$$

So, G-factor can be measured by taking the ratio of I_{HV} and I_{HH} and knowing the value of G-factor, anisotropy can be calculated using equation (2.23).

The time-dependent anisotropy of a sample can be measured using a TCSPC set-up, which is related to the rotational time of the molecule using the following equation.⁶

$$r(t) = r(0) \cdot e^{\frac{-t}{\tau_R}} \quad (2.28)$$

where, $r(t)$ is the time-dependent anisotropy, $r(0)$ is the anisotropy at zero time and τ_R is known as the rotational correlation time. In cases where there are more components of rotational correlation times either due to the different environments in which fluorophores are located or due to the presence of more fluorophore moieties, the anisotropy can be written as

$$r(t) = r(0) \cdot \sum_i \alpha_i e^{\frac{-t}{\tau_{R_i}}} \quad (2.29)$$

Here, τ_{R_i} 's are the components of rotational correlation times and α_i 's are the corresponding fractional amplitudes. For the fluorescent anisotropy measurements carried in my thesis, the same TCSPC setup has been used which was used for lifetime measurements.

2.1.5 Fluorescence correlation spectroscopy

Fluorescence correlation spectroscopy (FCS) helps us to monitor a system at the single molecular level.^{18–21} In FCS, we take a solution of a fluorescent molecule at very low concentrations, normally at nanomolar level and the detection is done in a tiny detection volume, typically of femtolitre level. As a result of the very small concentration used for experiments, a fluorescent molecule might not be present at all times inside the detection volume. In FCS experiments the fluorescence will be recorded only when there is a molecule present inside the detection volume. The small detection volume is achieved with the help of an objective lens, which focuses the laser to a very small area of the sample solution and with the help of a confocal pinhole placed before the detector. This makes sure that only the light coming from the focal point of the excitation beam is being detected.

Using a FCS set-up we measure the fluorescence intensity, $F(t)$, at different times. $F(t)$ will fluctuate depending on whether a molecule is present inside the detection volume. Then using an auto correlator card, we calculate the correlation between the intensity at a given time, $F(t)$ with that at a slightly later time $F(t + \tau)$. This correlation is formally expressed as a function known as the autocorrelation function which is defined as⁶

$$G(\tau) = \frac{\langle \delta F(t) \delta F(t + \tau) \rangle}{\langle F(t) \rangle^2} \quad (2.30)$$

where, $\langle F(t) \rangle$ is the average fluorescence intensity. $G(\tau)$ is calculated for a range of τ values. $G(\tau)$ values tend to be higher at small τ values as the intensity of

fluorescence is mostly similar within small time intervals and tend to be smaller for higher values of τ as intensity values will be less similar at higher time intervals.

The autocorrelation function contains information about the diffusion of the particle. For a system containing only one translational diffusing component of particles, an equation connecting the autocorrelation function and the diffusion time can be written as²²

$$G(\tau) = G(0) \left(1 + \frac{\tau}{\tau_D}\right)^{-1} \left(1 + \frac{\tau}{\omega^2 \tau_D}\right)^{-1/2} \quad (2.31)$$

where, $G(0)$ is the value of $G(\tau)$ at $\tau = 0$, τ_D is the diffusion time and ω is the depth to diameter ratio of the three dimensional detection volume. ω is calculated by globally fitting various autocorrelation traces of rhodamine-6G. For more complex systems containing multiple diffusion time components and relaxation time, more complex equations will be required. In my thesis work, I have made use of the auto correlation equation in which one additional relaxation term (τ_R) is incorporated.²²

$$G(\tau) = G(0) \left(1 + \frac{\tau}{\tau_D}\right)^{-1} \left(1 + \frac{\tau}{\omega^2 \tau_D}\right)^{-1/2} (1 + A \cdot e^{\frac{-\tau}{\tau_R}}) \quad (2.32)$$

Here, A is the amplitude of the process defined by τ_R . τ_D can be calculated by global fitting the obtained data using equations (2.31) or (2.32). Once we have calculated τ_D , we can calculate the diffusion coefficient (D), using the equation,

$$D = \frac{r^2}{4 \cdot \tau_D} \quad (2.33)$$

where, r is the transverse radius of the observation volume. To calculate r , we carry out the experiment using rhodamine-6G and calculate τ_D by global fitting of autocorrelation traces using equation (2.31). Knowing the value of τ_D , we can calculate r for rhodamine-6G from equation (2.33) as the diffusion coefficient, D of rhodamine-6G is already known ($4.14 \times 10^{-6} \text{ cm}^2\text{s}^{-1}$).²³ The value of r will be same for rhodamine-6G and for our sample as the observation volume is same for both. After calculating the value of D , the hydrodynamic radius can be calculated using the Stokes-Einstein equation.^{24,25}

$$r_H = \frac{k_B T}{6\pi\eta D} \quad (2.34)$$

where, r_H is the hydrodynamic radius, k_B is the Boltzmann constant, T is the absolute temperature, η is the viscosity of the medium.

For the studies mentioned in chapter 7, I have used fluorescent correlation spectroscopy to calculate the hydrodynamic radii of protein moieties for which I have made use of the home-built FCS setup of our laboratory. The setup is made on an inverted confocal microscope, IX-71, Olympus, Japan. The laser source used was MDL-III-405-5mW (405 nm), CNI, China. The detector and the correlator card used were SPCM-AQRH-13-FC-24420, Excelitas technologies and Flex 990EM-12E, USA.

2.1.6 Circular dichroism spectroscopy

Circular dichroism (CD) spectroscopy is based on the differential absorption of left and right circularly polarized light by some molecules.^{26,27} Optically active chiral molecules will preferentially absorb one of these polarized lights over the other. In CD spectroscopy, we measure and quantify this difference in absorbance to get information about the structure of molecules. The schematic representation of CD spectrometer is shown in figure 2.7. The circular dichroism spectroscope is a specialised version of absorption spectrophotometer. The light emitted from the light source passes through a monochromator, which enables the wavelength selection and then through a polarizer, which converts it into a plane polarized light. This light then passes through a photo-elastic modulator (PEM) which helps to convert the linearly polarized light into right and left circularly polarized lights. The circularly polarized light then passes through the sample. The transmitted light is detected by a detector and it is possible to measure the difference in intensity between the two circularly polarized lights. If the total light intensity is I_t and the difference between the intensity of two circularly polarized lights is I_d , then the CD signal will be²⁸

$$CD = \frac{I_d}{I_t} G \quad (2.35)$$

where, G is the calibration factor. For the recording of CD spectra reported in this thesis, I have used a commercial CD spectrometer, J-815, Jasco, Japan.

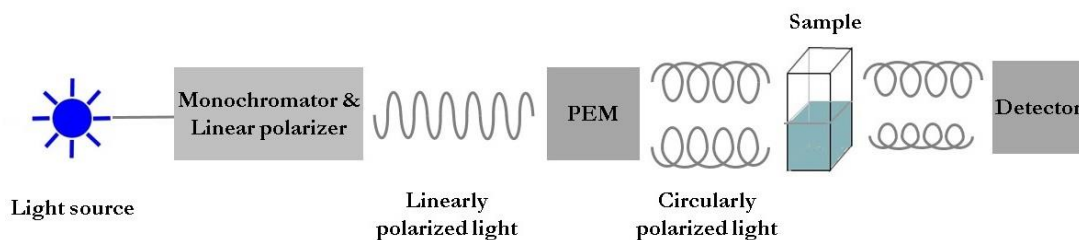


Figure 2.7. Schematic representation of the essential components of a circular dichroism spectrometer.

Optically active chiral molecules preferentially absorb one direction of circularly polarized lights. As most of the biological molecules are chiral, this method has been used widely for the study of biomolecules including proteins. Analysis of CD spectra can give information about the change in secondary and tertiary structure of proteins.^{29,30} In order to study the secondary structure of proteins, normally CD spectrum within the range 200-260 nm is recorded. For the analysis of secondary structure, the concentration of protein used is normally close to 5 μM and the path length of the cuvette used is 2 mm. For the purpose of monitoring the tertiary structure, a higher concentration of protein ($\sim 15 \mu\text{M}$) and a longer path length (10 mm) should be used and the spectra are recorded usually in the range 250-320 nm.³¹

The α -helical content of a protein can be calculated as,³²

$$\% \alpha \text{ helicity} = \frac{MRE_{222} - 3000}{-36000 - 3000} \times 100 \quad (2.36)$$

where the mean molar residual ellipticity at 222 nm (MRE_{222}) is defined as

$$MRE_{222} = \frac{\theta_{222} \times M}{n \cdot c \cdot l} \quad (2.37)$$

In the above equation, θ_{222} is the intensity of CD signal at 222 nm, M is the molecular weight of the protein, n is the number of amino acid residues, c is the concentration in g/l and l is the path length of the cuvette. Further, CD spectra could be analysed using CDNN software. This software helps to analyse and quantify the information

of far-UV CD spectra based on neural network theory as described by Gerald Böhm.³³ Using a neural network model, it is possible to deduce the five different secondary structure fractions (α -helix, parallel and antiparrel β -sheet, β -turn and random coil) of a protein molecule from its CD spectrum.

2.2 Materials used

The proteins used for my studies, human serum albumin (essential fatty acid free), papain, β -lactoglobulin and bromelain were purchased from Sigma-Aldrich, USA and were used as received. Among the probe molecules used to tag the proteins, DACIA (N-(7-dimethylamino-4-methylcoumarin-3-yl) iodoacetamide) was purchased from Molecular Probes Inc., CPM (7-diethylamino-3-(4-maleimidophenyl)-4-methylcoumarin) was purchased from Sigma-Aldrich and NPCE (*p*-nitrophenyl coumarin ester) was synthesised. The starting materials for synthesis of NPCE – coumarin 343, *p*-nitrophenyl, 4-dimethylamino pyridine (DMAP) and N,N-dicyclohexylcarbodiimide (DCC) were all purchased from Sigma-Aldrich. Dialysis membrane tubing (14 kDa cut-off) was also bought from Sigma-Aldrich and was used for dialysis to remove any unreacted probe molecules after removing the glycerol and sulfur compounds present on the membrane tubing. The centrifugal filter units (Amicon Ultra, 10kDa cut-off) were purchased from Merck Millipore, Germany. Analytical grade di-sodium hydrogen phosphate and sodium dihydrogen phosphate, used for the preparation of buffer solutions, were purchased from Merck. Urea, GnHCl and sucrose which have been used as the external agents added to proteins and sodium bis(2-ethylhexyl) sulfocinate (AOT) and cetyl trimethyl ammonium bromide (CTAB) which were used to make reverse micelles were purchased from Sigma-Aldrich. AOT and CTAB were dried under vacuum before each sample preparation. The solvents used in my experiments, HPLC grade dimethyl sulfoxide (DMSO), dichloromethane (DCM) and ethanol were bought from S. D. Fine chemicals limited and were used after distillation.

AOT reverse micelles of different water-pool sizes were prepared by injecting the required amount of protein sample (dissolved in buffer of pH 7.4) into

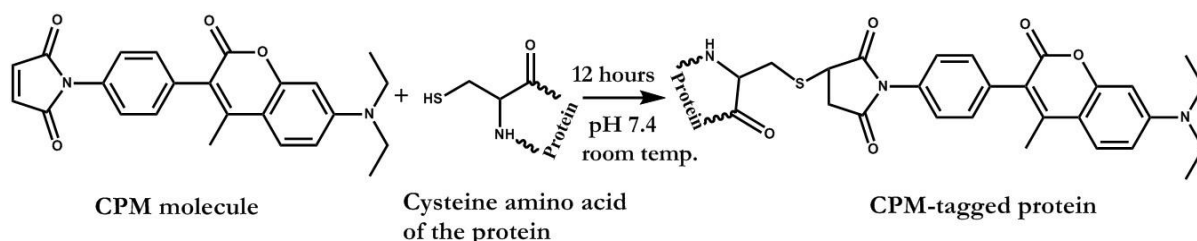
a solution of AOT in isooctane. For the preparation of CTAB reverse micelles, the protein sample was injected into a solution of CTAB in isooctane. In this case 250 μl of pentanol was added for stabilizing the reverse micelles. All experiments were done at 298 K, if not mentioned otherwise.

2.3 Tagging of proteins

Tagging of the proteins used for my experiments were carried out by following the already reported procedures.^{34–37} Upon the completion of tagging reaction, the reaction mixture was dialysed with a DMSO buffer (pH 7.4, 50 mM phosphate buffer) mixture, with the same DMSO : buffer ratio as in the reaction mixture at 4 °C to remove any unreacted dye. The dialysis medium was replaced at an interval of 12 hours for the first 5 days and then with buffer solution only for the next 5-8 days. In order to check for the completion of dialysis, the fluorescence spectra of each dialysed solution were recorded. The dialysis was stopped when the fluorescence spectra of the solution were not found to have any signal of the dye. The labelled protein was then concentrated using 10 kDa cut-off centrifugal filtration unit to obtain the tagged protein.

2.3.1 Tagging of proteins with CPM

CPM (7-diethylamino-3-(4-maleimidophenyl)-4-methylcoumarin) was used to tag three proteins, β -lactoglobulin, HSA and bromelain at their cysteine amino acid moieties. Cys-121, Cys-34 and Cys-26 were the tagging sites for β -lactoglobulin, HSA and bromelain respectively. In all the cases, the reaction procedure was very similar, which can be represented by the scheme below.³⁴



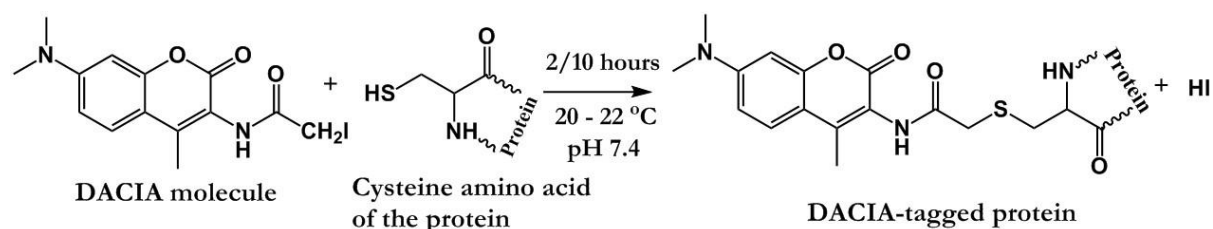
Scheme 2.1. Tagging of cysteine amino acid moieties of proteins with CPM (7-diethylamino-3-(4-maleimidophenyl)-4-methylcoumarin)

For tagging proteins with CPM, about 50 mg of the protein was dissolved in 4 ml of 50 mM phosphate buffer (pH 7.4). 400 μl of 5.5 mM CPM dissolved in

DMSO was added dropwise to the protein solution at room temperature under stirring condition. The reaction was carried on for 12 hours.

2.3.2 Tagging of proteins with DACIA

DACIA (N-(7-dimethylamino-4-methylcoumarin-3-yl) iodoacetamide) was used to tag Cys-34 of HSA and Cys-25 of papain using procedures reported by Wang *et. al.*³⁶ and Lindahl *et. al.*³⁵ respectively. Both the procedures are quite similar and can be represented by scheme 2.2.



Scheme 2.2. Tagging of cysteine amino acid moieties of proteins with DACIA (N-(7-dimethylamino-4-methylcoumarin-3-yl) iodoacetamide)

The protein (HSA or papain) was dissolved in buffer solution (pH 7.4) to make a solution 400 μM . DACIA (200 μM) was dissolved in 1 ml of DMSO and added to papain under stirring condition in a dropwise manner. The reaction was carried out at 20-22 $^\circ\text{C}$ and under low light conditions as DACIA is a light sensitive molecule. The reaction was carried out for 2 and 10 hours for tagging of papain and HSA respectively.

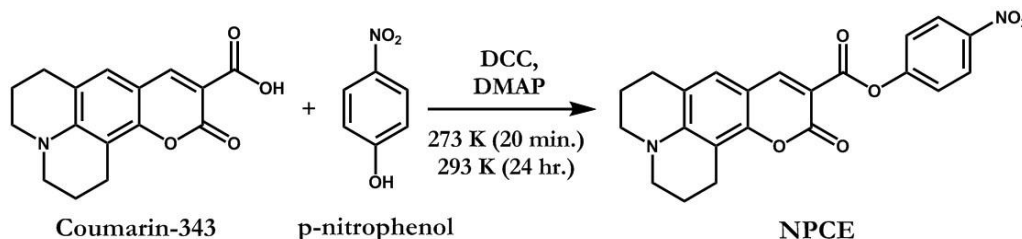
2.3.3 Tagging of HSA with NPCE

2.3.3.1 Synthesis of NPCE

NPCE (*p*-nitrophenyl coumarin ester) was synthesised following the common procedure of esterification³⁸ (scheme 2.3). Coumarin-343 (0.38 mmol), *p*-nitrophenol (0.38 mmol) and 4-dimethylamino pyridine (DMAP) (0.38 mmol) were taken in 5 ml DCM and stirred in an ice bath for 10 minutes. Following this, N,N-dicyclohexylcarbodiimide (DCC) was added under nitrogen atmosphere under stirring condition. The reaction mixture was stirred for 20 minutes at 0 $^\circ\text{C}$ and then for 24 hours at 20 $^\circ\text{C}$. After 24 hours, the organic layer was washed successively with 35 ml of 1.2 M HCl and 35 ml of saturated NaHCO_3 and then dried over MgSO_4 . The residue was suspended in methanol and the precipitate was washed with

methanol to remove any unreacted coumarin-343. The precipitate was collected in DCM and characterised with ^1H NMR. The ^1H NMR spectrum shows two doublet peaks at ca. 8.28 and 7.40 ppm, which indicates the formation of NPCE.

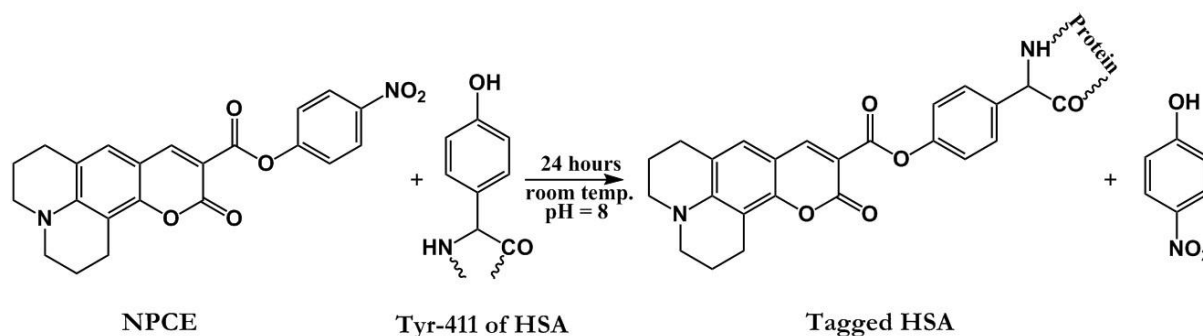
^1H NMR spectra of NPCE, 400MHz, solvent CDCl_3 : δ 8.472 (s, 1H), 8.276 (d, $J=9.16$ Hz, 2H), 7.401 (d, $J=9.16$ Hz, 2H), 6.979 (s, 1H), 3.34-3.39 (m, 4H), 2.890 (t, $J=6.4$ Hz, 2H), 2.764 (t, $J=6.44$ Hz, 2H), 1.947-2.010 (m, 4H).



Scheme 2.3. Synthesis of NPCE

2.3.3.2 Tagging of HSA

For tagging,³⁷ 40 mg of HSA was dissolved in 9 ml of 50 mM phosphate buffer (pH 8.0) and then 1 ml of NPCE dissolved in DMSO was slowly added under stirring conditions. The reaction was carried for 24 hours at room temperature. The scheme for the reaction is given in scheme 2.4.



Scheme 2.4. Tagging of Tyr-411 of HSA with NPCE

References

- (1) Beer, A. Bestimmung Der Absorption Des Rothen Lichts in Farbigen Flussigkeiten (Determination of the Absorption of Red Light in Colored Liquids). *Ann. Phys.* **1852**, 162, 78–88.
- (2) Lambert, J. H. *Photometrie: Photometria, Sive De Mensura et Gradibus Luminis, Colorum et Umbrae* (Photometry, or, On the Measure and Gradations of Light, Colors, and Shade) (1760); W. Engelmann, 1892; Vol. 31.
- (3) Owen, T. Fundamentals of Modern UV-Visible Spectroscopy, Agilent Technologies. Germany 2000.
- (4) Tkachenko, N. V. *Optical Spectroscopy: Methods and Instrumentations*; Elsevier, 2006.
- (5) Atkins, P.; De Paula, J.; Keeler, J. *Atkins' Physical Chemistry*, 11th ed.; Oxford university press: New York, 2018.
- (6) Lakowicz, J. R. *Principles of Fluorescence Spectroscopy*, 3rd ed.; Springer: Boston, MA, 2006.
- (7) Rohatgi-Mukherjee, K. K. *Fundamentals of Photochemistry*, 2nd ed.; New Age International: New Delhi, 1986.
- (8) O'Connor, D.; Phillips, D. *Time-Correlated Single Photon Counting*, 1st ed.; Academic Press: London, 1984.
- (9) Becker, W. *Advanced Time-Correlated Single Photon Counting Techniques*; Springer: New York, 2005.
- (10) Fleming, G. *Chemical Applications of Ultrafast Spectroscopy*; Oxford University Press: New York, 1986.
- (11) Bevington, P. R.; Robinson, D. K. Least-Squares Fit to an Arbitrary Function. *Data Reduct. Error Anal. Phys. Sci.* **1969**, 204–246.
- (12) Bevington, P. R. *Data Reduction and Error Analysis for Physicists*. McGraw Hill, New York 1969.
- (13) Grinvald, A.; Steinberg, I. Z. On the Analysis of Fluorescence Decay Kinetics by the Method of Least-Squares. *Anal. Biochem.* **1974**, 59, 583–598.
- (14) Easter, J. H.; DeToma, R. P.; Brand, L. Nanosecond Time-Resolved Emission Spectroscopy of a Fluorescence Probe Adsorbed to L-Alpha-Egg Lecithin Vesicles. *Biophys. J.* **1976**, 16, 571–583.
- (15) Horng, M. L.; Gardecki, J. A.; Papazyan, A.; Maroncelli, M. Subpicosecond Measurements of Polar Solvation Dynamics: Coumarin 153 Revisited. *J. Phys. Chem.* **1995**, 99, 17311–17337.
- (16) Fleming, G. R.; Gijzeman, O. L. J.; Freed, K. F.; Lin, S. H. Theory for Time Resolved Emission Spectra. *J. Chem. Soc. Faraday Trans. 2 Mol. Chem. Phys.* **1975**, 71, 773–780.
- (17) Maroncelli, M.; Fleming, G. R. Picosecond Solvation Dynamics of Coumarin 153: The Importance of Molecular Aspects of Solvation. *J. Chem. Phys.* **1987**, 86, 6221–6239.

-
- (18) Wolfbeis, O. S. *Fluorescence Spectroscopy: New Methods and Applications*; Springer Science & Business Media, 2012.
- (19) Widengren, J.; Mets, Ü. Conceptual Basis of Fluorescence Correlation Spectroscopy and Related Techniques as Tools in Bioscience. *Single Mol. Detect. Solut. Methods Appl.* **2002**, 69–120.
- (20) Schwille, P. Fluorescence Correlation Spectroscopy and Its Potential for Intracellular Applications. *Cell Biochem. Biophys.* **2001**, 34, 383–408.
- (21) Humpolíčková, J.; Gielen, E.; Benda, A.; Fagulova, V.; Vercammen, J.; Hof, M.; Ameloot, M.; Engelborghs, Y. Probing Diffusion Laws within Cellular Membranes by Z-Scan Fluorescence Correlation Spectroscopy. *Biophys. J.* **2006**, 91, L23–L25.
- (22) Sengupta, B.; Yadav, R.; Sen, P. Startling Temperature Effect on Proteins When Confined: Single Molecular Level Behaviour of Human Serum Albumin in a Reverse Micelle. *Phys. Chem. Chem. Phys.* **2016**, 18, 14350–14358.
- (23) Müller, C. B.; Loman, A.; Pacheco, V.; Koberling, F.; Willbold, D.; Richter, W.; Enderlein, J. Precise Measurement of Diffusion by Multi-Color Dual-Focus Fluorescence Correlation Spectroscopy. *EPL (Europhysics Lett.)* **2008**, 83, 46001.
- (24) Miller, C. C. The Stokes-Einstein Law for Diffusion in Solution. *Proc. R. Soc. London. Ser. A, Contain. Pap. a Math. Phys. Character* **1924**, 106, 724–749.
- (25) Edward, J. T. Molecular Volumes and the Stokes-Einstein Equation. *J. Chem. Educ.* **1970**, 47, 261.
- (26) Woody, R. W. Theory of Circular Dichroism of Proteins. In *Circular dichroism and the conformational analysis of biomolecules*; Springer, 1996; pp 25–67.
- (27) Greenfield, N. J. Using Circular Dichroism Spectra to Estimate Protein Secondary Structure. *Nat. Protoc.* **2006**, 1, 2876.
- (28) Berova, N.; Ellestad, G.; Harada, N.; Lew, N.; Hung-Wen, L. *Characterization by Circular Dichroism Spectroscopy*; 2010; Vol. 9.
- (29) Johnson Jr, W. C. Protein Secondary Structure and Circular Dichroism: A Practical Guide. *Proteins Struct. Funct. Bioinforma.* **1990**, 7, 205–214.
- (30) Whitmore, L.; Wallace, B. A. Protein Secondary Structure Analyses from Circular Dichroism Spectroscopy: Methods and Reference Databases. *Biopolym. Orig. Res. Biomol.* **2008**, 89, 392–400.
- (31) Zaidi, N.; Ajmal, M. R.; Rabbani, G.; Ahmad, E.; Khan, R. H. A Comprehensive Insight into Binding of Hippuric Acid to Human Serum Albumin: A Study to Uncover Its Impaired Elimination through Hemodialysis. *PLoS One* **2013**, 8, e71422.
- (32) Corrêa, D. H. A.; Ramos, C. H. I. The Use of Circular Dichroism Spectroscopy to Study Protein Folding, Form and Function. *J. Biochem.* **2009**, 3, 164–173.
- (33) Böhm, G.; Muhr, R.; Jaenicke, R. Quantitative Analysis of Protein Far UV Circular Dichroism Spectra by Neural Networks. *Protein Eng. Des. Sel.* **1992**, 5, 191–195.

- (34) Sasmal, D. K.; Mondal, T.; Sen Mojumdar, S.; Choudhury, A.; Banerjee, R.; Bhattacharyya, K. An FCS Study of Unfolding and Refolding of CPM-Labeled Human Serum Albumin: Role of Ionic Liquid. *J. Phys. Chem. B* **2011**, *115*, 13075–13083.
- (35) Lindahl, P.; Raub-Segall, E.; Olson, S. T.; Björk, I. Papain Labelled with Fluorescent Thiol-Specific Reagents as a Probe for Characterization of Interactions between Cysteine Proteinases and Their Protein Inhibitors by Competitive Titrations. *Biochem. J.* **1991**, *276*, 387–394.
- (36) Wang, R.; Sun, S.; Bekos, E. J.; Bright, F. V. Dynamics Surrounding Cys-34 in Native, Chemically Denatured, and Silica-Adsorbed Bovine Serum Albumin. *Anal. Chem.* **1995**, *67*, 149–159.
- (37) Sengupta, B.; Acharyya, A.; Sen, P. Elucidation of the Local Dynamics of Domain-III of Human Serum Albumin over the Ps-Ms Time Regime Using a New Fluorescent Label. *Phys. Chem. Chem. Phys.* **2016**, *18*, 28548–28555.
- (38) Aujard, I.; Benbrahim, C.; Gouget, M.; Ruel, O.; Baudin, J.; Neveu, P.; Jullien, L. O-Nitrobenzyl Photolabile Protecting Groups with Red-Shifted Absorption: Syntheses and Uncaging Cross-Sections for One-and Two-Photon Excitation. *Chem. Eur. J.* **2006**, *12*, 6865–6879.

Chapter 3

A Comparative Study of Hydration Dynamics inside Different Proteins: The Effect of Probe and the Protein Site

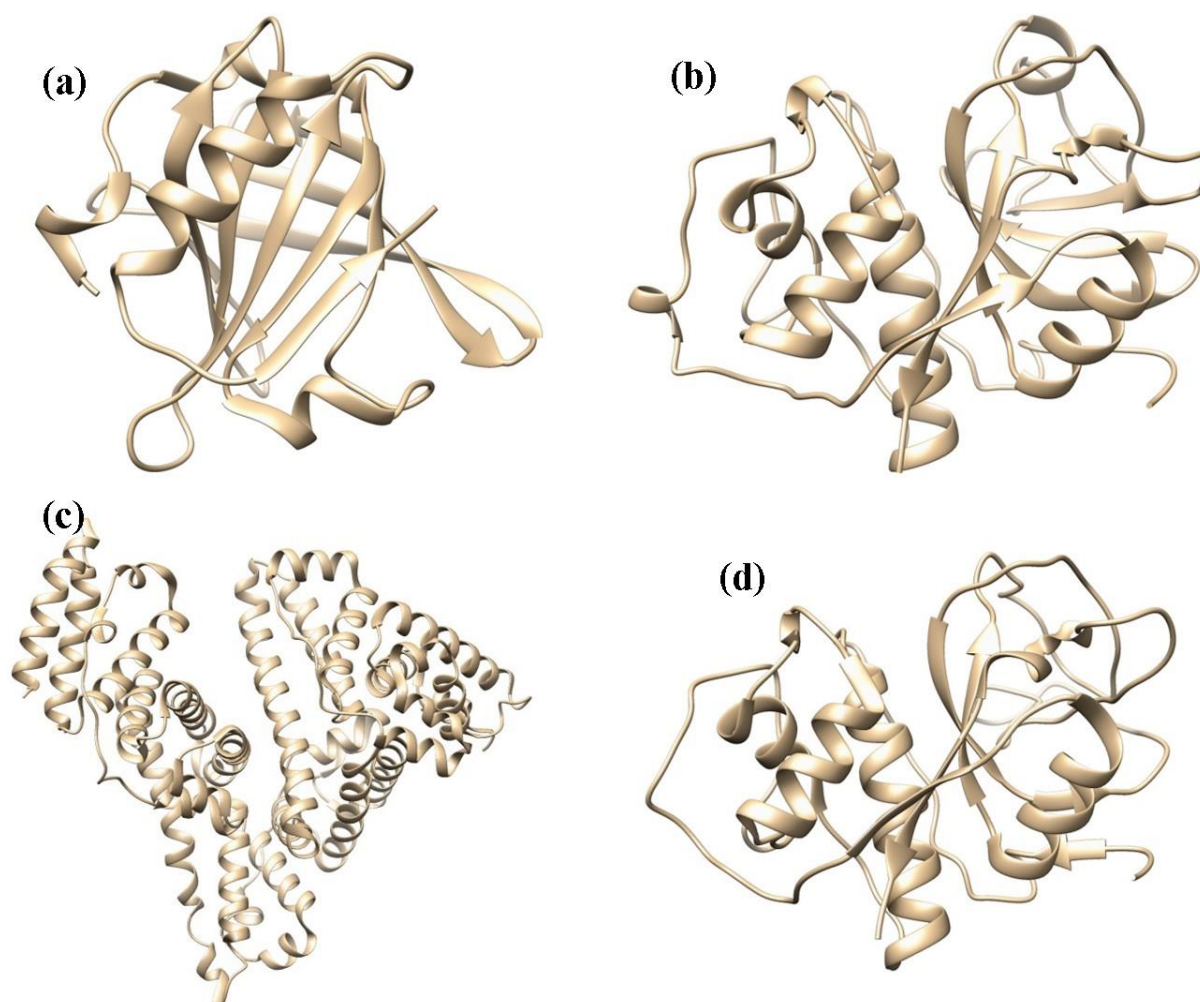
In this work, the solvation dynamics of water inside four different proteins was studied using three different fluorescent molecules as probes. The probe molecules were covalently bonded to a particular amino acid residue of the proteins. The average solvation time when monitored using probe molecules N-(7-dimethylamino-4-methylcoumarin-3-yl) iodoacetamide (DACIA) and 7-dimethylamino-3-(4-maleimidophenyl)-4-methylcoumarin (CPM) at Cys-34 position of human serum albumin (HSA), was found to vary only by 2.5%, indicating that the dynamics of solvation at a particular site does not depend on the probe molecule, as expected. However, when monitored at two different sites of HSA, Cys-34 and Tyr-411, the average solvation time was found to differ by 90 %. This points out at the difference in solvation time caused due to different local environments even within the same protein. Further, solvation dynamics at different proteins, were found to exhibit different rates of solvation depending on the environment in which the probe molecule is located. Among the proteins that we have studied, the solvation time was found to be slowest inside bromelain (at Cys-26) and was the fastest inside papain (at Cys-25).

3.1 Introduction

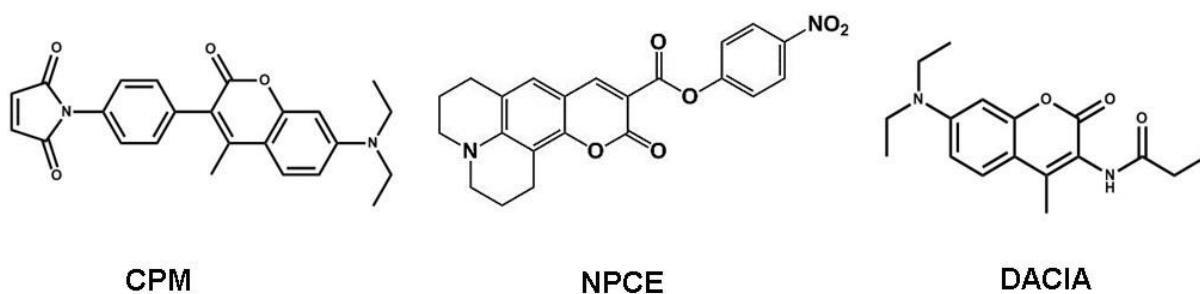
The dynamics of water inside biomolecules is one of the factors that determines their three-dimensional structure under small perturbation.¹⁻⁵ In the case of proteins, the local motion of water molecules also plays a crucial role in enzyme reactions and protein recognition.⁶⁻¹⁰ Due to its biological importance, hydration dynamics inside proteins has been studied extensively during the last two decades and it is a well-established fact that inside proteins, hydration is slower by many orders as compared to that in bulk water.¹¹⁻¹³ Solvation dynamics studies inside proteins are carried out either by exploiting the intrinsic fluorescence of the protein or by using covalent or non-covalent fluorescent probe molecules.¹⁴⁻²⁰ Some proteins do not possess any intrinsic fluorescence due to the absence of fluorescent amino acid moieties and some have more than one fluorescent amino acids which results in a loss of site-specific information. In these cases, a covalent or a non-covalent fluorescent probe molecule can be used to carry out the solvation dynamics studies. Covalent probe molecules have an advantage over the non-covalent probe molecules as they attach to a specific amino acid moieties and thus can provide more site-specific information.¹⁷⁻²⁰ Moreover, as in this case, the attachment is covalent, a change in protein structure does not alter the position of the probe molecule within the protein.

In the present work, we have covalently tagged four different proteins, human serum albumin (HSA), papain, β -lactoglobulin and bromelain (scheme 3.1) using different fluorescent probe molecules with a view to study the effect of probe molecules on the solvation dynamics and to compare the solvation dynamics at different sites of a protein and among various proteins. For most of our studies, we have used cysteine to attach the probe molecule.^{21,22} In all of the protein molecules we have studied, we had only one free cysteine residue, which was used for this covalent binding to a fluorescent probe. The probe molecules used for tagging the cysteine residues were 7-diethylamino-3-(4-maleimidophenyl)-4-methylcoumarin (CPM) and N-(7-dimethylamino-4-methylcoumarin-3-yl) iodoacetamide (DACIA).

In one of the cases, we have also used p-nitrophenyl coumarin ester (NPCE) to tag Tyr-411 of HSA. The structures of the used probe molecules are shown in scheme 3.2.



Scheme 3.1. Schematic representation of structures of (a) β -lactoglobulin (PDB: 2Q2M), (b) papain (PDB: 1PPN), (c) human serum albumin (PDB: 1HA2) and (d) bromelain (1Q0W).



Scheme 3.2. Structures of the probe molecules

3.2 Results

3.2.1 Solvation dynamics inside β -lactoglobulin monitored using CPM

The normalised absorption and emission spectra of CPM-tagged β -lactoglobulin are given in figure 3.1.

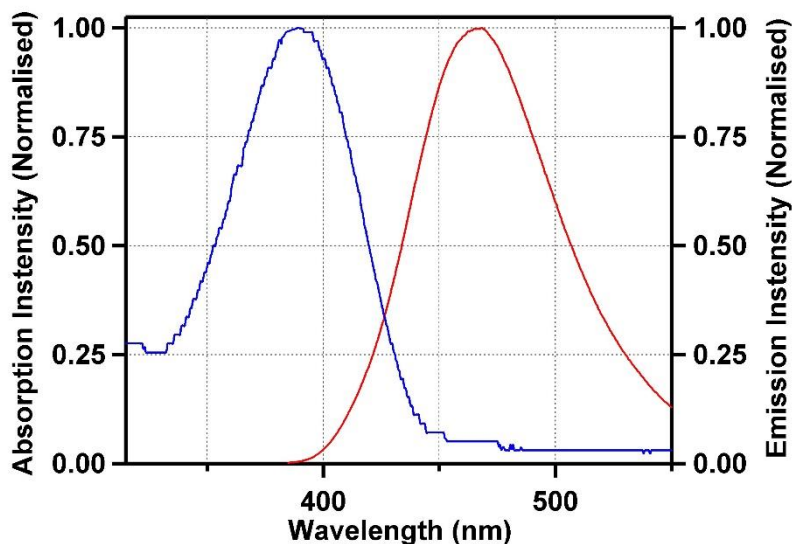


Figure 3.1. Normalised absorption and emission spectra ($\lambda_{ex}=390$ nm) of CPM-tagged β -lactoglobulin

In order to study the solvation dynamics around the CPM molecule covalently tagged to the Cys-121 site of β -lactoglobulin, the fluorescent transients were collected at 24 different wavelengths along the steady-state emission spectrum of the CPM-tagged β -lactoglobulin. A few of them are shown in figure 3.2(a). For better visualising the characteristics of the transients at a shorter time, the decays were also collected in a shorter time window, a few of which are shown in figure 3.2(b). The growth components in the fluorescence transients at higher wavelengths can be clearly seen here. The transients were best fitted using a triexponential function to obtain the lifetime components and their fractional amplitudes. The longest component of lifetime was obtained from the fitting of the decay profiles recorded at the larger time window, which were kept fixed during the fitting of the transients collected at shorter time window. However, the corresponding fractional components were not fixed. The three lifetime-components thus obtained for the emission collected at 400 nm were found to be 0.06 ns (38%), 0.72 ns (25%) and 3.15 ns (37%) with an average lifetime of 1.37 ns, whereas, for the emission

collected at 550 nm, the three lifetime-components were found to be 0.27 ns (-53%), 3.16 ns (105%) and 5.01 ns (48%) with an average lifetime of 5.58 ns. The negative fractional amplitude of the shortest component is an indicative of the solvation process. The lifetime components of the transients collected at different wavelengths are compiled in table 3.1. The time-resolved emission spectra (TRES) were constructed from the lifetime-components following the standard procedure.²³ A few of the time-resolved spectra along with the steady state emission spectrum are shown in figure 3.2(c). The dynamic Stokes shift was found to be 386 cm⁻¹. From the peak frequencies of TRES, the solvent correlation function was constructed (figure 3.2(d)). The solvent correlation function thus constructed is best fitted using a biexponential equation. The two components were found to be 0.22 ns (63%) and 0.78 ns (37%) with an average solvation time of 0.43 ns.

Table 3.1. Fitting parameters of the transient decays of CPM tagged to Cys-121 of β -lactoglobulin at different wavelengths. The sample was excited at 375.8 nm.

λ_{em} (nm)	a_1	τ_1 (ns) ^a	a_2	τ_2 (ns) ^b	a_3	τ_3 (ns) ^c	$\langle \tau \rangle$ (ns)
400	0.38	0.06	0.25	0.72	0.37	3.15	1.37
410	0.42	0.03	0.20	0.82	0.38	3.28	1.42
420	0.28	0.79	0.22	2.84	0.50	3.43	2.56
430	0.26	1.02	0.12	2.57	0.62	3.65	2.84
435	0.16	1.24	0.35	2.21	0.49	3.83	2.85
440	0.06	1.68	0.25	1.56	0.69	3.88	3.17
444	0.03	1.73	0.25	1.70	0.72	3.90	3.29
448	-0.16	0.24	0.27	1.14	0.89	3.99	3.82
452	-0.18	0.25	0.29	1.28	0.89	4.13	4.00
456	-0.19	0.27	0.34	1.49	0.85	4.25	4.07
460	-0.22	0.26	0.32	1.54	0.90	4.10	4.13
464	-0.26	0.24	0.26	1.42	1.00	4.05	4.36
468	-0.27	0.23	0.43	2.09	0.84	4.18	4.35
472	-0.28	0.25	0.46	2.20	0.82	4.24	4.42
476	-0.32	0.23	0.59	2.48	0.73	4.34	4.56
480	-0.33	0.23	0.63	2.55	0.70	4.45	4.65
485	-0.33	0.25	0.52	2.35	0.81	4.43	4.73
490	-0.38	0.26	0.67	2.49	0.71	4.64	4.87
495	-0.40	0.26	0.83	2.78	0.57	4.80	4.94
500	-0.41	0.28	0.97	2.91	0.45	4.56	4.76
510	-0.44	0.27	0.72	2.68	0.72	4.68	5.18
520	-0.46	0.27	0.85	2.93	0.61	4.81	5.30
535	-0.51	0.27	0.85	2.85	0.66	4.84	5.48
550	-0.53	0.27	1.05	3.16	0.48	5.01	5.58

^a± 0.02 ns, ^b± 0.05 ns, ^c± 0.20 ns

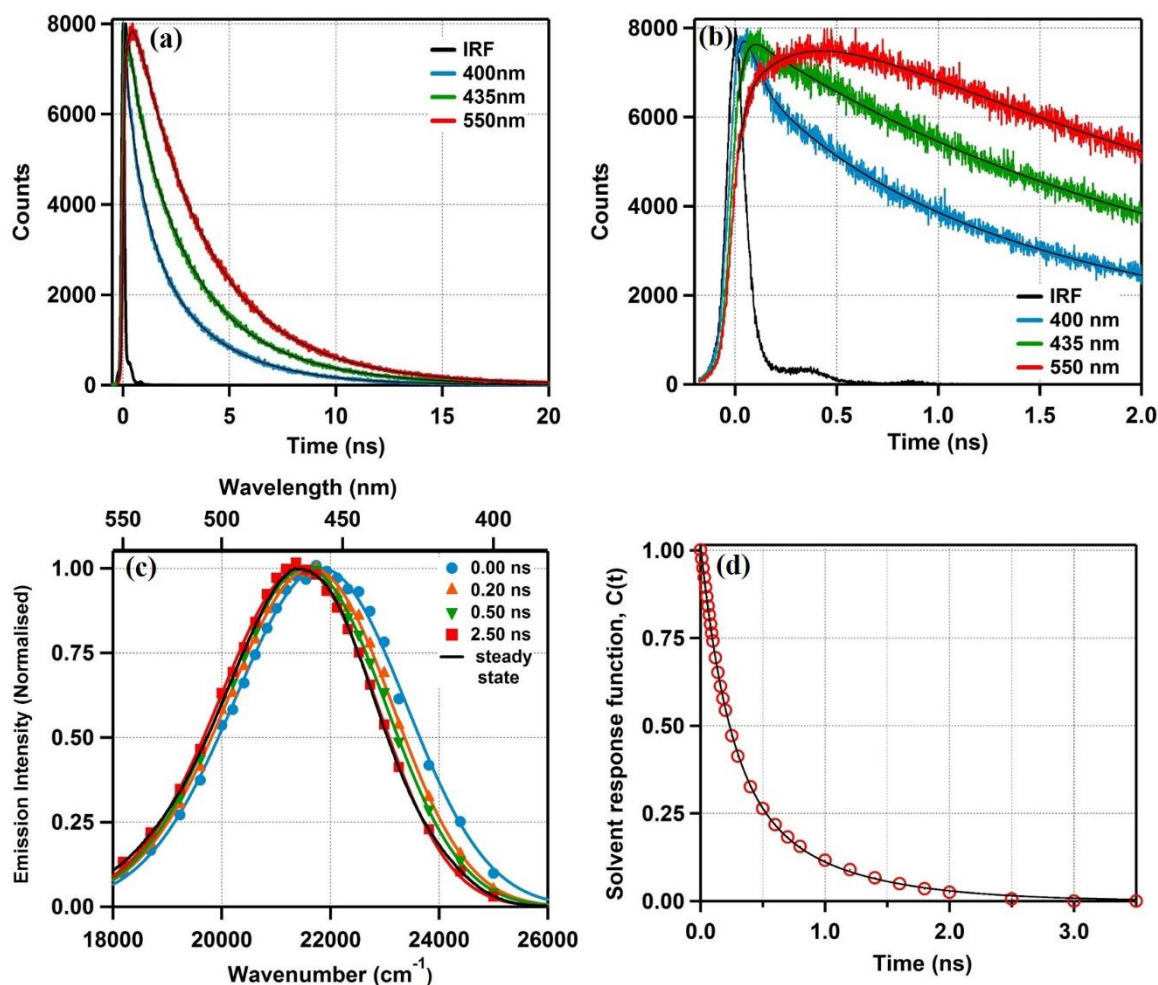


Figure 3.2. (a) & (b) A few representative transient decays of CPM tagged to Cys-121 of β -lactoglobulin collected at a longer (a) and a shorter (b) timescales. (c) Time-resolved emission spectra (TRES) constructed using the fitting parameters of the transient decays ($\lambda_{ex} = 375.8$ nm) and (d) the solvent response function calculated using the peak frequencies of TRES.

3.2.2 Solvation dynamics inside domain-I of HSA monitored using DACIA

The normalised absorption and emission spectra of DACIA tagged to Cys-34 of HSA located at its domain-I is given in figure 3.3. Solvation dynamics of this DACIA-tagged HSA was also carried out in a similar manner as mentioned in the previous section. In this case, the transients at 20 different wavelengths along the steady-state emission spectrum were recorded. Some of the decay profiles collected in longer and shorter time windows are shown in figure 3.4(a) and figure 3.4(b), respectively. The growth components at longer wavelengths can be clearly seen in the figures. The fitting of the transients was also done similarly as mentioned in the previous section. At 405 nm, the components of lifetime were found to be 0.13 ns (41%), 1.04 (30%) ns and 3.70 ns (29%) while at 550 nm, the three components were

found to be 0.37 ns (-18%), 1.26 ns (43%) and 4.86 ns (75%) with the average lifetime being 1.44 ns and 4.07 ns, respectively. The three lifetime-components at different wavelengths collected are given in table 3.2. The time-resolved emission spectra were constructed from the decay components, some of which along with the steady state emission spectrum are shown in figure 3.4(c). The solvent correlation function was constructed from the peak frequencies of TRES.

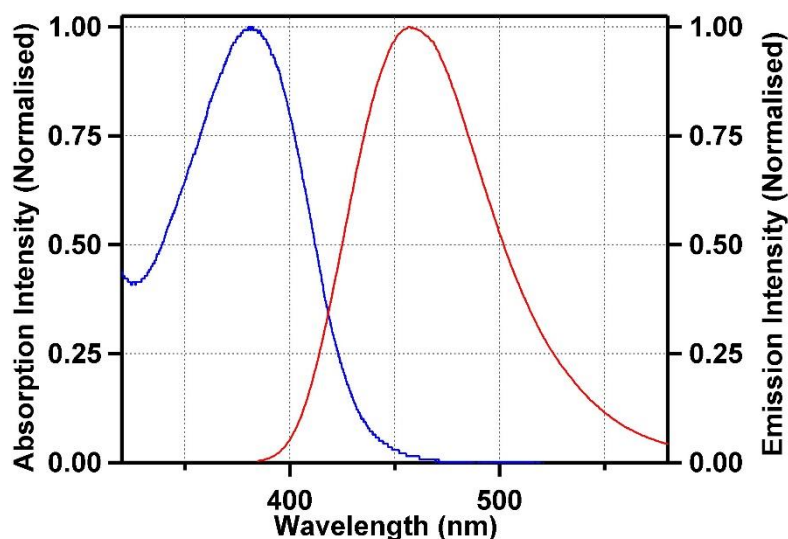


Figure 3.3. Normalised absorption and emission spectra ($\lambda_{ex}=381$ nm) of DACIA-tagged HSA

While constructing the solvent response function from TRES, we observed that the convergence of data was not very good, which may be arising due to the complex environment and constant fluctuations of the protein core.²⁴ In cases like this, choosing an appropriate $\nu(\infty)$ value could be challenging and any change in the chosen $\nu(\infty)$ value usually changes the value of the solvation time drastically. For our experiments, the time spectrum whose peak frequency closely matches to that of the steady-state spectrum has been chosen as the $\nu(\infty)$. The solvent correlation function thus constructed is shown in figure 3.4(d) along with its biexponential fitting. The two time components obtained are 0.15 ns (55%) and 0.68 ns (45%). The average solvation time is calculated to be 0.39 ns and the dynamic Stokes shift was found to be 479 cm^{-1} .

Table 3.2. Fitting parameters of the transient decays of DACIA tagged to Cys-34 of HSA at different wavelengths. The sample was excited at 375.8 nm.

λ_{em} (nm)	a_1	τ_1 (ns) ^a	a_2	τ_2 (ns) ^b	a_3	τ_3 (ns) ^c	$\langle\tau\rangle$ (ns)
405	0.41	0.13	0.30	1.04	0.29	3.67	1.43
415	0.35	0.13	0.30	1.09	0.35	3.88	1.73
420	0.32	0.13	0.31	1.10	0.37	3.92	1.83
425	0.29	0.14	0.31	1.14	0.40	3.98	1.99
430	0.28	0.14	0.32	1.22	0.40	4.10	2.07
435	0.24	0.17	0.33	1.29	0.43	4.18	2.26
440	0.22	0.18	0.33	1.33	0.45	4.29	2.41
445	0.19	0.19	0.32	1.35	0.49	4.26	2.56
450	0.18	0.19	0.33	1.44	0.49	4.35	2.64
455	0.15	0.21	0.33	1.50	0.52	4.43	2.83
460	0.13	0.19	0.33	1.50	0.54	4.44	2.92
465	0.06	0.22	0.36	1.40	0.58	4.56	3.16
470	0.02	0.21	0.36	1.35	0.62	4.53	3.30
475	-0.03	0.50	0.38	1.28	0.65	4.65	3.49
480	-0.04	0.45	0.42	1.38	0.62	4.82	3.55
490	-0.08	0.46	0.38	1.24	0.70	4.64	3.68
500	-0.10	0.42	0.41	1.32	0.69	4.76	3.78
510	-0.11	0.42	0.40	1.36	0.71	4.75	3.87
525	-0.11	0.40	0.38	1.38	0.73	4.72	3.93
550	-0.18	0.37	0.43	1.26	0.75	4.86	4.12

^a± 0.02 ns, ^b± 0.05 ns, ^c± 0.20 ns*This space intentionally left blank*

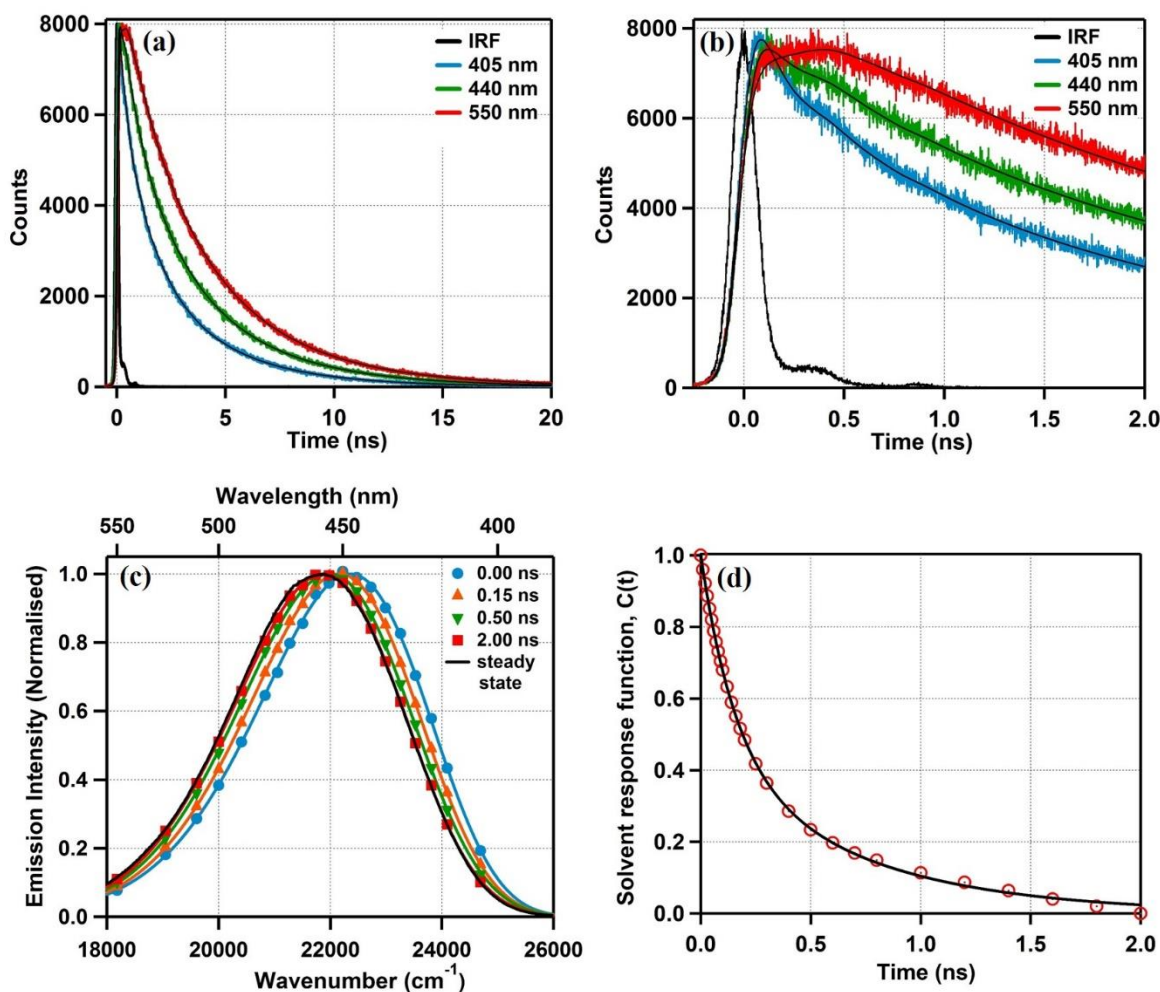


Figure 3.4. (a) & (b) A few representative transient decays of DACIA tagged to Cys-34 of HSA collected at a longer (a) and a shorter (b) timescales. (c) Time-resolved emission spectra (TRES) constructed using the fitting parameters of the transient decays ($\lambda_{ex} = 375.8$ nm) and (d) the solvent response function calculated using the peak frequencies of TRES.

3.2.3 Solvation dynamics inside domain-I of HSA monitored using CPM

The normalised absorption and emission spectra of 7-diethylamino-3-(4-maleimidophenyl)-4-methylcoumarin (CPM) tagged to Cys-34 of domain-I of HSA are shown in figure 3.5. In this case, transients were collected at 24 different wavelengths along the steady state emission spectrum. The lifetime-components obtained by fitting the transients at different wavelengths using a triexponential function are given in table 3.3. At higher wavelengths, the negative amplitudes of the shortest lifetime-components can be seen. At 410 nm, the average lifetime was found to be 0.57 ns with the three lifetime-components 0.08 ns (66%), 0.70 ns (22%) and 2.99 ns (12%) and at 550 nm the average lifetime was found to be 4.92 ns with lifetime-components 0.09 ns (-31%), 1.95 ns (49%) and 4.81 ns (47%).

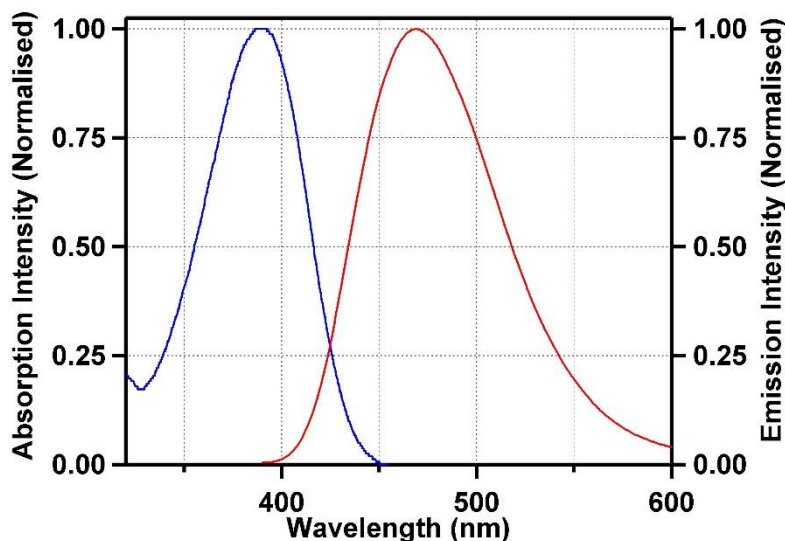


Figure 3.5. Normalised absorption and emission spectra (λ_{ex} = 390 nm) of CPM-tagged HSA.

Table 3.3. Fitting parameters of CPM tagged to Cys-34 of HSA at different wavelengths. The sample was excited at 375.8 nm.

λ_{em}	a_1	τ_1 (ns) ^a	a_2	τ_2 (ns) ^b	a_3	τ_3 (ns) ^c	$\langle \tau \rangle$ (ns)
410	0.66	0.08	0.22	0.70	0.12	2.99	0.57
420	0.57	0.09	0.26	0.77	0.16	3.32	0.78
425	0.55	0.10	0.27	0.83	0.18	3.45	0.90
430	0.5	0.10	0.28	0.86	0.22	3.61	1.09
435	0.46	0.11	0.29	0.93	0.25	3.74	1.26
440	0.41	0.12	0.29	0.96	0.30	3.75	1.45
445	0.37	0.12	0.30	1.03	0.33	3.86	1.63
450	0.34	0.13	0.29	1.14	0.37	3.90	1.82
455	0.31	0.15	0.28	1.25	0.40	3.96	1.98
460	0.28	0.12	0.29	1.15	0.42	4.09	2.08
465	0.27	0.12	0.28	1.18	0.45	4.08	2.20
470	0.22	0.15	0.31	1.44	0.47	4.16	2.43
475	0.20	0.20	0.30	1.50	0.50	4.19	2.59
480	0.17	0.23	0.31	1.60	0.52	4.26	2.75
485	0.13	0.24	0.33	1.62	0.54	4.25	2.86
490	0.10	0.22	0.37	1.56	0.54	4.51	3.03
495	0.06	0.22	0.32	1.33	0.62	4.33	3.12
500	0.02	0.21	0.33	1.27	0.65	4.39	3.28
505	-0.02	0.03	0.33	1.23	0.69	4.46	3.48
510	-0.07	0.04	0.39	1.44	0.68	4.64	3.71
515	-0.10	0.05	0.42	1.36	0.69	4.46	3.64
525	-0.17	0.08	0.4	1.58	0.78	4.64	4.24
535	-0.24	0.10	0.47	1.83	0.76	4.82	4.50
550	-0.31	0.09	0.49	1.95	0.83	4.81	4.92

^a ± 0.02 ns, ^b ± 0.05 ns, ^c ± 0.20 ns

The solvent correlation function constructed using the peak frequencies of the TRES showed a biexponential decay with solvation time components 0.11 ns

(55%) and 0.76 ns (45%) with an average solvation time of 0.40 ns and the Stokes shift was found to be 856 cm^{-1} .

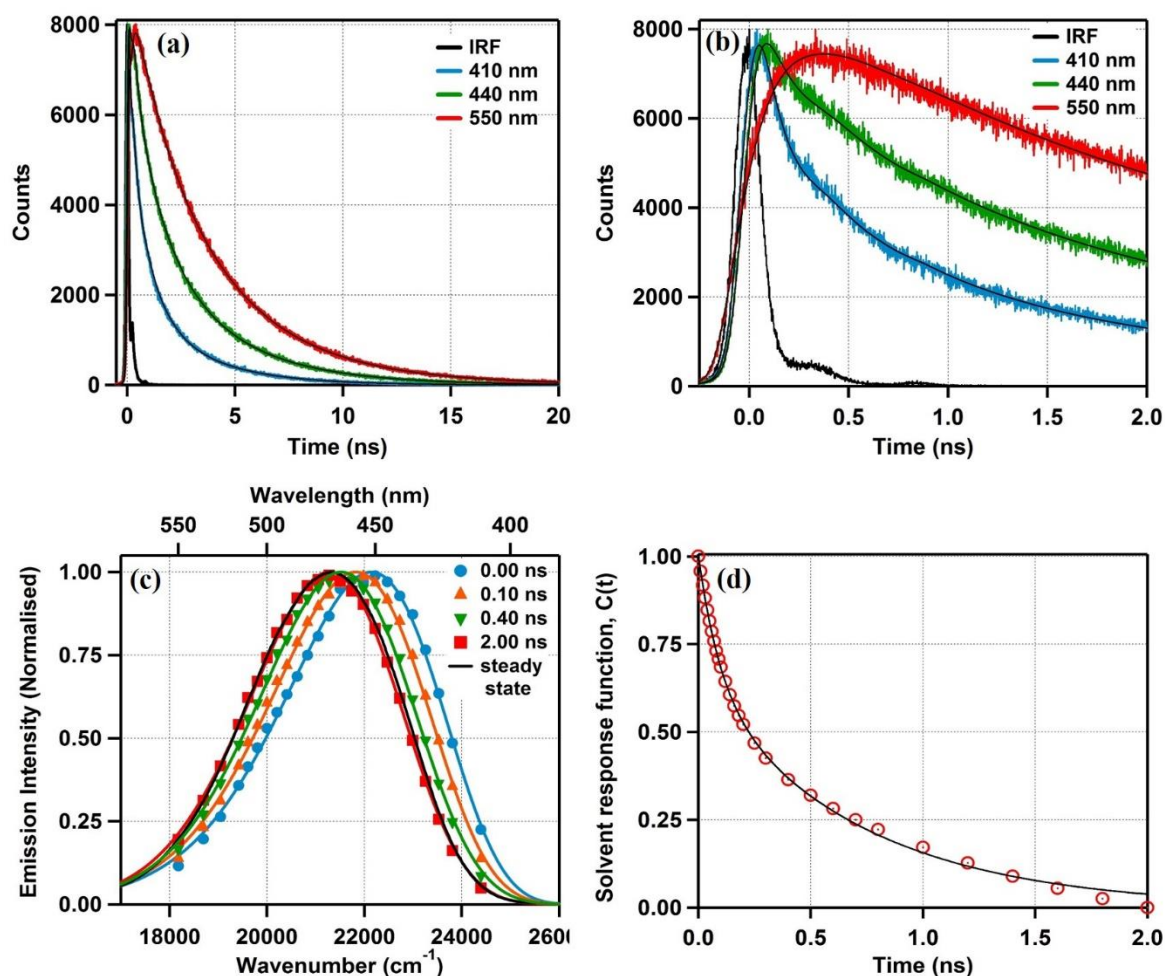


Figure 3.6. (a) & (b) A few representative transient decays of CPM tagged to Cys-34 of HSA collected at a longer (a) and a shorter (b) timescales. (c) Time-resolved emission spectra (TRES) constructed using the fitting parameters of the transient decays ($\lambda_{ex}=375.8$ nm) and (d) the solvent response function calculated using the peak frequencies of TRES.

3.2.4 Solvation dynamics inside domain-III of HSA monitored using NPCE

The normalised absorption and emission spectra of p-nitrophenyl coumarin ester (NPCE) tagged to Tyr-411 residue of domain-III of HSA are shown in figure 3.7. Solvation dynamics was studied by collecting fluorescence transients at 13 different wavelengths along the steady-state emission spectrum. The lifetime-components of the decay collected at 452 nm were found to be 0.27 ns (33%), 1.69 ns (30%) and 3.87 ns (37%) with an average lifetime of 2.03 ns while at 600 nm, the average lifetime was found to be 3.83 ns with lifetime components 0.43 ns (-6%), 2.60 ns (51%) and 4.60 ns (55%). Lifetime-components at all the wavelengths at

which the decay were collected are given in table 3.4 and some of the transients are plotted in figure 3.8(a) and (b).

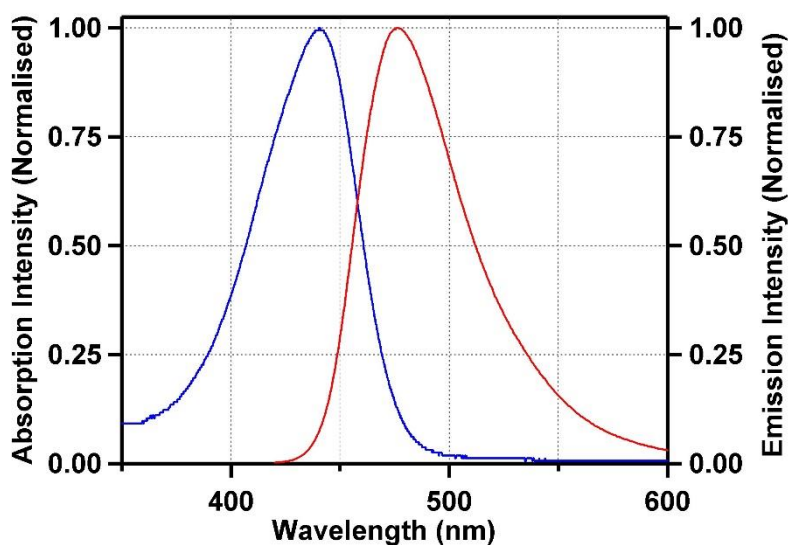


Figure 3.7. Normalised absorption and emission spectra ($\lambda_{ex} = 447$ nm) of NPCE-tagged HSA

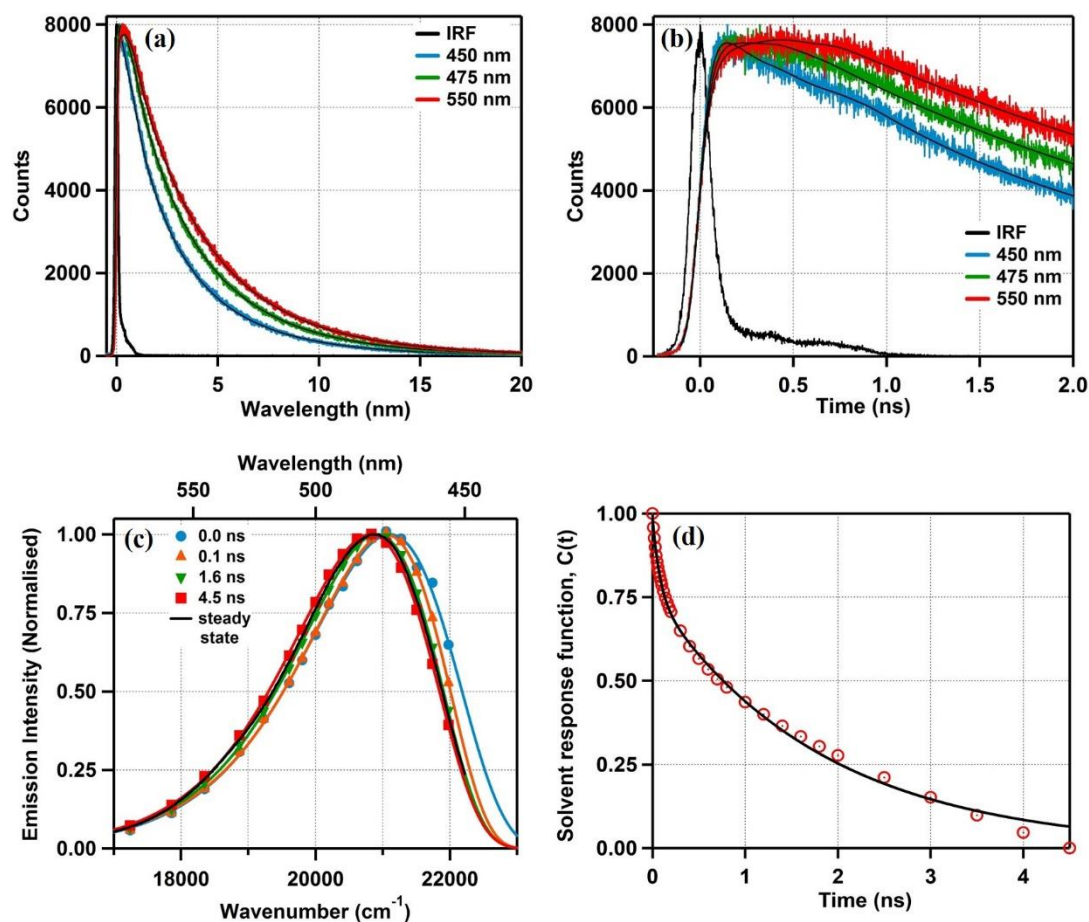


Figure 3.8. (a) & (b) A few representative transient decays of NPCE tagged to Tyr-411 of HSA collected at a longer (a) and a shorter (b) timescales. (c) Time-resolved emission spectra

(TRES) constructed using the fitting parameters of the transient decays ($\lambda_{ex}=442$ nm) and (d) the solvent response function calculated using the peak frequencies of TRES.

The TRES constructed using the decay components along with the steady-state spectrum are shown in figure 3.8(c). The dynamic Stokes shift was found to be 225 cm^{-1} in this case. The two components of solvation dynamics (figure 3.8 (d)) obtained by fitting the solvent correlation function using a biexponential equation were found to be 0.05 ns (23%) and 0.97 ns (77%) with an average solvation time of 0.76 ns.

Table 3.4. Fitting parameters of transient decays of NPCE tagged to Tyr-411 of HSA at different wavelengths. The sample are excited at 442 nm.

λ_{em} (nm)	a_1	τ_1 (ns) ^a	a_2	τ_2 (ns) ^b	a_3	τ_3 (ns) ^c	$\langle\tau\rangle$ (ns)
452	0.33	0.27	0.30	1.69	0.37	3.87	2.03
456	0.32	0.32	0.31	1.82	0.37	3.91	2.11
460	0.26	0.30	0.28	1.58	0.46	3.91	2.32
468	0.10	0.04	0.38	1.71	0.52	4.03	2.75
481	-0.41	0.01	0.73	2.39	0.68	4.42	4.75
487	-0.06	0.51	0.47	2.16	0.59	4.32	3.53
495	-0.08	0.47	0.51	2.38	0.57	4.40	3.68
500	-0.09	0.48	0.43	2.09	0.66	4.35	3.73
510	-0.09	0.46	0.49	2.37	0.60	4.40	3.76
520	-0.08	0.46	0.44	2.24	0.64	4.42	3.78
530	-0.09	0.43	0.46	2.40	0.63	4.47	3.88
550	-0.07	0.41	0.50	2.60	0.57	4.60	3.89
600	-0.06	0.43	0.51	2.60	0.55	4.60	3.83

^a ± 0.02 ns, ^b ± 0.05 ns, ^c ± 0.20 ns

3.2.5 Solvation dynamics inside papain monitored using DACIA

Solvation dynamics of N-(7-dimethylamino-4-methylcoumarin-3-yl) iodoacetamide (DACIA) inside papain was studied by tagging DACIA to Cys-25 amino acid residue of papain. (Normalised absorption and emission spectra are given in figure 3.9) The fluorescent transients were collected at 18 different wavelengths along the steady-state emission spectrum. The average lifetime at 410 nm was found to be 1.21 ns with the three lifetime-components 0.10 ns (40%), 0.85 ns (29%), 2.98 ns (31%) and at 550 nm the average lifetime was found to be 2.74 ns with three lifetime components 0.30 ns (-14%), 1.99 ns (86%) and 3.82 ns (28%). The transients collected at two different time windows are shown in figure 3.10(a) & (b) and the fitting parameters are tabulated in table 3.5. Figure 3.10(c) shows the time-

resolved emission spectra along with the steady-state emission spectrum. The solvent correlation function is shown in figure 3.10(d). The average solvation time was found to be 0.22 ns with two components 0.03 ns (17%) and 0.26 ns (83%) and the dynamic Stokes shift was found to be 124 cm^{-1} .

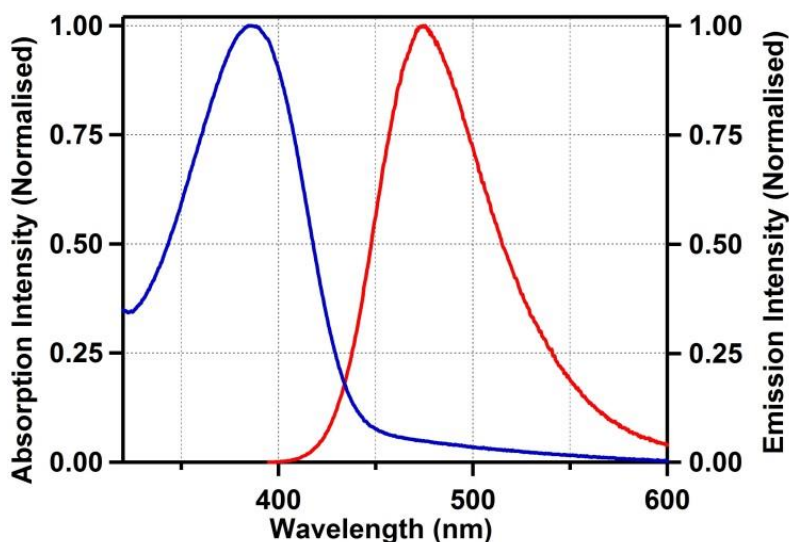


Figure 3.9. Normalised absorption and emission spectra (λ_{ex} = 389 nm) of DACIA-tagged papain.

Table 3.5. Fitting parameters of transient decays of DACIA tagged to papain at different wavelengths. The sample was excited at 375.8 nm.

λ_{em} (nm)	a_1	τ_1 (ns) ^a	a_2	τ_2 (ns) ^b	a_3	τ_3 (ns) ^c	$\langle \tau \rangle$ (ns)
410	0.40	0.09	0.29	0.85	0.31	2.98	1.21
420	0.35	0.11	0.26	0.87	0.39	3.07	1.46
430	0.23	0.11	0.24	0.74	0.53	3.08	1.84
440	0.17	0.11	0.34	1.23	0.49	3.35	2.08
450	0.08	0.08	0.44	1.51	0.48	3.48	2.34
460	0.03	0.05	0.51	1.70	0.46	3.59	2.52
465	0.01	0.03	0.52	1.78	0.47	3.62	2.63
470	0.01	0.01	0.54	1.80	0.45	3.63	2.61
474	-0.01	0.02	0.58	1.89	0.43	3.69	2.68
478	-0.10	0.51	0.78	1.90	0.33	3.72	2.66
483	-0.10	0.45	0.80	1.92	0.31	3.72	2.64
490	-0.11	0.33	0.79	1.94	0.32	3.74	2.69
500	-0.11	0.33	0.82	1.99	0.29	3.78	2.69
510	-0.12	0.38	0.82	1.95	0.30	3.72	2.67
520	-0.13	0.30	0.87	2.00	0.26	3.78	2.68
530	-0.13	0.28	0.91	2.06	0.22	3.89	2.69
540	-0.13	0.32	0.92	2.07	0.21	3.91	2.68
550	-0.14	0.30	0.86	1.99	0.28	3.82	2.74

^a ± 0.02 ns, ^b ± 0.05 ns, ^c ± 0.20 ns

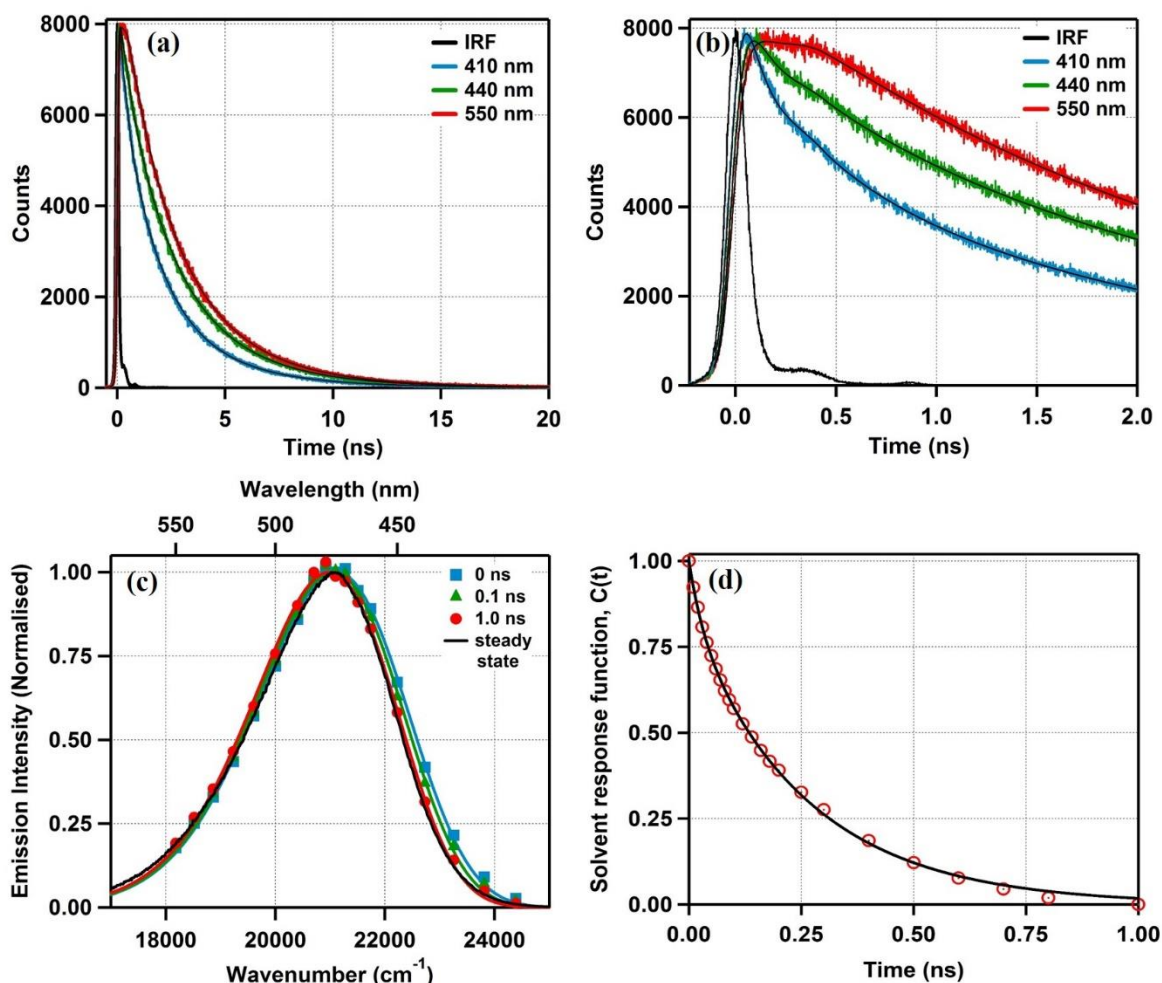


Figure 3.10. (a) & (b) A few representative transient decays of DACIA tagged to Cys-25 of Papain collected at a longer (a) and a shorter (b) timescales. (c) Time-resolved emission spectra (TRES) constructed using the fitting parameters of the transient decays ($\lambda_{ex} = 375.8$ nm) and (d) the solvent response function calculated using the peak frequencies of TRES.

3.2.6 Solvation dynamics inside bromelain monitored using CPM

Solvation dynamics of CPM molecule tagged to Cys-26 of bromelain was studied by recording the fluorescent transients at 21 different wavelengths (figure 3.12(a) and (b)) (the absorption and emission spectra are shown in figure 3.11). The excited state lifetime-components at each wavelength are compiled in table 3.6. At 405 nm, the three lifetime-components were found to be 0.16 ns (41%), 0.96 (23%) and 3.24 (36%), with an average lifetime of 1.45 ns. At 540 nm, the average lifetime was found to be 4.16 ns with three components of 0.28 ns (16%), 3.00 ns (81%) and 5.08 (35%). The time-resolved emission spectra along with the steady-state emission spectra are shown in figure 3.12 (c) from which the dynamic Stokes shift was

calculated as 392 cm^{-1} . The average solvation time was found to be 0.93 ns with the two components 0.29 ns (64%) and 2.07 ns (36%).

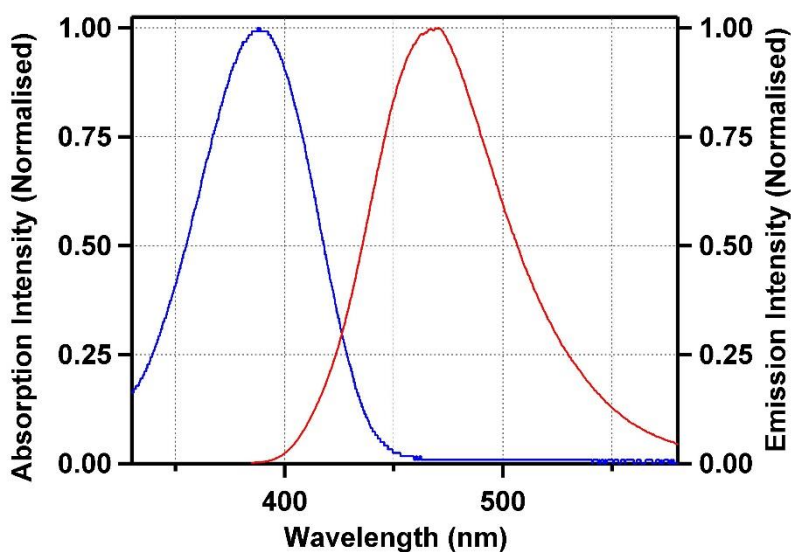


Figure 3.11. Normalised absorption and emission spectra ($\lambda_{ex} = 390 \text{ nm}$) of CPM-tagged Bromelain.

Table 3.6. Fitting parameters of transient decays of CPM tagged to bromelain at different wavelengths. The sample was excited at 375.8 nm.

λ_{em}	a_1	$\tau_1 \text{ (ns)}^a$	a_2	$\tau_2 \text{ (ns)}^b$	a_3	$\tau_3 \text{ (ns)}^c$	$\langle \tau \rangle \text{ (ns)}$
405	0.41	0.16	0.23	0.96	0.36	3.24	1.45
415	0.35	0.18	0.23	1.07	0.42	3.39	1.73
425	0.32	0.22	0.25	1.40	0.43	3.67	2.00
430	0.30	0.22	0.27	1.50	0.43	3.83	2.12
435	0.27	0.27	0.33	1.93	0.40	3.99	2.31
440	0.24	0.26	0.34	1.85	0.42	4.15	2.43
445	0.21	0.29	0.40	2.20	0.39	4.26	2.60
450	0.18	0.32	0.56	2.63	0.26	4.69	2.75
455	0.15	0.33	0.64	2.80	0.21	4.96	2.88
460	0.12	0.40	0.62	2.84	0.26	4.71	3.03
465	0.08	0.35	0.57	2.57	0.35	4.99	3.24
470	-0.27	2.06	0.80	2.05	0.47	5.25	3.55
475	-0.21	2.17	0.74	2.19	0.47	5.14	3.58
480	-0.23	2.30	0.79	2.35	0.44	5.00	3.53
485	-0.21	2.60	0.92	2.75	0.29	5.29	3.52
490	-0.27	1.83	0.98	2.48	0.29	5.59	3.56
495	-0.24	2.46	1.12	3.03	0.12	5.65	3.48
505	-0.07	0.11	0.89	3.10	0.18	5.47	3.74
515	-0.12	0.10	0.98	3.19	0.14	5.06	3.82
525	-0.21	0.85	0.66	1.77	0.55	4.87	3.67
540	-0.16	0.28	0.81	3.00	0.35	5.08	4.16

^a $\pm 0.02 \text{ ns}$, ^b $\pm 0.05 \text{ ns}$, ^c $\pm 0.20 \text{ ns}$

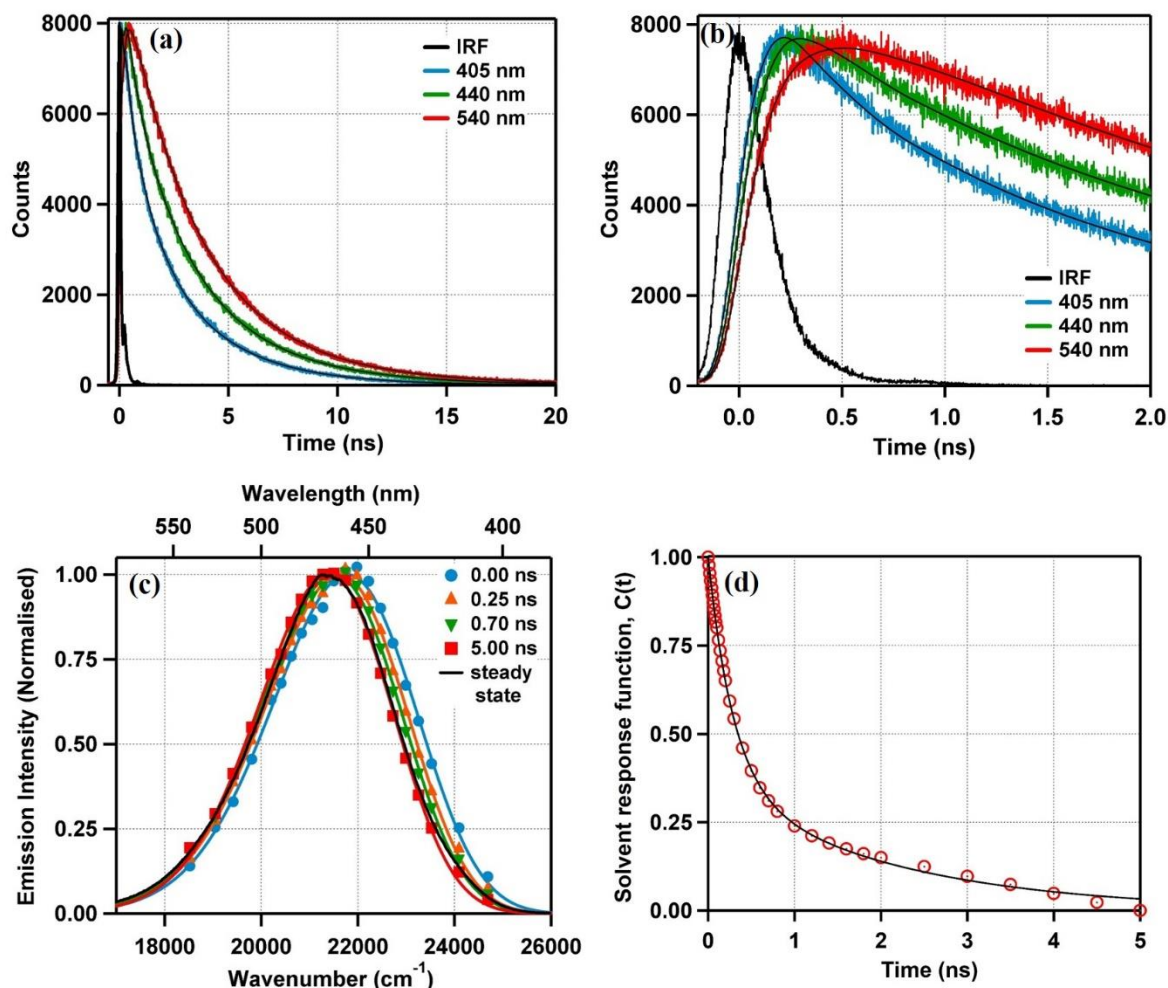


Figure 3.12. (a) & (b) A few representative transient decays of CPM tagged to Cys-26 of bromelain collected at a longer (a) and a shorter (b) timescales. (c) Time-resolved emission spectra (TRES) constructed using the fitting parameters of the transient decays ($\lambda_{ex} = 375.8$ nm) and (d) the solvent response function calculated using the peak frequencies of TRES.

3.3 Discussion

In this work, we have used four different proteins, β -lactoglobulin, human serum albumin, papain and bromelain and have studied the solvation dynamics at the core of these protein molecules using different fluorescent tags. The probe molecules, which were used to tag different proteins are CPM, DACIA and NPCE. One of the probe molecules, CPM was used to tag three of the proteins, β -lactoglobulin, HSA and bromelain. Cys-34 amino acid moiety of domain-I of HSA was tagged using two molecules, CPM and DACIA. Also, two different sites of HSA were tagged – Cys-34 of domain-I was tagged using DACIA and Tyr-411 of domain-III was tagged with NPCE – separately. In this manner, we intend to study (i) the effect of probe molecules on solvation dynamics, (ii) how solvation dynamics varies

among different proteins and (iii) the site-specific variation of solvation dynamics within a protein. The data obtained has been compiled in table 3.7 where the two components of solvation time, average solvation times and dynamic Stokes shifts are mentioned. In our experiments using ~100 ps time resolution, a significant portion of the total Stokes shift has not been observed and what we are observing here is the slowest part of the solvation dynamics. The missing components of dynamic Stokes shift in our set up were calculated using the method demonstrated by Fee and Maroncelli.²⁵ The emission frequency at time zero, $\nu_{em}^p(0)$ was calculated using

$$\nu_{em}^p(0) = \nu_{abs}^p - [\nu_{abs}^{np} - \nu_{em}^{np}] \quad (3.1)$$

where, ν_{abs}^p is the absorption frequency in a polar medium and ν_{abs}^{np} and ν_{em}^{np} denote the steady state absorption and emission frequencies of the probe molecule in a non-polar medium (in our case, cyclohexane). The missing components of Stokes shift are also listed in table 3.7.

Table 3.7. Solvation time components, average solvation times, dynamic Stokes shifts and the missing components of different probe molecules tagged to different protein molecules. The fractional components are given in parentheses.

Probe molecule	Protein molecule and the binding site	τ_{s1} (ns)	τ_{s2} (ns)	$\langle \tau_s \rangle$ (ns)	Stokes shift (cm ⁻¹)	Missing component (%)
CPM	β -lactoglobulin, Cys-121	0.22 (0.63)	0.78 (0.37)	0.43	386	80
DACIA	HSA, Cys-34	0.15 (0.55)	0.68 (0.45)	0.39	479	64
CPM	HSA, Cys-34	0.11 (0.55)	0.76 (0.45)	0.40	856	56
NPCE	HSA, Tyr-411	0.05 (0.23)	0.97 (0.77)	0.76	225	85
DACIA	Papain, Cys-25	0.03 (0.17)	0.26 (0.83)	0.22	124	94
CPM	Bromelain, Cys-26	0.29 (0.64)	2.07 (0.36)	0.93	392	82

From the above table, it could be noticed that the solvation dynamics at Cys-34 of HSA differs only by 2.5% when tagged with DACIA or CPM. Also, it could be seen that the solvation time components and their fractional amplitudes are also quite similar. This indicates that the solvation time does not depend on the probe molecule, and it is a characteristic of the environment. However, the dynamic Stokes shift in these two cases differ by 377 cm⁻¹ (479 cm⁻¹ in the case of DACIA-tagged

HSA and 856 cm^{-1} in the case of CPM-tagged HSA). This is because of the difference in the excited state dipole moment of the two molecules, which results in a difference in the energy gap between the ground state and excited state energy levels of the two probe molecules. To get an idea about the dependence of protein environment on solvation dynamics, we can compare the solvation dynamics at two different sites of HSA, Cys-34 of domain-I and Tyr-411 of domain-III tagged with DACIA and NPCE, respectively. As solvation time is not affected by the choice of probe molecule, any change in solvation time will be due to the difference in the protein environment in which the probe molecule is present. From table 3.7, it could be seen that the solvation dynamics at the two different sites of HSA, Cys-34 and Tyr-411 are quite different with average solvation times 0.39 ns and 0.76 ns, respectively. A comparison between the average solvation times monitored at Cys-34 of HSA monitored using DACIA and CPM probe molecules and that monitored at two different sites of HSA are given in figure 3.13.

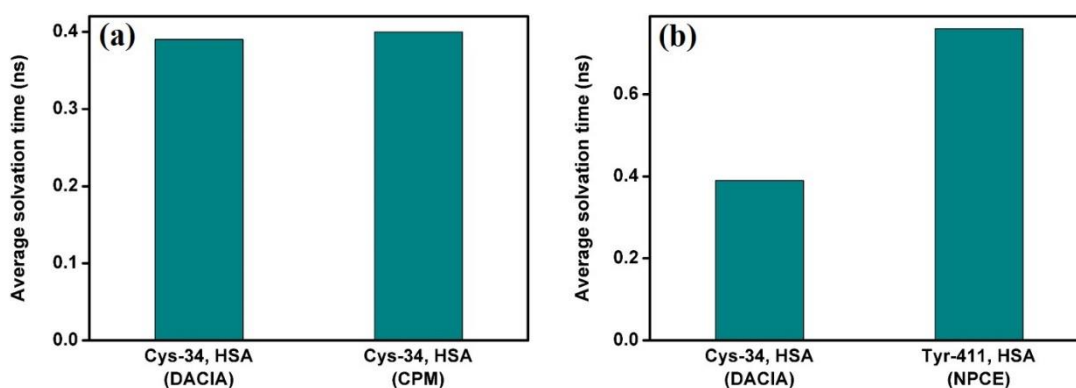
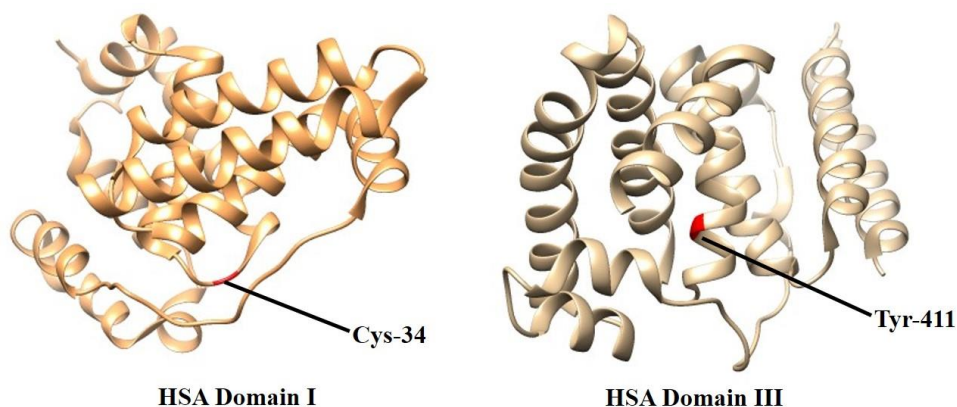


Figure 3.13. (a) Comparison of average solvation time monitored at Cys-34 site of HSA using two different probe molecules (b) comparison of average solvation time monitored at two different sites of HSA, Cys-34 and Tyr-411. The probe molecule used in each case is mentioned in parentheses.

The difference in solvation times at Cys-34 and Tyr-411 of HSA is due to the different environments in which the two amino acid moieties and their probe molecules are present. In scheme 3.3, the positions of DACIA and NPCE tagging sites inside domain-I and domain-III are shown using the structure of HSA obtained from the RCSB protein database.²⁶ The faster solvation inside domain-I can be

attributed to the less crowded environment around Cys-34 on which the DACIA is covalently attached.



Scheme 3.3. Figure showing the binding sites of DACIA (Cys-34) and NPCE (Tyr-411) on human serum albumin (PDB: 1HA2).

Finally, in figure 3.14, a comparison of solvation dynamics monitored in different proteins are shown. As evident from the figure, the average solvation time differs from protein to protein according to the environment in which the probe molecule is present. Among the proteins we have monitored, solvation dynamics is the fastest at Cys-25 site of papain and the slowest in the case of Cys-26 site of bromelain. This random variation in solvation time inside different proteins is expected as solvation time depends upon the mobility of water molecules around the solvatochromic probe which is affected by the nature of amino acid moieties in the immediate environment.

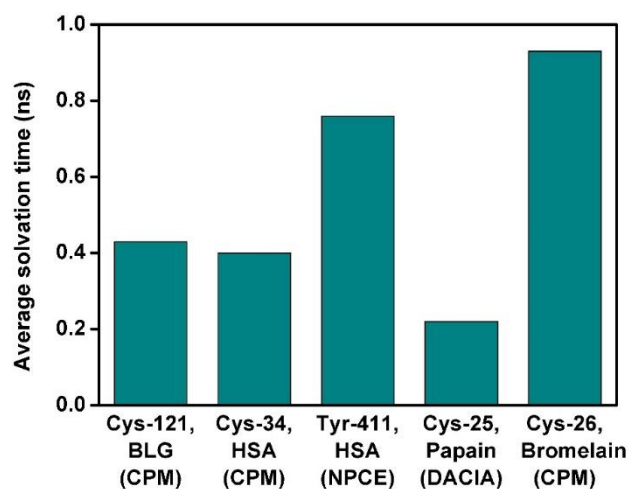


Figure 3.14. Average solvation time monitored at different sites of different proteins. The probe molecule used for monitoring the solvation are mentioned in parentheses.

3.4 Conclusion

We have studied the solvation dynamics of water inside four proteins, human serum albumin, papain, β -lactoglobulin and bromelain with the help of three fluorescent tags, namely, CPM, DACIA and NPCE. In the case of HSA, solvation dynamics at two different sites, at Cys-34 and Tyr-411, has been studied. Also at Cys-34 site of HSA, solvation was monitored with the help of two different probes, CPM and DACIA. The value of average solvation time at Cys-34 site while monitored using DACIA or CPM was found to be very similar, 0.39 ns and 0.40 ns respectively. This would suggest that the hydration dynamics at a particular site of a protein is independent of the probe molecule used for monitoring. However, the solvation time monitored at different sites of different proteins were found to vary widely depending on the environment of the probe molecule inside the protein, with the maximum value in the case of bromelain with 0.93 ns and the smallest being in the case of papain with 0.22 ns. Solvation time was also found to vary at different sites of the same protein. At Cys-34 and Tyr-411 of human serum albumin the average solvation time were found to be 0.40 ns and 0.76 ns respectively, indicating that solvation time varies according to the immediate environment of the probe molecule even within the same protein.

References

- (1) Bagchi, B. *Water in Biological and Chemical Processes: From Structure and Dynamics to Function*; Cambridge University Press: Cambridge, 2013.
- (2) Lynden-Bell, R. M.; Morris, S. C.; Barrow, J. D.; Finney, J. L.; Harper, C. *Water and Life: The Unique Properties of H₂O*, 1st ed.; CRC Press: Boca Raton, 2010.
- (3) Zhong, D.; Pal, S. K.; Zewail, A. H. *Biological Water: A Critique*. *Chem. Phys. Lett.* **2011**, 503, 1–11.
- (4) Meyer, E. Internal Water Molecules and H-Bonding in Biological Macromolecules: A Review of Structural Features with Functional Implications. *Protein Sci.* **1992**, 1, 1543–1562.
- (5) Ball, P. Water as an Active Constituent in Cell Biology. *Chem. Rev.* **2008**, 108, 74–108.
- (6) Bellissent-Funel, M.-C.; Hassanali, A.; Havenith, M.; Henchman, R.; Pohl, P.; Sterpone, F.; van der Spoel, D.; Xu, Y.; Garcia, A. E. Water Determines the Structure and Dynamics of Proteins. *Chem. Rev.* **2016**, 116, 7673–7697.
- (7) Bagchi, B. Water Dynamics in the Hydration Layer around Proteins and Micelles. *Chem. Rev.* **2005**, 105, 3197–3219.
- (8) Levy, Y.; Onuchic, J. N. Water Mediation in Protein Folding and Molecular Recognition. *Annu. Rev. Biophys. Biomol. Struct.* **2006**, 35, 389–415.
- (9) Levy, Y.; Onuchic, J. N. Water and Proteins: A Love–hate Relationship. *Proc. Natl. Acad. Sci. U. S. A.* **2004**, 101, 3325–3326.
- (10) Cheung, M. S.; García, A. E.; Onuchic, J. N. Protein Folding Mediated by Solvation: Water Expulsion and Formation of the Hydrophobic Core Occur after the Structural Collapse. *Proc. Natl. Acad. Sci.* **2002**, 99, 685–690.
- (11) Nandi, N.; Bagchi, B. Dielectric Relaxation of Biological Water. *J. Phys. Chem. B* **1997**, 101, 10954–10961.
- (12) Kuntz, I. D.; Kauzmann, W. Hydration of Proteins and Polypeptides; Anfinsen, C. B., Edsall, J. T., Richards, F. M. B. T.-A. in P. C., Eds.; Academic Press, 1974; Vol. 28, pp 239–345.
- (13) Pethig, R. Protein-Water Interactions Determined by Dielectric Methods. *Annu. Rev. Phys. Chem.* **1992**, 43, 177–205.
- (14) Ghisaidoobe, A. B. T.; Chung, S. J. Intrinsic Tryptophan Fluorescence in the Detection and Analysis of Proteins: A Focus on Förster Resonance Energy Transfer Techniques. *Int. J. Mol. Sci.* **2014**, 15, 22518–22538.
- (15) Chen, Y.; Barkley, M. D. Toward Understanding Tryptophan Fluorescence in Proteins. *Biochemistry* **1998**, 37, 9976–9982.
- (16) Vivian, J. T.; Callis, P. R. Mechanisms of Tryptophan Fluorescence Shifts in Proteins. *Biophys. J.* **2001**, 80, 2093–2109.
- (17) Romanini, D. W.; Cornish, V. W. Protein Labelling: Playing Tag with Proteins. *Nat. Chem.* **2012**, 4, 248.

- (18) Toseland, C. P. Fluorescent Labeling and Modification of Proteins. *J. Chem. Biol.* **2013**, 6, 85–95.
- (19) Kim, Y.; Ho, S. O.; Gassman, N. R.; Korlann, Y.; Landorf, E. V; Collart, F. R.; Weiss, S. Efficient Site-Specific Labeling of Proteins via Cysteines. *Bioconjug. Chem.* **2008**, 19, 786–791.
- (20) Klymchenko, A. S. Solvatochromic and Fluorogenic Dyes as Environment-Sensitive Probes: Design and Biological Applications. *Acc. Chem. Res.* **2017**, 50, 366–375.
- (21) Trivedi, M. V; Laurence, J. S.; Siahaan, T. J. The Role of Thiols and Disulfides in Protein Chemical and Physical Stability. *Curr. Protein Pept. Sci.* **2009**, 10, 614–625.
- (22) Zavodszky, M.; Chen, C.-W.; Huang, J.-K.; Zolkiewski, M.; Wen, L.; Krishnamoorthi, R. Disulfide Bond Effects on Protein Stability: Designed Variants of Cucurbita Maxima Trypsin Inhibitor-V. *Protein Sci.* **2001**, 10, 149–160.
- (23) Maroncelli, M.; Fleming, G. R. Picosecond Solvation Dynamics of Coumarin 153: The Importance of Molecular Aspects of Solvation. *J. Chem. Phys.* **1987**, 86, 6221–6239.
- (24) Sen, P.; Pal, S.; Bagchi, B. Solvation Dynamics in Biological Systems and Organized Assemblies. **2006**, 53, 169–180.
- (25) Fee, R. S.; Maroncelli, M. Estimating the Time-Zero Spectrum in Time-Resolved Emission Measurements of Solvation Dynamics. *Chem. Phys.* **1994**, 183, 235.
- (26) Petitpas, I.; Bhattacharya, A. A.; Twine, S.; East, M.; Curry, S. Crystal Structure Analysis of Warfarin Binding to Human Serum Albumin. *J. Biol. Chem.* **2001**, 276, 22804–22809.

Chapter 4

Region-Specific Double Denaturation of Human Serum Albumin: Combined Effects of Temperature and GnHCl on Structural and Dynamical Responses

Mohan, V.; Sengupta, B.; Acharyya, A.; Yadav, R.; Das, N.; Sen, P. Region-Specific Double Denaturation of Human Serum Albumin : Combined Effects of Temperature and GnHCl on Structural and Dynamical Responses. *ACS Omega* **2018**, 3, 10406–10417.

In this work, we have investigated the effects of two denaturing agents, guanidine hydrochloride (GnHCl) and temperature on the overall structure, domain-I and domain-III of human serum albumin (HSA) using circular dichroism (CD), steady state and time-resolved fluorescence spectroscopy. CD spectroscopy studies reveal the overall denaturation of the protein. Denaturation follows the expected direction in which protein is denatured with an increase in concentration of GnHCl or temperature. α -helicity of the native state of HSA was found to be 64.2% and the minimum value of α -helicity was found to be 14.8% in the presence of 6 M of GnHCl at room temperature. Steady state emission studies were carried out on domain-I and domain-III of HSA using site-specific fluorescent tags. The degree of folding of the two domains at different combinations of temperature and GnHCl concentration were calculated and were found to follow somewhat different courses of denaturation. Variation of solvation time was also found to be quite different for these two domains. Solvation time inside domain-I tends to decrease with the action of either temperature or GnHCl. On the other hand, inside domain-III of HSA, solvation time does not show any regular change at higher temperatures or in presence of GnHCl. This difference could be attributed to the different microenvironments inside the protein cores of the two domains.

4.1 Introduction

Human serum albumin (HSA) is the most abundant transport protein present in human blood serum.¹⁻³ Being a huge protein with 585 amino acid residues and 66.5 kDa molecular weight, it has a few hydrophobic pockets which can accommodate macromolecules and transport them to specific locations of human body.⁴⁻¹⁰ HSA is responsible for the transport of a variety of molecules including carbohydrates, fatty acids, drugs and hormones.^{4,9,10} Structurally, HSA is divided into three domains, each of which consists of two subdomains.³⁻⁵ It is to be noted that all proteins, including HSA, perform their biological actions at physiological conditions when they have a specific structure, known as the native state of protein. In the native state, protein chain is folded in a unique way to minimize the destabilizing interactions. Any loss in this folded three dimensional structure under the effect of any external factors is broadly identified as denaturation of the protein and it eventually leads to the loss in its functionality.¹¹⁻¹⁸ Understanding the complex mechanism of denaturation has remained a topic of research for several decades.^{14,19} Besides this, biological and biochemical researches have been carried out to monitor the functionality of proteins as a function of external parameters and to relate it with the structural perturbations.^{20,21}

Fluorescence techniques are being vastly applied to study proteins, owing to their sensitivity towards the local environment inside proteins.²²⁻³⁸ Tyrosine and tryptophan are the two main fluorescing amino acid residues which cause intrinsic fluorescence of proteins. In most proteins, the number of these amino acid residues is more than one and they are located at different parts of the protein. For this reason, site specific information is lost and the signal depicts an overall picture. Fortunately, HSA has a single tryptophan residue located at 214th position of domain-II, which serves as an efficient marker for monitoring this domain.^{36,37} But domain-I and domain-III do not have any site-specific intrinsic fluorophores and hence fluorescent labelling is necessary to perform unfolding studies specific to domain-I or domain-III. Several reports are available on the tagging of HSA with non-covalent and covalent fluorescent markers.^{32,33,38-40} Domain-I of HSA has a single free cysteine

residue at 34th position which can be tagged with thiol specific fluorescence probes.^{32,33,38,39} Domain-III, on the other hand, has a tyrosine residue at 411th position, which is much more active than the other tyrosine residues and can be selectively labelled by hydroxyl specific fluorescent probes.⁴¹ However, no suitable fluorescent marker is available commercially to tag tyrosine residue. In one of the reports from our research group, we have designed and synthesized a fluorescent marker p-nitrophenyl coumarin ester (NPCE), which can successfully tag Tyr-411 and delivers useful domain specific informations.³⁹

There are several reports on the effect of external parameters on the structure and dynamics of proteins but there are only a few reports on the effect of more than one denaturants simultaneously.⁴² Such a situation of multiple denaturing effect is important, as similar situations may be occurring in biological systems. Moreover, the effect of such multiple denaturation may not be uniform throughout the protein structure and thus a domain-specific study is warrant. Similar studies on the effect of more than one denaturants were carried out by Shaw et al., where they observed that the donor-acceptor distance of alkali-induced conformer of HSA does not change with temperature while in the case of acid-induced and native conformer, the distance was found to decrease with increase in temperature. The donor and acceptor in this case were Trp-214 and a photosensitizing drug, protoporphyrin IX respectively.⁴³ In another study carried out by Ahmad et al., domain specific ligands have been used to study the unfolding of different domains of HSA under the action of GnHCl and they reveal that in presence of GnHCl, domain-III is more labile to unfolding, as compared to the two other domains.⁴⁴

In the present study, we aim to map the unfolding behaviour of domain-I and domain-III of HSA under a double-denaturing condition with GnHCl (0 – 6 M) and temperature (283 – 353 K). We have used steady-state as well as time-resolved fluorescence measurements to understand the nature of unfolding.

4.2 Results

4.2.1 Effect of double denaturation on the overall structure of HSA

The overall structural features of unfolding of HSA was monitored by measuring the α -helicity content by circular dichroism spectroscopy using the following equation⁴⁵

$$\% \alpha \text{ helicity} = \frac{MRE_{222} - 3000}{-36000 - 3000} \times 100 \quad (4.1)$$

where the mean molar residual ellipticity at 222 nm (MRE_{222}) is defined as

$$MRE_{222} = \frac{\theta_{222} \times M}{n \cdot c \cdot l} \quad (4.2)$$

In the above equation, θ_{222} is the intensity of CD signal at 222 nm, M is the molecular weight of HSA, n is the number of amino acid residues, c is the concentration in g/l and l is the path length of the cuvette. The helicity of native state of HSA has been calculated as 64.2%, which is in good agreement with the reported value.^{38,39}

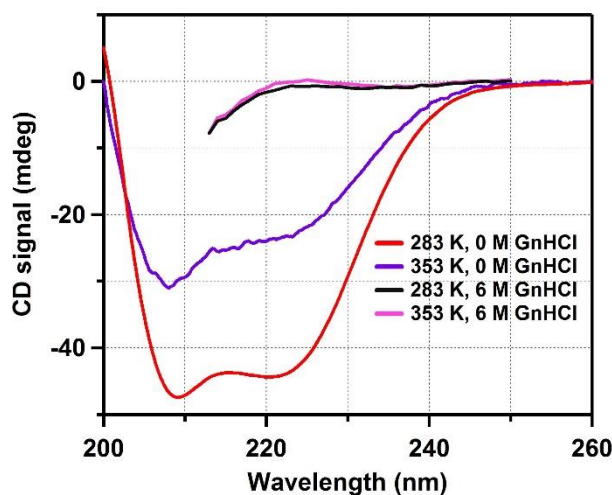


Figure 4.1. CD spectra of HSA at four different combinations of GnHCl concentration and temperature. Concentration of HSA in each case is 1.85 μ M and the path length in each case is 2 mm.

Upon denaturation, the α -helicity has been found to decrease both on increasing temperature and on increasing GnHCl concentration. At high concentrations of GnHCl, CD spectra could not be recorded below 210 nm due to significant interference from GnHCl. Figure 4.1 shows the CD spectra of HSA at

four different GnHCl – temperature combinations. The α -helicity for all the samples were calculated using the same set of equations as discussed. In the absence of GnHCl, α -helicity decreases to 38.0% at the highest temperature (353 K) whereas at room temperature, α -helicity was 14.8% at 6 M GnHCl. This value of α -helicity is the minimum value within our experimental range and it can be ascribed to the most unfolded state of HSA in our experiments. To quantify the extent of unfolding, we have written the following equation using the α -helicity content of HSA.

$$f_i = \frac{\alpha_i - \alpha_U}{\alpha_N - \alpha_U} \quad (4.3)$$

where, f_i is a measure of the degree of folding (varies between 1 and 0), α_i is the α -helicity at a particular denaturing condition (i.e. either at some specific temperature or at some specific GnHCl concentration or both together) and α_U and α_N are the α -helicities of HSA in its unfolded (i.e. in presence of 6 M GnHCl at 298 K) and native (i.e. in absence of GnHCl at 298 K) states, respectively. Figure 4.2 shows the contour diagram of the calculated extent of folding as a function of GnHCl concentration and temperature. From the contour diagram it is evident that the effect of temperature is less pronounced than the effect of GnHCl.

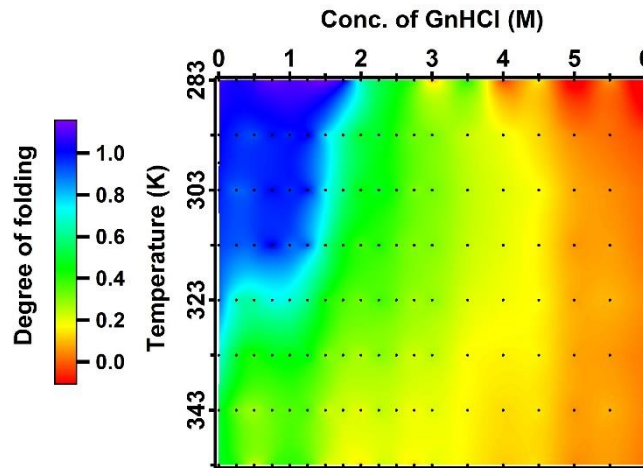


Figure 4.2. Degree of folding of HSA calculated from the CD spectra recorded at different temperatures and in presence of different concentrations of GnHCl. The black dots on the contour graph represent the measured data points.

4.2.2 Effect of double denaturation on domain-I of HSA

4.2.2.1 Steady state measurements

As mentioned earlier, domain-I of HSA was tagged with DACIA to study its unfolding behaviour in presence of GnHCl and temperature. However, first we have to be sure that tagging of DACIA does not alter the secondary structure of HSA, which was verified by measuring CD spectra of tagged and untagged HSA. The same study was also performed with NPCE-tagged HSA (note: NPCE binds to domain-III of HSA). Figure 4.3 shows CD spectra of native HSA, HSA tagged with DACIA and HSA tagged with NPCE. The calculated values of α -helicity and the spectral signatures are similar for all the three cases indicating that the attachment of the fluorescent label (either DACIA or NPCE) does not affect the secondary structure of HSA.

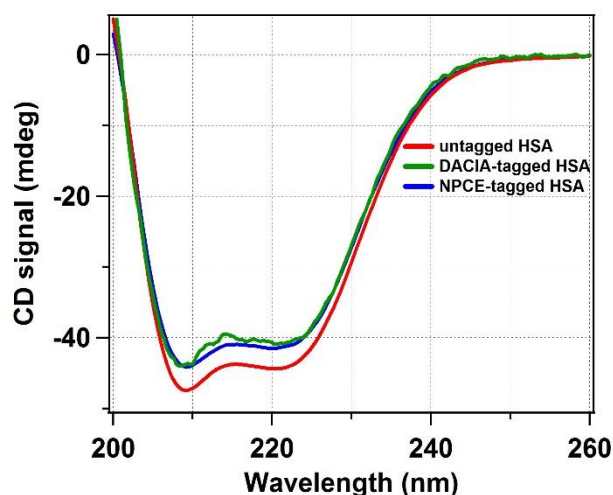


Figure 4.3. CD spectra of untagged HSA (red), HSA tagged with DACIA (green) and HSA tagged with NPCE (blue). The concentrations of untagged HSA, DACIA-tagged HSA and NPCE-tagged HSA were 1.85 μ M, 1.7 μ M and 1.65 μ M respectively. In each case, the path length used is 2 mm.

Further, to investigate the effect of tagging on the tertiary structure of HSA, we have recorded the near-UV CD spectra (250 – 320 nm) using a higher HSA concentration (15 μ M) and longer path length (10 mm). The resulting spectra of tagged and untagged HSA possess similar features indicating that the tertiary structure is also retained upon tagging with either DACIA or NPCE. In order to verify if the tags undergo any structural changes at elevated temperatures, we have recorded the excitation spectra of DACIA and NPCE at higher temperatures and

observed that the spectrum at 348 K is almost overlapping with that at 298 K. This confirms that both these dyes are stable within our experimental range of temperature.

The fluorescent tag DACIA which has been used to tag domain-I, is a solvatochromic probe, which shows strong solvent polarity dependence on emission spectra.³⁸ Upon being tagged to domain-I of HSA, DACIA shows a 20 nm blue shift ($\lambda_{em}^{max} = 457$ nm) in emission maximum from 477 nm in buffer, owing to the more hydrophobic environment inside the protein core. As HSA unfolds, the emission maximum shows a bathochromic shift as shown in figure 4.4 for four different GnHCl – temperature combinations.

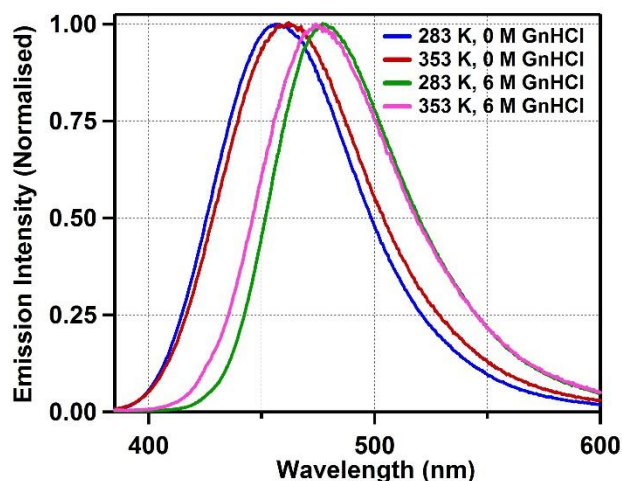


Figure 4.4. Emission spectra of DACIA tagged to HSA at four different combinations of GnHCl concentration and temperature. The sample were excited at 381 nm.

The amount of shift normalized by the maximum amount of shift has been used to denote the degree of folding as per the following equation.

$$f_i = \frac{\lambda_U - \lambda_i}{\lambda_U - \lambda_N} \quad (4.4)$$

where λ_N and λ_U are the emission maxima in the native and unfolded states, respectively and λ_i is the emission maxima at intermediate temperatures and GnHCl concentrations. The value of λ_i at 298 K in the absence of GnHCl has been taken as λ_N and the value of λ_i at 298 K in the presence of 6 M GnHCl has been taken as λ_U . The contour plot (figure 4.5) shows the variation of degree of folding at different GnHCl concentrations and temperatures. Expectedly, as per the definition, extent of

folding is unity at 298 K in the absence of GnHCl. Upon increasing either temperature or GnHCl concentration, the extent of folding decreases. As evident, effect of temperature is similar for all GnHCl concentrations and the denaturation effect of GnHCl is much more pronounced as compared to that of temperature. Apart from these regular observations, we observe two striking features. The first one is that, at 323 K in the absence of GnHCl concentration, the extent of folding is more than unity. Secondly, at 283 K in the absence of GnHCl, the extent of folding is less than unity.

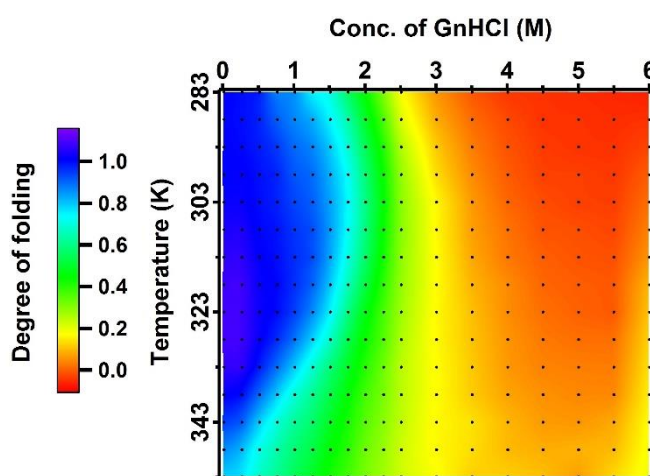


Figure 4.5. Degree of folding of domain-I of HSA calculated from the emission maxima of DACIA tagged to domain-I of HSA at different temperatures and in presence of different concentrations of GnHCl. The black dots on the contour graph represent the measured data points.

4.2.2.2 Lifetime measurements

To gather further information on the nature of heat and GnHCl-induced denaturation, fluorescence lifetime measurements were performed for a few samples. The excited state lifetime of free DACIA molecule was measured at its emission maximum and the fluorescent transients were fitted using a tri-exponential function. The decay components were found to be 0.28 ns (3%), 1.85 ns (85%) and 3.31 ns (12%) with average lifetime 1.98 ns. Once tagged to domain-I of HSA, the average lifetime was found to increase to 3.63 ns with three decay components 0.37 ns (3%), 1.81 ns (21%), and 4.28 ns (76%).

Lifetime measurements of DACIA-tagged HSA were carried out in the absence of GnHCl and in the presence of 2 and 5 M GnHCl, at three different

temperatures: 298 K, 328 K and 348 K at their respective emission maxima. In all cases, the fluorescence transients were fitted using a tri-exponential function. In the presence of 2 M GnHCl at 298 K, the average lifetime was found to decrease to 3.29 ns, while in the absence of GnHCl at 328 K, the average lifetime became 3.41 ns. The emission maxima and the average lifetime of each of the cases are given in table 4.1. It can be seen that the lifetime of DACIA-tagged to HSA decreases with an increase in concentration of GnHCl or with an increase in temperature, which indicates an increase in the non-radiative rate constant of excited DACIA molecule at higher temperatures and higher GnHCl concentrations. However, this study is not much informative and we proceed with solvation dynamics study to have a better picture of the dynamics of associated water molecules within the domain.

Table 4.1. Emission maxima ($\lambda_{ex} = 381$ nm) and average lifetimes of DACIA-tagged HSA in presence of different concentrations of GnHCl at different temperatures.

GnHCl concentration (M)	Temperature (K)	Emission maximum (nm)	Average τ (ns)
0	298	457.0	3.63
0	328	456.0	3.41
0	348	462.0	3.03
2	298	468.5	3.29
2	328	469.5	2.50
2	348	472.5	1.96
5	298	478.5	2.87
5	328	477.0	2.11
5	348	475.5	2.25

4.2.2.3 Solvation dynamics measurements

We have studied the dynamics of solvation within domain-I of HSA under different denaturing conditions by exploiting the solvatochromic property of DACIA. The solvation dynamics of DACIA-tagged HSA in its native state (at 298 K in absence of any external agents) had been mentioned in section 3.2.2 of chapter 3. In a similar fashion, solvation dynamics within domain-I of HSA has been studied for nine different combinations of temperatures and GnHCl concentrations. In each case, fluorescence transients at different wavelengths spread over the steady state emission spectrum were recorded at the magic angle condition (54.7°). The fluorescence transients collected at longer wavelengths showed distinct growth

components, which were absent at shorter wavelengths. All transients were fitted using a tri-exponential function. At 328 K and in presence of 2 M GnHCl, the average lifetime at 405 nm was found to be 0.95 ns with the three lifetime components, 0.10 ns (54%), 0.88 ns (27%) and 3.46 ns (19%). At 550 nm, the average lifetime was calculated to be 2.85 ns with components 0.25 ns (-20%), 1.11 ns (73%) and 4.44 ns (47%). Some of the transients are shown in figure 4.6 (a) & (b) and the fitting components at each wavelength are given in table 4.2. The time-resolved emission spectra (TRES) were constructed from the decay components following standard procedure, which is shown along with the steady state spectrum in figure 4.6(c).⁴⁶ The solvent response function (figure 4.6(d)) is best fitted using a single-exponential function with solvation time of 0.17 ns. The Stokes shift was observed to be 360 cm⁻¹.

Table 4.2. Fitting parameters of fluorescence decay of DACIA-tagged HSA in presence of 2 M GnHCl at 328 K monitored at different wavelengths. The sample was excited at 375.8 nm.

λ_{em} (nm)	a_1	τ_1 (ns) ^a	a_2	τ_2 (ns) ^b	a_3	τ_3 (ns) ^c	$\langle\tau\rangle$ (ns)
405	0.54	0.10	0.27	0.88	0.19	3.46	0.95
415	0.46	0.11	0.29	0.10	0.25	3.61	0.98
420	0.44	0.11	0.31	1.04	0.25	3.76	1.31
425	0.41	0.10	0.31	1.00	0.28	3.71	1.39
430	0.38	0.12	0.30	0.99	0.32	3.80	1.56
435	0.33	0.14	0.34	1.13	0.33	3.86	1.70
440	0.28	0.15	0.38	1.19	0.34	3.91	1.82
445	0.28	0.13	0.40	1.24	0.32	3.90	1.78
450	0.23	0.16	0.44	1.32	0.33	3.91	1.91
455	0.20	0.16	0.48	1.34	0.32	3.96	1.94
470	-0.02	0.54	0.60	1.19	0.42	4.28	2.50
475	-0.04	0.49	0.63	1.19	0.41	4.40	2.53
480	-0.08	0.45	0.64	1.14	0.44	4.36	2.61
485	-0.11	0.42	0.67	1.10	0.44	4.35	2.60
490	-0.15	0.38	0.66	1.03	0.49	4.19	2.68
500	-0.19	0.31	0.70	1.04	0.49	4.46	2.85
510	-0.24	0.28	0.69	1.00	0.55	4.43	3.06
525	-0.28	0.26	0.73	0.98	0.55	4.68	3.22
550	-0.20	0.25	0.73	1.11	0.47	4.44	2.85

^a ± 0.02 ns, ^b ± 0.05 ns, ^c ± 0.20 ns

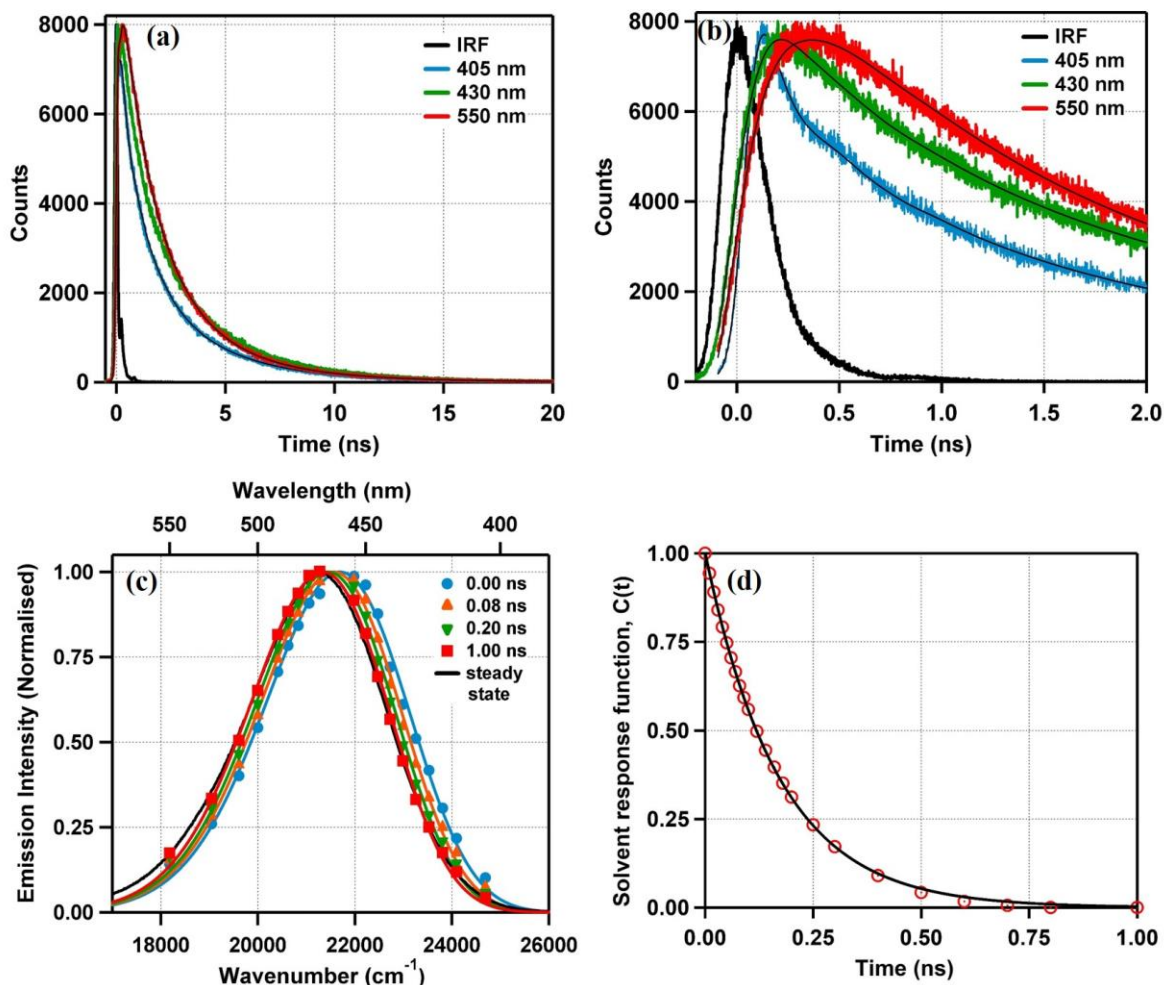


Figure 4.6. (a) & (b) A few representative transient decays of DACIA tagged to Cys-34 of HSA in presence of 2 M GnHCl at 328 K collected at a longer (a) and a shorter (b) timescales. (c) Time-resolved emission spectra (TRES) constructed using the fitting parameters of the transient decays (λ_{ex} = 375.8 nm) and (d) the solvent response function calculated using the peak frequencies of TRES.

Similarly, we have calculated the solvation times of DACIA-tagged HSA and the dynamic Stokes shifts for seven other combinations of temperature and GnHCl concentration. The solvent response functions were fitted either by a single-exponential or a bi-exponential function. The data for the same is compiled in table 4.3 and the nine solvent response functions along with their fittings are shown in figure 4.7. The missing components of dynamic Stokes shift in our instrument have also been mentioned in table 4.3.

Table 4.3. Solvent response time components, average solvation times, dynamic Stokes shifts and the missing components of DACIA-tagged HSA in the presence of different concentrations of GnHCl at different temperatures.

GnHCl conc. (M)	Temperature (K)	τ_{s1} (ns)	τ_{s2} (ns)	$\langle\tau_s\rangle$ (ns)	Stokes shift (cm ⁻¹)	Missing component (%)
0	298	0.15 (0.55)	0.68 (0.45)	0.39	480	64
0	328	0.25 (0.96)	1.29 (0.04)	0.29	430	67
0	348	0.20 (0.96)	1.80 (0.04)	0.26	360	79
2	298	0.10 (0.60)	0.33 (0.40)	0.19	400	73
2	328	0.17 (1.00)		0.17	360	80
2	348	0.24 (1.00)		0.24	200	93
5	298	0.07 (0.80)	0.53 (0.20)	0.16	250	85
5	328	0.08 (0.45)	0.21 (0.55)	0.15	130	93
5	348	0.09 (0.13)	0.28 (0.87)	0.26	110	94

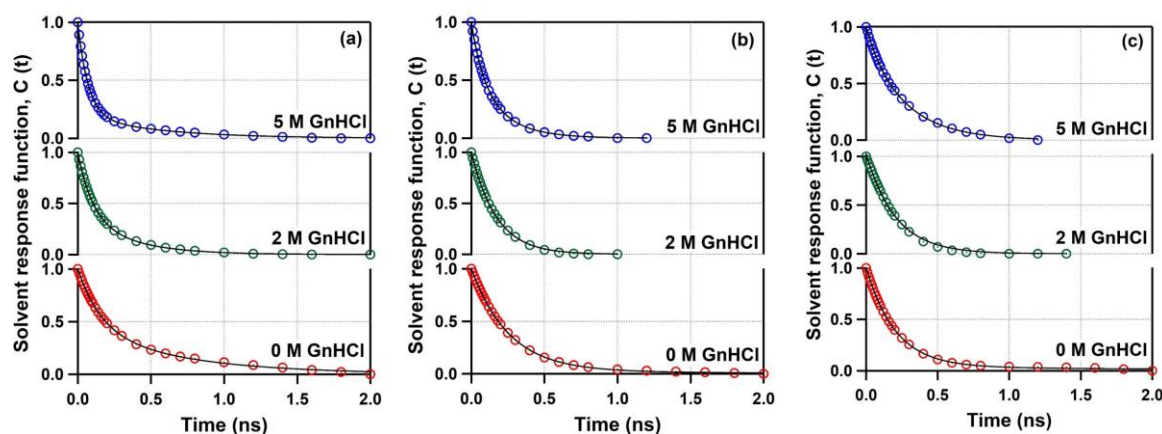


Figure 4.7. Decay of the solvent response function of DACIA tagged to domain-I of HSA in presence of 0 M, 2 M and 5 M GnHCl (a) at 298 K (b) at 328 K and (c) at 348 K.

From table 4.3, it can be seen that either an increasing temperature or a high concentration of GnHCl results in a decrease in solvation time. However, the effect of temperature in presence of GnHCl (2 or 5 M) is quite strange. In these two cases, we observed that the solvation time is unaffected by rising the temperature from 298 K to 328 K, however, further increase in the temperature to 348 K leads to slower

solvation. Another important observation is that at 348 K, the solvation time hardly depends on the GnHCl concentration. The dynamic Stokes shift was found to decrease with an increase in temperature or an increase in the concentration of GnHCl in each of the cases we monitored.

4.2.3 Effect of double denaturation on domain-III of HSA

4.2.3.1 Steady state measurements

The fluorescent label NPCE which is used to tag domain-III of HSA shows the emission maximum at 493 nm in phosphate buffer. After being covalently attached to HSA, the emission maximum shifts to 478 nm. The solvatochromic behaviour of NPCE is utilized to study the double denaturation effect of this specific domain. The fluorescence maximum of NPCE-tagged HSA gets red shifted monotonously with an increase in temperature almost at all GnHCl concentrations. Figure 4.8 shows the emission spectra of NPCE-tagged HSA at two different GnHCl concentrations and at two different temperatures. Using equation (4.4), the change in degree of folding of this domain has been calculated from the shifts in emission maxima of NPCE. Here also, the same nomenclature of λ_N and λ_U has been used. The variation of extent of folding upon thermal and chemical denaturation is shown in the contour plot in figure 4.9.

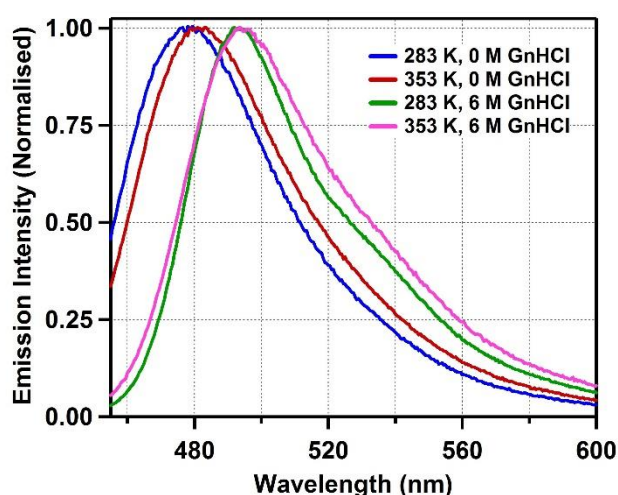


Figure 4.8. Emission ($\lambda_{ex}=447$ nm) spectra of NPCE tagged to domain-III of HSA at four different combinations of GnHCl concentration and temperature.

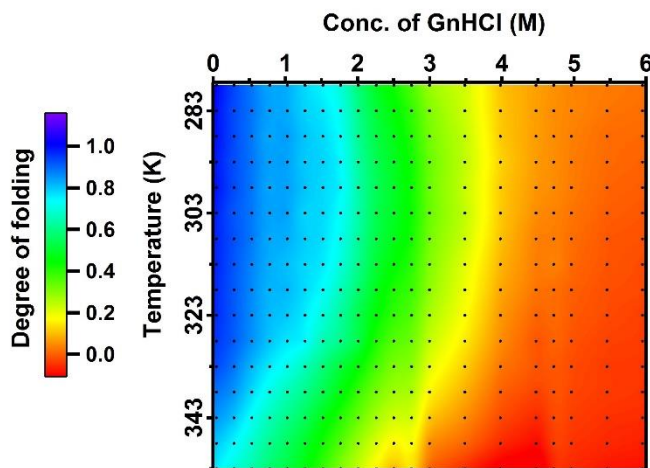


Figure 4.9. Degree of folding of domain-III of HSA calculated from the emission maxima of NPCE tagged to domain-III of HSA at different temperatures and in presence of different concentrations of GnHCl. The black dots on the contour graph represent the measured data points.

4.2.3.2 Lifetime measurements

The excited state lifetime of NPCE in phosphate buffer was measured at its emission maximum and the decay transient was best fitted using a single-exponential function where the lifetime was found to be 4.1 ns. After tagging to domain-III of HSA, the decay transient becomes tri-exponential with average lifetime 3.7 ns. Similar to the experiments carried out with DACIA-tagged domain-I, lifetime of NPCE-tagged HSA was also measured in presence of denaturing agents – GnHCl and temperature and in all cases the fluorescence transients were fitted with a tri-exponential function. The average lifetimes of NPCE-tagged to domain-III of HSA in presence of different concentrations of GnHCl at various temperatures are given in table 4.3. It can be seen that there is only a small variation in lifetime of NPCE-tagged to domain-III of HSA with increase in temperature and with increase in GnHCl concentration.

Table 4.4. Emission maxima ($\lambda_{ex} = 447$ nm) and average lifetimes of NPCE-tagged HSA in presence of different concentrations of GnHCl at different temperatures.

GnHCl concentration (M)	Temperature (K)	Emission maximum (nm)	Average τ (ns)
0	298	479.0	3.70
0	328	478.5	3.69
0	348	480.0	3.79
2	298	485.0	3.68
2	328	482.5	3.32
2	348	489.5	3.32
5	298	494.0	3.81
5	328	494.0	3.67
5	348	495.0	3.76

4.2.3.3 Solvation dynamics measurements

Solvation dynamics within domain-III of HSA in presence of different amounts of GnHCl at different temperatures were measured using the tagged probe molecule, NPCE. The fluorescence transients at different wavelengths along the steady state emission spectrum of the molecule were measured and using the wavelength dependent lifetime data, TRES was constructed. Following this, the solvent correlation function has been constructed as described in section 4.2.2.3. The observed solvation times, dynamic Stokes shifts and the missing components of Stokes shift within the domain-III of HSA for nine different combinations of GnHCl and temperatures are tabulated in table 4.5 and the solvation response functions are shown in figure 4.10. Surprisingly, for domain-III, unlike domain-I, we could not observe any definite trend in the variation of solvation time with change in temperature or concentration of GnHCl.

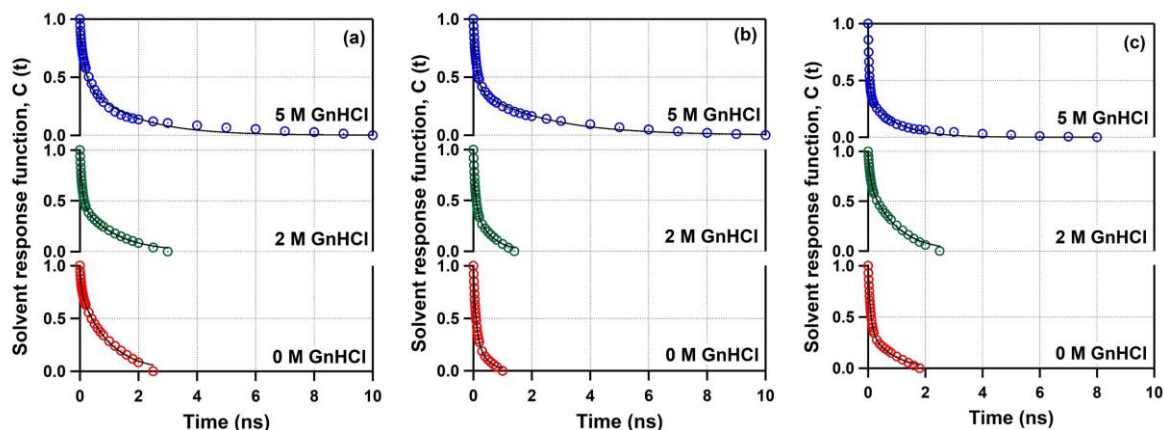
**Figure 4.10.** Decay of the solvent response function of NPCE tagged to domain-III of HSA in presence of 0 M, 2 M and 5 M GnHCl (a) at 298 K (b) at 328 K and (c) at 348 K.

Table 4.5. Solvent response time components, average solvation times, dynamic Stokes shifts and the missing component of NPCE-tagged HSA in presence of different concentrations of GnHCl at different temperatures.

GnHCl conc. (M)	Temperature (K)	τ_{s1} (ns)	τ_{s2} (ns)	$\langle\tau_s\rangle$ (ns)	Stokes shift (cm ⁻¹)	Missing component (%)
0	298	0.05 (0.23)	0.97 (0.77)	0.76	225	85
0	328	0.08 (0.62)	0.36 (0.38)	0.19	290	81
0	348	0.08 (0.61)	0.74 (0.39)	0.34	350	81
2	298	0.08 (0.52)	1.15 (0.48)	0.59	370	77
2	328	0.07 (0.55)	0.55 (0.45)	0.29	340	78
2	348	0.08 (0.43)	0.93 (0.57)	0.56	240	87
5	298	0.15 (0.51)	1.69 (0.49)	0.91	160	90
5	328	0.11 (0.59)	2.31 (0.41)	1.01	220	87
5	348	0.99 (0.34)	1.55 (0.66)	1.36	130	93

4.3 Discussion

It is well known that definite interactions between amino acid residues guide a protein to fold into its characteristic native three dimensional structure that determines its functional specificity.^{47–49} The secondary structures of proteins are stabilized by hydrogen bonding whereas other non-covalent interactions like electrostatic interactions and hydrophobicity are responsible for the formation of the tertiary structure of the proteins.^{47–49} Under the action of denaturants, these interactions are broken. Understanding the complex mechanism of denaturation has remained a topic of considerable research for several decades. Temperature, pH and chemical-induced denaturation pathways of various proteins have been extensively studied by several groups.^{12–19,50,51} In case of GnHCl, this unfolding is driven by the attractive interaction of protein surface with GnHCl molecule. When this interaction overcomes the hydrogen bonding network of the protein, which is responsible for the native state stabilization, the protein gets denatured.⁵² To understand the thermal unfolding of protein in aqueous solution, a proper understanding of the role of water

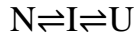
molecules is necessary. Inside an aqueous solution, hydrophobic protein molecules tend to disrupt the intermolecular hydrogen bond network between water molecules. In order to retain the network, water molecules tend to form cage like ordered structures around the hydrophobic core at the cost of high entropic loss. In order to minimize the effect of unfavourable entropy change, the protein molecules tend to fold so as to reduce the surface area of contact with the water molecules. An interesting fact is that this entropy change associated with hydrophobic effect depends on temperature. With an increase in temperature, the ordered cage like structure tends to break down, thus leading to a decrease in negative entropy effect. This leads to the gradual unfolding of protein with increasing temperature.⁵³ The course of denaturing action of GnHCl is related with their capacity to break down the salt bridges that are responsible to stabilize the folded structure of the protein.

In our experiments where we have monitored the denaturation of HSA at a temperature range 283 - 353 K and in presence of 0 – 6 M GnHCl, we could find that temperature has a lesser effect to cause the denaturation of the two domains of the protein as compared to GnHCl. In the absence of GnHCl, degree of folding of both domain-I and domain-III was found to decrease from 1.0 at 298 K to ~0.7 at 353 K (figure 4.5, figure 4.9). However, the overall unfolding of the protein was found to be more sensitive to temperature as the degree of folding was found to vary from 1.0 at 298 K to ~0.4 at 353 K (figure 4.2). Also, at any given concentration of GnHCl, the degree of folding due to the change in temperature was not found to vary to a great extent. On the contrary, the degree of folding of both the domains as well as the overall protein decreased from 1 to 0 with an increase in concentration of GnHCl from 0 to 6 M (by definition, the degree of folding is 1 at 0 M GnHCl, 298 K and is 0 at 6 M GnHCl, 298 K).

The two domains were also found to show some differences in their nature of unfolding due to GnHCl. In the case of domain-I, the extent of unfolding due to GnHCl was more pronounced at lower temperature (283 K) than at higher temperature (353 K), whereas in the case of domain-III this unfolding occurs more

at higher temperature than at lower temperature. This also leads to a surprising scenario where the most unfolded state of domain-I of HSA in our temperature-GnHCl combinations occurs near 283 K, 6 M GnHCl instead of 353 K, 6 M GnHCl. However, in the case of domain-III, the most unfolded states occurred near to 353 K, 6 M GnHCl as expected. The overall denaturation of protein above 298 K follows an intermediate path followed by domain-I and domain-III. The stabilizing effect of domain-I at higher temperature suggests that the DACIA molecule, which is bound to the Cys-34 position of domain-I of HSA is somehow pushed into a more hydrophobic environment due to the movement of protein side chains near that site of the protein at higher temperatures.

The associated free energy change of different parts of HSA was evaluated by considering either a two-step or a three-step process as given below.



where N denotes the native state, I denotes intermediate state and U denotes the unfolded state. The measured degree of folding as a function of denaturant concentration for the two-state and three-state processes can be represented by equations (4.5) and (4.6), respectively⁵⁴

$$Y = \frac{Y_N + Y_U \times e^{-x}}{1 + e^{-x}} \quad (4.5)$$

$$Y = \frac{Y_N + Y_I \times e^{-x} + Y_U \times e^{-y}}{1 + e^{-x} + e^{-y}} \quad (4.6)$$

$$x = \frac{(\Delta G^0 - m[Denaturant])}{RT} \quad (4.7)$$

$$y = \frac{\Delta G_1^0 + \Delta G_2^0 - (m_1 + m_2)[Denaturant]}{RT} \quad (4.8)$$

In the above equation, Y is the degree of folding and Y_N , Y_I and Y_U being the degree of folding for the native, intermediate and unfolded states respectively. ΔG^0 , ΔG_1^0 and ΔG_2^0 are the free energy changes associated with the concerned transitions,

m denotes the slope of the free energy change plotted against the denaturant. R and T are the universal gas constant and temperature in Kelvin respectively.

Using the above model, we have calculated the free energy change associated with the domain-specific unfolding of HSA by either temperature or GnHCl. A three state model was adopted for the temperature-induced unfolding of domain-I of HSA and for all the other cases, a two-state model was sufficient to fit the data (see figure 4.11). The corresponding ΔG^0 values are tabulated in table 4.6. The change in free energy associated with each of the unfolding processes is positive, indicating that none of these processes happen spontaneously. It could also be noted that the free energy change associated with the GnHCl-induced unfolding is much lesser than that of the temperature-induced unfolding, showing that GnHCl is much more effective for HSA denaturation. The free energy change of domain-III is lesser than that of domain-I, indicating that domain-III is more vulnerable than domain-I of HSA.

Table 4.6. The change in free energy associated with the domain-specific and overall unfolding of HSA.

	Domain-I	Domain-III	Overall structure
ΔG^0 associated with GnHCl-induced unfolding (kcal mol ⁻¹)	($N \rightleftharpoons U$) 2.8	($N \rightleftharpoons U$) 1.7	($N \rightleftharpoons U$) 1.8
ΔG^0 associated with temp-induced unfolding (kcal mol ⁻¹)	($\Delta G_1^0, N \rightleftharpoons I$) 25.4 ($\Delta G_2^0, I \rightleftharpoons U$) 4.7	($N \rightleftharpoons U$) 18.6	($N \rightleftharpoons U$) 22.2

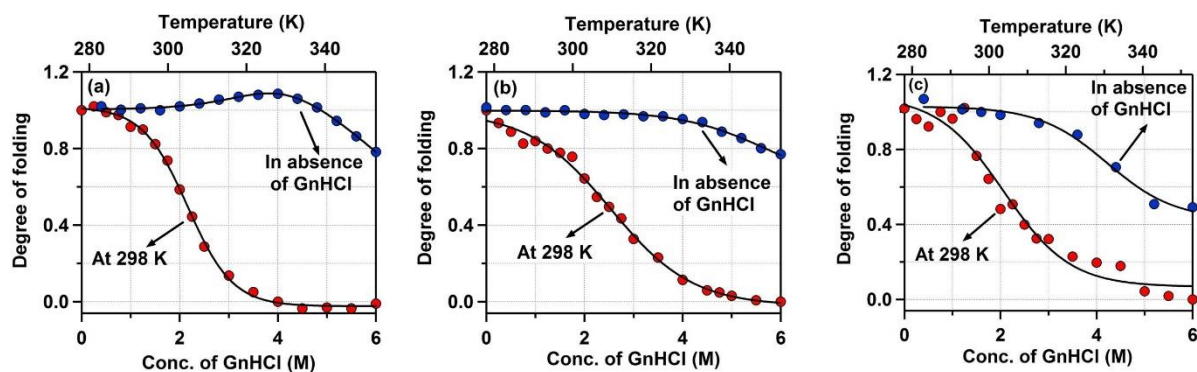


Figure 4.11. The change in degree of folding of (a) domain-I of HSA, (b) domain-III of HSA and (c) the overall structure of HSA due to the action of GnHCl (red circles) and temperature (blue circles). The fitting of the data using either a two-state or a three-state model are also shown.

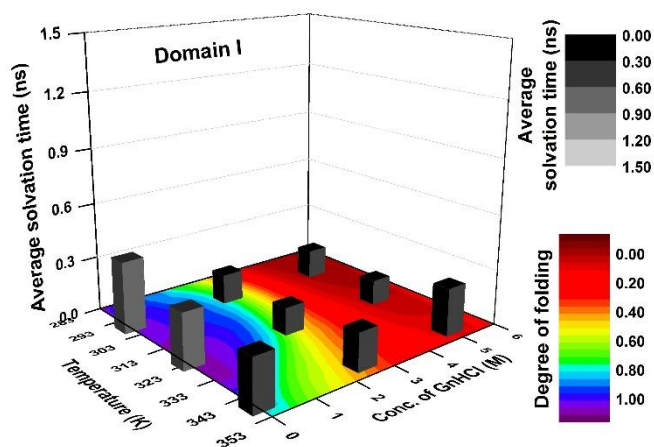


Figure 4.12. The average solvation times of DACIA-tagged HSA at different temperatures in the presence of different concentrations of GnHCl plotted over the contour plot of extent of folding calculated from the steady state emission spectra.

Solvation times of DACIA tagged to domain-I of HSA at different temperatures and different concentrations of GnHCl are illustrated in figure 4.12. The solvation time is found to generally decrease with an increase in temperature or with an increase in GnHCl concentration. This change is expected as the denaturation of HSA results in DACIA being located in a less hydrophobic environment away from the protein core, where the dynamics of water molecules are faster. As a result, the average solvation time of DACIA tagged to domain-I of HSA decreased by 0.1 ns from 0.39 ns to 0.29 ns when temperature was increased from 298 K to 328 K and further decreased by 0.03 ns when the temperature was increased to 348 K, in the absence of any GnHCl. The value of dynamic Stokes shift also decreased monotonously when temperature was changed from 298 K to 348 K.

In presence of 2 M GnHCl, the solvation time decreased with an increase in temperature from 298 K to 328 K, but the change was only 0.02 ns (from 0.19 ns to 0.17 ns) which is only 1/5th of the change we had observed for the corresponding change in temperature in the absence of GnHCl. With further increase in temperature, the average solvation time increased to 0.24 ns. This suggests that increasing the temperature closer to 348 K would somehow result in the DACIA molecule being located in a more confined environment. Similar changes could be observed in presence of 5 M GnHCl where average solvation time decreases only by 0.01 ns (from 0.16 ns to 0.15 ns) when the temperature is increased from 298 K to 328 K and then increased to 0.26 ns at 348 K. However, at all concentration of GnHCl, the value of dynamic Stokes shift decreases monotonously with temperature.

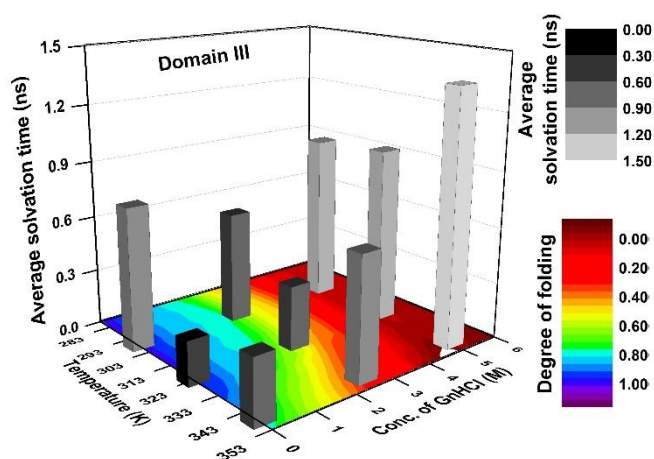
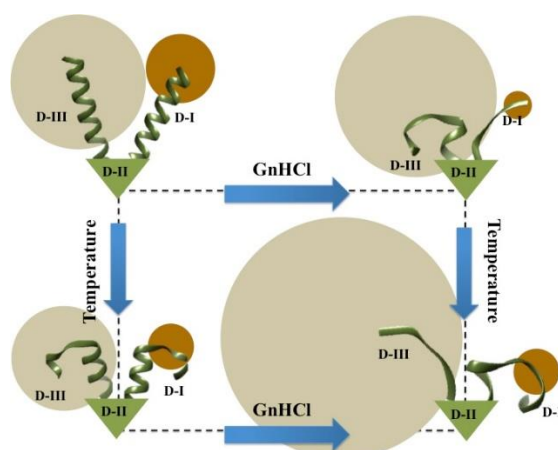


Figure 4.13. The average solvation times of NPCE-tagged HSA at different temperatures in the presence of different concentrations of GnHCl plotted over the contour plot of extent of folding calculated from the steady state emission spectra.

The solvation dynamics of NPCE tagged to domain-III of HSA was found to be more intriguing than domain-I of HSA (see figure 4.13). When temperature was increased from 298 K to 328 K, the average solvation time decreased sharply by a factor of 4 and 2 in presence of 0 M and 2 M GnHCl respectively, implying that temperature has an immediate denaturing effect on the domain-III of HSA. However, a further increase in temperature to 348 K results in an increase in solvation time suggesting that the denaturation near the binding site does not occur

anymore and the increase in temperature has water structure making property near domain-III. In presence of 5 M GnHCl, such phenomenon starts even at a lower temperature and as a result, the average solvation time increases with temperature. At 328 K and 348 K, the average solvation time shows a monotonous increase with the increase in the concentration of GnHCl. At lower temperature (298 K), the solvation time decreases when GnHCl concentration is increased from 0 M GnHCl to 2 M GnHCl and then increases in presence of 5 M GnHCl (Scheme 4.1).



Scheme 4.1. Schematic representation of domain-specific unfolding of human serum albumin in double denaturing condition. The nature of change of associated solvation dynamics is also represented through circular disc representation (larger the circle means large solvation time).

This study reveals that the course of denaturation for domain-I and domain-III of HSA are somewhat different, which also differs from the nature of the overall denaturation of the protein. The solvation dynamics studies in presence of denaturing agents, temperature and GnHCl, at two particular regions of the protein (domain-I and domain-III) shows that the dynamics at these two regions follow quite different pathways in response to the denaturing agents. This must be due to the different confined environments in which the fluorophores are located. The much slower solvation times of the NPCE molecule tagged to domain-III of HSA suggests that the relaxation of water molecules is slower inside domain-III as compared to that of domain-I. Also, in the case of DACIA-tagged HSA, denaturing agents cause a decrease in solvation time in most of the experiments we had carried out, which is expected. On the other hand, the solvation dynamics inside domain-III reveals no trend on imposing the denaturation either by temperature or GnHCl. Increase in

temperature or concentration of GnHCl sometimes resulted in more confinement in the motion of water molecules inside the protein core, which resulted in slower solvation at these sites. The confinement of water molecules could have been caused due to the orientation of side chains near the binding site of the fluorophore or the stronger bonding of water molecules with the amino acid moieties.

4.4 Conclusion

To conclude, we have studied the effect of GnHCl and temperature on the overall structure, domain-I and domain-III of HSA, using covalent fluorescent labels. The overall unfolding of HSA calculated using circular dichroism spectroscopy showed that the unfolding of the protein molecule is following the expected trend, where it is more unfolded at higher temperatures and in presence of GnHCl . The domain-specific unfolding of domains I and III of HSA, calculated using steady state emission spectroscopy also exhibited somewhat different behaviours compared to the overall unfolding. Thus we proved that different parts of HSA do not unfold sequentially. From solvation dynamics studies it was seen that solvation inside the core of domain-III is much slower than that inside domain-I, which is attributed to the different micro environments at the core of the two domains, which restrict the motion of water molecules at the respective sites. This difference in local environments inside the two domains also results in different response of their solvation dynamics to the denaturing agents, as the domain-I of HSA shows a more regular decrease in solvation time due to higher temperature or presence of GnHCl , whereas for domain-III of HSA the change in solvation time with temperature or concentration of GnHCl is more random.

References

- (1) Dugaiczyk, A.; Law, S. W.; Dennison, O. E. Nucleotide Sequence and the Encoded Amino Acids of Human Serum Albumin mRNA. *Proc. Natl. Acad. Sci. U. S. A.* **1982**, *79*, 71–75.
- (2) Theodore Peters, J. *All about Albumin. Biochemistry, Genetics, and Medical Applications*, 1st ed.; Academic Press: San Diego, 1996.
- (3) He, X. M.; Carter, D. C. Atomic Structure and Chemistry of Human Serum Albumin. *Nature* **1992**, *358*, 209.
- (4) Sudlow, G.; Birkett, D. J.; Wade, D. N. The Characterization of Two Specific Drug Binding Sites on Human Serum Albumin. *Mol. Pharmacol.* **1975**, *11*, 824 – 832.
- (5) Curry, S.; Mandelkow, H.; Brick, P.; Franks, N. Crystal Structure of Human Serum Albumin Complexed with Fatty Acid Reveals an Asymmetric Distribution of Binding Sites. *Nat. Struct. Biol.* **1998**, *5*, 827.
- (6) Sugio, S.; Kashima, A.; Mochizuki, S.; Noda, M.; Kobayashi, K. Crystal Structure of Human Serum Albumin at 2.5 Å Resolution. *Protein Eng. Des. Sel.* **1999**, *12*, 439–446.
- (7) Kragh-Hansen, U.; Chuang, V. T. G.; Otagiri, M. Practical Aspects of the Ligand-Binding and Enzymatic Properties of Human Serum Albumin. *Biol. Pharm. Bull.* **2002**, *25*, 695–704.
- (8) Kosa, T.; Maruyama, T.; Otagiri, M. Species Differences of Serum Albumins: I. Drug Binding Sites. *Pharm. Res.* **1997**, *14*, 1607–1612.
- (9) Hoang, H.; Manyanga, F.; Morakinyo, M. K.; Pinkert, V.; Sarwary, F.; Fish, D. J.; Brewood, G. P.; Benight, A. S. Effects of Selective Biotinylation on the Thermodynamic Stability of Human Serum Albumin. *J. Biophys. Chem.* **2016**, *7*, 9–29.
- (10) Fasano, M.; Curry, S.; Terreno, E.; Galliano, M.; Fanali, G.; Narciso, P.; Notari, S.; Ascenzi, P. The Extraordinary Ligand Binding Properties of Human Serum Albumin. *IUBMB Life* **2008**, *57*, 787–796.
- (11) Neurath, H.; Greenstein, J. P.; Putnam, F. W.; Erickson, J. A. The Chemistry of Protein Denaturation. *Chem. Rev.* **1944**, *34*, 157–265.
- (12) Dinner, A. R.; Šali, A.; Smith, L. J.; Dobson, C. M.; Karplus, M. Understanding Protein Folding via Free-Energy Surfaces from Theory and Experiment. *Trends Biochem. Sci.* **2000**, *25*, 331–339.
- (13) Loughlin, W. J. The Denaturation of Proteins: The Effect of the Addition of Electrolytes on the Viscosity of Solutions of Crystalline Egg-Albumin. *Biochem. J.* **1932**, *26*, 1557–1565.
- (14) Camilloni, C.; Guerini Rocco, A.; Eberini, I.; Gianazza, E.; Broglia, R. A.;

- Tiana, G. Urea and Guanidinium Chloride Denature Protein L in Different Ways in Molecular Dynamics Simulations. *Biophys. J.* **2008**, *94*, 4654–4661.
- (15) Kishore, D.; Kundu, S.; Kayastha, A. M. Thermal, Chemical and PH Induced Denaturation of a Multimeric β -Galactosidase Reveals Multiple Unfolding Pathways. *PLoS One* **2012**, *7*, e50380.
- (16) Daggett, V.; Levitt, M. Protein Unfolding Pathways Explored Through Molecular Dynamics Simulations. *J. Mol. Biol.* **1993**, *232*, 600–619.
- (17) Malecki, J.; Wasylewski, Z. The Sequential Mechanism of Guanidine Hydrochloride-Induced Denaturation of CAMP Receptor Protein from Escherichia Coli. A Fluorescent Study Using 8-Anilino-1-Naphthalenesulfonic Acid. *J. Protein Chem.* **1998**, *17*, 745–755.
- (18) Wang, Q.; Christiansen, A.; Samiotakis, A.; Wittung-Stafshede, P.; Cheung, M. S. Comparison of Chemical and Thermal Protein Denaturation by Combination of Computational and Experimental Approaches. II. *J. Chem. Phys.* **2011**, *135*, 175102-1-12.
- (19) Lim, W. K.; Rösgen, J.; Englander, S. W. Urea, but Not Guanidinium, Destabilizes Proteins by Forming Hydrogen Bonds to the Peptide Group. *Proc. Natl. Acad. Sci. U. S. A.* **2009**, *106*, 2595–2600.
- (20) Hegyi, H.; Gerstein, M. The Relationship between Protein Structure and Function: A Comprehensive Survey with Application to the Yeast Genome 11 Edited by G. von Heijne. *J. Mol. Biol.* **1999**, *288*, 147–164.
- (21) Strosberg, A. D. Structure/Function Relationship of Proteins Belonging to the Family of Receptors Coupled to GTP-Binding Proteins. *Eur. J. Biochem.* **2018**, *196*, 1–10.
- (22) Vivian, J. T.; Callis, P. R. Mechanisms of Tryptophan Fluorescence Shifts in Proteins. *Biophys. J.* **2001**, *80*, 2093–2109.
- (23) Chen, Y.; Barkley, M. D. Toward Understanding Tryptophan Fluorescence in Proteins. *Biochemistry* **1998**, *37*, 9976–9982.
- (24) Ghisaidoobe, A. B. T.; Chung, S. J. Intrinsic Tryptophan Fluorescence in the Detection and Analysis of Proteins: A Focus on Förster Resonance Energy Transfer Techniques. *Int. J. Mol. Sci.* **2014**, *15*, 22518–22538.
- (25) Royer, C. A. Probing Protein Folding and Conformational Transitions with Fluorescence. *Chem. Rev.* **2006**, *106*, 1769–1784.
- (26) Sengupta, B.; Das, N.; Sen, P. Monomerization and Aggregation of β -Lactoglobulin under Adverse Condition: A Fluorescence Correlation Spectroscopic Investigation. *Biochim. Biophys. Acta - Proteins Proteomics* **2018**, *1866*, 316–326.
- (27) Romanini, D. W.; Cornish, V. W. Protein Labelling: Playing Tag with Proteins. *Nat. Chem.* **2012**, *4*, 248.

- (28) Kim, Y.; Ho, S. O.; Gassman, N. R.; Korlann, Y.; Landorf, E. V.; Collart, F. R.; Weiss, S. Efficient Site-Specific Labeling of Proteins via Cysteines. *Bioconjug. Chem.* **2008**, *19*, 786–791.
- (29) Toseland, C. P. Fluorescent Labeling and Modification of Proteins. *J. Chem. Biol.* **2013**, *6*, 85–95.
- (30) Krall, N.; da Cruz, F. P.; Boutureira, O.; Bernardes, G. J. L. Site-Selective Protein-Modification Chemistry for Basic Biology and Drug Development. *Nat. Chem.* **2015**, *8*, 103.
- (31) Klymchenko, A. S. Solvatochromic and Fluorogenic Dyes as Environment-Sensitive Probes: Design and Biological Applications. *Acc. Chem. Res.* **2017**, *50*, 366–375.
- (32) Yadav, R.; Sengupta, B.; Sen, P. Effect of Sucrose on Chemically and Thermally Induced Unfolding of Domain-I of Human Serum Albumin: Solvation Dynamics and Fluorescence Anisotropy Study. *Biophys. Chem.* **2016**, *211*, 59–69.
- (33) Flora, K.; Brennan, J. D.; Baker, G. A.; Doody, M. A.; Bright, F. V. Unfolding of Acrylodan-Labeled Human Serum Albumin Probed by Steady-State and Time-Resolved Fluorescence Methods. *Biophys. J.* **1998**, *75*, 1084–1096.
- (34) Sasmal, D. K.; Mondal, T.; Sen Mojumdar, S.; Choudhury, A.; Banerjee, R.; Bhattacharyya, K. An FCS Study of Unfolding and Refolding of CPM-Labeled Human Serum Albumin: Role of Ionic Liquid. *J. Phys. Chem. B* **2011**, *115*, 13075–13083.
- (35) Gerasov, A.; Shandura, M.; Kovtun, Y.; Losytskyy, M.; Negrutka, V.; Dubey, I. Fluorescent Labeling of Proteins with Amine-Specific 1,3,2-(2H)-Dioxaborine Polymethine Dye. *Anal. Biochem.* **2012**, *420*, 115–120.
- (36) Yadav, R.; Sen, P. Mechanistic Investigation of Domain Specific Unfolding of Human Serum Albumin and the Effect of Sucrose. *Protein Sci.* **2013**, *22*, 1571–1581.
- (37) Santra, M. K.; Banerjee, A.; Krishnakumar, S. S.; Rahaman, O.; Panda, D. Multiple-Probe Analysis of Folding and Unfolding Pathways of Human Serum Albumin. *Eur. J. Biochem.* **2004**, *271*, 1789–1797.
- (38) Yadav, R.; Sengupta, B.; Sen, P. Conformational Fluctuation Dynamics of Domain I of Human Serum Albumin in the Course of Chemically and Thermally Induced Unfolding Using Fluorescence Correlation Spectroscopy. *J. Phys. Chem. B* **2014**, *118*, 5428–5438.
- (39) Sengupta, B.; Acharyya, A.; Sen, P. Elucidation of the Local Dynamics of Domain-III of Human Serum Albumin over the Ps-[Small Mu]s Time Regime Using a New Fluorescent Label. *Phys. Chem. Chem. Phys.* **2016**, *18*, 28548–28555.

-
- (40) Wang, R.; Sun, S.; Bekos, E. J.; Bright, F. V. Dynamics Surrounding Cys-34 in Native, Chemically Denatured, and Silica-Adsorbed Bovine Serum Albumin. *Anal. Chem.* **1995**, *67*, 149–159.
- (41) Hagag, N.; Birnbaum, E. R.; Darnall, D. W. Resonance Energy Transfer between Cys-34, Trp-214, and Tyr-411 of Human Serum Albumin. *Biochemistry* **1983**, *22*, 2420–2427.
- (42) Xia, Z.; Das, P.; Shakhnovich, E. I.; Zhou, R. Collapse of Unfolded Proteins in a Mixture of Denaturants. *J. Am. Chem. Soc.* **2012**, *134*, 18266–18274.
- (43) Shaw, A. K.; Pal, S. K. Spectroscopic Studies on the Effect of Temperature on pH-Induced Folded States of Human Serum Albumin. *J. Photochem. Photobiol. B Biol.* **2008**, *90*, 69–77.
- (44) Ahmad, B.; Ahmed, M. Z.; Haq, S. K.; Khan, R. H. Guanidine Hydrochloride Denaturation of Human Serum Albumin Originates by Local Unfolding of Some Stable Loops in Domain III. *Biochim. Biophys. Acta - Proteins Proteomics* **2005**, *1750*, 93–102.
- (45) Corrêa, D. H. A.; Ramos, C. H. I. The Use of Circular Dichroism Spectroscopy to Study Protein Folding , Form and Function. *J. Biochem.* **2009**, *3*, 164–173.
- (46) Maroncelli, M.; Fleming, G. R. Picosecond Solvation Dynamics of Coumarin 153: The Importance of Molecular Aspects of Solvation. *J. Chem. Phys.* **1987**, *86*, 6221– 6239.
- (47) Anfinsen, C. B. Principles That Govern the Folding of Protein Chains. *Science* **1973**, *181* (4096), 223 – 230.
- (48) Dobson, C. M. Protein Folding and Misfolding. *Nature* **2003**, *426*, 884.
- (49) Betz, S. F. Disulfide Bonds and the Stability of Globular Proteins. *Protein Sci.* **1993**, *2*, 1551–1558.
- (50) Tanford, C. Isothermal Unfolding of Globular Proteins in Aqueous Urea Solutions. *J. Am. Chem. Soc.* **1964**, *86*, 2050–2059.
- (51) Anderson, D. E.; Becktel, W. J.; Dahlquist, F. W. PH-Induced Denaturation of Proteins: A Single Salt Bridge Contributes 3-5 Kcal/Mol to the Free Energy of Folding of T4 Lysozyme. *Biochemistry* **1990**, *29*, 2403–2408.
- (52) Meuzelaar, H.; Panman, M. R.; Woutersen, S. Guanidinium-Induced Denaturation by Breaking of Salt Bridges. *Angew. Chemie Int. Ed.* **2015**, *54* (50), 15255–15259.
- (53) Dias, C. L.; Ala-Nissila, T.; Wong-ekkabut, J.; Vattulainen, I.; Grant, M.; Karttunen, M. The Hydrophobic Effect and Its Role in Cold Denaturation. *Cryobiology* **2010**, *60*, 91–99.
- (54) Naidu, K. T.; Prabhu, N. P. Protein-Surfactant Interaction: Sodium Dodecyl Sulfate-Induced Unfolding of Ribonuclease A. *J. Phys. Chem. B* **2011**, *115*, 14760–14767.

Chapter 5

Domain-Specific Stabilization of Structural and Dynamical Responses of Human Serum Albumin by Sucrose

Mohan, V.; Das, N.; Banerjee I.; Sengupta, B.; Sen, P. Domain-Specific Stabilization of Structural and Dynamical Responses of Human Serum Albumin by Sucrose. *Protein Pept. Lett.* **2019**, *1*, 287-300.

In the present work, we have investigated the denaturing and renaturing effects of urea and sucrose respectively, on the overall structure and on two different domains (domain-I and domain-III) of human serum albumin (HSA). From circular dichroism measurements it could be seen that, the α -helicity of the overall structure, which is 64% in its native state, decreases to 11% in presence of 9 M urea and further increases to 25% with the addition of 1 M sucrose. In order to study the domain-specific responses towards these external agents, HSA covalently tagged with fluorescent probes N-(7-dimethylamino-4-methylcoumarin-3-yl) iodoacetamide (DACIA) and p-nitrophenyl coumarin ester (NPCE) at Cys-34 of domain-I and Tyr-411 of domain-III, respectively were used. The domain-wise unfolding/folding studies of HSA by steady state fluorescence spectroscopy reveal that the renaturing effect of sucrose is more pronounced on domain-I. The calculation of free energy change during denaturation due to urea divulges the presence of an intermediate state, which gets stabilized in the presence of sucrose. The renaturing or stabilizing effect of sucrose is attributed to the stabilization of this intermediate state. From solvation dynamics studies it could be seen that the solvation dynamics near the binding site of DACIA inside domain-I becomes faster in presence of urea and it becomes slower in presence of sucrose. However, in the case of NPCE-tagged domain-III, the effect of sucrose on solvation time is evident only at high concentrations of urea and the denaturing effect of urea is evident only at very low or zero concentration of sucrose.

5.1 Introduction

Proteins are regarded as one of the most essential macromolecules inside the human body as they perform a wide range of functions including transport and storage of molecules, providing structural support to cells, helping the body to protect against foreign bodies like viruses and bacteria, and carrying out enzymatic and hormonal functions.¹⁻³ For a protein to carry out its regular function or activity, it should remain in an optimized form, which it had acquired during the post-translational modification after the biosynthesis of the protein. Any change in environmental conditions including alterations in temperature, salinity or pressure may disrupt the native structure of the protein.^{4,5} Such a loss of quaternary, tertiary or secondary structure of a protein which can lead to the loss of its functionality is called denaturation of the protein. However, in many cases, the denaturation process has been found to be reversible, and the structure and functionality of the protein can be regained by the reversal of the change in the environment that caused the denaturation or by the action of other external agents.⁶ Due to their high biological importance, denaturation of proteins has been studied extensively with the help of denaturing agents including acids, salts, surfactants, temperature, urea and guanidine hydrochloride.⁷⁻¹¹ In a similar way, the renaturation of proteins by external agents like polyols, macromolecular crowders and sugars including glucose, sucrose and trehalose have also been studied by various research groups.¹²⁻¹⁶

In the present study, we have looked at the effects of denaturing and renaturing agents on multi-domain protein, human serum albumin (HSA), which plays a significant role in the transportation of hormones, drugs and fatty acids throughout the human body.¹⁷⁻²⁴ Previously, several studies have been carried out to understand the denaturation profile of HSA and also the effect of renaturing agents like sugars to combat this denaturing effect.²²⁻³⁷ In a work carried out by González-Jiménez *et al.*, it is reported that the denaturation of HSA due to urea takes place as a two-state transition and that even in the presence of 8 M urea, some residual secondary structure remains.²⁵ In the previous chapter, we had described the domain-

specific effects of the two denaturing agents, guanidine hydrochloride (GnHCl) and temperature simultaneously.⁴¹ The ability of external agents to renature the unfolded structure of HSA has also been investigated previously.^{42,43} In a study carried out by Muzammil *et al.*, it was found that different salts of sodium and potassium can stabilize the structure of human serum albumin in the presence of urea. The anions were found to be responsible for this stabilizing effect.⁴² Our research group had previously reported the domain-specific effect of GnHCl and sucrose on HSA, where we found that the stabilizing impact of sucrose is more on domain-I as compared to the other two domains.⁴³ In the present study, we have investigated the effects of urea and sucrose on domain-I, domain-III, and overall structure of HSA. For studying domain-specific effects, we have exploited the solvatochromic effects of N-(7-dimethylamino-4-methylcoumarin-3-yl) iodoacetamide (DACIA) and *p*-nitrophenyl coumarin ester (NPCE) which were tagged to domain-I and domain-III respectively.^{44,45} The fluorescence characteristics of these fluorescent tags situated inside the proteins were used to study the unfolding/folding nature of the protein domains. The overall unfolding and folding of the protein were monitored with the help of circular dichroism spectroscopy.

Water molecules present inside and around biomolecules like proteins, DNA, RNA or cellular membranes usually exhibit properties that are distinct from those of aqueous bulk. These water molecules are generally referred to as biological water.^{46,47} In the case of proteins, the slow dynamics of water within a protein plays an important role in maintaining the structural integrity of the proteins.^{48,49} Many research groups including Zewail, Bagchi and Bhattacharyya have studied the solvation of water molecules inside different protein molecules during the last two decades.^{50–57} The solvation time around a probe molecule inside a protein varies with the amount of denaturation that has occurred to the protein. During denaturation, the probe molecule attached to it becomes exposed to the hydrophilic environment of bulk water, leading to faster solvation dynamics. In a previous report by our research group, the change in such dynamics inside domain-I of HSA caused due to GnHCl,

temperature and sucrose was studied.⁵⁸ In the present work we have investigated the solvation dynamics inside domain-I and domain-III, under the action of different concentrations of urea and sucrose. From this study, we gain information about the changes taking place at the immediate environment of the tagging sites due to the action of the external agents.

5.2 Results

5.2.1 Effect of urea and sucrose on the overall structure of HSA

The change in overall structural features of HSA due to the action of urea and sucrose was monitored by calculating the α -helicity from the circular dichroism (CD) spectra of HSA in the presence of different concentrations of urea and sucrose, by the methods mentioned in section 4.2.1 of chapter 4. α -helicity of HSA decreased monotonously with increasing concentration of urea and in the presence of 9 M urea, the α -helicity was found to be 11%. This value of α -helicity is ascribed to the most unfolded state of HSA in our experiments. The α -helicity of HSA in the presence of different concentrations of sucrose was found to be more than that in the native state of HSA (64%) with its maximum value of 70% being observed in the presence of 1 M sucrose. The presence of sucrose is also found to alleviate the denaturing effect of urea on HSA. In the presence of 1 M sucrose, α -helicity of HSA in presence of 8 M urea was found to be 25%, which is considerably higher than the corresponding value in the absence of sucrose (11%). The stabilizing effect of sucrose is evident in other cases as well, where the presence of sucrose increases the value of α -helicity even in the presence of urea.

The extent of unfolding has been quantified using the same method as used in section 4.2.1 of chapter 4, using the following equation.

$$f_i = \frac{\alpha_i - \alpha_U}{\alpha_N - \alpha_U} \quad (5.1)$$

In the above equation, f_i is the degree of folding, which varies from 0 to 1, α_i is the α -helicity of HSA in presence of a particular concentration of urea and

sucrose and α_U and α_N are the α -helicities of HSA in its unfolded state (ie. in the presence of 9 M urea at 298 K) and native state (in the absence of either urea or sucrose at 298 K), respectively. The contour diagram of the calculated extent of folding as a function of urea and sucrose concentration is shown in figure 5.1, where, the stabilizing effect of sucrose can be clearly seen at its higher concentrations. It can be noted that, at concentrations of sucrose above 0.5 M at very small concentrations of urea, the degree of folding of HSA is more than one, which indicates a more folded state than the native state of HSA. It is interesting to note that, while in the absence of sucrose the denaturation of HSA starts at about 4 M urea, in presence of 1 M sucrose, denaturation starts at about 5.5 M urea.

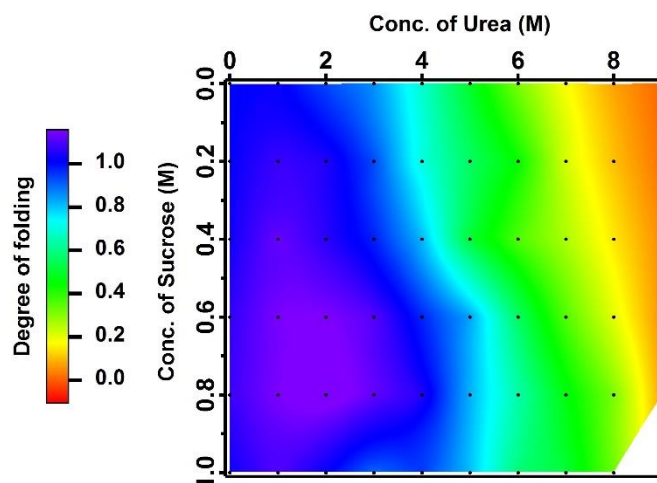


Figure 5.1. Degree of folding of HSA calculated from the CD spectra recorded in the presence of different concentrations of urea and sucrose. The black dots on the contour graph represent the measured data points.

5.2.2 Effect of urea and sucrose on domain-I of HSA

5.2.2.1 Steady state measurements

The domain-I of HSA was tagged with DACIA to study its folding/unfolding behaviour in the presence of urea and sucrose. We had confirmed that the tagging with DACIA does not induce any structural changes in HSA by recording the CD spectrum of HSA in its tagged and untagged states and it was found that both of them show similar spectral features.

The emission spectra of DACIA-tagged HSA under four different combinations of urea and sucrose are shown in figure 5.2. It can be noted that, in the presence of 9 M urea, the spectrum gets red shifted to 476 nm, which is due to the denaturation of domain-I of HSA by the action of urea. In the presence of both 9 M urea and 1 M sucrose, the emission maximum is found at 472 nm. This 4 nm blue shift in emission spectrum in the presence of sucrose is due to the renaturation or refolding occurring at domain-I of HSA in the presence of sucrose. It can also be noted that in the absence of urea, the emission spectra of DACIA-tagged HSA in the presence and absence of sucrose overlaps, which indicates that under these conditions, almost no structural change occurs to domain-I of HSA.

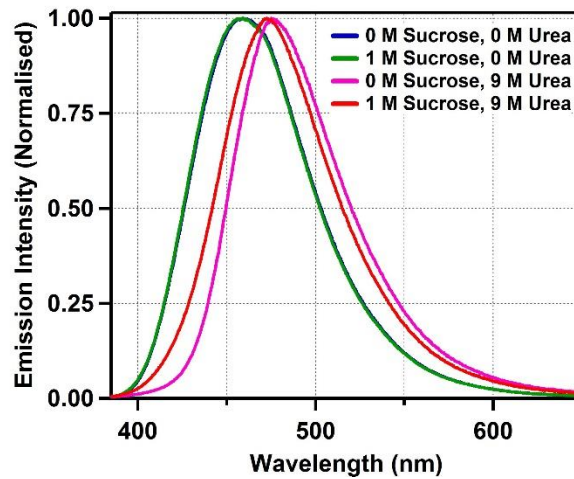


Figure 5.2. Emission spectra of DACIA-tagged HSA at four different combinations of concentrations of urea and sucrose. The samples were excited at 381 nm.

The degree of folding for domain-I of HSA is also calculated using the following equation in which the amount of shift in each case is normalized by the maximum amount of shift.

$$f_i = \frac{\lambda_U - \lambda_i}{\lambda_U - \lambda_N} \quad (5.2)$$

In this case, λ_N and λ_U are the emission maxima in the native and unfolded states respectively and λ_i is the emission maxima at intermediate concentrations of urea and sucrose. The value of λ_i in the absence of both urea and sucrose is taken as the value of λ_N and the value of λ_i in the presence of 9 M urea (maximum amount of

urea used in our experiments) is taken as λ_U . The contour plot (Figure 5.3) shows the variation of degree of folding of domain-I of HSA with variations in the concentrations of urea and sucrose. From the contour plot, it can be seen that even in the absence of sucrose, denaturation of domain-I does not occur to a great extent even after the addition of 4 M urea. But with further addition of urea, degree of folding decreases rapidly and is almost fully denatured in the presence of 9 M urea. With an increase in the concentration of sucrose in presence of 9 M urea, an increase in the degree of folding can be seen and in presence of 1 M sucrose, the degree of folding reaches the value of 1. Also, it can be noted that in some cases, where sucrose concentration is maximum, the value of degree of folding is more than unity.

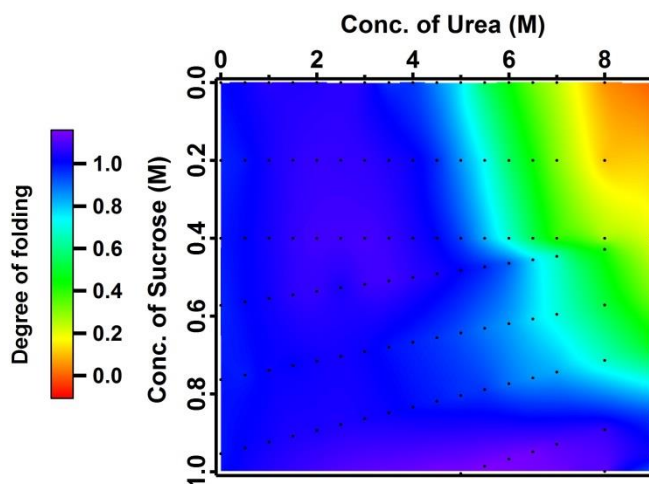


Figure 5.3. Degree of folding of domain-I of HSA calculated from the emission maxima of DACIA-tagged domain-I of HSA in presence of different concentrations of urea and sucrose. The black dots on the contour graph represent the measured data points.

5.2.2.2 Lifetime measurements

To gather more information about the nature of unfolding, we carried out fluorescent lifetime measurements on a few samples. The excited state lifetime measurements were carried out for different samples at their respective emission maxima. As mentioned in section 4.2.2.2, DACIA molecule exhibits a triexponential decay with an average lifetime of 1.98 ns in buffer solution, which increases to 3.63 ns once it is tagged to Cys-34 of domain-I of HSA. Lifetime measurements of DACIA-tagged HSA at three different concentrations of urea and three different

concentrations of sucrose have been carried out and the collected data is shown in table 5.1. All fluorescent decays were fitted using a tri-exponential function. The average lifetime of DACIA-tagged HSA was found to decrease in the presence of both urea and sucrose. In the presence of 5 M urea, average lifetime was found to decrease to 3.2 ns and in the presence of 0.5 M sucrose, it becomes 2.9 ns. The decrease in excited state lifetime is an indication of an increase in the non-radiative rate constant of excited DACIA molecule. However, a definitive trend of change could not be observed with further variation in the concentrations of either urea and sucrose.

Table 5.1. Emission maxima ($\lambda_{ex}=381$ nm) and average lifetimes of DACIA-tagged HSA in presence of different concentrations of sucrose and urea.

Sucrose concentration (M)	Urea concentration (M)	Emission maximum (nm)	Average τ (ns)
0	0	457.0	3.6
0	5	474.0	3.2
0	9	476.0	3.2
0.5	0	460.0	2.9
0.5	5	470.0	3.2
0.5	9	470.5	3.4
1	0	458.0	2.8
1	5	460.0	2.9
1	9	472.0	3.2

5.2.2.3 Solvation dynamics measurements

We have carried out solvation dynamics studies of DACIA inside domain-I of HSA in presence of different concentrations of urea and sucrose. To calculate solvation times and Stokes shifts, fluorescent transients for each samples were collected at the magic angle condition (54.7°) at different wavelengths along the steady-state emission spectrum. In all cases, the decay curves were fitted using a tri-exponential function. The solvation dynamics of DACIA-tagged HSA in buffer solution in the absence of urea and sucrose had been mentioned in section 3.2.2 (chapter 3) where we found the average solvation time to be 0.39 ns and Stokes shift 480 cm^{-1} . In presence of 5 M urea, the three lifetime components at 425 nm were found to be 0.14 ns (29 %), 1.15 ns (30 %) and 3.80 ns (41 %) with an average

lifetime of 1.94 ns. At 550 nm, the lifetime components are 0.33 ns (-18 %), 1.44 ns (55 %) and 5.53 ns (63%) and the average lifetime is 4.22 ns. The three lifetime components and their respective amplitudes at 18 different wavelengths at which the decays were monitored are mentioned in table 5.2. The growth at longer wavelengths are marked by the negative components of the shortest lifetime component.

Table 5.2. Fitting parameters of fluorescence decay of DACIA-tagged HSA in presence of 5 M urea monitored at different wavelengths. The sample was excited at 375.8 nm.

λ_{em} (nm)	a_1	τ_1 (ns) ^a	a_2	τ_2 (ns) ^b	a_3	τ_3 (ns) ^c	$\langle \tau \rangle$ (ns)
425	0.29	0.14	0.31	1.15	0.40	3.82	1.93
435	0.27	0.11	0.27	1.11	3.89	0.46	2.12
445	0.22	0.10	0.26	1.31	0.52	3.95	2.42
450	0.17	0.25	0.17	2.19	0.45	4.09	2.26
455	0.14	0.23	0.35	2.03	0.51	4.17	2.87
460	0.14	0.11	0.31	1.69	0.55	4.27	2.89
465	0.11	0.27	0.61	2.86	0.28	4.35	2.99
470	0.09	0.23	0.62	2.71	0.29	4.94	3.13
475	0.06	0.31	0.57	2.68	0.37	4.60	3.25
480	0.04	0.28	0.51	2.47	0.45	4.56	3.32
485	0.02	0.25	0.43	2.27	0.55	4.39	3.4
490	-0.02	0.28	0.45	2.01	0.57	4.64	3.54
495	-0.06	0.22	0.47	1.80	0.61	4.95	3.85
500	-0.11	0.28	0.43	1.53	0.68	4.82	3.9
510	-0.13	0.32	0.46	1.53	0.67	4.91	3.95
520	-0.18	0.31	0.45	1.35	0.73	4.88	4.11
535	-0.23	0.32	0.50	1.23	0.73	5.10	4.26
550	-0.18	0.33	0.55	1.44	0.63	5.53	4.22

^a ± 0.02 ns, ^b ± 0.05 ns, ^c ± 0.20 ns

Some of the decay transients are shown in figure 5.4 (a) and (b). The time-resolved emission spectra were constructed from the decay components following the standard procedure.⁵⁹ A few of the time-resolved spectra are shown in figure 5.4 (c) along with steady-state spectra. Solvent correlation function was constructed from the peak frequencies of time-resolved emission spectra. While calculating the solvent response function, I have chosen $\nu(\infty)$ as the peak frequency of the time-resolved spectrum whose emission maximum matches closely with that of the steady-state spectrum. The solvent response function thus constructed (figure 5.4 (d)) is best fitted using a biexponential function. The two components were found to

be 0.85 (25 %) and 0.16 (75 %) with average solvation time 0.33 ns. The dynamic Stokes shift was calculated to be 253 cm^{-1} .

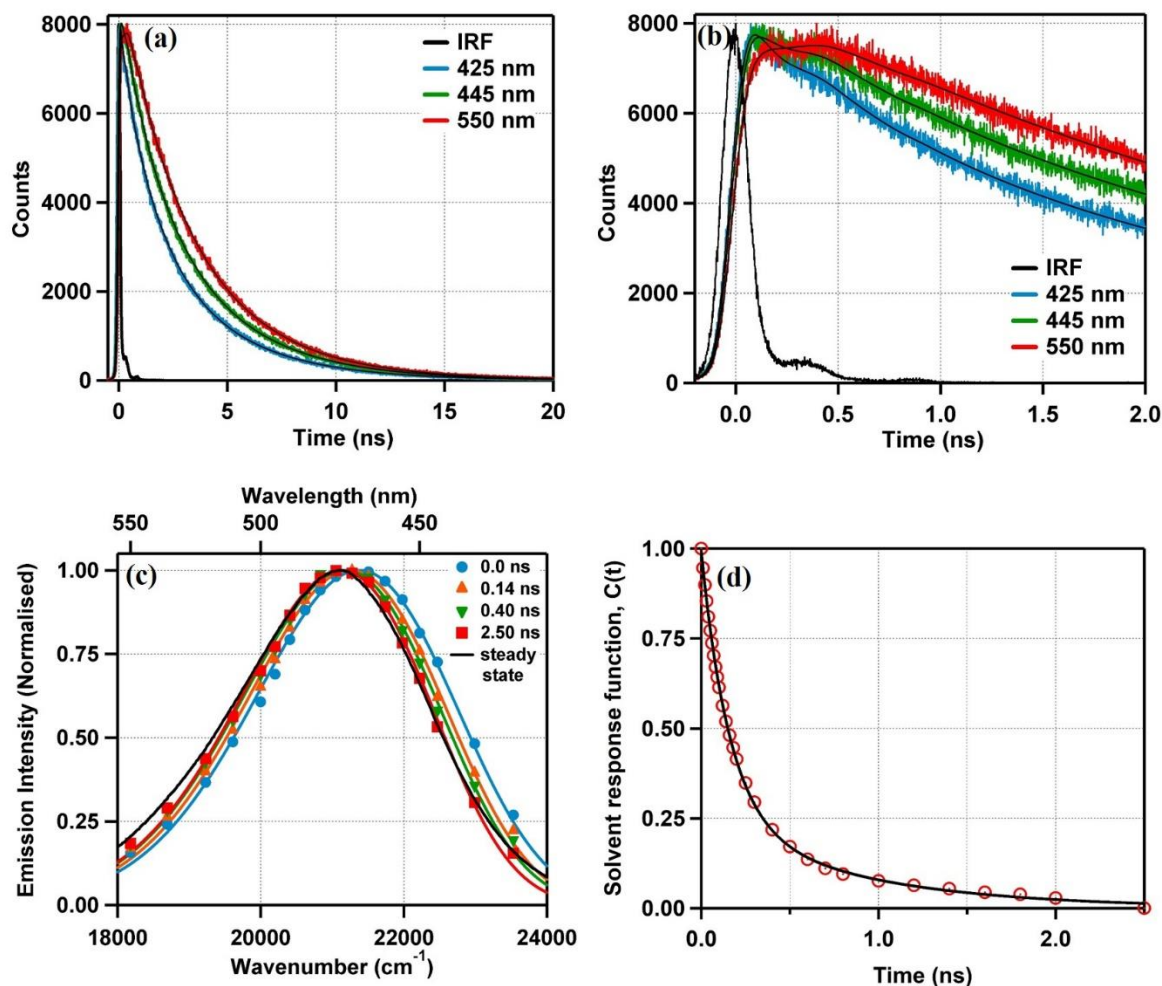


Figure 5.4. A few representative transient decays of DACIA tagged to Cys-34 of HSA in presence of 5 M urea collected at a longer (a) and a shorter (b) timescales. (c) Time-resolved emission spectra (TRES) constructed using the fitting parameters of the transient decays ($\lambda_{ex}=375.8\text{ nm}$) and (d) the solvent response function calculated using the peak frequencies of TRES.

In a similar fashion, solvation times and dynamic Stokes shifts of DACIA-tagged HSA in presence of different concentrations of urea and sucrose were calculated. The solvent response functions and their fitting using biexponential function are shown in figure 5.5 and the solvation time components, observed Stokes shifts and the missing components of Stokes shift are compiled in table 5.3.

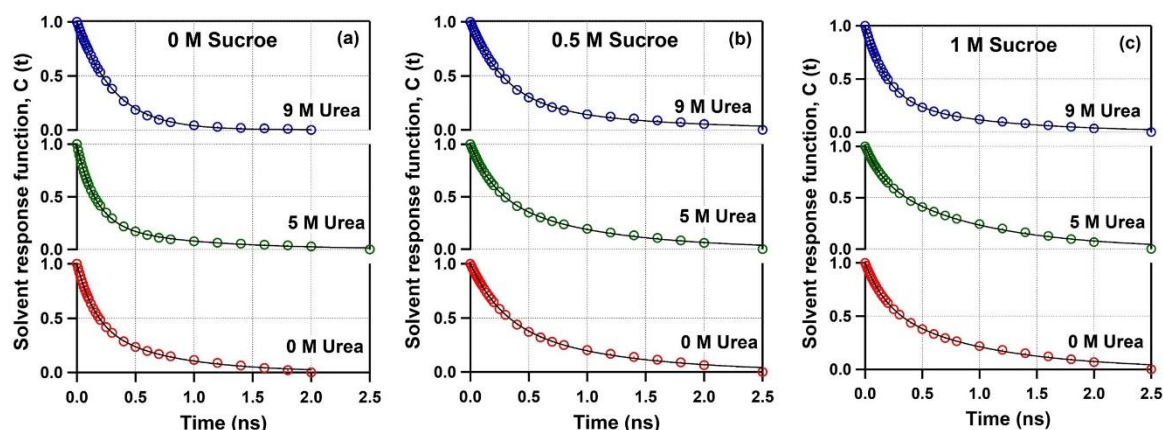


Figure 5.5. Solvent response functions of DACIA-tagged HSA in presence of (a) 0 M, (b) 0.5 M and (c) 1 M sucrose. The solid lines represent the fitting using a biexponential function.

Table 5.3. Solvent response time components, average solvation times, observed dynamic Stokes shifts and the missing component of Stokes shift of DACIA-tagged HSA in presence of different concentrations of urea and sucrose.

Concentration (M)		τ_{s1} (ns)	τ_{s2} (ns)	$\langle \tau_S \rangle$ (ns)	Observed Stokes shift (cm ⁻¹)	Missing component (%)
Sucrose	Urea					
0	0	0.15 (0.55)	0.68 (0.45)	0.39	480	44
0	5	0.16 (0.75)	0.85 (0.25)	0.33	253	86
0	9	0.31 (1.00)		0.31	168	91
0.5	0	0.25 (0.49)	0.98 (0.51)	0.62	444	55
0.5	5	0.20 (0.46)	0.93 (0.54)	0.59	349	75
0.5	9	0.29 (0.73)	1.22 (0.27)	0.54	355	78
1	0	0.18 (0.39)	0.94 (0.61)	0.64	488	46
1	5	0.16 (0.31)	0.91 (0.69)	0.68	465	62
1	9	0.19 (0.68)	0.96 (0.32)	0.44	413	79

From table 5.3, it can be seen that in most of the cases, solvation time of DACIA inside domain-I of HSA decreases with an increase in the concentration of urea. This decrease in solvation time is expected as HSA undergoes denaturation in the presence of urea. In the presence of 0.5 M sucrose, the solvation time increases to 0.62 ns from 0.39 ns in the native state, which further increases to 0.64 ns as the concentration of sucrose is increased to 1 M. The increase in solvation time indicates

that domain-I of HSA becomes more folded in the presence of sucrose. In the presence of 0.5 M sucrose, solvation time decreases from 0.62 ns in the absence of urea to 0.59 ns at 5 M urea and further to 0.54 ns at 9 M urea. As a whole, we have clearly observed that solvation time becomes higher in presence of sucrose and the extent of increase depends on the concentration of sucrose. A similar change was observed with Stokes shift, where the value of Stokes shift decreases with an increase in concentration of urea and increases with an increase in concentration of sucrose in majority of cases I have monitored.

5.2.3 Effect of urea and sucrose on domain-III of HSA

5.2.3.1 Steady state measurements

In order to study the folding and unfolding behaviour of domain-III of HSA, it was tagged with a solvatochromic probe NPCE on Tyr-411. The emission spectra of NPCE-tagged HSA was recorded in the presence of different combinations of urea and sucrose concentrations. Four of them are shown in figure 5.6. In presence of 9 M urea, the emission spectrum of NPCE-tagged HSA gets red shifted to 491 nm due to the denaturation of the domain and gets blue shifted back to 486 nm in presence of both 9 M urea and 1 M sucrose due to the stabilizing or folding effect of sucrose on this domain. Also, the spectra of the native state in presence and absence of sucrose alone almost overlap, indicating very similar degree of folding of both of them.

This space intentionally left blank

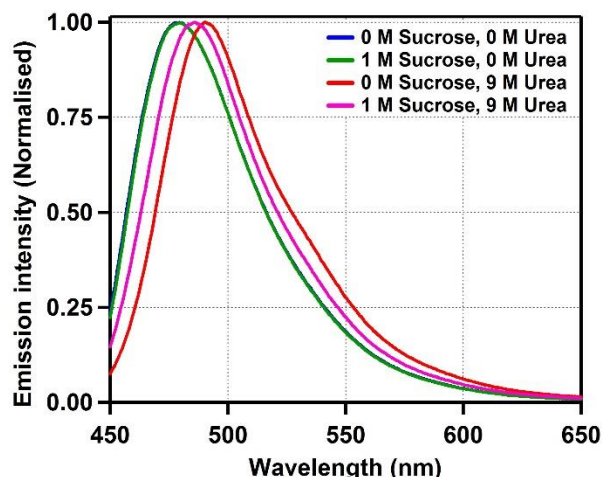


Figure 5.6. Emission spectra of NPCE-tagged HSA at four different combinations of concentrations of urea and sucrose. The samples were excited at 447 nm.

The degree of folding for various concentrations of urea and sucrose were calculated using equation (5.2) and is represented using a contour graph as given in figure 5.7. Similar to the case of domain-I of HSA, the denaturing and renaturing effects of urea and sucrose respectively are evident from the contour plot.

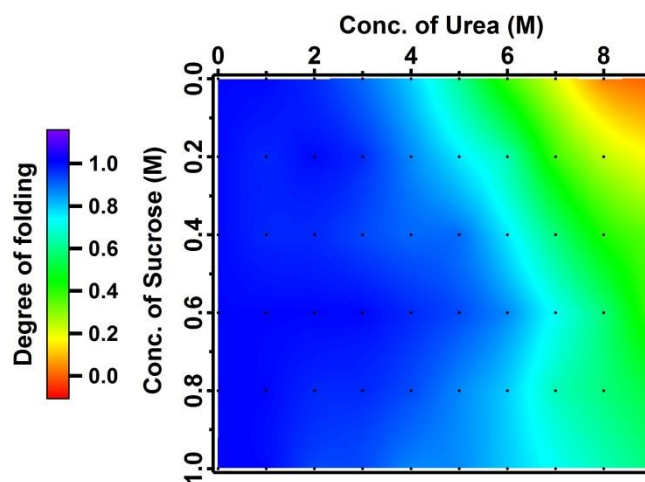


Figure 5.7. Degree of folding of domain-III of HSA calculated from the emission maxima of NPCE-tagged domain-III of HSA in presence of different concentrations of urea and sucrose. The black dots on the contour graph represent the measured data points.

5.2.3.2 Lifetime measurements

Excited state lifetime of NPCE in buffer solution and NPCE tagged to domain-III of HSA in the presence of different concentrations of urea and sucrose were measured at their respective emission maxima. The average lifetime of NPCE-tagged HSA in the presence of different concentrations of urea and sucrose are

compiled in table 5.4. It can be seen that very small variation in lifetime occurs due to the action of either urea or sucrose and also no regular increase/decrease of lifetime can be seen.

Table 5.4. Emission maxima ($\lambda_{ex}= 447$ nm) and average lifetimes of NPCE-tagged HSA in presence of different concentrations of urea and sucrose.

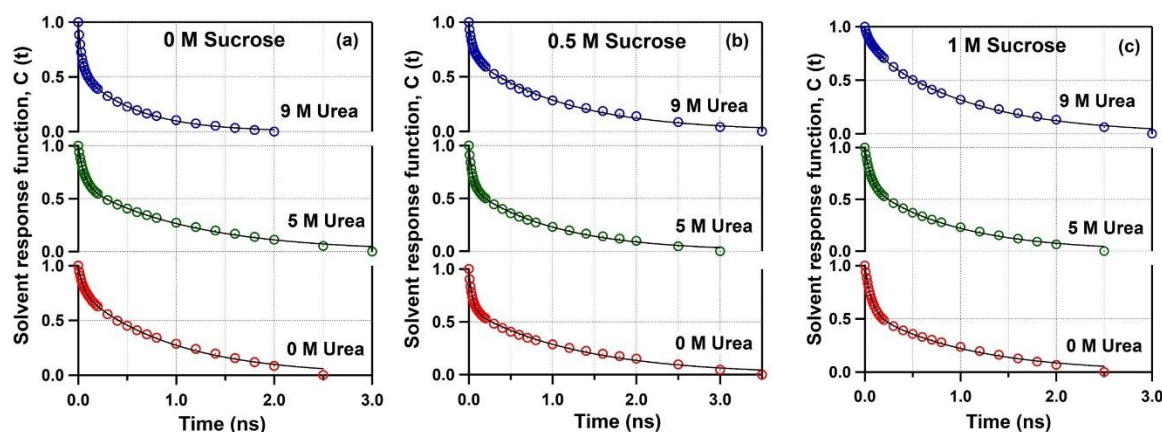
Sucrose concentration (M)	Urea concentration (M)	Emission maximum (nm)	Average τ (ns)
0	0	478.0	3.7
0	5	483.0	3.4
0	9	491.0	3.9
0.5	0	476.5	3.1
0.5	5	480.5	3.2
0.5	9	486.0	3.6
1	0	478.5	2.8
1	5	480.0	3.1
1	9	486.0	3.5

5.2.3.3 Solvation dynamics measurements

Dynamics of solvation inside domain-III of HSA in the presence of 9 different combinations of urea and sucrose were measured using NPCE as the solvatochromic probe. Following the measurement of transients at different wavelengths along the steady-state emission spectrum, TRES were constructed using the wavelength dependent lifetime data. The solvent correlation functions were constructed by using the method mentioned in section 5.2.2.3. The Stokes shifts, solvation time components and average solvation times of different samples are compiled in table 5.5 and the solvent response functions for the same are shown in figure 5.8. From the table, it can be seen that even though the average solvation times tend to decrease with increasing concentration of urea and tend to increase with increasing concentration of sucrose, the trend is not as consistent as we had observed in the case of domain-I of HSA. Stokes shift also does not show a regular trend in this case.

Table 5.5. Solvation time components, average solvation times, dynamic Stokes shifts and the missing component of NPCE-tagged HSA in presence of different concentrations of sucrose and urea.

Concentration (M)		τ_{s1} (ns)	τ_{s2} (ns)	$\langle \tau_S \rangle$ (ns)	Observed Stokes shift (cm ⁻¹)	Missing component (%)
Sucrose	Urea					
0	0	0.05 (0.23)	0.97 (0.77)	0.76	225	80
0	5	0.06 (0.37)	1.14 (0.63)	0.74	293	78
0	9	0.04 (0.45)	0.58 (0.55)	0.34	237	85
0.5	0	0.05 (0.38)	1.32 (0.62)	0.84	337	72
0.5	5	0.05 (0.40)	1.05 (0.60)	0.65	328	74
0.5	9	0.06 (0.31)	1.15 (0.69)	0.81	285	82
1	0	0.07 (0.43)	1.05 (0.57)	0.63	281	77
1	5	0.06 (0.36)	0.94 (0.64)	0.62	283	78
1	9	0.09 (0.16)	1.04 (0.84)	0.89	241	85

**Figure 5.8.** Solvent response functions of NPCE-tagged HSA in presence of (a) 0 M, (b) 0.5 M and (c) 1 M sucrose. The solid line represents the fitting using a biexponential function.

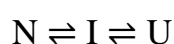
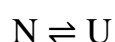
5.3 Discussion

In the present study, the ability of sucrose to alleviate the denaturing effect caused by urea on domain-I and domain-III could be clearly observed. It could also be seen from figure 5.3 that domain-I does not get denatured in the presence of low concentrations of urea and that denaturation begins only after the addition of 4 M

urea. In the presence of 5 M urea, the degree of folding is found to be 0.8 and with a further increase in concentration, the degree of folding decreases rapidly and becomes 0 in the presence of 9 M urea. However, domain-III was found to be more labile towards denaturation as compared to domain-I. Domain-III begins to denature with the addition of 3 M of urea and after the addition of 5 M urea, the degree of folding was found to be less than 0.6. It can also be seen that the stabilizing or renaturing effect of sucrose is more on domain-I as compared to domain-III. In the presence of 1 M sucrose, the denaturation of the domain-I of HSA does not occur (degree of denaturation remain 1.0) even in the presence of 9 M urea. However, in the case of domain-III, the degree of folding in the presence of 1 M sucrose and 9 M urea is found to be 0.5, indicating that a considerable amount of denaturation has occurred under these conditions. Our observation is consistent with some previous works, in which domain-III of HSA is found to be more susceptible to denaturation as compared to the other two domains.⁴⁰

The contour diagram of the degree of folding of the overall HSA (Figure 5.1) shows characteristics of domain-I as well as domain-III. At low concentrations of urea (less than 4 M), the protein appears to be very stabilized in the presence of sucrose. It could be noted that the degree of folding is more than 1 in many cases, which is similar to the behaviour of domain-I of HSA. However, at higher concentrations of urea, the overall structure of protein shows the unfolding behaviour similar to that of domain-III.

We have calculated the free energy changes associated with the unfolding of HSA due to the action of urea in the absence and presence of sucrose using the same models that we had used in section 4.3 using either a two-step or a three-step process as given below.⁶⁰



Here, N, I and U represent the native, intermediate and the unfolded states of the protein, respectively. The degree of folding, Y, can be represented as

$$Y = \frac{Y_N + (Y_U \times e^{-x})}{1 + e^{-x}} \quad (5.3)$$

$$Y = \frac{Y_N + (Y_I \times e^{-x}) + (Y_U \times e^{-y})}{1 + e^{-x} + e^{-y}}. \quad (5.4)$$

Equation (5.3) could be applied to a two-state model and equation (5.4) to a three-state model. In the above equations, Y_N , Y_I and Y_U are the spectroscopic signals for native, intermediate and the unfolded states, respectively. Here, x and y are defined as,⁶⁰

$$x = \frac{(\Delta G^o - m[D])}{RT} \quad (5.5)$$

$$y = \frac{\Delta G_1^o + \Delta G_2^o - (m_1 + m_2)[D]}{RT} \quad (5.6)$$

where, ΔG^o , ΔG_1^o and ΔG_2^o are the free energy changes associated with the corresponding processes, $[D]$ is the concentration of urea and m , m_1 and m_2 denote the slopes of the free energy change plotted against concentration of urea. R and T are the universal gas constant and temperature (in Kelvin), respectively.

The free energy changes for domain-wise and overall unfolding of the protein in the absence and presence of 1 M sucrose were calculated using the above models. The three-state model was adopted for the unfolding of domain-I monitored using the shift of emission maximum as well as for the unfolding of the overall structure monitored using CD spectra. However, for the unfolding of domain-III, where the presence of an intermediate state could not be found, the two-state model was used. The fitting of the data using the two models are shown in figure 5.9 and the changes in free energy calculated using these models are compiled in table 5.6. From the table it could be seen that all ΔG^o values mentioned are positive indicating the non-spontaneity of the unfolding of the protein. It could also be seen that ΔG^o

values for the denaturation of domain-III is lesser than that of domain-I in the absence as well as in the presence of sucrose, which is expected, as domain-III is more feasible towards denaturation as compared to domain-I.

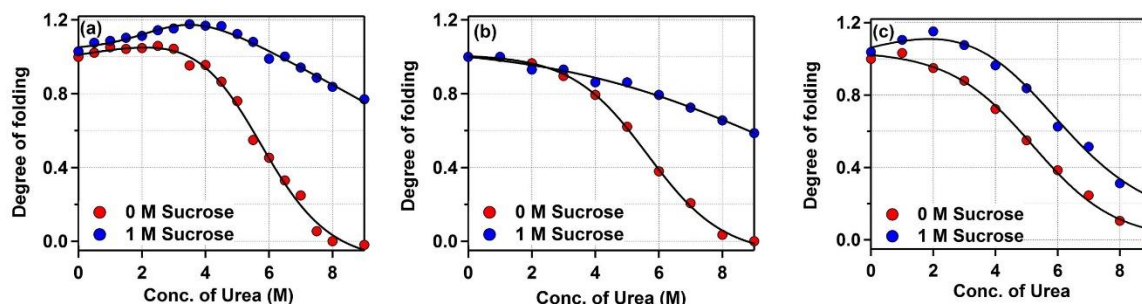


Figure 5.9. The change of degree of folding of (a) domain-I, (b) domain-III and (c) overall structure of HSA with change in concentration of urea in the absence of sucrose (red circles) and presence of 1 M sucrose (blue circles). The fitting of the data using either a two-state or a three-state model are also shown.

Table 5.6. The change in free energy associated with the domain-specific and overall unfolding of HSA in absence and presence of sucrose.

	Domain-I	Domain-III	Overall
ΔG^o associated with urea-induced unfolding in absence of sucrose (kcal mol ⁻¹)	($\Delta G_1^o, N \rightleftharpoons I$) 4.2 ($\Delta G_2^o, I \rightleftharpoons U$) 0.5	($N \rightleftharpoons U$) 2.8	($\Delta G_1^o, N \rightleftharpoons I$) 1.9 ($\Delta G_2^o, I \rightleftharpoons U$) 0.5
ΔG^o associated with urea-induced unfolding in presence of 1 M sucrose (kcal mol ⁻¹)	($\Delta G_1^o, N \rightleftharpoons I$) 2.1 ($\Delta G_2^o, I \rightleftharpoons U$) 1.3	($N \rightleftharpoons U$) 1.6	($\Delta G_1^o, N \rightleftharpoons I$) 0.2 ($\Delta G_2^o, I \rightleftharpoons U$) 1.7

In the case of unfolding of domain-I, the value of ΔG^o corresponding to the $N \rightleftharpoons I$ transition (ΔG_1^o) was found to be 4.2 kcal mol⁻¹ in the absence of sucrose, which decreased to 2.1 kcal mol⁻¹ in presence of 1 M sucrose. However, the value of ΔG_2^o (which corresponds to the value of ΔG^o for $I \rightleftharpoons U$ transition) was found to increase from 0.5 to 1.3 kcal mol⁻¹ when the concentration of sucrose was increased from 0 to 1 M. These changes in ΔG_1^o and ΔG_2^o indicate that the intermediate state during the unfolding process is getting stabilized in presence of sucrose. The stabilization of the intermediate state could be observed for the overall unfolding of the protein also, where ΔG_1^o decreases from 1.9 to 0.2 kcal mol⁻¹ and ΔG_2^o increases from 0.5 to 1.7 kcal mol⁻¹, when the concentration of sucrose was increased from 0 to 1 M. It would be safe to conclude that the stabilization effect of sucrose on HSA

is due to the stabilization of this intermediate state in these cases. In the case of domain-III, where the presence of an intermediate could not be found, ΔG^o was found to decrease from 2.8 to 1.6 kcal mol⁻¹ with an increase in concentration of sucrose from 0 to 1 M, even though one would expect an increase in the value of ΔG^o as presence of sucrose would make the denaturation of the protein less facile. However, this observation could be explained by noting that in our experiments, the degree of folding of domain-III decreases only to a minimum value of 0.7 in presence of sucrose while in the absence of sucrose it decreases to a minimum of 0. So the ΔG^o values indicated in the table for domain-III in the presence of sucrose only represent the free energy change for partial denaturation as compared to the case in the absence of sucrose and as a result, the ΔG^o value is smaller than expected.

While circular dichroism spectra give us information about the degree of folding of the whole protein and steady-state fluorescence spectra using covalently bound solvatochromic probes give us information about the degree of folding of particular domains, the solvation dynamics study provide us with the knowledge of the dynamics of the immediate environment of the tagged sites (in our case, Cys-34 of domain-I and Tyr-411 of domain-III). The average solvation times of DACIA tagged to Cys-34 of domain-I of HSA at nine different combinations of concentrations of urea and sucrose plotted over the contour diagram of degree of folding is shown in figure 5.10. The average solvation time of DACIA tagged to domain-I of HSA decreases by 0.06 ns from 0.39 ns to 0.33 ns with the addition of 5 M urea. This decrease in solvation time is assigned to the unfolding of domain-I. With a further increase in the concentration of urea to 9 M, the solvation time decreases only by 0.02 ns. This suggests that unlike the overall unfolding of domain-I, the unfolding near Cys-34 occurs to a considerable amount at the low concentrations of urea.

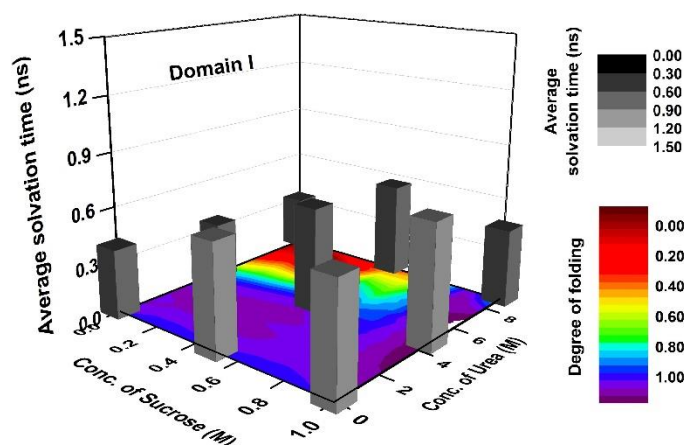


Figure 5.10. Average solvation times of DACIA-tagged HSA in presence of different concentrations of urea and sucrose are represented over the contour plot for the degree of folding of domain-I of HSA.

The addition of sucrose also had a similar effect on the solvation time of DACIA-tagged HSA, but in the opposite direction. The average solvation time of DACIA increased by 0.23 ns in presence of 0.5 M sucrose but increased further only by 0.02 ns when concentration of sucrose is 1 M. This would indicate that the folding/unfolding effects induced by the external agents are prominent at their lower concentrations, but the effect gets saturated above a particular concentration. In the presence of 0.5 M sucrose, the solvation time decreases monotonously with the addition of urea. Surprisingly, in the presence of 1 M sucrose the solvation time increases slightly by 0.04 ns (from 0.64 to 0.68 ns) when the concentration of urea is increased from 0 M to 0.5 M. With a further increase in sucrose concentration, solvation time decreases to 0.44 ns. The small increase in solvation time suggests that at a high concentration of sucrose, smaller concentrations of urea is not enough to cause the unfolding effect near the binding site of DACIA.

The solvation times of NPCE-tagged HSA projected over the contour diagram of degree of folding for domain-III is shown in figure 5.11. From table 5.5, it can be seen that the average solvation time of NPCE inside domain-III decreases with an increase in urea concentration, but significant changes in solvation time occur only when the concentration of urea is more than 5 M. The average solvation time decreases by 0.02 ns when concentration of urea is increased from 0 to 5 M,

while it decreases by 0.40 ns when urea concentration is further increased to 9 M. This is unlike the behaviour observed with domain-I but this change is consistent with the steady state emission changes observed with NPCE-tagged HSA, where the decrease in degree of folding is prominent at urea concentration above 5 M. With the addition of 0.5 M sucrose, the average solvation time of NPCE increases by 0.08 ns, but with a further increase of sucrose concentration to 1 M, it decreases by 0.21 ns from 0.84 to 0.63 ns. As it can be seen from table 5.5, in the presence of 5 M urea, the solvation time decreases from 0.74 ns in the absence of sucrose to 0.65 ns in the presence of 0.5 M sucrose and further to 0.62 ns in the presence of 1 M sucrose. Only in presence of the maximum amount urea used (9 M), a regular renaturing effect of sucrose represented by a prominent increase in solvation time could be seen. In this case, the solvation time increased from 0.34 ns in the absence of sucrose to 0.81 ns in the presence of 0.5 M sucrose and then to 0.89 ns in the presence of 1 M sucrose.

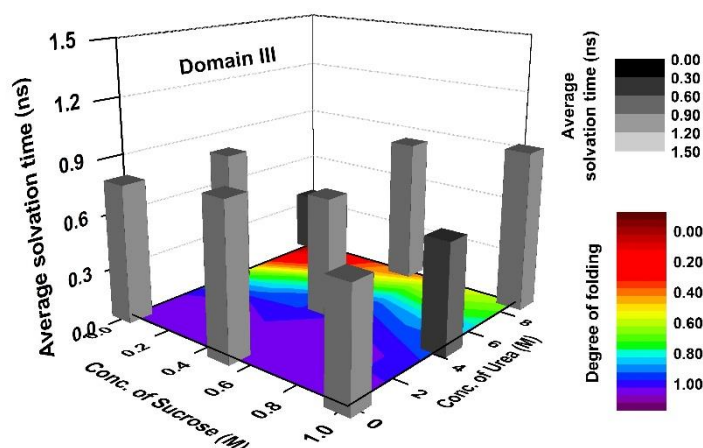
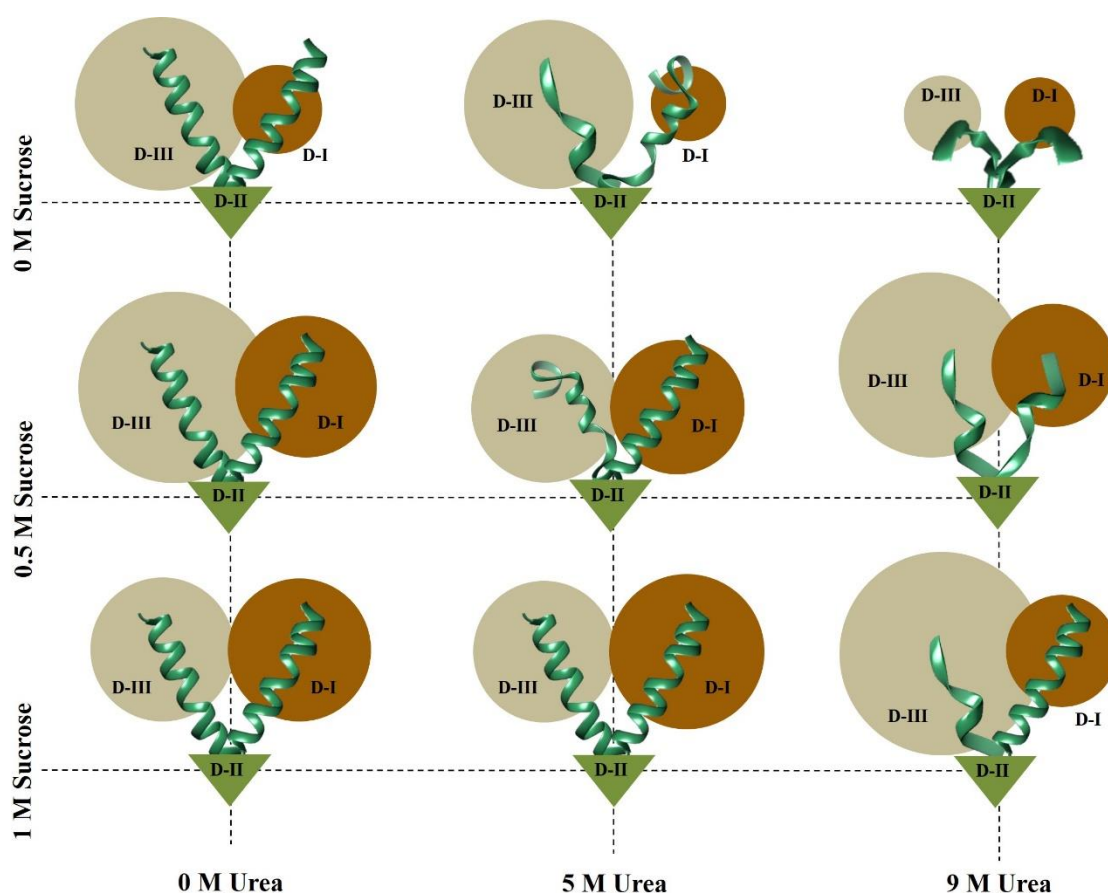


Figure 5.11. Average solvation times of NPCE-tagged HSA in the presence of different concentrations of urea and sucrose are represented over the contour plot for the degree of folding of domain-III of HSA.

From the present study, it could be concluded that even though urea and sucrose result in denaturation and renaturation of both domain-I and domain-III of HSA, the extents are different. Sucrose succumbs to the denaturing effect of urea better in domain-III than in domain-I. On the other hand, domain-I was found to be much more stable in the presence of urea and was more stabilized/renatured when

sucrose is present. Solvation dynamics at the two domains were also found to be different. The faster solvation of DACIA inside domain-I can be attributed to a less confined environment within domain-I of HSA. While for domain-I, the renaturing effect of sucrose could be seen at all different concentrations of urea, in the case of domain-III, the effect is prominent only at very high concentrations of urea when the protein is mostly denatured. It could also be seen that while a monotonous denaturing effect of urea can be seen from the variation of solvation time in presence of different concentrations of sucrose in case of domain-I, such a decrease in solvation time with urea concentration could be seen only in the absence of sucrose in the case of domain-III.



Scheme 1. A schematic representation of variation of degree of folding of domain-I and domain-III of HSA with change in concentration of urea and sucrose. The nature of change of solvation time inside the two domains is also represented by the circles, with a larger circle being an indication of a longer solvation time.

5.4 Conclusion

In the present contribution, we have studied the overall and domain-specific responses of human serum albumin towards two external agents, urea and sucrose, using circular dichroism spectroscopy, steady state emission and solvation dynamics. In order to carry out the domain-specific studies, HSA was tagged separately at Cys-34 and Tyr-411 sites using DACIA and NPCE molecules respectively. The denaturing nature of urea and renaturing nature of sucrose could be clearly seen on the overall structure, domain-I and domain-III of HSA. The domain-III was found to be more prone to urea denaturation with less renaturing effect imposed by sucrose compared to domain-I. The overall unfolding of HSA shows characteristics of domain-I at low concentrations and that of domain-III at higher concentrations of urea. From the circular dichroism and steady state data, the presence of an intermediate state could be found during the unfolding of domain-I and the overall HSA. From the free energy calculations, it was found that this intermediate state stabilizes in the presence of sucrose, which results in the stabilization of protein. The solvation dynamics at domain-III was found to be slower than that in domain-I, which is due to the more confined environment of domain-III. Also, while the solvation time inside domain-I increases regularly due to the action of sucrose at different levels of denaturation, in the case of domain-III, this regular increase in solvation time with increase in sucrose concentration can only be observed when high concentrations of urea is present. This suggests that the renaturing effect of sucrose is not very evident in domain-III when the protein is in its native state.

References

- (1) Berg, J.; Tymoczko, J.; Stryer, L. *Biochemistry*, 5th ed.; W. H. Freeman and company: New York, 2002.
- (2) Nelson, D.; Cox, M. *Lehninger Principles of Biochemistry*, 5th ed.; W. H. Freeman and company: New York, 2008.
- (3) Pace, C. N.; Treviño, S.; Prabhakaran, E.; Scholtz, J. M. Protein Structure, Stability and Solubility in Water and Other Solvents. *Philos. Trans. R. Soc. B Biol. Sci.* **2004**, 359 (1448), 1225–1235.
- (4) Gromiha, M. M. *Protein Bioinformatics from Sequence to Function*, 1st ed.; Elsevier Inc.: New Delhi, 2010.
- (5) Vorobjev, Y. N.; Hermans, J. Free Energies of Protein Decoys Provide Insight into Determinants of Protein Stability. *Protein Sci.* **2001**, 10 (12), 2498–2506.
- (6) Reece, J. B.; Campbell, N. A.; Myers, N.; Urry, L. A.; Cain, M. L.; Wasserman, S. A.; Minorsky, P. V.; Jackson, R. B.; Cooke, B. N. *Campbell Biology*; Pearson Education Australia: Sydney, 2011.
- (7) López-Alonso, J. P.; Bruix, M.; Font, J.; Ribó, M.; Vilanova, M.; Jiménez, M. A.; Santoro, J.; González, C.; Laurents, D. V. NMR Spectroscopy Reveals That RNase A Is Chiefly Denatured in 40% Acetic Acid: Implications for Oligomer Formation by 3D Domain Swapping. *J. Am. Chem. Soc.* **2010**, 132 (5), 1621–1630.
- (8) Sawyer, W. H.; Puckridge, J. The Dissociation of Proteins by Chaotropic Salts. *J. Biol. Chem.* **1973**, 248 (24), 8429–8433.
- (9) Bhuyan, A. K. On the Mechanism of SDS-Induced Protein Denaturation. *Biopolymers* **2009**, 93 (2), 186–199.
- (10) Scholtz, J. M.; Baldwin, R. L. Perchlorate-Induced Denaturation of Ribonuclease A: Investigation of Possible Folding Intermediates. *Biochemistry* **1993**, 32 (17), 4604–4608.
- (11) Leggio, C.; Galantini, L.; Konarev, P. V.; Pavel, N. V. Urea-Induced Denaturation Process on Defatted Human Serum Albumin and in the Presence of Palmitic Acid. *J. Phys. Chem. B* **2009**, 113 (37), 12590–12602.
- (12) Vagenende, V.; Yap, M. G. S.; Trout, B. L. Mechanisms of Protein Stabilization and Prevention of Protein Aggregation by Glycerol. *Biochemistry* **2009**, 48 (46), 11084–11096.
- (13) Abe, M.; Abe, Y.; Ohkuri, T.; Mishima, T.; Monji, A.; Kanba, S.; Ueda, T. Mechanism for Retardation of Amyloid Fibril Formation by Sugars in V λ 6 Protein. *Protein Sci.* **2013**, 22 (4), 467–474.
- (14) Kumar, N.; Kishore, N. Protein Stabilization and Counteraction of Denaturing Effect of Urea by Glycine Betaine. *Biophys. Chem.* **2014**, 189, 16–24.

-
- (15) Wang, Y.; Sarkar, M.; Smith, A. E.; Krois, A. S.; Pielak, G. J. Macromolecular Crowding and Protein Stability. *J. Am. Chem. Soc.* **2012**, *134* (40), 16614–16618.
- (16) Cottone, G. A Comparative Study of Carboxy Myoglobin in Saccharide-Water Systems by Molecular Dynamics Simulation. *J. Phys. Chem. B* **2007**, *111* (13), 3563–3569.
- (17) He, X. M.; Carter, D. C. Atomic Structure and Chemistry of Human Serum Albumin. *Nature* **1992**, *358*, 209.
- (18) Dockal, M.; Carter, D. C.; Rüker, F. The Three Recombinant Domains of Human Serum Albumin: Structural Characterization and Ligand Binding Properties. *J. Biol. Chem.* **1999**, *274* (41), 29303–29310.
- (19) Ghuman, J.; Zunszain, P. A.; Petitpas, I.; Bhattacharya, A. A.; Otagiri, M.; Curry, S. Structural Basis of the Drug-Binding Specificity of Human Serum Albumin. *J. Mol. Biol.* **2005**, *353* (1), 38–52.
- (20) Yamasaki, K.; Chuang, V. T. G.; Maruyama, T.; Otagiri, M. Albumin–drug Interaction and Its Clinical Implication. *Biochim. Biophys. Acta - Gen. Subj.* **2013**, *1830* (12), 5435–5443.
- (21) Li, S.; Zhao, X.; Mo, Y.; Cummings, P. T.; Heller, W. T. Human Serum Albumin Interactions with C60 Fullerene Studied by Spectroscopy, Small-Angle Neutron Scattering, and Molecular Dynamics Simulations. *J. Nanoparticle Res.* **2013**, *15* (7), 1769.
- (22) Abou-Zied, O. K. Investigating 2,2′-Bipyridine-3,3′-Diol as a Microenvironment-Sensitive Probe: Its Binding to Cyclodextrins and Human Serum Albumin. *J. Phys. Chem. B* **2007**, *111* (33), 9879–9885.
- (23) Jana, S.; Dalapati, S.; Ghosh, S.; Guchhait, N. Study of Microheterogeneous Environment of Protein Human Serum Albumin by an Extrinsic Fluorescent Reporter: A Spectroscopic Study in Combination with Molecular Docking and Molecular Dynamics Simulation. *J. Photochem. Photobiol. B Biol.* **2012**, *112*, 48–58.
- (24) Singh, R. B.; Mahanta, S.; Bagchi, A.; Guchhait, N. Interaction of Human Serum Albumin with Charge Transfer Probe Ethyl Ester of N,N-Dimethylamino Naphthyl Acrylic Acid: An Extrinsic Fluorescence Probe for Studying Protein Micro-Environment. *Photochem. Photobiol. Sci.* **2009**, *8* (1), 101–110.
- (25) González-Jiménez, J.; Cortijo, M. Urea-Induced Denaturation of Human Serum Albumin Labeled with Acrylodan. *J. Protein Chem.* **2002**, *21* (2), 75–79.
- (26) Flora, K.; Brennan, J. D.; Baker, G. A.; Doody, M. A.; Bright, F. V. Unfolding of Acrylodan-Labeled Human Serum Albumin Probed by Steady-State and Time-Resolved Fluorescence Methods. *Biophys. J.* **1998**,

- 75 (2), 1084–1096.
- (27) Ahmad, B.; Ankita; Khan, R. H. Urea Induced Unfolding of F Isomer of Human Serum Albumin: A Case Study Using Multiple Probes. *Arch. Biochem. Biophys.* **2005**, *437* (2), 159–167.
- (28) Galantini, L.; Leggio, C.; Pavel, N. V. Human Serum Albumin Unfolding: A Small-Angle X-Ray Scattering and Light Scattering Study. *J. Phys. Chem. B* **2008**, *112* (48), 15460–15469.
- (29) Del Giudice, A.; Leggio, C.; Balasco, N.; Galantini, L.; Pavel, N. V. Ibuprofen and Propofol Cobinding Effect on Human Serum Albumin Unfolding in Urea. *J. Phys. Chem. B* **2014**, *118* (34), 10043–10051.
- (30) Del Giudice, A.; Dicko, C.; Galantini, L.; Pavel, N. V. Time-Dependent PH Scanning of the Acid-Induced Unfolding of Human Serum Albumin Reveals Stabilization of the Native Form by Palmitic Acid Binding. *J. Phys. Chem. B* **2017**, *121* (17), 4388–4399.
- (31) Heller, W. T. Comparison of the Thermal Denaturing of Human Serum Albumin in the Presence of Guanidine Hydrochloride and 1-Butyl-3-Methylimidazolium Ionic Liquids. *J. Phys. Chem. B* **2013**, *117* (8), 2378–2383.
- (32) Zhuo, W.; Peng, X.; Lin, X. Insights into the Interaction Mechanism between Tiagabine Hydrochloride and Two Serum Albumins. *RSC Adv.* **2018**, *8* (44), 24953–24960.
- (33) Shaw, A. K.; Pal, S. K. Spectroscopic Studies on the Effect of Temperature on PH-Induced Folded States of Human Serum Albumin. *J. Photochem. Photobiol. B Biol.* **2008**, *90* (1), 69–77.
- (34) Wallewik, K. Reversible Temperature, Denaturation of Human Serum Albumin and Guanidine Hydrochloride Followed by Optical Rotation. *J. Biol. Chem.* **1973**, *248* (8), 2650–2655.
- (35) Wetzel, R.; Becker, M.; Behlke, J.; Billwitz, H.; Böhm, S.; Ebert, B.; Hamann, H.; Krumbiegel, J.; Lassmann, G. Temperature Behaviour of Human Serum Albumin. *Eur. J. Biochem* **1980**, *104* (2), 469–478.
- (36) Abou-zied, O. K.; Al-Shihi, O. I. K. Characterization of Subdomain IIA Binding Site of Human Serum Albumin in Its Native, Unfolded, and Refolded States Using Small Molecular Probes. *J. Am. Chem. Soc.* **2008**, *130* (32), 10793–10801.
- (37) Picó, G. A. Thermodynamic Features of the Thermal Unfolding of Human Serum Albumin. *Int. J. Biol. Macromol.* **1997**, *20* (1), 63–73.
- (38) Krishnakumar, S. S.; Panda, D. Spatial Relationship between the Prodan Site, Trp-214, and Cys-34 Residues in Human Serum Albumin and Loss of Structure through Incremental Unfolding. *Biochemistry* **2002**, *41* (23), 7443–7452.

- (39) Ahmad, B.; Khan, M. K. A.; Haq, S. K.; Khan, R. H. Intermediate Formation at Lower Urea Concentration in “B” Isomer of Human Serum Albumin: A Case Study Using Domain Specific Ligands. *Biochem. Biophys. Res. Commun.* **2004**, *314* (1), 166–173.
- (40) Ahmad, B.; Ahmed, M. Z.; Haq, S. K.; Khan, R. H. Guanidine Hydrochloride Denaturation of Human Serum Albumin Originates by Local Unfolding of Some Stable Loops in Domain III. *Biochim. Biophys. Acta - Proteins Proteomics* **2005**, *1750* (1), 93–102.
- (41) Mohan, V.; Sengupta, B.; Acharyya, A.; Yadav, R.; Das, N.; Sen, P. Region-Specific Double Denaturation of Human Serum Albumin: Combined Effects of Temperature and GnHCl on Structural and Dynamical Responses. *ACS Omega* **2018**, *3* (8), 10406–10417.
- (42) Muzammil, S.; Kumar, Y.; Tayyab, S. Anion-induced Stabilization of Human Serum Albumin Prevents the Formation of Intermediate during Urea Denaturation. *Proteins Struct. Funct. Bioinforma.* **2000**, *40* (1), 29–38.
- (43) Yadav, R.; Sen, P. Mechanistic Investigation of Domain Specific Unfolding of Human Serum Albumin and the Effect of Sucrose. *Protein Sci.* **2013**, *22* (11), 1571–1581.
- (44) Wang, R.; Sun, S.; Bekos, E. J.; Bright, F. V. Dynamics Surrounding Cys-34 in Native, Chemically Denatured, and Silica-Adsorbed Bovine Serum Albumin. *Anal. Chem.* **1995**, *67* (1), 149–159.
- (45) Sengupta, B.; Acharyya, A.; Sen, P. Elucidation of the Local Dynamics of Domain-III of Human Serum Albumin over the Ps-Ms Time Regime Using a New Fluorescent Label. *Phys. Chem. Chem. Phys.* **2016**, *18* (41), 28548–28555.
- (46) Zhong, D.; Pal, S. K.; Zewail, A. H. Biological Water: A Critique. *Chem. Phys. Lett.* **2011**, *503* (1–3), 1–11.
- (47) Jungwirth, P. Biological Water or Rather Water in Biology? *J. Phys. Chem. Lett.* **2015**, *6* (13), 2449–2451.
- (48) Bellissent-Funel, M.-C.; Hassanali, A.; Havenith, M.; Henchman, R.; Pohl, P.; Sterpone, F.; van der Spoel, D.; Xu, Y.; Garcia, A. E. Water Determines the Structure and Dynamics of Proteins. *Chem. Rev.* **2016**, *116* (13), 7673–7697.
- (49) Nandi, N.; Bagchi, B. Dielectric Relaxation of Biological Water. *J. Phys. Chem. B* **1997**, *101* (50), 10954–10961.
- (50) Kamal, J. K. A.; Zhao, L.; Zewail, A. H. Ultrafast Hydration Dynamics in Protein Unfolding: Human Serum Albumin. *Proc. Natl. Acad. Sci. U. S. A.* **2004**, *101* (37), 13411–13416.
- (51) Das, D. K.; Mondal, T.; Mandal, U.; Bhattacharyya, K. Probing Deuterium

- Isotope Effect on Structure and Solvation Dynamics of Human Serum Albumin. *ChemPhysChem* **2011**, *12* (4), 814–822.
- (52) Chowdhury, R.; Mojumdar, S. Sen; Chattoraj, S.; Bhattacharyya, K. Effect of Ionic Liquid on the Native and Denatured State of a Protein Covalently Attached to a Probe: Solvation Dynamics Study. *J. Chem. Phys.* **2012**, *137* (5), 55104.
- (53) Bagchi, B. Water Dynamics in the Hydration Layer around Proteins and Micelles. *Chem. Rev.* **2005**, *105* (9), 3197–3219.
- (54) Mondal, S.; Mukherjee, S.; Bagchi, B. Origin of Diverse Time Scales in the Protein Hydration Layer Solvation Dynamics: A Simulation Study. *J. Chem. Phys.* **2017**, *147* (15), 154901-1–11.
- (55) Ben Ishai, P.; Tripathi, S. R.; Kawase, K.; Puzenko, A.; Feldman, Y. What Is the Primary Mover of Water Dynamics? *Phys. Chem. Chem. Phys.* **2015**, *17* (23), 15428–15434.
- (56) Popov, I.; Ishai, P. Ben; Khamzin, A.; Feldman, Y. The Mechanism of the Dielectric Relaxation in Water. *Phys. Chem. Chem. Phys.* **2016**, *18* (20), 13941–13953.
- (57) Kurzweil-Segev, Y.; Popov, I.; Eisenberg, I.; Yochelis, S.; Keren, N.; Paltiel, Y.; Feldman, Y. Confined Water Dynamics in a Hydrated Photosynthetic Pigment–protein Complex. *Phys. Chem. Chem. Phys.* **2017**, *19* (41), 28063–28070.
- (58) Yadav, R.; Sengupta, B.; Sen, P. Effect of Sucrose on Chemically and Thermally Induced Unfolding of Domain-I of Human Serum Albumin: Solvation Dynamics and Fluorescence Anisotropy Study. *Biophys. Chem.* **2016**, *211*, 59–69.
- (59) Maroncelli, M.; Fleming, G. R. Picosecond Solvation Dynamics of Coumarin 153: The Importance of Molecular Aspects of Solvation. *J. Chem. Phys.* **1987**, *86* (11), 6221–6239.
- (60) Naidu, K. T.; Prabhu, N. P. Protein-Surfactant Interaction: Sodium Dodecyl Sulfate-Induced Unfolding of Ribonuclease A. *J. Phys. Chem. B* **2011**, *115* (49), 14760–14767.

This page intentionally left blank

Chapter 6

Elucidation of Active Site Dynamics of Papain and the Effect of Encapsulation within Cationic and Anionic Reverse Micelles

Mohan, V. Sen, P. Elucidation of active site dynamics of papain and the effect of encapsulation within cationic and anionic reverse micelles. *Spectrochim. Acta Part A Mol. Biomol. Spectrosc.* **2018**, *200*, 202–211.

In this study, steady state, solvation dynamics and rotational dynamics experiments have been carried out on DACIA-tagged papain in bulk water and inside the water pool of cationic (cetyltrimethylammonium bromide, CTAB) and anionic (sodium bis(2-ethylhexyl)sulfosuccinate, AOT) reverse micelles with varying water contents ($W_0 = 20$ to 50). While the absorption and emission maxima and the excited state lifetime did not show any noticeable change with the variation of the size of the reverse micelle, the change in solvation time, Stokes shift, rotational correlation time and residual anisotropy with the change in reverse micellar size were quite revealing. The average solvation time and Stokes shift of papain in bulk water are 0.22 ns and 125 cm^{-1} respectively, which increase to 0.96 ns and 718 cm^{-1} while inside CTAB reverse micelle of $W_0 = 20$. The solvation time and Stokes shift values decrease with the increase in the size of reverse micelle, approaching the corresponding values in bulk water when $W_0 = 50$. The solvation time and Stokes shift of the DACIA-tagged papain was also found to be high while inside AOT reverse micelle (0.47 ns and 438 cm^{-1} respectively when $W_0 = 20$), but there was no monotonous variation with the change in size of reverse micelle size as in the case with CTAB reverse micelle. From the anisotropy studies, it was seen that inside CTAB and AOT reverse micelles, there is a significant amount of residual anisotropy, which is absent in the case of DACIA-tagged papain in bulk water. The rotational correlation times were also found to be higher inside the reverse micelles than those in bulk water. Both residual anisotropy and rotational correlation time were found to be more in the case with AOT reverse micelle than with CTAB reverse micelle. These behaviours could be explained based on the electrostatic forces acting between the papain having a positive surface charge and the reverse micelles of cationic CTAB and anionic AOT.

6.1 Introduction

Knowledge about the interaction between solvent and solute molecules, which leads to the stabilization of solute in the solution gives us information about dynamical properties of the solvent and is referred as solvation dynamics. This turns out to be an important tool to understand the nature of water present in biological assemblies. Naturally, the study of solvation dynamics was performed in varieties of biomolecules over the last couple of decades.^{1–8} Being one of the most important biomolecules, proteins have been studied extensively to understand their solvation properties. Apomyoglobin,^{9–12} protein G,^{13,14} human and bovine serum albumins,^{15–25} K-ATPase, Na-ATPase and glutaminyl-tRNA synthetase^{26–30} are some of the protein molecules whose solvation behaviour has been studied. However, a large majority of these studies have been carried out *in vitro* where experiments are carried outside the environment in which proteins naturally exist. In nature, proteins remain confined to a small volume i.e. within a biological cell and consequently there is a large interest to understand the structure, dynamics and biological functions of proteins in a confined and crowded environment.^{31,32}

A protein encapsulated in the water pool of a microemulsion closely resembles the *in vivo* conditions of a biological cell, where water is present in a confined medium.³³ There is a significant difference in the solvation behaviour of the free solvent as compared to confined solvent as reported by several researchers. Bhattacharyya and co-workers studied the solvation dynamics of coumarin 480 in reverse micelles and found that the dynamics in bulk water is significantly faster than in AOT reverse micelle.³⁴ They concluded that the relaxation of micelle bound water is several fold slower than the free water. Corbeil *et al.* studied the solvation dynamics in quaternary micellar systems and found it to be significantly slower than that in ternary micellar systems.³⁵ Pant *et al.* studied the solvation dynamics inside nonionic reverse micelles and reported that the polar solvation dynamics becomes slower inside reverse micelles and new slow relaxation modes arise, which are not observed in bulk water.³⁶

A microemulsion is basically a nano-droplet of water surrounded by a layer of surfactant and dispersed in hydrocarbon medium. If the protein resides in the core of the water pool, one may expect that it retains the structure and biological activity as in bulk water. However, if the protein carries a net charge opposite to that of the surfactant, strong electrostatic interaction may induce some structural alteration of the protein within the water pool. The presence of a big protein molecule within a small water pool is likely to cause serious restrictions on the motion of the water molecules. In bulk water, movement of water is fast and solvation dynamics occurs in <1 ps time scale. However, in the case of water present inside a protein molecule or that of water present in the water pool of a microemulsion, the solvation dynamics exhibits a component in 100-1000 ps time scale, which has been confirmed with a numerous number of studies over the last two decades, pioneered by Bhattacharyya and co-workers. Unfortunately, we do not have a clear idea about how the solvation dynamics will be affected when protein is present in a confined environment, which is the main emphasis of the present work.

Over the last few decades, many experimental as well as theoretical studies have been carried out to gain knowledge about the change in structural properties and enzymatic activities of proteins when confined inside a water pool created by a reverse micelle.³⁷⁻⁴⁷ Grandi *et al.* have studied lysozyme solubilized inside reverse micelle of AOT.³⁷ They reported that the enzymatic activity of protein depends on the water content of the reverse micellar system and also that the helical content of lysozyme increases from 34% in bulk water to 48% inside reverse micelle. Mukherjee *et al.* have carried out similar studies in more details wherein they studied the correlation between the structural properties with the size of the water pool for a series of alanine rich peptides.³⁸ They have found that even though a decrease in the size of water pool helps to stabilize the helical conformation of peptides, the concomitant decrease in pool size forces the peptides to adopt another conformation. Malik *et al.* have studied the interaction of HSA with 1-anilinonaphthalenesulphonate (ANS) inside AOT reverse micelles and they

observed that the binding between the two has considerably decreased inside the reverse micelle due to the distortion in secondary structure of the protein and the disruption happened to the ANS binding sites.³⁹ Molecular dynamic simulations carried out in this regard revealed that even though the peptide molecule (alanine-rich AKA₂ peptide in this case) retained its helical conformation within a spherically constrained AOT reverse micelle, it partially unfolded when simulated inside an unconstrained reverse micelle.⁴⁰ In one of the previous works carried out by our group, we have investigated the effect of confinement of HSA to the water pool created by AOT reverse micelle by fluorescence correlation spectroscopy.⁴⁸ It was observed that the conformational fluctuation time of HSA inside reverse micelle is about 6 times smaller than that in bulk water and the fluctuation time increases with increase in size of water pool, approaching the value of the same in bulk water.

In the present work, we report the effect of encapsulation of a protein, papain on the slow component of solvation dynamics in the water pools of reverse micelles. Even though many studies have been carried out on protein molecules trapped inside the water pool of a reverse micelle, the solvation dynamic studies of the same have not been performed to the best of our knowledge. Also, we have tried to look at the effect of surface charge of reverse micelle on solvation dynamics of papain, which itself has a net positive surface charge. For this purpose, we have used reverse micelles of cetyl trimethyl ammonium bromide (CTAB), which is positively charged and sodium bis(2-ethylhexyl)sulfosuccinate (AOT) which is negatively charged for creating the water pool in which papain is confined.

Papain, the protein which has been investigated in this work, is a plant protease enzyme isolated from papaya.^{49,50} Due to its proteolytic activity, papain has found application in pathological studies, drug design and pharmaceutical preparations. This globular protein has a molecular weight of 23.4 kDa and has a single chain with 212 amino acid residues. The three dimensional structure consists of two distinct structural domains (R and L) with a cleft between them. Cysteine-25 and histidine-159 located in the cleft are responsible for the enzymatic activities of

papain.⁴⁹ Papain's enzymatic use was first discovered in 1873 by G. C. Roy, while the structure of papain was determined by X-ray crystallography by Drenth *et al.* in 1968.⁵¹ For our experiments the single free cysteine residue at position 25 in domain-L is covalently labelled with N-(7-dimethylamino-4-methylcoumarin-3-yl) iodoacetamide (DACIA).⁵²

AOT reverse micelles of different water-pool sizes were prepared by injecting the required amount of protein sample (dissolved in buffer of pH 7.4) into a solution of AOT in isooctane. For the preparation of CTAB reverse micelles, the protein sample was injected into a solution of CTAB in isooctane. In this case a 250 μ L of pentanol was added for stabilizing the reverse micelles.

6.2 Results

6.2.1 Steady state experiments

The absorption spectrum of DACIA in 50 mM phosphate buffer (pH 7.4) shows a band centred at 389 nm and upon excitation at 389 nm it gives an emission spectrum with maximum at 478.5 nm. After tagging of papain with DACIA, tagged papain shows an absorption maximum at 386 nm and emission maximum at 474.5 nm (upon excitation at 386 nm). The normalized absorption and emission spectra of DACIA tagged papain were shown in figure 3.9 of chapter 3.

In its native state, papain shows an absorption maximum at 278 nm and after tagging with DACIA the absorption maximum remains the same. The normalised absorption spectra of papain before and after tagging with DACIA are shown in figure 6.1(a). The circular dichroism (CD) spectra of papain were recorded before and after the tagging process to make sure that the secondary structure of papain has not undergone any significant change due to tagging, which are shown in figure 6.1(b).

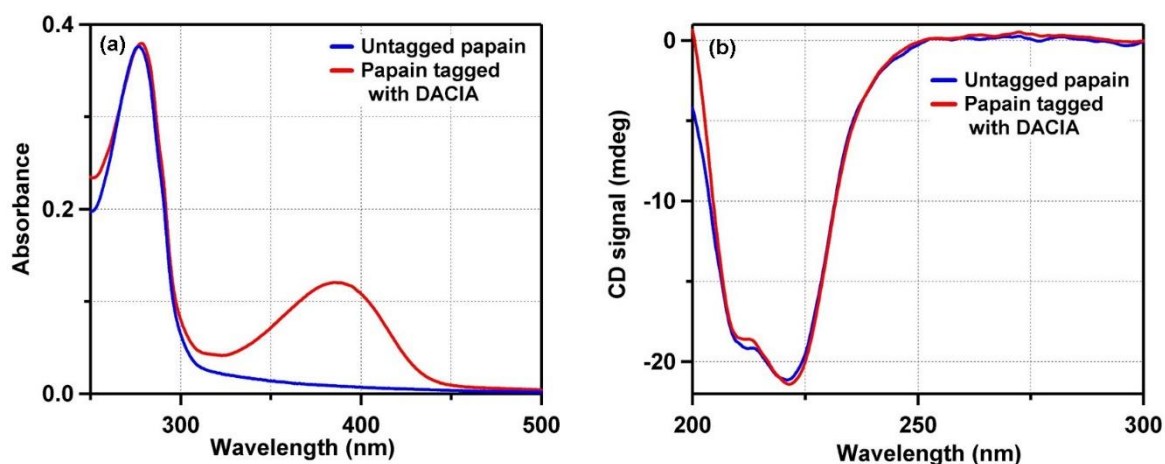


Figure 6.1. Absorption spectra (a) and CD spectra (b) of papain molecule before and after tagging with DACIA molecule

Steady state absorption and emission studies were carried out on DACIA-tagged papain encapsulated inside AOT and CTAB reverse micelles of size varying from $W_0 = 20$ to 50. Here W_0 is a parameter used to characterise microemulsions, which indicates the water content within the reverse micelle. As W_0 increases, the diameter of the water-pool increases. W_0 is defined as,

$$W_0 = \frac{[water]}{[surfactant]} \quad (6.1)$$

The absorption and emission maxima of DACIA-tagged papain inside CTAB and AOT reverse micelles of different W_0 are listed in table 6.1. Inside the water pool of AOT reverse micelle the absorption band centred at 386 nm has been blue shifted. The shift varied with the size of water pool but generally a shift of 3 – 4 nm was observed. The emission spectra also showed similar blue shifts of 1 – 2 nm. In the case of papain inside water pool of positively charged CTAB reverse micelle, similar blue shifts in absorption and emission maxima were observed but the shifts of spectra were much higher in this case as compared to that of AOT reverse micelle. The absorption maxima were shifted by 10 – 12 nm and emission maxima by 2 – 3 nm.

Table 6.1. Absorption and emission maxima (λ_{ex} = 389 nm) of DACIA-tagged papain encapsulated inside AOT and CTAB reverse micelle of different W_0 values.

W_0 of reverse micelle	AOT reverse micelle		CTAB reverse micelle	
	Absorption maxima (nm)	Emission maximum (nm)	Absorption maxima (nm)	Emission maximum (nm)
Bulk water	278.0, 386.0	474.5		
20	276.0, 382.5	472.5	276.5, 373.0	471.5
30	277.0, 383.0	472.0	276.5, 372.5	471.5
40	277.0, 382.0	472.0	277.0, 376.0	472.5
50	279.0, 383.0	473.0	276.0, 374.0	472.5

6.2.2 Lifetime measurements

Excited state lifetime of free DACIA in phosphate buffer was measured at its emission maximum. The fluorescence transient was fitted with a tri-exponential function with the three decay components as 0.28 ns (3%), 1.85 ns (85%) and 3.31 ns (12%) with an average lifetime of 1.98 ns. Once tagged to papain, the average lifetime increases to 2.68 ns with the three lifetime components 0.02 ns (-1%), 1.89 ns (58%) and 3.69 ns (43%). This change in lifetime could be attributed to the change in environment around the fluorescent probe after tagging upon papain.

Fluorescent transients were collected for DACIA-tagged papain inside AOT and CTAB reverse micelles of different W_0 . In all the cases, the transients were fitted using a tri-exponential function. The emission maxima, average lifetime and lifetime components along with their fractional amplitudes are tabulated in table 6.2 and table 6.3. The excited state lifetimes of DACIA tagged papain inside CTAB reverse micelles measured at their respective emission maxima were found to be slightly lower than that in bulk water. Average lifetime was not found to vary considerably with change in W_0 of reverse micelle and in all cases from $W_0 = 20$ to 50 and the values of average lifetime were found to be very close to 2.50 ns. The change in the average lifetime of DACIA-tagged papain inside AOT reverse micelle was found to be even smaller with the values close to 2.60 ns in all the cases.

Table 6.2. Lifetime components and average lifetimes measured at emission maxima of DACIA tagged papain in bulk water and inside CTAB reverse micelle. The fractional amplitudes are given in parentheses.

W₀ of CTAB reverse micelle	Emi. max. (nm)	τ_1 (ns)	τ_2 (ns)	τ_3 (ns)	average τ (ns)
20	471.5	0.84 (0.17)	2.46 (0.62)	3.89 (0.21)	2.48
30	471.5	0.86 (0.16)	2.56 (0.70)	4.13 (0.14)	2.52
40	472.5	0.79 (0.10)	2.44 (0.73)	4.07 (0.17)	2.55
50	472.5	1.10 (0.15)	2.54 (0.76)	4.52 (0.09)	2.50
Bulk water	474.5	0.02 (-0.01)	1.89 (0.58)	3.69 (0.43)	2.68

Table 6.3. Lifetime components and average lifetimes measured at emission maxima of DACIA tagged papain in bulk water and inside AOT reverse micelle. The fractional amplitudes are given in parentheses.

W₀ of AOT reverse micelle	Emi. max. (nm)	τ_1 (ns)	τ_2 (ns)	τ_3 (ns)	average τ (ns)
20	472.5	0.67 (0.11)	2.34 (0.60)	3.87 (0.29)	2.60
30	472.0	0.59 (0.08)	2.26 (0.56)	3.81 (0.37)	2.72
40	472.0	0.64 (0.13)	2.32 (0.58)	3.89 (0.29)	2.56
50	473.0	0.74 (0.12)	2.38 (0.60)	3.97 (0.28)	2.63
Bulk water	474.5	0.02 (-0.01)	1.89 (0.58)	3.69 (0.43)	2.68

6.2.3 Solvation Dynamics Study

Solvation dynamics of DACIA-tagged papain in buffer solution had been described in section 3.2.5 of chapter 3. In a similar fashion, solvation dynamics of DACIA-tagged papain inside CTAB and AOT reverse micelles having W_0 values 20, 30, 40 and 50 was performed. The lifetime components of DACIA-tagged papain encapsulated inside CTAB reverse micelle of $W_0=20$ collected at 23 different wavelengths are shown in table 6.4.

Table 6.4. Lifetime components of DACIA-tagged papain collected at different wavelengths. The sample was excited at 375.8 nm.

λ_{em} (nm)	a_1	τ_1 (ns) ^a	a_2	τ_2 (ns) ^b	a_3	τ_3 (ns) ^c	$\langle\tau\rangle$ (ns)
405	0.63	0.11	0.34	0.89	0.03	2.83	0.46
420	0.59	0.13	0.31	0.95	0.10	2.82	0.65
430	0.49	0.18	0.34	1.13	0.17	3.02	0.99
435	0.43	0.21	0.35	1.20	0.22	3.08	1.19
440	0.40	0.24	0.35	1.33	0.25	3.16	1.35
444	0.36	0.26	0.36	1.44	0.28	3.21	1.51
448	0.31	0.29	0.37	1.51	0.32	3.25	1.69
452	0.26	0.31	0.39	1.59	0.35	3.28	1.85
456	0.22	0.33	0.40	1.67	0.38	3.32	2
460	0.20	0.45	0.42	1.90	0.38	3.40	2.18
464	0.18	0.56	0.48	2.10	0.34	3.50	2.3
467	0.18	0.72	0.58	2.34	0.25	3.76	2.43
470	0.17	0.84	0.62	2.46	0.21	3.89	2.48
473	0.17	0.95	0.66	2.58	0.17	4.02	2.55
477	0.18	1.14	0.66	2.66	0.16	4.03	2.61
481	0.21	1.43	0.64	2.74	0.15	4.05	2.66
485	0.23	1.64	0.65	2.83	0.12	4.29	2.73
490	0.08	2.11	0.50	2.19	0.42	3.56	2.76
500	-0.28	0.09	0.83	2.30	0.45	3.70	3.55
510	-0.24	0.13	0.87	2.41	0.38	3.80	3.51
520	-0.25	0.16	0.90	2.46	0.34	3.87	3.49
535	-0.29	0.19	0.97	2.51	0.32	3.98	3.65
560	-0.28	0.24	1.03	2.57	0.25	4.20	3.63

^a ± 0.02 ns, ^b ± 0.05 ns, ^c ± 0.20 ns

The lifetime components at 405 nm were found to be 0.11 ns (63%), 0.89 (34%) ns and 2.83 ns (3%) with an average lifetime of 0.46 ns. At 560 nm, the components are 0.24 ns (-28%), 2.57 ns (103%) and 4.20 ns (25%) with an average lifetime of 3.63 ns. A distinct growth component can be observed at higher wavelengths, which is indicated by negative fractional amplitudes of the shortest lifetime component. The fluorescence transients at some wavelengths are shown in figure 6.2 (a). TRES were constructed (figure 6.2(b)) and a dynamic stokes shift of 718 cm⁻¹ was observed. The decay of the solvent correlation function (figure 6.2(c)) can be fitted using a bi-exponential function and the two decay components are 0.24 ns (65%) and 2.31 ns (35%) with an average solvation time of 0.96 ns.

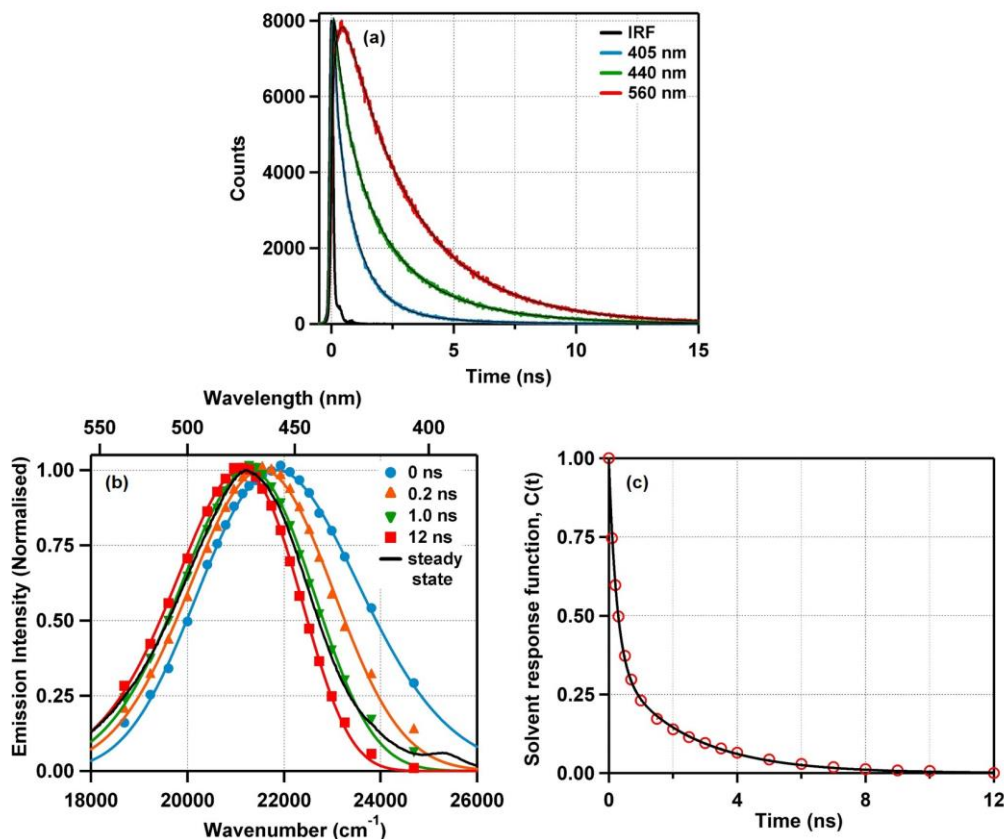


Figure 6.2. (a) A few representative transient decays of DACIA-tagged papain inside CTAB reverse micelle of $W_0 = 20$, (b) time-resolved emission spectra (TRES) constructed using the fitting parameters of the transient decays ($\lambda_{ex} = 375.8$ nm) and (c) the solvent response function calculated using the peak frequencies of TRES

The components of solvent response functions and the dynamic Stokes shift of DACIA-tagged papain inside CTAB reverse micelles of different W_0 are tabulated in table 6.5. The plots of solvent response functions of DACIA-tagged papain inside CTAB reverse micelles of various W_0 values are shown in figure 6.3.

This space intentionally left blank

Table 6.5. Solvent correlation time components, average solvation time and Stokes shift of DACIA-tagged papain inside CTAB reverse micelles of different W_0 . The fractional amplitudes of the solvent correlation time components are given in parentheses.

W_0	τ_{s1} (ns)	τ_{s2} (ns)	$\langle \tau_S \rangle$ (ns)	Observed Stokes shift (cm^{-1})	Missing component (%)
20	0.24 (0.65)	2.30 (0.35)	0.96	718	73
30	0.20 (0.63)	1.46 (0.37)	0.68 ± 0.08	585 ± 20	79
40	0.18 (0.59)	1.00 (0.41)	0.52	560	78
50	0.12 (0.49)	0.59 (0.51)	0.36	636	76
Bulk water	0.03 (0.17)	0.26 (0.83)	0.22 ± 0.06	124 ± 15	94

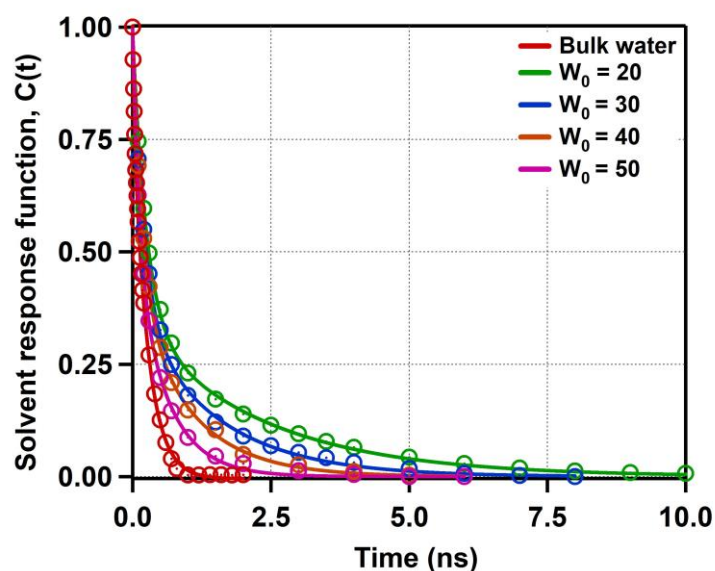


Figure 6.3. The solvent response functions of the active site of papain in bulk water and inside the water pool of CTAB reverse micelles with W_0 varying from 20 to 50 fitted using a biexponential equation.

As can be seen from table 6.5, the average solvation time and stokes shifts are much higher when papain is encapsulated inside the water pool of CTAB reverse micelle. When encapsulated, the motion of water within papain as well as the surrounding water molecules would be restricted, which causes an increase in the time of solvation. It can be seen from table 6.5 that the solvation time and dynamic stokes shift are maximum for $W_0 = 20$ and solvation time decreases monotonously with the increase in size of reverse micelle, approaching the value of solvation time

in bulk water. The value of Stokes shift tends to decrease with increase in the size of the reverse micelle.

Solvation dynamics measurements were also carried out for DACIA-tagged papain inside AOT reverse micelles. The lifetime components at 405 nm for DACIA-tagged papain encapsulated inside AOT reverse micelle of $W_0 = 20$ are 0.12 ns (73%), 0.71 ns (21%) and 2.57 ns (6%) with an average lifetime of 0.39 ns while at 560 nm, the components are 0.19 ns (-27%), 2.36 ns (87%) and 3.93 ns (40%) showing a growth component at higher wavelengths as in the previous cases. Likewise, as stated above, we have constructed the TRES and solvent response function. The decay components of the solvent response function were found to be 0.21 ns (76%) and 1.31 ns (24%) with an average solvation time of 0.47 ns. The dynamic Stokes shift calculated from TRES in this case is 438 cm^{-1} . The solvation time components, Stokes shifts and the missing components of Stokes shift of papain inside AOT reverse micelles of different W_0 are tabulated in table 6.6. As can be seen from table 6.6, the solvation times of DACIA-tagged papain is longer inside the water pools of AOT reverse micelles and the dynamic Stokes shifts are also higher. But unlike papain inside CTAB reverse micelle case, there is no monotonous change in the solvation time or Stokes shift with change of the size of the reverse micelle. The solvent response functions of DACIA-tagged papain inside AOT reverse micelle of various W_0 are shown in figure 6.4.

This space intentionally left blank

Table 6.6. Solvent correlation time components, average solvation time and Stokes shift of DACIA-tagged papain inside AOT reverse micelles of different W_0 . The fractional amplitudes of the solvent correlation time components are given in parentheses.

W_0	τ_{s1} (ns)	τ_{s2} (ns)	$\langle \tau_S \rangle$ (ns)	Observed Stokes shift (cm^{-1})	Missing component (%)
20	0.21 (0.76)	1.31 (0.24)	0.47	438	79
30	0.24 (0.71)	1.65 (0.29)	0.60 ± 0.10	472 ± 25	76
40	0.23 (0.81)	1.61 (0.19)	0.49	464	78
50	0.21 (0.76)	1.76 (0.24)	0.58	564	73
Bulk water	0.03 (0.17)	0.26 (0.83)	0.22 ± 0.06	124 ± 15	94

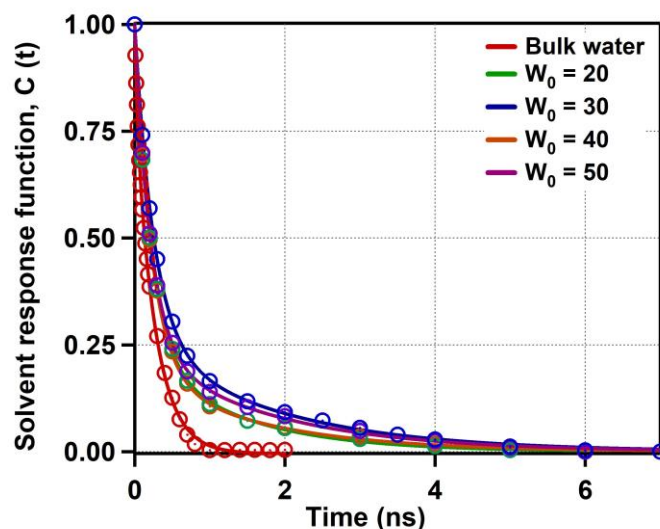


Figure 6.4. The decay curves of solvent correlation function of the active site of papain in bulk water and inside AOT reverse micelles with W_0 varying from 20 to 50 fitted using a biexponential equation.

6.2.4 Fluorescence Anisotropy Study

We carried out time-resolved fluorescence anisotropy studies on DACIA-tagged papain in bulk water and inside CTAB and AOT reverse micelles. The anisotropy decays of DACIA-tagged papain in bulk water and inside CTAB reverse micelles are shown in figure 6.5. As can be seen in the figure, the anisotropy decay inside CTAB reverse micelle is slower with large residual anisotropy as compared to that in bulk water. Also, the decay time tends to become faster with increase in size of reverse micelle. The anisotropy decays are fitted using the equation

$$r(t) = r(\infty) + [r(0) - r(\infty)] \cdot [a_1 e^{(-t/\tau_{R1})} + a_2 e^{(-t/\tau_{R2})}] \quad (6.2)$$

where, $r(t)$ is the anisotropy at time t , $r(\infty)$ is the residual anisotropy, $r(0)$ is the intrinsic anisotropy, τ_{R1} and τ_{R2} are the two components of rotational correlation time with their fractional amplitudes a_1 and a_2 , respectively.⁵³ In bulk water, the shorter component of rotational correlation time was found to be 0.20 ns and the longer component, 9.50 ns. Inside CTAB reverse micelle, the value of the shorter and longer components rises to about 0.5 ns and 10.0 ns, respectively in all cases. The residual anisotropy of DACIA-tagged papain in bulk water is very small (0.01), while inside CTAB reverse micelle the residual anisotropy values are much higher (0.10 ± 0.02). The values of the rotational decay time components along with their fractional amplitudes and the residual anisotropy are shown in table 6.6.

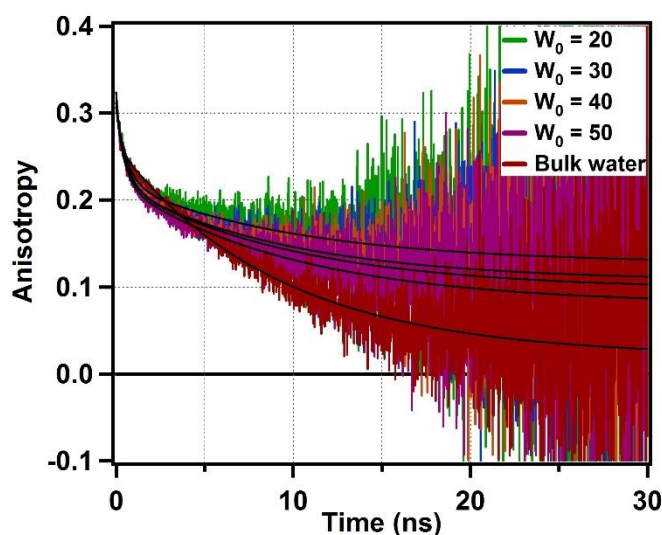


Figure 6.5. Fluorescence anisotropy decay curves of papain in bulk water and inside CTAB reverse micelles of size varying from $W_0=20$ to $W_0=50$

Table 6.7. The components of rotational correlation time and the residual anisotropy of DACIA-tagged papain in bulk water and inside CTAB and AOT reverse micelles of $W_0=20$ to 50.

W_0	CTAB reverse micelle			AOT reverse micelle		
	τ_{R1} (ns)	τ_{R2} (ns)	$r(\infty)$	τ_{R1} (ns)	τ_{R2} (ns)	$r(\infty)$
20	0.60 (0.48)	9.95 (0.52)	0.12	0.53 (0.35)	12.92 (0.65)	0.14
30	0.55 (0.46)	9.55 (0.54)	0.10	0.45 (0.38)	13.12 (0.62)	0.15
40	0.53 (0.43)	9.79 (0.57)	0.09	0.44 (0.38)	13.10 (0.62)	0.15
50	0.47 (0.39)	9.99 (0.61)	0.08	0.42 (0.43)	12.97 (0.57)	0.14
Bulk water	0.20 (0.20)	9.50 (0.80)	0.01			

The anisotropy decays of DACIA-tagged papain inside AOT reverse micelles were also measured and are shown in figure 6.6. As shown in the figure, the rotational decay inside AOT reverse micelle is much slower than that in bulk water. But unlike the case with CTAB reverse micelle, it does not vary much with the size of the reverse micelle. These decay curves were also fitted using equation (6) and the values of the rotational time components and residual anisotropy obtained after fitting are shown in table 6.7. The shorter decay time components of DACIA-tagged papain inside AOT reverse micelle remain very similar to the corresponding values inside CTAB reverse micelle, while the values of the longer rotational decay components are found to be higher (13 ns) than that inside CTAB reverse micelle, in all cases. Residual anisotropies of DACIA-tagged papain inside AOT reverse micelles were also found to be higher (0.14 – 0.15) inside AOT reverse micelles.

This space intentionally left blank

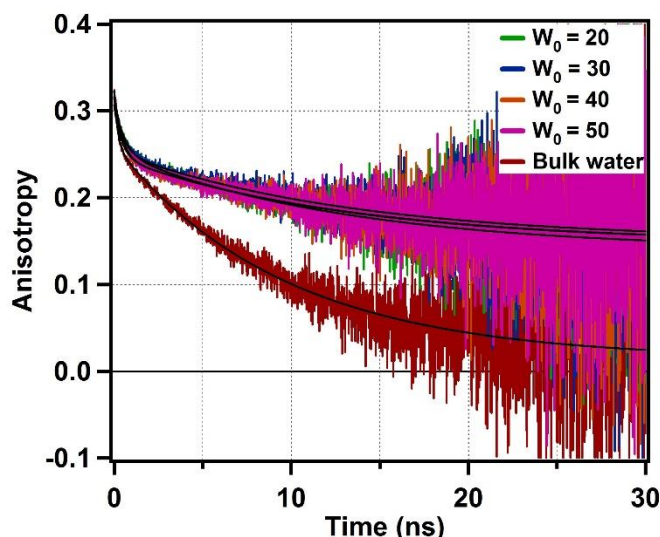


Figure 6.6. Fluorescence anisotropy decay curves of papain in bulk water and inside AOT reverse micelle of size varying from $W_0=20$ to $W_0=50$

6.3 Discussion

The emission maximum of DACIA in water is at 478.5 nm and upon tagging to papain it underwent a blue shift of 4 nm. The absorption peak was also found to undergo a blue shift of 3 nm from 389 nm to 386 nm after the tagging process. These blue shifts in absorption and emission spectra are due to the more hydrophobic, non-polar environment in which DACIA molecule is located inside papain as compared to that in bulk water. When incorporated inside the water-pool of AOT reverse micelles of different W_0 , the emission spectrum of DACIA tagged to papain further underwent a blue shift of about 1.5 – 2.5 nm. Similar blue shifts of 2 – 3 nm were observed while DACIA-tagged papain is encapsulated within the water-pool of CTAB reverse micelles. The shifts in spectra could be an indicative of the more hydrophobic environment inside the reverse micelles. But the position of spectral peak does not vary noticeably with the variation of size of the CTAB reverse micelles. This could indicate that there is not much change in the microenvironment surrounding the DACIA molecule with the change in W_0 of the reverse micelle, which in turn indicates that the structure of protein does not change with change of size of the reverse micelle. The excited state lifetime of DACIA-tagged papain at its emission maxima in bulk water was found to be 2.68 ns. Inside CTAB reverse micelle of $W_0 = 20$, the lifetime reduced by only 0.2 ns. The lifetime was not found

to vary much with the variation in W_0 of CTAB reverse micelle and it was found to be 2.52 ns, 2.55 ns and 2.50 ns for W_0 30, 40 and 50 respectively. When encapsulated inside AOT reverse micelle, the variation of excited state lifetime was found to be even smaller as compared to the case in which DACIA-tagged papain was encapsulated inside CTAB reverse micelle. The average lifetime value of DACIA-tagged papain inside AOT reverse micelle of $W_0 = 20$ was found to be reduced by only 0.08 ns and the maximum variation was found in the case of $W_0 = 40$ in which case the lifetime was found to be reduced by 0.12 ns. The absence of any significant variation in lifetime of DACIA-tagged papain while encapsulated inside the water pool of either CTAB or AOT reverse micelles could be a further indication to the fact that the protein does not undergo any appreciable change in its secondary structure upon encapsulation.

Unlike the steady state absorption and emission maxima and the excited state lifetime, the solvation times and the values of Stokes shift of DACIA-tagged papain inside CTAB and AOT reverse micelles were distinctly different from that in bulk water. In bulk water, DACIA-tagged papain showed an average solvation time of 0.22 ns with the two components 0.03 ns (17%) and 0.26 ns (83%) and a dynamic Stokes shift of 124 cm^{-1} . While encapsulated inside CTAB reverse micelle of $W_0 = 20$, the average solvation time and dynamic Stokes shift were found to increase by about 4.3 and 5.8 times to 0.96 ns and 718 cm^{-1} respectively. With the increase in W_0 values of the reverse micelle, in which papain was encapsulated, the value of solvation time was found to monotonously decrease, and inside $W_0 = 50$, solvation time (0.36 ns) is closest to that in bulk water. The hydrodynamic radius of papain can be found from literature to be 18.4 \AA .⁵⁴ The hydrodynamic radii of CTAB reverse micelle could be found in the literature and was found to vary from 44.9 \AA when $W_0 = 20$ to 89.3 \AA when $W_0 = 50$.⁵⁵ From the given size of papain and the reverse micelles, it would be safe to assume that a papain molecule could be confined inside a reverse micelle without disrupting the structure of the protein. The electrostatic surface potential calculation on papain shows that papain is having

largely positive charge on the surface (figure 6.7). The coulombic surface charge of papain was calculated using UCSF Chimera program using the structure of papain from Research collaborator for structural bioinformatics (RCSB) protein data base reported by Pickersgill et al.⁵⁶ The repulsion between positively charged papain surface and positively charged inner surface of the CTAB reverse micelle will force the protein to remain towards the centre of the water pool. When papain is encapsulated inside CTAB reverse micelle with $W_0 = 20$, the electrostatic repulsion as well as the effect of confinement towards the restriction of motion of molecules will be more as compared to that inside the bigger reverse micelles. This causes the maximum value of solvation time of DACIA-tagged papain when encapsulated inside CTAB reverse micelle with $W_0 = 20$ and its monotonous decrease with increase in the size of the reverse micelle. A plot showing the decrease of solvation time of DACIA-tagged papain with increasing diameter of water pool is shown in figure 6.8. The diameter of water pool was calculated using the known values of hydrodynamic radii of reverse micelle⁵⁴ and the length of a CTAB molecule.

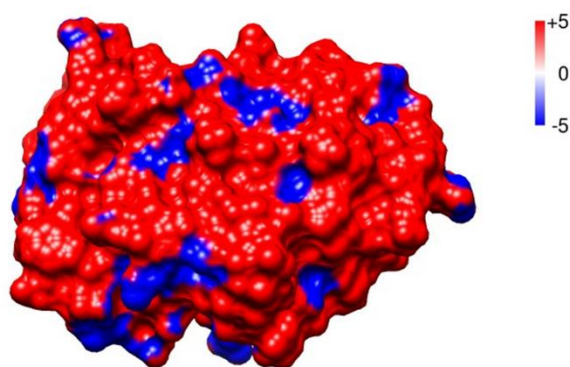


Figure 6.7. Electrostatic potential map of papain. The values of potential mentioned in the colour code are in kcal/mol.e.

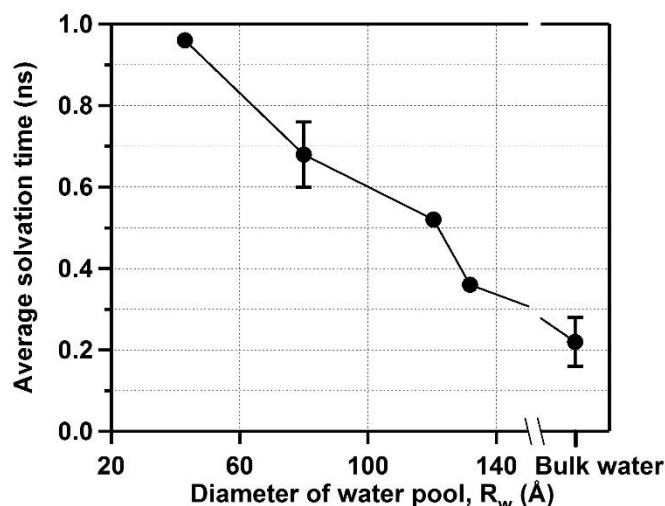


Figure 6.8. The average solvation time of DACIA-tagged papain encapsulated inside the water pool of CTAB reverse micelle plotted against the diameter of the water pool.

Similar to the case as with CTAB reverse micelle, encapsulation of DACIA-tagged papain inside AOT reverse micelle also resulted in a significant increase in solvation time and dynamic Stokes shift. The average solvation time and Stokes shift inside AOT reverse micelle of $W_0=20$ are 0.47 ns and 438.2 cm^{-1} respectively, which are 2.1 and 3.5 times as compared to the corresponding values for DACIA-tagged papain in bulk water. But unlike the case with CTAB reverse micelle, neither solvation time nor Stokes shift shows any monotonous change in values with increase in the size of reverse micelle. The plot showing the variation of solvation time with the diameter of the water pool inside AOT reverse micelles is shown in figure 6.9. The size of AOT reverse micelles could also be found from literature. The hydrodynamic radii varied from 51.1 Å for $W_0=20$ to 118.0 Å for $W_0=50$,⁵⁷ which indicates that a papain molecule would be able to be located inside AOT reverse micelles. The protein having a positive surface charge will be electrostatically attracted towards the negatively charged inner surface of the AOT reverse micelle. This causes papain to be located towards the inner surface of the reverse micelle regardless of its size. As a result, the solvation will not depend on the size of reverse micelle, but the solvation will still be slower inside reverse micelle as compared to that in bulk water due to the restrictions induced by the confined space.

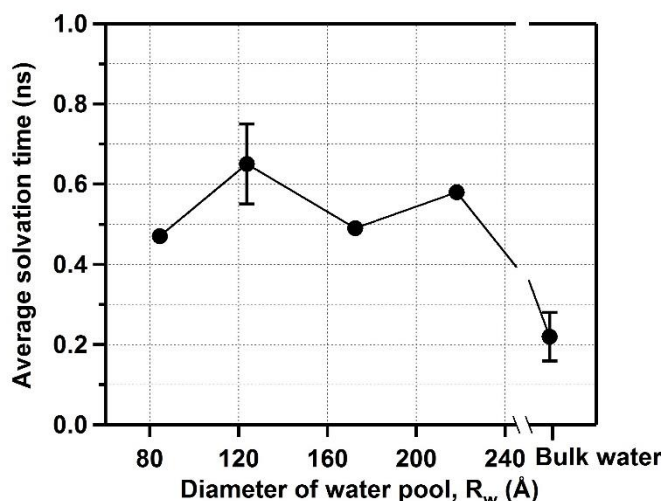


Figure 6.9. The average solvation time of DACIA-tagged papain encapsulated inside the water pool of AOT reverse micelle plotted against the diameter of the water pool.

From the rotational anisotropy studies it was seen that in bulk water, DACIA-tagged papain exhibits negligible residual anisotropy (0.01), while inside CTAB and AOT reverse micelles the residual anisotropy was found to be much higher. Inside CTAB and AOT reverse micelles the value of residual anisotropy was found to be ~ 10 times and ~ 13 times respectively as compared to that in bulk water. The presence of residual anisotropies indicates that the rotation of the protein molecule as well as the probe molecule is hindered inside the reverse micelles as compared to that in bulk water. Also, it can be seen that the residual anisotropy values are higher for DACIA-tagged papain inside AOT reverse micelles compared to that inside CTAB reverse micelles, which would be due to the close proximity of the protein molecule to the inner surface of AOT reverse micelle due to the electrostatic attraction between the protein with a positive surface charge and the micelle surface having negative charge. The anisotropy decay of papain displays two different components, an initial fast component and a slow component. The faster component of decay corresponds to the rotation of covalently bound DACIA molecule inside papain and the slower component corresponds to the rotation of the whole protein molecule. In bulk water, the shorter decay component was found to be 0.20 ns while its value increased to 0.60 ns inside CTAB reverse micelle of $W_0 = 20$, which decreases slightly with an increase in size of the reverse micelle, and has a value of 0.47 inside when $W_0 = 50$. Inside the AOT reverse micelle also, the shorter

decay component has a higher value as compared to that in bulk water. The decay component decreases from 0.53 ns when $W_0 = 20$ to 0.42 when $W_0 = 50$. The higher value of shorter rotational time component indicates that the local motion of the probe molecule inside the protein is hindered when encapsulated inside the water pool of the reverse micelles. With an increase in the size of reverse micelle, the rotational motion becomes more relaxed and faster, resulting in a decrease in the value of the corresponding time component. The slower rotational decay time component, which corresponds to the overall motion of the protein, was found to be 9.50 ns in bulk water. The slower time component does not vary much while the protein is encapsulated inside CATB reverse micelle, with maximum variation occurring in the case of $W_0 = 50$ where the time component increases by 0.5 ns, implying that the encapsulation inside CATB reverse micelle does not affect the rotational motion of protein to any noticeable degree. However, while situated inside the water pool of AOT, the slower rotational time component increases and has a value of 13.0 ± 0.2 in all cases. This indicates that the overall rotation of papain inside AOT reverse micelle is restricted than that inside CTAB reverse micelle or in bulk water, which is because the protein molecule is situated very near to the inner surface of AOT reverse micelle due to the attraction between protein and reverse micellar surface.

6.4 Conclusion

The solvation dynamics at the active site of papain was found to be affected when confined inside a water pool of a reverse micelle. In the case of a cationic (CTAB) reverse micelle the solvation time was found to decrease with increase in the size of water-pool and gradually approaches the bulk water value. This behaviour is because of the fact that the protein molecule would be located towards the centre of water pool in all the cases due to the electrostatic repulsion between the positively charged protein surface and the positive charge on the inner surface of the cationic reverse micelle. Inside a water pool of smaller size, the effect of confinement would be more and hence a higher solvation time was observed. In the case of papain inside

an anionic (AOT) reverse micelle even though the solvation time was found to be longer as compared to that in bulk water, it was found to be independent on the size of the reverse micelle. This is because of the fact that the electrostatic attraction between the papain with positive charge and the negatively charged reverse micellar surface resulted in the protein being located near the inner surface of the reverse micelle in all cases and thus the effect of confinement would be the same irrespective of the size of the reverse micelle. The change in anisotropy also justified the above arguments. The anisotropy decay time of papain was found to be more while confined inside CTAB reverse micelle, decreasing slightly with an increase in size of the reverse micelle. This is due to the restriction in rotation offered by the water pool within the reverse micelle, which also results in high values of residual anisotropy. When confined inside AOT reverse micelle, DACIA-tagged papain shows an increase in anisotropy decay time, but no change in decay time with the change of micelle size could be seen. The rotational restriction offered by AOT reverse micelle would be higher than that of CTAB reverse micelle due to the proximity of papain to the inner surface of reverse micelle, which results in higher values of residual anisotropy and higher rotational correlation times as compared to that inside CTAB reverse micelle.

References

- (1) DeToma, R. P.; Easter, J. H.; Brand, L. Dynamic Interactions of Fluorescence Probes with the Solvent Environment. *J. Am. Chem. Soc.* **1976**, *98*, 5001–5007.
- (2) Lakowicz, J. R.; Cherek, H.; Laczko, G.; Gratton, E. Time-Resolved Fluorescence Emission Spectra of Labeled Phospholipid Vesicles, as Observed Using Multi-Frequency Phase-Modulation Fluorometry. *Biochim. Biophys. Acta - Biomembr.* **1984**, *777*, 183–193.
- (3) Chakrabarty, D.; Hazra, P.; Chakraborty, A.; Sarkar, N. Solvation Dynamics of Coumarin 480 in Bile Salt–Cetyltrimethylammonium Bromide (CTAB) and Bile Salt–Tween 80 Mixed Micelles. *J. Phys. Chem. B* **2003**, *107*, 13643–13648.
- (4) Egelhaaf, H.-J.; Lehr, B.; Hof, M.; Häfner, A.; Fritz, H.; Schneider, F. W.; Bayer, E.; Oelkrug, D. Solvation and Solvent Relaxation in Swellable Copolymers as Studied by Time-Resolved Fluorescence Spectroscopy. *J. Fluoresc.* **2000**, *10*, 383–392.
- (5) Hutterer, R.; Hof, M. Dynamics in Diether Lipid Bilayers and Interdigitated Bilayer Structures Studied by Time-Resolved Emission Spectra, Decay Time and Anisotropy Profiles. *J. Fluoresc.* **2001**, *11*, 227–236.
- (6) Muramatsu, M.; Nagasawa, Y.; Miyasaka, H. Ultrafast Solvation Dynamics in Room Temperature Ionic Liquids Observed by Three-Pulse Photon Echo Peak Shift Measurements. *J. Phys. Chem. A* **2011**, *115*, 3886–3894.
- (7) Balasubramanian, S.; Bagchi, B. Slow Solvation Dynamics near an Aqueous Micellar Surface. *J. Phys. Chem. B* **2001**, *105*, 12529–12533.
- (8) Peon, J.; Pal, S. K.; Zewail, A. H. Hydration at the Surface of the Protein Monellin: Dynamics with Femtosecond Resolution. *Proc. Natl. Acad. Sci.* **2002**, *99*, 10964–10969.
- (9) Gafni, A.; DeToma, R. P.; Manrow, R. E.; Brand, L. Nanosecond Decay Studies of a Fluorescence Probe Bound to Apomyoglobin. *Biophys. J.* **1977**, *17*, 155–168.
- (10) Lakowicz, J. R.; Cherek, H. Proof of Nanosecond Timescale Relaxation in Apomyoglobin by Phase Fluorometry. *Biochem. Biophys. Res. Commun.* **1981**, *99*, 1173–1178.
- (11) Pierce, D. W.; Boxer, S. G. Dielectric Relaxation in a Protein Matrix. *J. Phys. Chem.* **1992**, *96*, 5560–5566.
- (12) Lakowicz, J. R.; Gratton, E.; Cherek, H.; Maliwal, B. P.; Laczko, G. Determination of Time-Resolved Fluorescence Emission Spectra and Anisotropies of a Fluorophore-Protein Complex Using Frequency-Domain Phase-Modulation Fluorometry. *J. Biol. Chem.* **1984**, *259*, 10967–10972.
- (13) Cohen, B. E.; McAnaney, T. B.; Park, E. S.; Jan, Y. N.; Boxer, S. G.; Jan, L.

- Y. Probing Protein Electrostatics with a Synthetic Fluorescent Amino Acid. *Science* **2002**, 296, 1700–1703.
- (14) Park, S.-H.; Shastry, M. C. R.; Roder, H. Folding Dynamics of the B1 Domain of Protein G Explored by Ultrarapid Mixing. *Nat. Struct. Biol.* **1999**, 6, 943.
- (15) Buzády, A.; Erostyák, J.; Somogyi, B. Phase-Fluorometry Study on Dielectric Relaxation of Acrylodan-Labeled Human Serum Albumin. *Biophys. Chem.* **2001**, 94, 75–85.
- (16) Pal, S. K.; Mandal, D.; Sukul, D.; Sen, S.; Bhattacharyya, K. Solvation Dynamics of DCM in Human Serum Albumin. *J. Phys. Chem. B* **2001**, 105, 1438–1441.
- (17) Wang, R.; Sun, S.; Bekos, E. J.; Bright, F. V. Dynamics Surrounding Cys-34 in Native, Chemically Denatured, and Silica-Adsorbed Bovine Serum Albumin. *Anal. Chem.* **1995**, 67, 149–159.
- (18) Mukherjee, S. K.; Gautam, S.; Biswas, S.; Kundu, J.; Chowdhury, P. K. Do Macromolecular Crowding Agents Exert Only an Excluded Volume Effect? A Protein Solvation Study. *J. Phys. Chem. B* **2015**, 119, 14145–14156.
- (19) Dhar, S.; Rana, D. K.; Sarkar, A.; Mandal, T. K.; Bhattacharya, S. C. Fluorescence Resonance Energy Transfer from Serum Albumins to 1-Anthracene Sulphonate Entrapped in Reverse Micellar Nanocavities. *Colloids Surfaces A Physicochem. Eng. Asp.* **2010**, 369, 57–64.
- (20) Vlasova, I. M.; Saletskii, A. M. Fluorescence of Tryptophan in the Denaturation of Human Serum Albumin under the Action of Sodium Dodecyl Sulfate. *Russ. J. Phys. Chem. B* **2009**, 3 (6), 976–980.
- (21) Banerjee, D.; Pal, S. K. Solvation Dynamics of LDS 750 in Micelles, Reverse Micelles and Proteins. *Chem. Phys. Lett.* **2008**, 451, 237–242.
- (22) Quentmeier, C. C.; Wehling, A.; Walla, P. J. A Bioassay Based on the Ultrafast Response of a Reporter Molecule. *J. Biomol. Screen.* **2007**, 12, 341–350.
- (23) Sengupta, B.; Acharyya, A.; Sen, P. Elucidation of the Local Dynamics of Domain-III of Human Serum Albumin over the Ps-[Small Mu]s Time Regime Using a New Fluorescent Label. *Phys. Chem. Chem. Phys.* **2016**, 18, 28548–28555.
- (24) Biswas, S.; Mukherjee, S. K.; Lal, H.; Karmakar, S.; Chowdhury, P. K. PH Dependent Domain Dynamics of HSA Controlled by Protein Based Crowding Agents. *Chem. Phys. Lett.* **2017**, 688, 98–105.
- (25) Yadav, R.; Sengupta, B.; Sen, P. Effect of Sucrose on Chemically and Thermally Induced Unfolding of Domain-I of Human Serum Albumin: Solvation Dynamics and Fluorescence Anisotropy Study. *Biophys. Chem.* **2016**, 211, 59–69.
- (26) Mandal, D.; Sen, S.; Sukul, D.; Bhattacharyya, K.; Mandal, A. K.; Banerjee,

- R.; Roy, S. Solvation Dynamics of a Probe Covalently Bound to a Protein and in an AOT Microemulsion: 4-(N-Bromoacetylamino)-Phthalimide. *J. Phys. Chem. B* **2002**, *106*, 10741–10747.
- (27) Sen, P.; Mukherjee, S.; Dutta, P.; Halder, A.; Mandal, D.; Banerjee, R.; Roy, S.; Bhattacharyya, K. Solvation Dynamics in the Molten Globule State of a Protein. *J. Phys. Chem. B* **2003**, *107*, 14563–14568.
- (28) Demchenko, A. P.; Apell, H.-J.; Stürmer, W.; Feddersen, B. Fluorescence Spectroscopic Studies on Equilibrium Dipole-Relaxational Dynamics of Na,K-ATPase. *Biophys. Chem.* **1993**, *48*, 135–147.
- (29) Samaddar, S.; Mandal, A. K.; Mondal, S. K.; Sahu, K.; Bhattacharyya, K.; Roy, S. Solvation Dynamics of a Protein in the Pre Molten Globule State. *J. Phys. Chem. B* **2006**, *110* (42), 21210–21215.
- (30) Guha, S.; Sahu, K.; Roy, D.; Mondal, S. K.; Roy, S.; Bhattacharyya, K. Slow Solvation Dynamics at the Active Site of an Enzyme: Implications for Catalysis. *Biochemistry* **2005**, *44*, 8940–8947.
- (31) Zhou, H.-X. Protein Folding in Confined and Crowded Environments. *Arch. Biochem. Biophys.* **2008**, *469*, 76–82.
- (32) Harada, R.; Tochio, N.; Kigawa, T.; Sugita, Y.; Feig, M. Reduced Native State Stability in Crowded Cellular Environment Due to Protein–Protein Interactions. *J. Am. Chem. Soc.* **2013**, *135*, 3696–3701.
- (33) Bhattacharyya, K. Solvation Dynamics and Proton Transfer in Supramolecular Assemblies. *Acc. Chem. Res.* **2003**, *36*, 95–101.
- (34) Sarkar, N.; Das, K.; Datta, A.; Das, S.; Bhattacharyya, K. Solvation Dynamics of Coumarin 480 in Reverse Micelles. Slow Relaxation of Water Molecules. *J. Phys. Chem.* **1996**, *100*, 10523–10527.
- (35) Corbeil, E. M.; Levinger, N. E. Dynamics of Polar Solvation in Quaternary Microemulsions. *Langmuir* **2003**, *19*, 7264–7270.
- (36) Pant, D.; Levinger, N. E. Polar Solvation Dynamics in Nonionic Reverse Micelles and Model Polymer Solutions. *Langmuir* **2000**, *16*, 10123–10130.
- (37) Barbaric, S.; Luisi, P. L. Micellar Solubilization of Biopolymers in Organic Solvents. 5. Activity and Conformation of .Alpha.-Chymotrypsin in Isooctane-AOT Reverse Micelles. *J. Am. Chem. Soc.* **1981**, *103*, 4239–4244.
- (38) Mukherjee, S.; Chowdhury, P.; Gai, F. Tuning the Cooperativity of the Helix–Coil Transition by Aqueous Reverse Micelles. *J. Phys. Chem. B* **2006**, *110*, 11615–11619.
- (39) Malik, A.; Kundu, J.; Karmakar, S.; Lai, S.; Chowdhury, P. K. Interaction of ANS with Human Serum Albumin under Confinement: Important Insights and Relevance. *J. Lumin.* **2015**, *167*, 316–326.
- (40) Martinez, A. V.; DeSensi, S. C.; Dominguez, L.; Rivera, E.; Straub, J. E.

- Protein Folding in a Reverse Micelle Environment: The Role of Confinement and Dehydration. *J. Chem. Phys.* **2011**, *134*, 55107.
- (41) Babu, C. R.; Flynn, P. F.; Wand, A. J. Preparation, Characterization, and NMR Spectroscopy of Encapsulated Proteins Dissolved in Low Viscosity Fluids. *J. Biomol. NMR* **2003**, *25*, 313–323.
- (42) Peterson, R. W.; Lefebvre, B. G.; Wand, A. J. High-Resolution NMR Studies of Encapsulated Proteins in Liquid Ethane. *J. Am. Chem. Soc.* **2005**, *127*, 10176–10177.
- (43) Pometun, M. S.; Peterson, R. W.; Babu, C. R.; Wand, A. J. Cold Denaturation of Encapsulated Ubiquitin. *J. Am. Chem. Soc.* **2006**, *128*, 10652–10653.
- (44) Nicot, C.; Waks, M. Proteins as Invited Guests of Reverse Micelles: Conformational Effects, Significance, Applications. *Biotechnol. Genet. Eng. Rev.* **1996**, *13*, 267–314.
- (45) Yeung, P. S.-W.; Eskici, G.; Axelsen, P. H. Infrared Spectroscopy of Proteins in Reverse Micelles. *Biochim. Biophys. Acta - Biomembr.* **2013**, *1828*, 2314–2318.
- (46) Murakami, H.; Toyota, Y.; Nishi, T.; Nashima, S. Terahertz Absorption Spectroscopy of Protein-Containing Reverse Micellar Solution. *Chem. Phys. Lett.* **2012**, *519–520*, 105–109.
- (47) Melo, E. P.; Fojan, P.; Cabral, J. M. S.; Petersen, S. B. Dynamic Light Scattering of Cutinase in AOT Reverse Micelles. *Chem. Phys. Lipids* **2000**, *106*, 181–189.
- (48) Sengupta, B.; Yadav, R.; Sen, P. Startling Temperature Effect on Proteins When Confined: Single Molecular Level Behaviour of Human Serum Albumin in a Reverse Micelle. *Phys. Chem. Chem. Phys.* **2016**, *18*, 14350–14358.
- (49) Mamboya, E. A. F. Papain, a Plant Enzyme of Biological Importance: A Review. *Am. J. Biochem. Biotechnol.* **2012**, *8*, 99–104.
- (50) Lowe, G. The Structure and Mechanism of Action of Papain. *Phil. Trans. R. Soc. Lond. B* **1970**, *257*, 237–248.
- (51) Drenth, J.; Jansonius, J. N.; Koekoek, R.; Swen, H. M.; Wolthers, B. G. Structure of Papain. *Nature* **1968**, *218*, 929.
- (52) Lindahl, P.; Raub-Segall, E.; Olson, S. T.; Björk, I. Papain Labelled with Fluorescent Thiol-Specific Reagents as a Probe for Characterization of Interactions between Cysteine Proteinases and Their Protein Inhibitors by Competitive Titrations. *Biochem. J.* **1991**, *276*, 387–394.
- (53) Lakowicz, J. R. *Principles of Fluorescence Spectroscopy*, 3rd ed.; Springer: Boston, MA, 2006.
- (54) Sengupta, B.; Chaudhury, A.; Das, N.; Sen, P. Single Molecular Level Probing of Structure and Dynamics of Papain Under Denaturation. *Protein Pept. Lett.*

2017, 24, 1073–1081.

- (55) Khan, M. F.; Singh, M. K.; Sen, S. Measuring Size, Size Distribution, and Polydispersity of Water-in-Oil Microemulsion Droplets Using Fluorescence Correlation Spectroscopy: Comparison to Dynamic Light Scattering. *J. Phys. Chem. B* **2016**, 120, 1008–1020.
- (56) Pickersgill, R. W.; Harris, G. W.; Garman, E. Structure of Monoclinic Papain at 1.60 Å Resolution. *Acta Crystallogr. Sect. B* **1992**, 48, 59–67.
- (57) Pal, N.; Verma, S. D.; Singh, M. K.; Sen, S. Fluorescence Correlation Spectroscopy: An Efficient Tool for Measuring Size, Size-Distribution and Polydispersity of Microemulsion Droplets in Solution. *Anal. Chem.* **2011**, 83, 7736–7744.

Chapter 7

A Spectroscopic Insight on Ethanol Induced Aggregation of Papain

Mohan, V.; Das, N.; Das A.; Mishra, V.; Sen, P. A Spectroscopic Insight on Ethanol Induced Aggregation of Papain. *J. Phys. Chem. B* **2019**, *123*, 2280-2290.

In this study, the structural and dynamical changes occurring to papain molecules in ethanol-water binary solvent mixture have been investigated and compared with its denatured state induced by guanidine hydrochloride. Steady-state fluorescence, solvation dynamics, time-resolved rotational anisotropy, circular dichroism and single molecular level fluorescence correlation spectroscopic studies were carried out for this purpose. In ethanol-water mixture with $X_{EtOH} = 0.6$, DACIA-tagged papain was found to undergo a blue shift of 12 nm, while in the presence of 5 M GnHCl, a red shift of 5 nm was observed. Solvation dynamics of the system was also found to be different in presence of these external agents. In ethanol-water mixture, the average solvation time was found to increase almost 2 fold as compared to that in water, while in presence of GnHCl only a marginal increase could be observed. These changes of DACIA-tagged papain in ethanol-water mixture is attributed to the aggregation of the protein in presence of ethanol. Rotational anisotropy study further confirmed the formation of aggregates as the residual anisotropy was found to increase 14 fold and the rotational time component corresponding to the rotation of the probe molecule was found to increase by 4 fold in the ethanol-water mixture. From fluorescent correlation spectroscopic (FCS) study, the hydrodynamic radius of the protein aggregates in ethanol-water mixture was calculated to be ~ 155 Å as compared to the corresponding value of 18.4 Å in the case of native papain molecule. Also, it is confirmed that aggregate formation takes place even in nanomolar concentration of papain. Analysis of circular dichroism spectra of papain showed that an increase in the β -sheet content of papain at the expense of α -helix and the random coil with an increase of ethanol mole fraction may be responsible for this aggregation process.

7.1 Introduction

It has been long known that alcohol-water mixtures show interesting anomalies in many thermodynamic and physiochemical properties including partial molar volume, viscosity, compressibility and diffusion coefficient.¹⁻⁸ Many experimental techniques and theoretical methods have been used to understand these anomalous behaviour of alcohol-water mixtures including Raman spectroscopy, mass spectroscopy and molecular dynamics simulation.⁹⁻¹⁸ The effect of these alcohol-water mixtures on proteins and other macromolecules of biological importance has also been widely studied.¹⁹⁻³³

Bhattacharya and co-workers have looked at the effect of ethanol-water mixture on lysozyme where they found that both the size of the protein and its time constant of conformational relaxation oscillate with increasing concentration of ethanol.¹⁹ They have proposed that this oscillating behaviour is due to the competition between the ethanol-protein, water-protein, ethanol-water, protein-protein, ethanol-ethanol and water-water interactions. Bagchi and co-workers have used molecular dynamics simulations to study another protein, chicken villin headpiece, in ethanol-water mixture and found that the protein unfolds partially under ambient conditions.²⁰ They have also noticed an anomalous behaviour in the unfolding pathway. While most of the reports show that proteins get denatured in presence of aqueous mixture of ethanol,^{20,29,33} some of them reveal that under certain conditions proteins can also get stabilized in ethanol-water mixtures.^{21,28}

Proteins may also form aggregates in presence of aqueous mixture of alcohols.^{25,30,34} Nemzer *et. al* have reported the formation of aggregates of lysozyme under acidic conditions with an 'ethanol shock' of 16% (v/v) ethanol.³⁰ Studies on such protein aggregation are important as they have found to play important role in neurodegenerative diseases in humans, including Alzheimer's disease and Parkinson's disease.³⁵⁻³⁷ Also, the ability to modulate the structure, and in turn functionality, of a protein by changing the alcohol concentration could prove to be helpful under many circumstances.

In the present work, we have investigated the effect of ethanol-water mixture on the structure and dynamics of papain. The effect of aqueous mixture of organic solvents on papain has been previously investigated.^{38–40} It has been reported that papain exhibits high stability in aqueous ethanol and that the activity of papain decreases at ethanol concentrations above 60%.³⁸ It was also found that the stability of papain could be improved by chemically modifying it.³⁹ Even though many works related to proteins including papain in different alcohol-water mixtures can be found, systematic studies on the structural and dynamical responses are rare till date. Here, with a view of acquiring detailed structural and dynamical changes occurring to papain under the influence of aqueous mixture of ethanol, we have carried out steady state fluorescence, solvation dynamics, rotational anisotropy, fluorescence correlation spectroscopy and circular dichroism studies on papain in ethanol-water mixtures of different mole fractions varying from 0 to 0.6.

7.2 Results

7.2.1 Steady state fluorescence spectroscopy study

As mentioned in section 6.2.1 of chapter 6, DACIA-tagged papain shows an emission maximum at 474.5 nm in its native state. In order to look at the effects of an ethanol-water mixture on papain, first we recorded the emission spectra of DACIA-tagged papain in ethanol-water mixtures of different mole fractions. The emission maximum was found to undergo a blue shift with an increase in mole fraction of ethanol. The emission maxima at different mole fractions of ethanol are given in table 7.1. It can be seen that at $\chi_{\text{EtOH}} = 0.6$, the emission spectra underwent a blue shift of 12 nm as compared to that in water. It is well known that papain undergoes denaturation in presence of external agents like guanidine hydrochloride (GnHCl).^{41–43} To compare the effect of GnHCl on papain with that caused by ethanol-water binary mixture, we recorded the emission spectra of DACIA-tagged papain in presence of different concentrations of GnHCl. It can be seen that in the presence of GnHCl the emission spectrum undergoes a red shift due to the denaturation of papain as opposed to the blue shift that occurred due to the effect of

ethanol-water mixture. The emission maxima of DACIA-tagged papain in presence of different concentrations of GnHCl are also compiled in table 7.1. Emission spectra of DACIA-tagged papain in water, in ethanol-water mixture ($\chi_{\text{EtOH}} = 0.6$) and in presence of 5 M GnHCl are shown in figure 7.1, from which the difference in effects that a binary mixture and a denaturing agent have on papain can be clearly seen.

Table 7.1. Emission maxima ($\lambda_{\text{ex}} = 389$ nm) of DACIA-tagged papain in presence of different concentrations of GnHCl and in ethanol-water mixtures of different mole fractions.

χ_{EtOH}	Emi. max. (nm)	Conc. of GnHCl (M)	Emi. max. (nm)
0.00	474.5 ± 1.0	0.00	474.5 ± 1.0
0.05	471.5 ± 1.5	0.50	478.0 ± 1.5
0.10	466.5 ± 1.5	1.00	478.5 ± 2.0
0.20	466.0 ± 1.0	2.00	479.0 ± 1.0
0.30	465.0 ± 0.5	3.00	479.5 ± 1.5
0.40	462.5 ± 1.5	4.00	479.5 ± 1.0
0.60	462.5 ± 1.0	5.00	479.5 ± 2.0

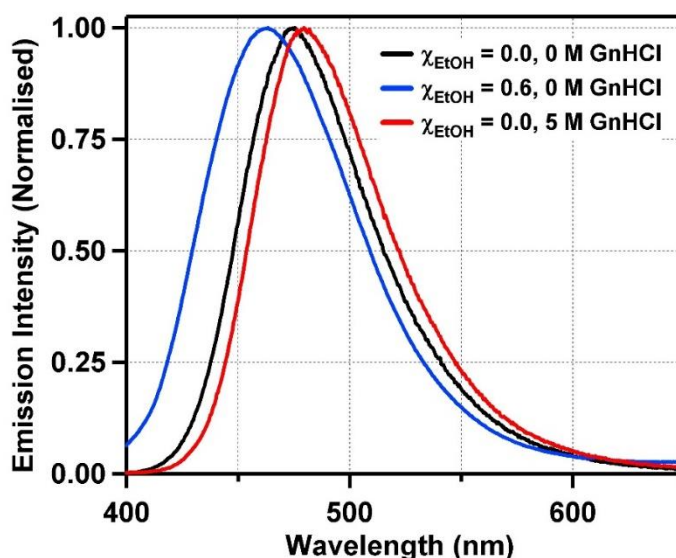


Figure 7.1. Normalized emission spectra of DACIA-tagged papain (black), DACIA-tagged papain in ethanol-water mixture, $\chi_{\text{EtOH}} = 0.6$ (blue) and DACIA-tagged papain in presence of 5 M GnHCl (red). The samples were excited at 389 nm.

7.2.2 Solvation dynamics study

To understand the effects of ethanol-water mixture on the dynamics of interstitial water molecules within papain, we carried out solvation dynamics measurements in ethanol-water binary mixture of different mole fractions. The solvation dynamics of DACIA-tagged papain in water has already been mentioned

in section 3.2.5 of chapter 3. In a similar manner, solvation dynamics studies were carried out in different ethanol-water mixtures. As a representative example, the fitting components of fluorescence transient of DACIA-tagged papain in ethanol-water mixture with $\chi_{\text{EtOH}} = 0.1$ is given in table 7.2. At 420 nm, the three lifetime components were found to be 0.05 ns (49%), 1.19 ns (37%) and 3.70 ns (14%) with an average lifetime of 0.98 ns and at 550 nm, the three components are 0.28 ns (-61%), 3.17 ns (114%) and 4.35 ns (47%) with an average lifetime of 5.49 ns. Some of the transients are shown in figure 7.2 (a) and (b) in which the rise part of fluorescence transient at a higher wavelength could be clearly seen. The time-resolved emission spectra, constructed using lifetime components at different wavelengths and the solvent correlation function are shown in figure 7.2 (c) and figure 7.2 (d) respectively. The dynamic Stokes shift was found to be 720 cm^{-1} and the solvation time components were found to be 0.06 ns (45%) and 0.74 ns (55%) with the average solvation time of 0.43 ns.

Table 7.2. Fitting parameters of fluorescence decay of DACIA-tagged papain in ethanol-water mixture of $\chi_{\text{EtOH}} = 0.1$. The sample was excited at 375.8 nm.

λ_{em} (nm)	a_1	τ_1 (ns) ^a	a_2	τ_2 (ns) ^b	a_3	τ_3 (ns) ^c	$\langle \tau \rangle$ (ns)
420	0.49	0.05	0.37	1.19	0.14	3.70	0.98
430	0.36	0.05	0.41	1.31	0.23	3.75	1.42
450	-0.24	0.50	0.46	0.90	0.78	3.80	3.26
455	-0.57	0.57	0.73	0.79	0.84	3.83	3.47
460	-0.43	0.50	0.54	0.86	0.89	3.85	3.68
464	-0.26	0.36	0.32	1.07	0.94	3.88	3.9
468	-0.36	0.41	0.36	0.93	0.99	3.90	4.05
472	-0.31	0.32	0.28	1.12	1.03	3.93	4.26
476	-0.30	0.30	0.27	1.39	1.03	3.95	4.35
480	-0.33	0.27	0.28	1.55	1.05	4.00	4.54
485	-0.35	0.27	0.37	1.92	0.98	4.05	4.58
490	-0.37	0.27	0.44	2.21	0.93	4.10	4.69
500	-0.44	0.27	0.59	2.48	0.85	4.15	4.87
510	-0.47	0.27	0.76	2.75	0.71	4.25	4.98
520	-0.52	0.26	1.10	3.15	0.42	4.30	5.14
535	-0.57	0.28	1.11	3.07	0.46	4.35	5.25
550	-0.61	0.28	1.14	3.17	0.47	4.35	5.49

^a ± 0.02 ns, ^b ± 0.05 ns, ^c ± 0.20 ns

In a similar manner, solvation studies were carried out on DACIA-tagged papain in ethanol-water mixtures with mole fraction of ethanol 0.05, 0.30 and 0.60.

The data obtained are compiled in table 7.3. It can be seen from the table that with an increase in mole fraction of ethanol, the average solvation time tends to increase up to $\chi_{\text{EtOH}} = 0.10$ and with further increase in χ_{EtOH} , the solvation time remains almost constant. The solvent response functions of DACIA-tagged papain in different ethanol-water mixtures are shown in figure 7.3 where the increase in solvation time can be seen.

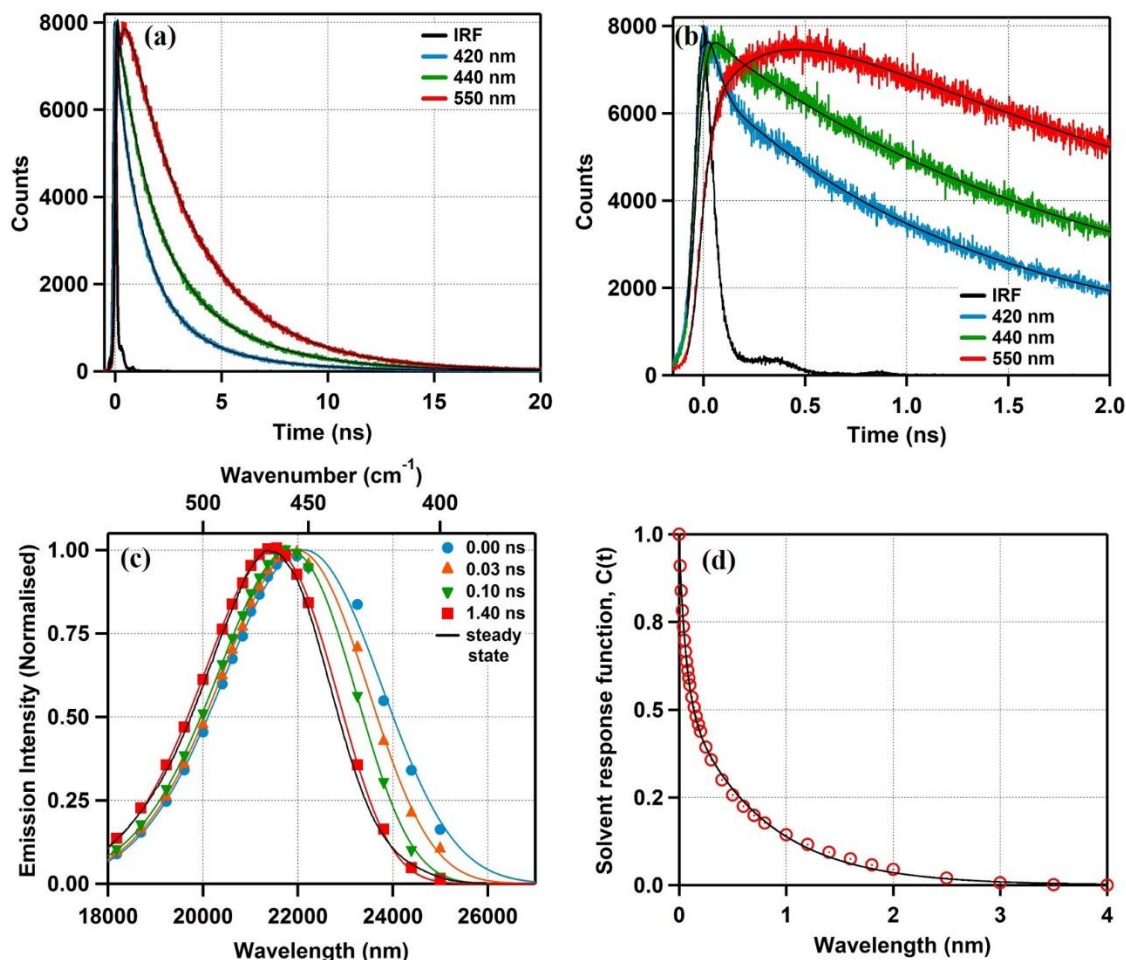


Figure 7.2. A few representative transient decays of DACIA-tagged papain in ethanol-water mixture of $\chi_{\text{EtOH}} = 0.1$ collected at a longer (a) and a shorter (b) timescales. (c) Time-resolved emission spectra (TRES) constructed using the fitting parameters of the transient decays ($\lambda_{\text{ex}} = 375.8$ nm) and (d) the solvent response function calculated using the peak frequencies of TRES.

Table 7.3. Solvation time components, average solvation times, Stokes shifts and missing components of Stokes shift of DACIA-tagged papain in ethanol-water mixtures of different mole fractions. The fractional amplitudes of the solvation time components are given in parentheses. The standard deviations of some of the values are also mentioned.

χ_{EtOH}	τ_1 (ns)	τ_2 (ns)	$\langle \tau_S \rangle$ (ns)	Observed Stokes shift (cm^{-1})	Missing component (%)
0.00	0.03 (0.17)	0.26 (0.83)	0.22 ± 0.06	124 ± 15	94
0.05	0.08 (0.42)	0.56 (0.58)	0.36	300	85
0.10	0.06 (0.45)	0.74 (0.55)	0.43 ± 0.03	720 ± 20	57
0.30	0.12 (0.37)	0.63 (0.63)	0.44	690	58
0.60	0.05 (0.29)	0.55 (0.71)	0.41	680	61

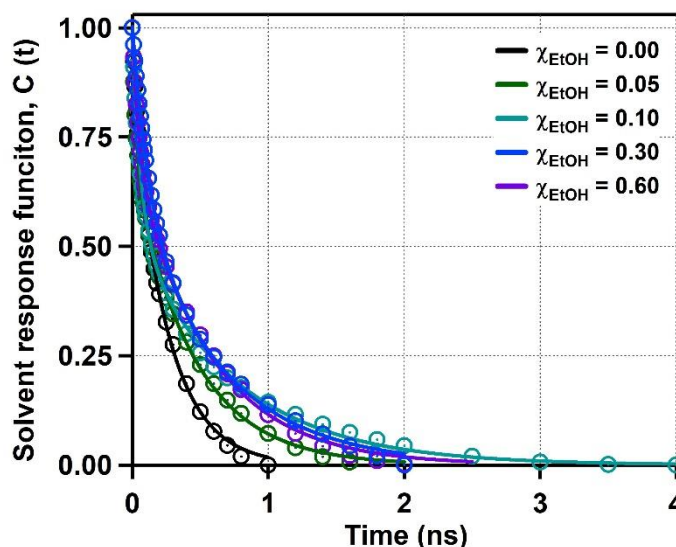


Figure 7.3. Solvent response functions of DACIA-tagged papain in ethanol-water mixtures of different mole fractions.

To compare the solvation dynamics of DACIA-tagged papain in ethanol-water mixture with that in the denatured state of the protein, we carried out solvation dynamics study of the tagged protein in presence of GnHCl. The solvation times are compiled in table 7.4 and the solvent response functions are shown in figure 7.4. As can be seen from table 7.4, the average solvation time in presence of GnHCl increases only slightly as compared to the increase in solvation time in ethanol-water mixtures.

Table 7.4. Solvation time components, average solvation times, Stokes shifts and missing components of Stokes shift of DACIA-tagged papain in presence of different concentrations of GnHCl.

Conc. of GnHCl (M)	τ_1 (ns)	τ_2 (ns)	$\langle \tau_S \rangle$ (ns)	Observed Stokes shift (cm^{-1})	Missing component (%)
0 M	0.03 (0.17)	0.26 (0.83)	0.22 ± 0.06	124 ± 15	94
1 M	0.20 (0.69)	0.48 (0.31)	0.29	130	93
2 M	0.25 (0.40)	0.26 (0.60)	0.26	105	94
3 M	0.17 (0.45)	0.35 (0.55)	0.25 ± 0.04	159 ± 15	91
5 M	0.07 (0.21)	0.34 (0.79)	0.28	240	86

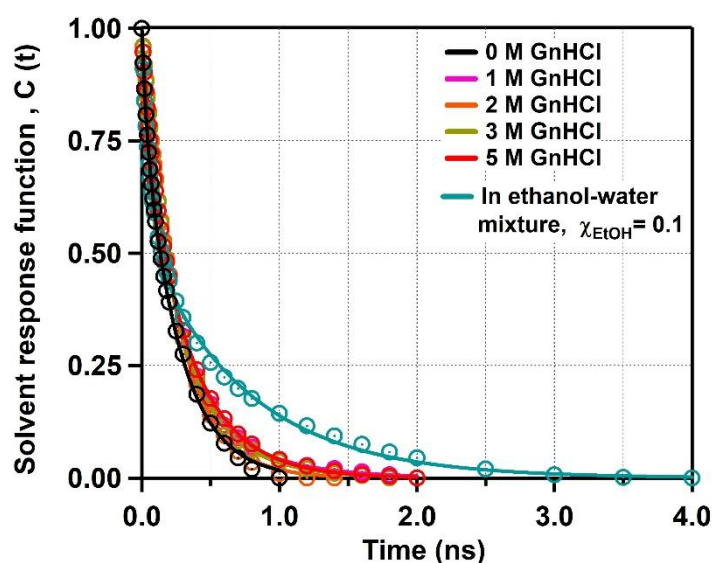


Figure 7.4. The solvent response functions of DACIA-tagged papain in presence of different concentrations of GnHCl. The solvent response function of DACIA-tagged papain in ethanol-water mixture of $\chi_{\text{EtOH}}=0.1$ is also shown for comparison.

7.2.3 Fluorescence anisotropy study

Time-resolved fluorescence anisotropy study was also carried out on DACIA-tagged papain, both in presence of GnHCl and also in ethanol-water mixtures of different mole fractions. The anisotropy decays are shown in figure 7.5. As can be seen from the figure, anisotropy decays are much slower in presence of ethanol as compared to the decay in water. In presence of GnHCl (figure 7.5(b)), even though the rotational dynamics is slower than that in the absence of GnHCl, the decay seems to be faster than that of DACIA-tagged papain in ethanol-water mixtures.

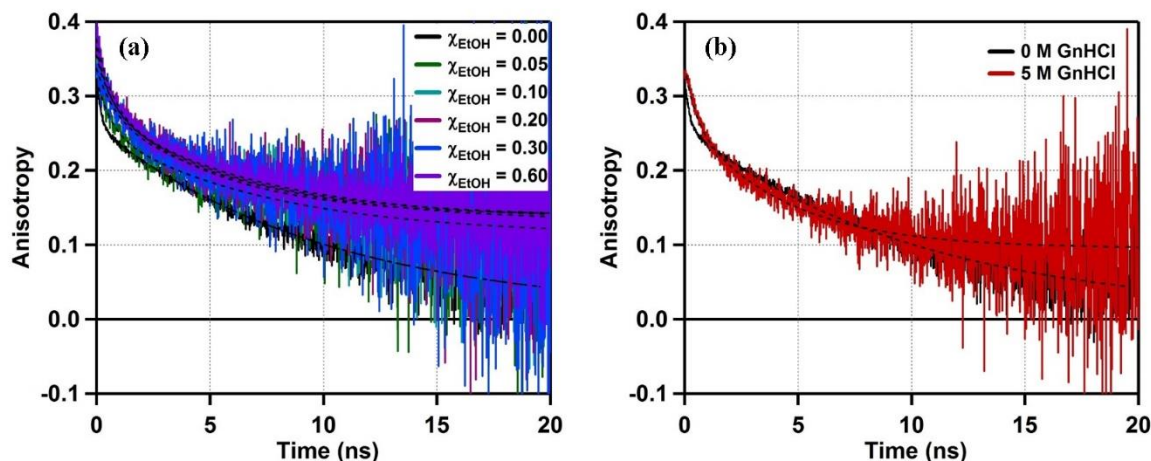


Figure 7.5. Fluorescence anisotropy decay of DACIA-tagged papain in (a) ethanol-water mixtures of different mole fractions and in (b) absence and presence of GnHCl (5 M).

The rotational anisotropy decays are fitted using the equation (6.2) and the rotational time constants and the residual anisotropies are tabulated in table 7.5. As can be seen from the table, DACIA-tagged papain exhibits negligible residual anisotropy in water, while in ethanol-water mixtures the residual anisotropy is much higher. In the presence of GnHCl, the residual anisotropy is higher than that of non-denatured protein, but still is lesser than that in the ethanol-mixtures. In the case of rotational time components, the value of shorter time component increases in presence of GnHCl and in ethanol-water mixture, while the value of longer time component decreases.

Table 7.5. The components of rotational correlation times of DACIA-tagged papain in ethanol-water mixtures and in presence of 5 M GnHCl.

χ_{EtOH}	τ_{R_1} (ns)	τ_{R_2} (ns)	$r(\infty)$	GnHCl conc. (M)	τ_{R_1} (ns)	τ_{R_2} (ns)	$r(\infty)$
0.00	0.20 (0.20)	9.50 (0.80)	0.01	0	0.20 (0.20)	9.50 (0.80)	0.01
0.05	0.63 (0.32)	7.33 (0.68)	0.11	5	0.49 (0.29)	4.28 (0.71)	0.08
0.10	0.56 (0.26)	4.90 (0.74)	0.14				
0.20	0.61 (0.34)	5.91 (0.66)	0.14				
0.40	0.82 (0.30)	6.78 (0.70)	0.13				
0.60	0.72 (0.40)	6.89 (0.60)	0.14				

7.2.4 Fluorescence correlation spectroscopy study

Having studied the solvation dynamics and the rotational anisotropy of DACIA-tagged papain in ethanol-water mixtures and in presence of GnHCl, we proceeded to carry out the fluorescence correlation spectroscopy measurements of the system in order to quantify the changes during the structural changes of papain

in ethanol-water mixture and GnHCl . From FCS data, we can get information about diffusion time-scale (τ_D) and conformational fluctuation time scale (τ_R) of papain for which fluctuation of fluorescence intensity arises. From τ_D , direct assessment of size is possible, whereas, τ_R furnishes information about the local dynamics around the probe. Mathematically, we get these timescales after fitting the auto-correlation curves by equation (2.32) mentioned in chapter 2. Here, it is to be mentioned that, in one of the previous publications from our research group, we have proved that the auto-correlation traces for papain cannot be fitted satisfactorily with equation (2.31) and we have to move on to equation (2.32) for proper fitting.⁴⁴

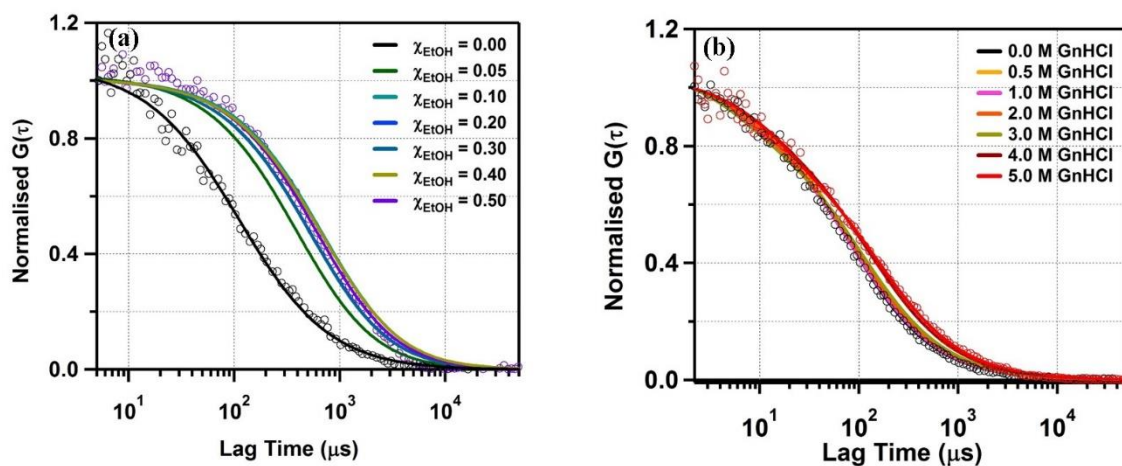


Figure 7.6. Normalized autocorrelation curves and their fittings of DACIA-tagged papain in (a) ethanol-water mixtures of different χ_{EtOH} and (b) in presence of different concentrations of GnHCl . The concentration of protein was maintained at about 50 nM in all the experiments.

The hydrodynamic radii were calculated using equation (2.34) for papain in presence of GnHCl and in ethanol-water mixtures. In all cases, the auto correlation curves were fitted using equation (2.32). The hydrodynamics radii thus obtained are tabulated in table 7.6. Here, it is to mention that, the presence of ethanol or GnHCl results in the change of viscosity or refractive index of the sample solutions that may interfere in the diffusion timescale of the protein. To ensure that, these changes does not hamper our measurement, we take two precautions.⁴⁵ Firstly, the objective collar position is adjusted in such a way to obtain an optimized focal volume that gives the lowest τ_D . In this way, we nullify the effect of the change of refractive index. And secondly, the viscosity effect is cancelled by doing the control experiment at every

experimental point, taking rhodamine-6G (a rigid molecule, which is assumed to not undergo any structural change in the presence of ethanol or GnHCl) as the probe and then normalizing the data using equation (7.1).

$$r_H^{papain} = r_H^{R6G} \cdot \frac{\tau_D^{papain}}{\tau_D^{R6G}} \quad (7.1)$$

Table 7.6. Hydrodynamic radii of papain in ethanol-water mixtures of different χ_{EtOH} and in presence of different concentrations of GnHCl.

χ_{EtOH}	Hydrodynamic radii, r_H (Å)	GnHCl conc. (M)	Hydrodynamic radii, r_H (Å)
0.00	18.4 ± 0.6	0.0	18.4 ± 0.6
0.05	95.4 ± 20	0.5	19.3 ± 1.1
0.10	159.8 ± 25	1.0	19.7 ± 1.1
0.20	127.9 ± 26	2.0	19.7 ± 1.3
0.30	136.5 ± 30	3.0	20.7 ± 1.2
0.40	181.7 ± 24	4.0	22.8 ± 1.8
0.50	155.2 ± 30	5.0	23.3 ± 1.7

7.2.5 Circular dichroism spectroscopy study

Circular dichroism (CD) studies can help us to get information regarding the secondary structural components of a protein. We recorded the CD spectra of papain in different ethanol-water mixtures and in presence of different concentrations of GnHCl to get an idea about the changes occurring to the α -helix and β -sheet structures of papain. Some of the representative spectra are shown in figure 7.7 (a) and (b).

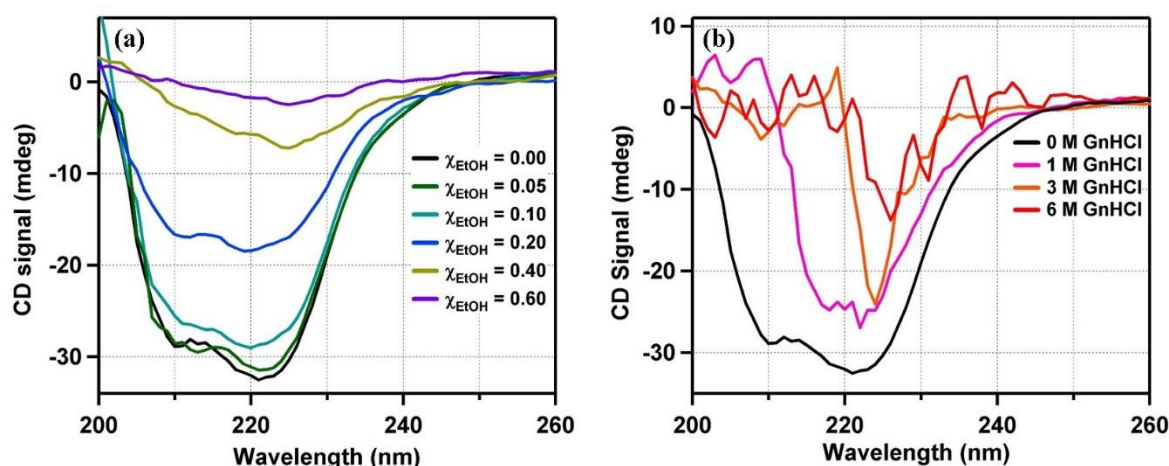


Figure 7.7. Circular dichroism spectra of papain (a) in ethanol-water mixture of different mole fractions and (b) in presence of different concentrations of GnHCl. In each case, concentration of papain was 5 μ M and the pathlength of cuvette was 2 mm.

From figure 7.7, the difference in the changes occurring due to the effect of ethanol-water binary mixture and that of GnHCl can be seen clearly. Further, we have analysed the CD data using CDNN software, which helps to get quantitative information about the secondary structures.⁴⁶ The data has been compiled in table 7.7 and table 7.8.

Table 7.7. Fractional components of different secondary structural elements of papain at different mole fractions of ethanol calculated using circular dichroism spectra.

χ_{EtOH}	Fractional component (%)			
	α -helix	β -sheet	β -turn	Random coil
0.00	25	21	17	37
0.05	23	24	17	36
0.10	21	26	17	36
0.20	16	31	18	35
0.40	12	37	17	34
0.60	10	41	17	32

Table 7.8. Fractional components of different secondary structural elements of papain in presence of different concentrations of GnHCl calculated from circular dichroism spectra.

GnHCl conc. (M)	Fractional component (%)			
	α -helix	β -sheet	β -turn	Random coil
0	25	21	17	37
1	16	26	18	40
2	14	27	17	42
3	10	30	17	43
4	10	31	17	42
5	11	30	17	42
6	10	31	17	42

7.3 Discussion

The steady state emission spectra of DACIA-tagged papain in ethanol-water mixtures of different mole fractions revealed that the emission maximum of the system undergoes a monotonous blue shift with an increase in mole fraction of ethanol. The emission maximum was found to be at 474.5 nm in water, which shifts by 12 nm to 462.5 nm when mole fraction of ethanol is 0.6. This shift in emission maximum could be due to some structural changes occurring to the protein, repositioning the fluorescent tag DACIA molecule into a more hydrophobic environment. In chapter 4 and chapter 5 we had looked at the effects of different denaturing agents on human serum albumin. During those studies, we had seen that

emission maximum of the tagged protein undergoes a red shift due to the action of denaturing agents as they expose the probe molecule to a less hydrophobic environment. So it would be safe to assume that the blue shift of emission maximum of DACIA-tagged papain in ethanol-water mixture is not due to the denaturation of papain as denaturation could have caused a red shift. Nevertheless, in order to make sure that the change in steady state spectrum in ethanol-water mixture is not caused due to denaturation, we have looked at the change in emission maximum of DACIA-tagged papain caused due to a denaturing agent, GnHCl. As expected, the emission maximum underwent a 5 nm red shift from 474.5 nm in the native state to 479.5 nm in presence of 5 M GnHCl. The variations of emission maximum in ethanol-water mixtures and that due to the action of denaturing agent are shown in figure 7.8, where the opposite effects caused by these two external agents could be clearly seen. From these observations, it becomes clear that some structural change of papain other than denaturation is causing the blue shift in emission spectrum in ethanol-water binary mixture. From figure 7.8 it could also be noted that a major change in emission maximum occurs between χ_{EtOH} values 0 and 0.1, where a blue shift of 8 nm is observed, while further increasing χ_{EtOH} to 0.6 only causes a shift of 4 nm.

This space intentionally left blank

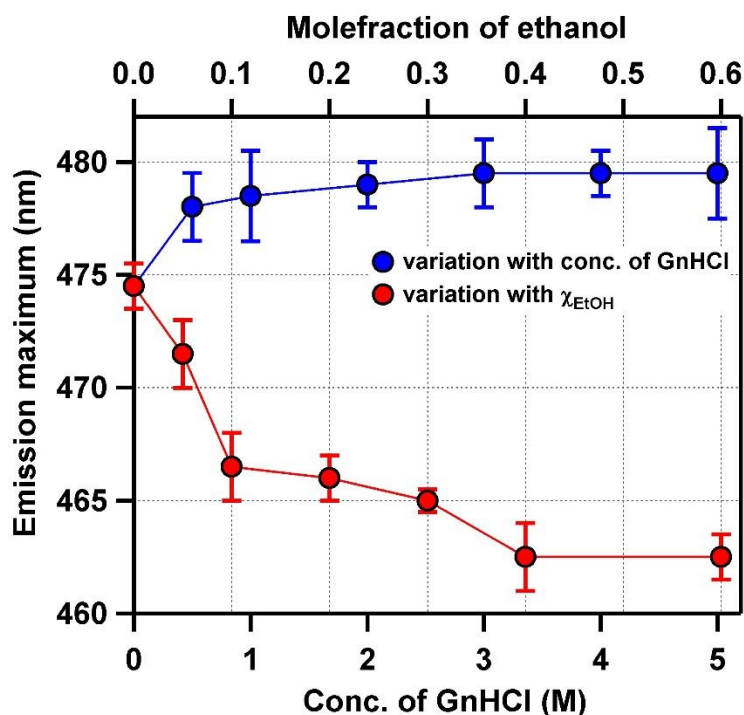


Figure 7.8. Variation of emission maximum ($\lambda_{ex} = 389$ nm) of DACIA-tagged papain with change in concentration of GnHCl and with change in mole fraction of ethanol.

Solvation time in papain increases about 2 fold in ethanol-water mixture as compared to that in water. In the case of denaturation of a protein, we expect the solvation to be either faster or to have a similar rate, as unfolding of peptide chains would make the environment of the probe molecule less confined.⁴¹ We were able to observe this effect when we had studied the solvation of papain in presence of GnHCl. The presence of denaturant caused only a marginal increase in solvation time of DACIA-tagged papain as compared to the increase in solvation time observed in the solvent mixture. Figure 7.9 shows the variation of solvation time of DACIA-tagged papain in ethanol-water mixtures and in presence of GnHCl. These observations further confirm that the structural changes in papain in presence of ethanol is not the denaturation of protein.

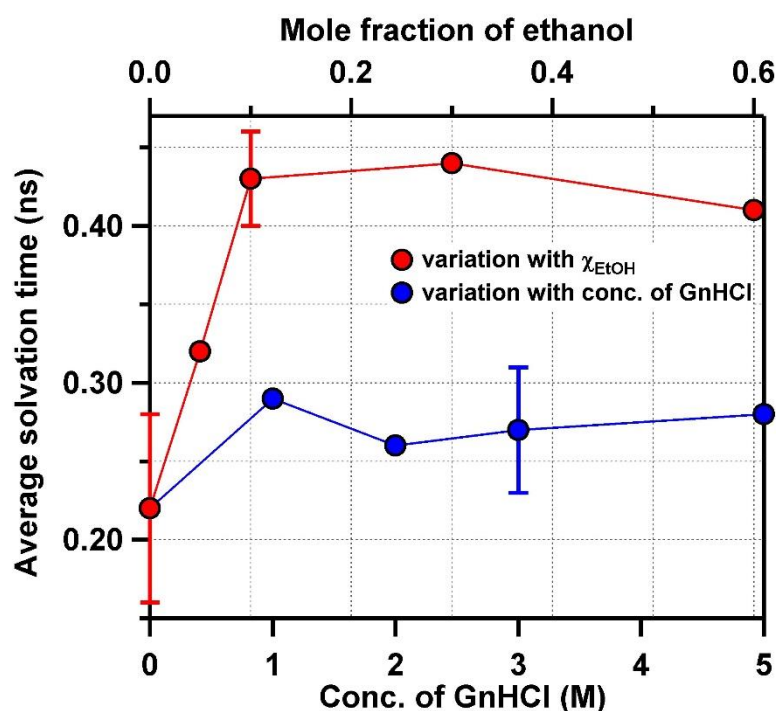


Figure 7.9. Variation of the average solvation time of DACIA-tagged papain with change in concentration of GnHCl and with change in mole fraction of ethanol.

It has been previously reported that solvation dynamics inside macromolecules becomes slower when they form aggregates.^{47–49} This slower solvation has been attributed to the greater restriction on the mobility of solvent molecules trapped inside macromolecules when they form aggregates. In view of this, we propose that papain undergoes aggregation in aqueous mixture of ethanol, which results in a more confined environment of the probe molecule, thus resulting in slower solvation. The aggregation of the protein would also result in a more hydrophobic environment of DACIA, which results in the blue shift in emission spectrum.

Rotational anisotropy study further helps to elucidate the aggregate formation of papain in ethanol-water mixtures. As it was discussed in chapter 6, the shorter component of anisotropy decay corresponds to the rotation of DACIA molecule covalently bound to the protein, while the longer component represents the rotation of the overall protein. From table 7.5 it can be seen that the shorter component of rotational time is slower in ethanol-water mixtures as compared to that in water. In the ethanol-water mixtures with mole fractions 0.05 and 0.40 the shorter

rotational components are 3 and 4 times slower than that in water. The aggregation of the protein in the binary mixture can be causing a restriction in the rotation of DACIA, which in turn results in slower rotational time. It can be noted that in the presence of GnHCl also, the shorter component becomes slower indicating that denaturation of the protein is also somehow hindering the rotation of the probe molecule.

Although the values of the longer component of rotational time, which corresponds to the overall rotation of the protein decrease in ethanol-water mixtures, the amount of residual anisotropy has increased appreciably. While, in water, papain is having negligible residual anisotropy (0.01), in ethanol-water mixtures of ethanol mole fractions 0.05 and 0.60, the residual anisotropy values are 0.11 and 0.14 respectively. The higher residual anisotropy values of papain in ethanol-water mixtures could be due to the larger aggregates which do not complete the reorientation within 4-5 lifetimes of the probe molecule. The higher residual anisotropy may also be the reason for the lower values of longer components of rotational times.

Fluorescence correlation spectroscopic study helps us to get information about the size of diffusing species by the calculation of the hydrodynamic radius from the measured diffusion time. In water, the hydrodynamic radius of papain has been calculated to be 18.4 Å.⁴⁴ The variation of hydrodynamic radii of papain with increasing amount of ethanol as well as with increasing concentration of GnHCl are shown in figure 7.10. In ethanol-water mixture, the hydrodynamic radius increases to 95.4 Å at $\chi_{\text{EtOH}} = 0.05$ and then to 159.8 Å at $\chi_{\text{EtOH}} = 0.10$. With further increase in the mole fraction of ethanol, the size remains almost constant. On the other hand, the size of protein moiety increases only to a much smaller extent due to the action of the denaturant, GnHCl. In presence of 5 M GnHCl, hydrodynamic radius increases to a value of 23.3 Å, which is due to the denaturation of papain. This huge increase in the value of hydrodynamic radius of papain in presence of ethanol-water mixture as compared to that of native state of papain and also to the denatured state

of papain further confirms aggregate formation in the alcohol-water mixture. In many of the previous reports on protein aggregation, the aggregate formation was found to occur when the concentration of protein is in micromolar range or higher.^{25,30,34,50,51} For our FCS experiments, we have used protein samples of concentration in the nanomolar order. The fact that we were able to detect the presence of aggregates in these samples reveal that papain can form aggregates in ethanol-water mixture even at such low concentrations.

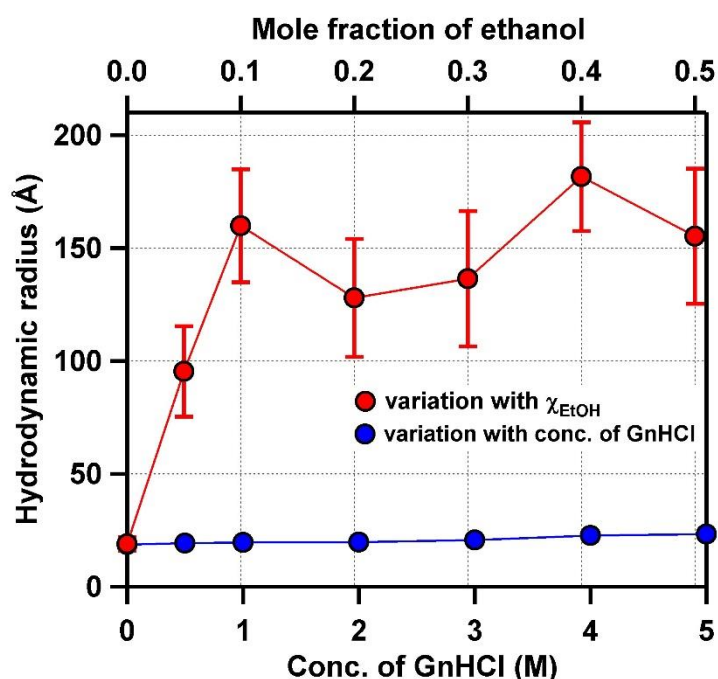


Figure 7.10. Hydrodynamic radii of papain in ethanol-water mixtures of different χ_{EtOH} and in presence of different concentrations of GnHCl.

Circular dichroism measurements can help us to get a clearer picture about the secondary structure of proteins and the changes induced on it due to the changes in its environment. Analysis of CD spectra using CDNN software can deliver us information about the fractional components of different secondary structural elements including α -helix, β -sheet and β -turn and the fraction of random coil in the protein moiety. It has been previously reported in literature that, proteins like human serum albumin and bovine serum albumin aggregates by the formation of β -sheet.^{52–54} Also, in most of the cases, the aggregates of proteins are found to be rich in β -sheet. We have monitored the change in the fraction of different secondary elements of papain with increasing mole fraction of ethanol (figure 7.11(a)). It could be seen

that the percentage component of β -sheet increases from 21% in water to 41% in ethanol-water mixture with $\chi_{\text{EtOH}}=0.60$, at the expense of α -helix structure (25% to 10%) and random coil (37% to 32%) content. It could also be noted that the amount of β -turn remains almost the same during this process. From this analysis, we can see that papain forms aggregates at higher mole fraction of ethanol in ethanol-water mixture by formation of β -sheets. Similar analysis for papain in presence of GnHCl (figure 7.11(b)) showed a decrease in the amount of α -helix structures and an increase in the amount of random coil which is expected during denaturation. An increase in the amount of β -sheet is also observed during the denaturation process (from 21% to 31%), even though this increase is smaller than the corresponding change occurred in the case of papain in ethanol-water mixtures, while the amount of β -turn remains almost constant in this case as well.

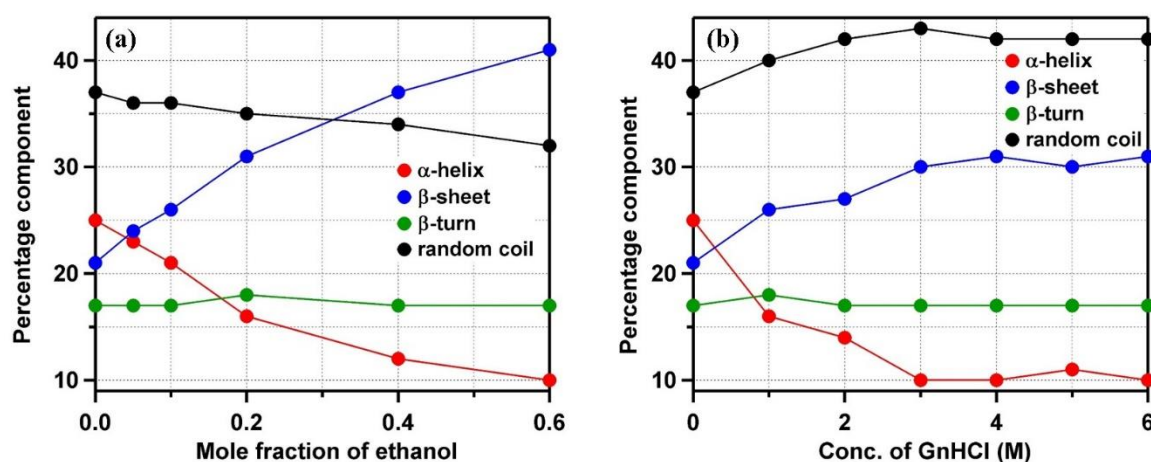


Figure 7.11. Variation in the amount of different secondary structural components of papain with (a) change in mole fraction of ethanol and (b) with change in concentration of ethanol.

7.4 Conclusion

In this study we have scrutinized the effect of ethanol-water binary solvent mixture on the structural response of papain by various bulk and single molecular level spectroscopic measurements and have compared the result with GnHCl induced structural change of papain. From the spectroscopic studies, we can conclude that GnHCl denaturates papain, whereas ethanol induces its aggregation. A strong correlation between structural change at single molecular level measurement and secondary structural change from the circular dichroism

measurements have been found. Chemical denaturation of papain by GnHCl is associated with the loss of helicity with a concomitant increase of random-coil and a small increase of β -sheet. Whereas, ethanol induced aggregation of papain is associated with the formation of high percentage of β -sheet. The findings are supported by steady-state experiment, solvation dynamics and the rotational anisotropy of the protein in ethanol-water mixture and in GnHCl. Our results suggest that two chemical constituents can interact with a protein in very different ways, reminding us of the tremendous degree of complexity involved in the biological system. Another surprising highlight of the study is that papain was found to form aggregates in ethanol-water mixture at concentrations as low as 50 nM. As a whole, the global and local structural change of papain in ethanol-water binary solvent mixture and also in the presence of GnHCl has been summarised, quantified and explained. Papain, being tremendously important in industry, are required to be protected against aggregation. In this study, we showed that papain is very much prone to aggregation in the presence of ethanol.

References

- (1) Frank, H. S.; Evans, M. W. Free Volume and Entropy in Condensed Systems III. Entropy in Binary Liquid Mixtures; Partial Molal Entropy in Dilute Solutions; Structure and Thermodynamics in Aqueous Electrolytes. *J. Chem. Phys.* **1945**, *13*, 507–532.
- (2) Lama, R. F.; Lu, B. C.-Y. Excess Thermodynamic Properties of Aqueous Alcohol Solutions. *J. Chem. Eng. Data* **1965**, *10*, 216–219.
- (3) Franks, F. t; Ives, D. J. G. The Structural Properties of Alcohol–water Mixtures. *Q. Rev. Chem. Soc.* **1966**, *20*, 1–44.
- (4) Nakanishi, K.; Kato, N.; Maruyama, M. Excess and Partial Volumes of Some Alcohol-Water and Glycol-Water Solutions. *J. Phys. Chem.* **1967**, *71*, 814–818.
- (5) Schott, H. Hydration of Primary Alcohols. *J. Chem. Eng. Data* **1969**, *14*, 237–239.
- (6) McGlashan, M. L.; Williamson, A. G. Isothermal Liquid-Vapor Equilibria for System Methanol-Water. *J. Chem. Eng. Data* **1976**, *21*, 196–199.
- (7) Wakisaka, A.; Abdoul-Carime, H.; Yamamoto, Y.; Kiyozumi, Y. Non-Ideality of Binary Mixtures Water-Methanol and Water-Acetonitrile from the Viewpoint of Clustering Structure. *J. Chem. Soc. Faraday Trans.* **1998**, *94*, 369–374.
- (8) Wakisaka, A.; Ohki, T. Phase Separation of Water–alcohol Binary Mixtures Induced by the Microheterogeneity. *Faraday Discuss.* **2005**, *129*, 231–245.
- (9) Egashira, K.; Nishi, N. Low-Frequency Raman Spectroscopy of Ethanol–water Binary Solution: Evidence for Self-Association of Solute and Solvent Molecules. *J. Phys. Chem. B* **1998**, *102*, 4054–4057.
- (10) Nishi, N.; Yamamoto, K. Conversion of Liquids to Cluster Beams by Adiabatic Expansion of Liquid Jets: Mass Spectrometric Analysis of Molecular Association in Aqueous Solution Systems. *J. Am. Chem. Soc.* **1987**, *109*, 7353–7361.
- (11) Nishi, N.; Koga, K.; Ohshima, C.; Yamamoto, K.; Nagashima, U.; Nagami, K. Molecular Association in Ethanol-Water Mixtures Studied by Mass Spectrometric Analysis of Clusters Generated through Adiabatic Expansion of Liquid Jets. *J. Am. Chem. Soc.* **1988**, *110*, 5246–5255.
- (12) Matsumoto, M.; Nishi, N.; Furusawa, T.; Saita, M.; Takamuku, T.; Yamagami, M.; Yamaguchi, T. Structure of Clusters in Ethanol–water Binary Solutions Studied by Mass Spectrometry and X-Ray Diffraction. *Bull. Chem. Soc. Jpn.* **1995**, *68*, 1775–1783.

- (13) Nishi, N.; Takahashi, S.; Matsumoto, M.; Tanaka, A.; Muraya, K.; Takamuku, T.; Yamaguchi, T. Hydrogen-Bonded Cluster Formation and Hydrophobic Solute Association in Aqueous Solutions of Ethanol. *J. Phys. Chem.* **1995**, *99*, 462–468.
- (14) Wakisaka, A.; Komatsu, S.; Usui, Y. Solute-Solvent and Solvent-Solvent Interactions Evaluated through Clusters Isolated from Solutions: Preferential Solvation in Water-Alcohol Mixtures. *J. Mol. Liq.* **2001**, *90*, 175–184.
- (15) Nishikawa, K.; Hayashi, H.; Iijima, T. Temperature Dependence of the Concentration Fluctuation, the Kirkwood-Buff Parameters, and the Correlation Length of Tert-Butyl Alcohol and Water Mixtures Studied by Small-Angle X-Ray Scattering. *J. Phys. Chem.* **1989**, *93*, 6559–6565.
- (16) Takamuku, T.; Saisho, K.; Nozawa, S.; Yamaguchi, T. X-Ray Diffraction Studies on Methanol–water, Ethanol–water, and 2-Propanol–water Mixtures at Low Temperatures. *J. Mol. Liq.* **2005**, *119*, 133–146.
- (17) Kusalik, P. G.; Lyubartsev, A. P.; Bergman, D. L.; Laaksonen, A. Computer Simulation Study of Tert-Butyl Alcohol. 1. Structure in the Pure Liquid. *J. Phys. Chem. B* **2000**, *104*, 9526–9532.
- (18) Gereben, O.; Pusztai, L. Investigation of the Structure of Ethanol–Water Mixtures by Molecular Dynamics Simulation I: Analyses Concerning the Hydrogen-Bonded Pairs. *J. Phys. Chem. B* **2015**, *119*, 3070–3084.
- (19) Chatteraj, S.; Mandal, A. K.; Bhattacharyya, K. Effect of Ethanol-Water Mixture on the Structure and Dynamics of Lysozyme: A Fluorescence Correlation Spectroscopy Study. *J. Chem. Phys.* **2014**, *140*, 115105-1–8.
- (20) Ghosh, R.; Roy, S.; Bagchi, B. Solvent Sensitivity of Protein Unfolding: Dynamical Study of Chicken Villin Headpiece Subdomain in Water-Ethanol Binary Mixture. *J. Phys. Chem. B* **2013**, *117*, 15625–15638.
- (21) Martin, S. R.; Esposito, V.; De Los Rios, P.; Pastore, A.; Temussi, P. A. Cold Denaturation of Yeast Frataxin Offers the Clue to Understand the Effect of Alcohols on Protein Stability. *J. Am. Chem. Soc.* **2008**, *130*, 9963–9970.
- (22) Avdulov, N. A.; Chochina, S. V.; Daragan, V. A.; Schroeder, F.; Mayo, K. H.; Wood, W. G. Direct Binding of Ethanol to Bovine Serum Albumin: A Fluorescent and ¹³C NMR Multiplet Relaxation Study. *Biochemistry* **1996**, *35*, 340–347.
- (23) Goda, S.; Takano, K.; Yamagata, Y.; Nagata, R.; Akutsu, H.; Maki, S.; Namba, K.; Yutani, K. Amyloid Protofilament Formation of Hen Egg Lysozyme in Highly Concentrated Ethanol Solution. *Protein Sci.* **2000**, *9*, 369–375.

-
- (24) Calandrini, V.; Onori, G.; Santucci, A. Effect of 1-Alkanols on the Native Conformation of Lysozyme. *Phys. Chem. Chem. Phys.* **2000**, *2*, 4143–4146.
- (25) Tanaka, S.; Oda, Y.; Ataka, M.; Onuma, K.; Fujiwara, S.; Yonezawa, Y. Denaturation and Aggregation of Hen Egg Lysozyme in Aqueous Ethanol Solution Studied by Dynamic Light Scattering. *Biopolym. Orig. Res. Biomol.* **2001**, *59*, 370–379.
- (26) Sasahara, K.; Nitta, K. Effect of Ethanol on Folding of Hen Egg-white Lysozyme under Acidic Condition. *Proteins Struct. Funct. Bioinforma.* **2006**, *63*, 127–135.
- (27) Ortore, M. G.; Mariani, P.; Carsughi, F.; Cinelli, S.; Onori, G.; Teixeira, J.; Spinuzzi, F. Preferential Solvation of Lysozyme in Water/Ethanol Mixtures. *J. Chem. Phys.* **2011**, *135*, 245103-1–9.
- (28) Lousa, D.; Baptista, A. M.; Soares, C. M. Analyzing the Molecular Basis of Enzyme Stability in Ethanol/Water Mixtures Using Molecular Dynamics Simulations. *J. Chem. Inf. Model.* **2012**, *52*, 465–473.
- (29) Sashi, P.; Yasin, U. M.; Bhuyan, A. K. Unfolding Action of Alcohols on a Highly Negatively Charged State of Cytochrome C. *Biochemistry* **2012**, *51*, 3273–3283.
- (30) Nemzer, L. R.; Flanders, B. N.; Schmit, J. D.; Chakrabarti, A.; Sorensen, C. M. Ethanol Shock and Lysozyme Aggregation. *Soft Matter* **2013**, *9*, 2187–2196.
- (31) Sirotkin, V. A.; Kuchierskaya, A. A. α -Chymotrypsin in Water-Ethanol Mixtures: Effect of Preferential Interactions. *Chem. Phys. Lett.* **2017**, *689*, 156–161.
- (32) Sarkar, S.; Biswas, B.; Singh, P. C. Spectroscopic and Molecular Dynamics Simulation Study of Lysozyme in the Aqueous Mixture of Ethanol: Insights into the Nonmonotonic Change of the Structure of Lysozyme. *J. Phys. Chem. B* **2018**, *122*, 7811–7820.
- (33) Nikolaidis, A.; Moschakis, T. On the Reversibility of Ethanol-Induced Whey Protein Denaturation. *Food Hydrocoll.* **2018**, *84*, 389–395.
- (34) Yoshida, K.; Vogtt, K.; Izaola, Z.; Russina, M.; Yamaguchi, T.; Bellissent-Funel, M.-C. Alcohol Induced Structural and Dynamic Changes in β -Lactoglobulin in Aqueous Solution: A Neutron Scattering Study. *Biochim. Biophys. Acta (BBA)-Proteins Proteomics* **2012**, *1824*, 502–510.
- (35) Ross, C. A.; Poirier, M. A. Protein Aggregation and Neurodegenerative Disease. *Nat. Med.* **2004**, *10*, S10–S17.
- (36) Koo, E. H.; Lansbury, P. T.; Kelly, J. W. Amyloid Diseases: Abnormal Protein Aggregation in Neurodegeneration. *Proc. Natl. Acad. Sci.* **1999**, *96*,

- 9989–9990.
- (37) Hashimoto, M.; Rockenstein, E.; Crews, L.; Masliah, E. Role of Protein Aggregation in Mitochondrial Dysfunction and Neurodegeneration in Alzheimer's and Parkinson's Diseases. *Neuromolecular Med.* **2003**, *4*, 21–35.
- (38) Szabó, A.; Kotormán, M.; Laczkó, I.; Simon, L. M. Spectroscopic Studies of Stability of Papain in Aqueous Organic Solvents. *J. Mol. Catal. B Enzym.* **2006**, *41*, 43–48.
- (39) Szabó, A.; Kotormán, M.; Laczkó, I.; Simon, L. M. Improved Stability and Catalytic Activity of Chemically Modified Papain in Aqueous Organic Solvents. *Process Biochem.* **2009**, *44*, 199–204.
- (40) Szabó, A.; Kotormán, M.; Laczkó, I.; Simon, L. M. Influence of Carbohydrates on Stability of Papain in Aqueous Tetrahydrofuran Mixture. *J. Chem. Technol. Biotechnol. Int. Res. Process. Environ. Clean Technol.* **2009**, *84*, 133–138.
- (41) Mohan, V.; Sengupta, B.; Acharyya, A.; Yadav, R.; Das, N.; Sen, P. Region-Specific Double Denaturation of Human Serum Albumin: Combined Effects of Temperature and GnHCl on Structural and Dynamical Responses. *ACS Omega* **2018**, *3*, 10406–10417.
- (42) Ahmad, B.; Ahmed, M. Z.; Haq, S. K.; Khan, R. H. Guanidine Hydrochloride Denaturation of Human Serum Albumin Originates by Local Unfolding of Some Stable Loops in Domain III. *Biochim. Biophys. Acta - Proteins Proteomics* **2005**, *1750*, 93–102.
- (43) Yadav, R.; Sen, P. Mechanistic Investigation of Domain Specific Unfolding of Human Serum Albumin and the Effect of Sucrose. *Protein Sci.* **2013**, *22*, 1571–1581.
- (44) Sengupta, B.; Chaudhury, A.; Das, N.; Sen, P. Single Molecular Level Probing of Structure and Dynamics of Papain Under Denaturation. *Protein Pept. Lett.* **2017**, *24*, 1073–1081.
- (45) Müller, C. B.; Loman, A.; Pacheco, V.; Koberling, F.; Willbold, D.; Richter, W.; Enderlein, J. Precise Measurement of Diffusion by Multi-Color Dual-Focus Fluorescence Correlation Spectroscopy. *EPL (Europhysics Lett.)* **2008**, *83*, 46001.
- (46) Böhm, G.; Muhr, R.; Jaenicke, R. Quantitative Analysis of Protein Far UV Circular Dichroism Spectra by Neural Networks. *Protein Eng. Des. Sel.* **1992**, *5*, 191–195.
- (47) Dutta, P.; Sukul, D.; Sen, S.; Bhattacharyya, K. Solvation Dynamics of 4-Aminophthalimide in a Polymer (PVP)–surfactant (SDS) Aggregate. *Phys.*

- Chem. Chem. Phys.* **2003**, *5*, 4875–4879.
- (48) Halder, A.; Sen, P.; Burman, A. Das; Bhattacharyya, K. Solvation Dynamics of DCM in a Polypeptide–Surfactant Aggregate: Gelatin–Sodium Dodecyl Sulfate. *Langmuir* **2004**, *20*, 653–657.
- (49) Sen, S.; Sukul, D.; Dutta, P.; Bhattacharyya, K. Solvation Dynamics in Aqueous Polymer Solution and in Polymer–Surfactant Aggregate. *J. Phys. Chem. B* **2002**, *106*, 3763–3769.
- (50) Barteri, M.; Gaudiano, M. C.; Mei, G.; Rosato, N. New Stable Folding of β -Lactoglobulin Induced by 2-Propanol. *Biochim. Biophys. Acta (BBA)-Protein Struct. Mol. Enzymol.* **1998**, *1383*, 317–326.
- (51) Rašković, B.; Popović, M.; Ostojić, S.; Anđelković, B.; Tešević, V.; Polović, N. Fourier Transform Infrared Spectroscopy Provides an Evidence of Papain Denaturation and Aggregation during Cold Storage. *Spectrochim. Acta Part A Mol. Biomol. Spectrosc.* **2015**, *150*, 238–246.
- (52) Bhattacharya, A.; Prajapati, R.; Chatterjee, S.; Mukherjee, T. K. Concentration-Dependent Reversible Self-Oligomerization of Serum Albumins through Intermolecular β -Sheet Formation. *Langmuir* **2014**, *30*, 14894–14904.
- (53) Biancalana, M.; Koide, S. Molecular Mechanism of Thioflavin-T Binding to Amyloid Fibrils. *Biochim. Biophys. Acta (BBA)-Proteins Proteomics* **2010**, *1804*, 1405–1412.
- (54) Dasgupta, M.; Kishore, N. Selective Inhibition of Aggregation/Fibrillation of Bovine Serum Albumin by Osmolytes: Mechanistic and Energetics Insights. *PLoS One* **2017**, *12*, 1–26.

This page intentionally left blank

List of Publications

- * 1. A spectroscopic insight on the ethanol induced aggregation of papain
Vaisakh Mohan, Nilimesh Das, Aritra Das, Vipin Mishra and Pratik Sen.
J. Phys. Chem. B **2019**, 123, 2280-2290.

- * 2. Domain-specific stabilization of structural and dynamic responses of human serum albumin by sucrose
Vaisakh Mohan, Nilimesh Das, Indrani Banerjee, Bhaswati Sengupta and Pratik Sen.
Protein Pept. Lett. **2019**, 26, 287-300.

- * 3. Region-specific double denaturation of human serum albumin: Combined effects of temperature and GnHCl on structural and dynamic responses.
Vaisakh Mohan, Bhaswati Sengupta, Arusha Acharyya, Rajeev Yadav, Nilimesh Das and Pratik Sen.
ACS Omega **2018**, 3, 10406–10417.

- * 4. Elucidation of active site dynamics of papain and the effect of encapsulation within cationic and anionic reverse micelles.
Vaisakh Mohan and Pratik Sen.
Spectrochim. Acta Part A Mol. Biomol. Spectrosc. **2018**, 200, 202–211.

- 5. Highly sensitive visual detection of Fe^{3+} at ppm level.
Md. Serajul Haque Faizi, Shradhey Gupta, **Vaisakh Mohan**, Vipin Kumar Jain and Pratik Sen.
Sensors Actuators B Chem. **2016**, 222, 15–20.

- 6. Photophysical and density functional studies on the interaction of a new nitrobenzoxadiazole derivative with anions.
Sudhir Kumar Das, Smruti Snigdha Misra, Prabhat Kumar Sahu, A. Nijamudheen, **Vaisakh Mohan** and Moloy Sarkar.

Chem. Phys. Lett. **2012**, 546, 90–95.

7. Ion Interactions with a new ditopic naphthalimide-based receptor: A photophysical, NMR and theoretical (DFT) study.

Vaisakh Mohan, A. Nijamudheen, Sudhir Kumar Das, Prabhat Kumar Sahu, Usha Pallabhi Kar, Abdur Rahman and Moloy Sarkar

ChemPhysChem **2012**, 13, 3882–3892.

8. Structures and electronic properties of Si-substituted benzenes and their transition metal complexes.

Vaisakh Mohan and Ayan Datta.

J. Phys. Chem. Lett. 2010, 1, 136–140.

* Included in thesis.